Tracing Massive Star Formation through a Galactic Census of Compact & Ultracompact HII Regions

Author:
Julie Djordjevic

Supervised by:
Mark Thompson
Jan Forbrich

Centre for Astrophysics Research
School of Physics, Astronomy and Mathematics
University of Hertfordshire

Submitted to the University of Hertfordshire in partial fulfilment of the requirements of the degree of Doctor of Philosophy.

July 2019

Abstract

The following dissertation details the work undertaken to compile the most complete compact and ultracompact H II region catalogue to date via multi-wavelength inspection of survey data. We utilise data from the recently available SASSy 850 μm survey and explain the data reduction process leading to the final Outer Galaxy Survey. Combined with the earlier SASSy component that focuses on the Perseus arm, we were able to use the catalogue to identify massive star forming clumps in the Outer Galaxy ($R_{GC} > 8.5$ kpc) and cross-match with infrared and radio data of known UC H II regions from the RMS database. We sought to compare this sample with previous existing catalogues in the Inner Galaxy to examine massive star formation as a function of galactocentric radius and particularly focusing on two distinct environmental regions (Inner and Outer Galaxy) with overall different average metallicities and gas-to-dust ratios. For this Inner Galaxy sample ($R_{GC} < 8.5$ kpc), we adopted the compact H II regions from works that used similar methods to cross-match ATLASGAL with either CORNISH or RMS, depending on the location within the Galactic plane. We present a new UC H II region catalogue that more than doubles the original sample size of previous work, totalling 536 embedded H II regions and 445 host clumps. We examine the distance independent values of N_{Ly}/M and L_{bol}/M as proxies for massive star formation efficiency and overall star formation efficiency, respectively. We find a significant trend showing that L_{bol}/M decreases with increasing R_{GC}, suggesting that the overall star formation per unit mass of the molecular clump is less in the Outer Galaxy. Further investigations with the VLA into the Outer Galaxy for 200 unmatched SASSy molecular clumps revealed seven additional 5 GHz continuum emission sources embedded within the clumps. We conclude that massive star formation is not dependent on Galactic position or environmental factors such as metallicity and the gas-to-dust ratio that are known to vary with galactocentric radius. These results will be relevant to future models attempting to use the Milky Way as a template for evolutionary and formation models of nearby galaxies where similar conditions are found but not observable to the degree of detail as seen in our own Galaxy.

Declaration

I declare that no part of this work is being submitted concurrently for another award of the University or any other awarding body or institution. This thesis contains a substantial body of work that has not previously been submitted successfully for an award of the University or any other awarding body or institution.

The following parts of this submission have been published previously and/or undertaken as part of a previous degree or research programme:

1. Chapter 4: this has been published as Djordjevic et. al, 2019, *Monthly Notices of the Royal Astronomical Society*, **487**, 1.

Except where indicated otherwise in the submission, the submission is my own work and has not previously been submitted successfully for any award.

Acknowledgements

Thank you to the University of Hertfordshire for funding me and sponsoring my student visa. Thank you to JCMT and VLA staff for your help and answers. Also to STFC, RAS, NRAO, ESO, YERAC, and IRAM staff.

I would like to extend additional thanks to the PAM faculty and staff for their support and advice throughout my academic journey, including, but limited to- James U, David E, Sean, Elias, Antonio, Martin, Janet, Kristen, Jim, Emma, Salah, Kuldeep, Kathy, Hugh, Wendy, and Nick. Additional thanks to Jan Forbrich for stepping in as my secondary supervisor halfway through and eagerly listening to my research ideas. To the friends and colleagues I made here- Lord, Mubela (go X's and O's), Gaius, Chris, Jonathan (Horsa Gardens), David, Joanna, Carla, Federico, Neil, Samantha, Hywel, Andre, Garreth, Shaun, Giulio and my whole top-notch outreach team from the undergraduates to the post-docs, wherever they are now. Special thanks to Emma and Nancy without whom I would never have made it this far be it because of their shoulders to lean on or an ear to vent to.

Thanks tor my family and friends who cheered me on from across the pond throughout all the weddings, and new babies. Thanks especially to Bethanne and Ana who visited and kept my motivation up. To Kaitlyn, Aman, Wresha, Kristi, Kelly, Sam, Ashley, Bryan, Caitlin, Brian, and Fiona who all continued to support me from afar. Thank you to my mentors especially Elise, Brad, and Don. Special love and thank you to my sister and brother in law for their unending faith in me. To my parents- Mom who instilled a love and passion for problem-solving in me early on, and to Dad, the "first doctor" Djordjevic.

Second to last, but not least, thank you to my examiners Phil (also for every other year!) and Sarah who are putting their time and effort into making sure this viva happens.

Thank you to my supervisor, Mark. Thanks for putting up with the pushy American girl. Thanks for letting me hammer on your door whenever I needed to and for giving me all of the incredible opportunities I've gotten to experience over the last few years. Thank you for your advice, both of the academic and real world variety.

And finally, with all my love that's brighter than any star in the Galaxy, thanks to Neal and River.

Contents

List of Figures

List of Tables

List of Abbreviations

ATLASGAL	APEX Telescope Large Area Survey of the Galaxy
CORNISH	Co-Ordinated Radio 'N' Infrared Survey for High-mass star formation
EBHIS	The Effelsberg-Bonn H I Survey
FCF	Flux Correction Factor
FWHM	Full Width Half Max
GALF-Hi	Galactic Arecibo L-band Feed Array H I
GASS	GALEX Arecibo SDSS Survey
GBT	Green Bank Telescope
Hi-GAL	Herschel Galactic Plane Survey
HR	Hertzsprung-Russell (diagram)
HRDS	H II Region Discovery Survey
IMF	Initial Mass Function
IR	Infrared
IRAS	Infrared Astronomical Survey
ISM	Interstellar Medium
JCMT	James Clark Maxwell Telescope
JPS	JCMT Plane Survey
KDA	Kinematic Distance Ambiguity
LAB	Leiden-Argentine-Bonn Survey of Galactic H I
MMB	Maser MultiBeam Survey
MS	Main Sequence
MSX	Mid-Course Space Experiment
NRAO	National Radio Astronomy Observatories
OGS	Outer Galaxy Survey
RMS	Red MSX Survey

SASSy	Scuba-2 Ambitious Sky Survey
SASPER	SASSy-Perseus
SCUBA-2	Submillimetre Common-User Bolometer Array 2
SDSS	Sloan Digital Sky Survey
SFE	Star Formation Efficiency
SFF	Star Forming Fraction
SFR	Star Formation Rate
UC	Ultra-Compact
VLA	Very Large Array
WISE	Wide-Field Infrared Survey Explorer
(M)YSO	(Massive) Young Stellar Object

Chapter 1

Introduction

"Do not look at stars as bright spots only. Try to take in the vastness of the universe." - Maria Mitchell, Astronomer

The Milky Way Galaxy contains approximately 100 billion stars. There are over 10 billion galaxies visible in the known Universe. Assuming this is a typical value for the average galaxy, that is over one billion trillion stars scattered throughout the vastness of space. The light from each of those stars carries vital information that is used to understand the nature of the stars and their host galaxies. It allows astronomers to probe stellar photons for clues hinting all the way back to their original formation and to determine what that means for their future evolution. The light is dominated by the biggest, the brightest, and the most massive stars ($M_* > 8\,\mathrm{M}_\odot$ and $L_* > 10^3\,\mathrm{L}_\odot$; Martins 1996). They are an essential piece of the puzzle for explaining the nature of galaxies and yet, a conclusive model for the underlying physics that drives massive star formation and how it varies across different environments found within the Galactic plane remains a challenge. Some of the most important questions can be summarised as follows:

1. Where do massive stars form?
2. How common is massive star formation?
3. How can we confirm with confidence that there is either ongoing or recent massive star formation at these sites?
4. What are the key environmental factors of the local interstellar medium that might impact massive star formation?

5. What percentage of the Galactic plane is home to massive star formation?

6. Is there a noticeable change in the efficiency of massive star formation as a function of galactocentric radius (R_{GC}), or more simply, between the Inner and Outer Galactic environments (with a boundary defined by the position of the Sun at $R_{GC} = R_0 = 8.5$ kpc)?

In this chapter, I will address each of these questions and the work that has been done to help answer them. As will be shown, there has been a great deal of effort towards addressing points (1)-(4); however, few studies have gone far enough to fully examine the real impact of these earlier results on (5) and (6). Little to no observations have been acquired for the Outer Galaxy and wide-area Galactic plane surveys with high enough angular resolution capabilities have only recently become available (see Chapter 2). How the massive star formation efficiency varies with galactocentric radius is the primary question that I seek to address in this dissertation.

1.1 The Interstellar Medium

The road to understanding the mechanics that lie behind the formation of massive stars begins by examining the physical make-up of the environments that give rise to them. The interstellar medium (ISM) is the tenuous material between the stars that consists of low-density gas and dust. It forms the reservoir of material that ultimately becomes molecular clouds that eventually produce star formation. The gaseous component is dominated by hydrogen (91%) which exists primarily in three forms: atomic (H I), molecular (H_2), and ionised (H II). Figure 1.1 shows their corresponding surface densities as a function of galactocentric radius as given by Stahler and Palla 2004. The remaining 9% of the gas is made up of helium and traces of heavier elements (Ferrière, 2001). The gas dominates the ISM mass and only a small percentage of the total ISM is comprised of material dust grains. However, this relatively small amount of dust does little to diminish their significant impact on the local environment. In this section, we will examine each of the primary components of the ISM and their respective influences on star formation.

1.1.1 Interstellar Hydrogen

The total H I gas mass makes up the majority of the interstellar mass in the Galaxy. Atomic hydrogen produces a unique emission line at 21.1 cm that allows us to trace its distribution across the Galactic disk (see Figure 1.1, long dashed line). The corresponding energy of this line for

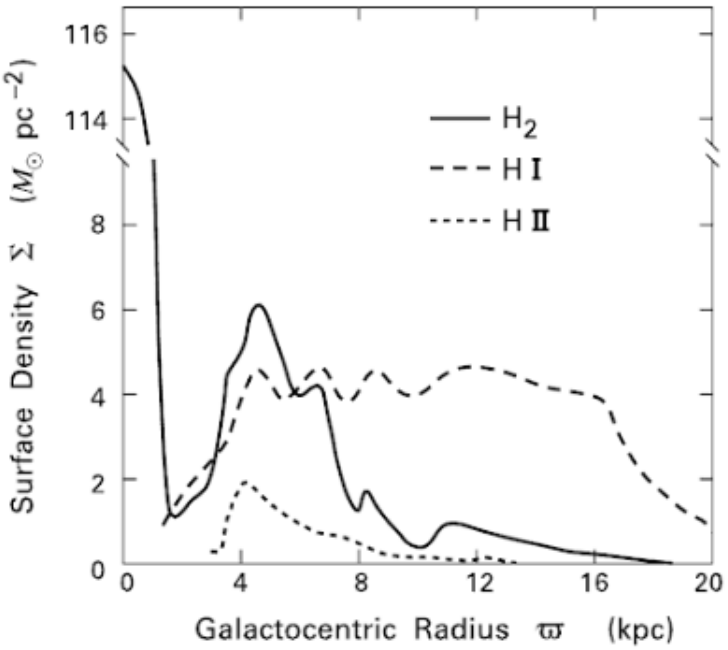

FIGURE 1.1: Galactic surface densities of H_2, H I, and H II as a function of galactocentric radius as given in Figure 2.3 by Stahler and Palla 2004. The symbol ω used here is equivalent to our use of R_{GC} throughout the text. The ionised component shown is that produced only by H II regions.

a system consisting of a single election of mass m_e and charge e bound to a proton of mass m_p can be expressed by the following equation based on the non-relativistic model of Schrodinger's formula,

$$E = -\frac{\mu_{ep} e^4}{2\hbar^2 n^2} = 13.6\,\text{eV}\; n^{-2} \tag{1.1}$$

where n is the principle quantum number (1, 2, 3, etc.) and μ_{ep} is the reduced mass defined as $\mu_{ep} \equiv m_e m_p/(m_e + m_p)$. Spectral lines in the ultraviolet regime that are generated by downward transitions to $n = 1$ form the Lyman series. For example, the Lα line at 1216 Å (121.6 nm) is produced when $n = 2 \rightarrow 1$ and so forth. To observe this energy, a hydrogen atom must first be collisionally excited to a higher state where the spins of the proton and election are parallel. Later, the atom will de-excite (usually by another collision) with the election flipping its spin to return to the ground state in which the spins are anti-parallel. There is a small probability that the radiation emitted will occur via a 21 cm photon with the time period between these two events approximately 1 x 10^7 yr on average (for spontaneous emission). However, with the large abundance of atomic hydrogen across the Galaxy, the probability of detecting this transition is very high. A measurable radio signal can be built up by a sufficiently large number of atoms

undergoing this transition along a particular line of sight. This column density, or the number of atoms per unit area along a line of sight, is directly proportional to the received intensity of the 21 cm radiation. We will return to the discussion of column density in massive star forming regions in Chapter 4.

Radio surveys such as Leiden-Argentine-Bonn (LAB; Kalberla et al. 2005), Arecibo Galactic ALFA Survey (GALFA-H I; Stanimirović et al. 2006), Parkes Galactic All-Sky Survey (GASS; McClure-Griffiths et al. 2009) and the Effelsberg-Bonn H I Survey (EBHIS, Kerp et al. 2009) have mapped the distribution of H I across the Galactic plane to high resolution and when combined with observations in the optical and ultraviolet regimes, have revealed that the atomic hydrogen tends to accumulate into discrete clumps known as H I clouds (e.g. Lockman 2002). These clouds have typical number densities within 10-100 cm^{-3} and diameters from 1 to 100 pc with representative temperatures around 80 K (Stahler and Palla, 2004). As seen in Figure 1.1, the surface density of H I is very low towards the Galactic centre but rises and remains level from 4 kpc to 16 kpc. At larger radii, the surface density begins to decline sharply and studies such as Kalberla and Kerp 2009 have modelled the expected distribution out to R_{GC} = 35 kpc. H I is a valuable tracer for identifying the physical conditions of the ISM allowing for derivations of the local temperature and volume densities that will be critical for determining the presence of ongoing or recent massive star formation later on.

The second main component of the ISM is the molecular hydrogen gas but it is not easy to observe directly as H_2 does not radiate at the temperatures expected in these environments. Instead, it may be traced via CO emission which has a shorter wavelength than 21 cm and provides higher spatial resolution. The distribution for H_2 is seen in Figure 1.1 (solid line). There is a peak of H_2 at the Galactic centre that rapidly declines but rises again at 4 kpc, corresponding with the H I peak discussed earlier. This secondary peak centres around 6 kpc before falling off after 8 kpc and has historically been known as the 'molecular ring' (Stecker et al., 1975; Cohen and Thaddeus, 1977; Roman-Duval et al., 2010). However, some work in the simulations of spiral galaxies has suggested this is not truly a ring and the feature is a result of emission from nearby spiral arms (e.g. Englmaier and Gerhard 1999; Rodriguez-Fernandez and Combes 2008; Junichi et al. 2010). CO maps that trace the molecular component can be used to map the Milky Way and determine its structure at various levels (e.g. Dame et al. 2001). These maps are essential to calculating accurate distances to objects (see Section 1.1.1.1) and the molecular component has long been known to have a strong correlation with areas associated with star formation (e.g. Talbot 1980; Wong and Blitz 2002; Heyer and Brunt 2004; Gao and Solomon 2004; Krumholz

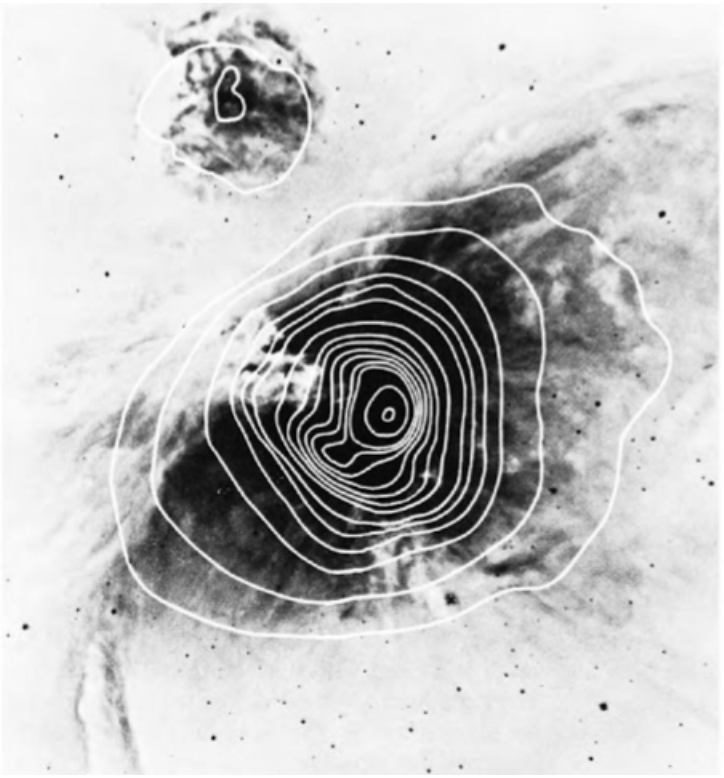

FIGURE 1.2: The Orion Nebula H II region. The white contours are representative of 1.3 cm radio continuum emission. These are overlaid on a negatively coloured optical Hα photograph which illustrates the effect of extinction by dust in the region. The contours are centred on the YSOs where star formation is known to be occurring. Figure from Wilson and Pauls 1984.

and Bonnell 2007; Krumholz and Matzner 2009; Kennicutt et al. 2007; Bigiel et al. 2008, 2011; Gnedin et al. 2010; Schruba et al. 2011; Rahman et al. 2011). This agrees with the trend seen in Figure 1.1 as the surface density of H_2 declines quickly after $R_{GC} \sim 8.5$ kpc. Multiple works (e.g. Braine et al. 2001; Wong and Blitz 2002; Bigiel et al. 2008, 2011; Genzel et al. 2010) have shown that the star formation rate is inherently linked with the amount of molecular gas present. Bolatto et al. 2011 have calculated that the relation between star formation rate and neutral gas surface density is steep with a power-law index of $\sim 2.2 \pm 0.1$. This value is similar to that observed in the outer disks of other large spiral galaxies. Further details on Galactic star formation rates will be discussed in Section 1.5.

Finally, interstellar hydrogen also exists in an ionised form with much of it being concentrated around H II regions that surround individual O and B stars. These regions originate around developing massive young protostars and will be the main focus in subsequent chapters of this dissertation as they can be excellent tracers of the early stages of massive star formation. A well known example of an H II region is the Orion Nebula shown in Figure 1.2 as presented by Wilson and Pauls 1984. The image shows 1.3 cm radio continuum contours overlaid on the negative

Hα optical photograph. The radio emission is much more symmetrical than the optical data which is subject to dust extinction. Observations can detect H II regions like those found in the Orion Nebula across the Galactic plane and sum the flux found over the radio peaks to obtain the total H II surface density (see Figure 1.1; short dashed lines). Similar to H_2, H II peaks around a galactocentric radius of 5 kpc, yielding further evidence of the relationship between molecular gas and star formation. Both the ionised and molecular gas also decease drastically between 8 and 12 kpc with very little material evident in the Outer Galaxy.

The presence of a massive star will yield photon energies that exceed 13.6 eV, producing hydrogen recombination line emission or Lyman continuum radiation. The radiation ionises a spherical area up to several parsecs across. In addition to the Lyman series, other hydrogen recombination lines are produced when the excited election falls from a higher state to $n = 2$, producing nanometer to centimetre range wavelengths that are visible in both the optical and radio spectrums, with radio allowing for observations to be made for H II regions over large distances.

Additionally, free elections within the H II regions may collide with other atoms present in trace amounts, exciting electrons associated with these heavier elements (metals; or all elements beyond hydrogen and helium) which later decay back to the ground state and generate forbidden lines. In general, the stronger these forbidden lines, the higher the metallicity (i.e. the respective abundance of elements heavier than hydrogen and helium) of the surrounding gas using the standard comparison of the solar composition, or the elemental distribution found in the solar photosphere. Metals located in H II regions will have significantly lower abundances than those found in the solar standard. In general, the metallicity of the ISM is expected to decrease as one moves away from the Galactic centre, as the amount of molecular and ionised gas decreases and there is less star formation to enrich the local medium (e.g. Elia et al. 2013, 2017; König et al. 2017). From this concept, we can define a value called the mean molecular weight μ. This quantity represents the average mass of a particle of gas relative to the hydrogen mass, m_H, and may be used to define the number density of particles in a gas with mass density ρ as,

$$n_{tot} = \frac{\rho}{\mu\, m_H} \tag{1.2}$$

The mean molecular weight in the ionised hydrogen regions will be of use for calculating the properties of the compact and ultracompact H II regions that host massive star formation later on

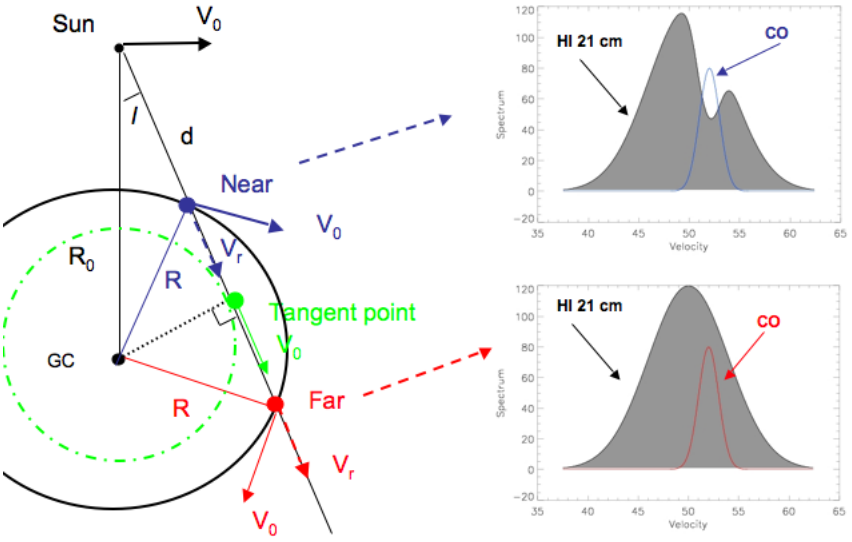

FIGURE 1.3: An illustration of the Kinematic Distance Ambiguity as given by Roman-Duval et al. 2009. For an observation of a source at some angle, there are two distance solutions that could be appropriate. Observations of a source at the far distance point (red), when observed through a molecular cloud along the line of sight, will show emission lines Doppler shifted such that the cloud's velocity will be measured to be up to and including the source's tangent point velocity. At the near distance point (blue), the measured cloud velocity will be less than the source's radial velocity.

in Chapter 4.

1.1.1.1 A Note on Distance Derivations

Distances are key when attempting to estimate flux and luminosity properties for various objects. The most accurate distances come from parallax and spectroscopic studies (e.g. Urquhart et al. 2013a,b, 2014c) but are restricted to objects that are relatively close to the sun. For objects further than a few hundred parsecs, kinematic distances must be derived. Radial velocities of the chosen source must be obtained and combined along with a Galactic rotation model to determine the appropriate distance. The most commonly used Galactic model is that of Brand and Blitz 1993 where v_0 =220 km/s and R_0 = 8.5 kpc, with v_0 being the circular rotation speed and R_0 is the sun's distance to the Galactic centre. This is a straight forward calculation for the Outer Galaxy but care must be taken for sources within the solar circle due to the near-far Kinematic Distance Ambiguity (KDA). For such objects, there will be two possible distance solutions that are equally spaced on either side of the tangent position known as the near and far distances (refer to Figure 1.3). To resolve the KDA, additional observations of the object's absorption spectra will be required. This technique was first used by Wilson 1972 who observed the $1_{11} \rightarrow 1_{10}$

transition line of formaldehyde toward 73 Galactic H II regions. However, the more reliably ubiquitous absorber of H_1 (recall the high surface density across galactocentric radii as shown in Figure 5.1) has since been adopted. If an interstellar H_1 cloud exists between the source and the observer, then 21 cm line may be used (Kuchar and Bania, 1994). Emission from the original source will be absorbed by the intervening cloud, yielding a Doppler shift according to the radial motion of the cloud. For sources at the far kinematic distance (red), the observed Doppler shift can yield velocities up to and including the tangent point velocity. For sources at the near distance (blue), the maximum radial velocity detected must be less than the radial velocity of the source. This technique of determining the maximum radial velocity of the absorption spectrum allows astronomers to differentiate between the near or far distance provided that the source's velocity is known and that there are several absorbing interstellar clouds along the line of sight (Kolpak et al., 2003). Typically, radial velocities will have an assumed error of ±10 km/s due to streaming motions (Reid et al., 2009) corresponding to a kinematic distance uncertainty of $\sim 0.6 - 1$ kpc.

1.1.2 Interstellar Dust

Dust grains make up less than 1% of the total mass of the interstellar medium (Boulanger et al., 2001), and yet, their presence can be a frustration as they absorb surrounding radiation to produce reddening and extinction effects. Dust grains will absorb and scatter photons at short wavelengths and re-radiate them at longer wavelengths. Reddening may cause observed stars to be mistaken for later spectral types, incorrectly assigning them too small luminosities or placing them at inappropriately large distances. A summary of how dust can impact observations is shown in Figure 1.4 as presented by Chiang and Ménard 2018. The arrow shows the expected shift in wavelength when temperature or redshift is varied. All wavelengths and frequencies will be affected by dust to some degree and thus it is important to understand the emission produced by dust when heated by stellar radiation.

Any radiation field may be described by its specific intensity I_ν which is defined such that $I_\nu \Delta\nu \Delta\mathcal{A} \Delta\Omega$ is the energy per unit time with frequency between ν and $\nu + \Delta\nu$ that propagates perpendicular to the area $\Delta\mathcal{A}$ within solid angle $\Delta\Omega$. Therefore, we may define the total energy density per unit frequency at a fixed location as,

$$u_\nu \equiv \frac{1}{c} \int I_\nu \, d\Omega \tag{1.3}$$

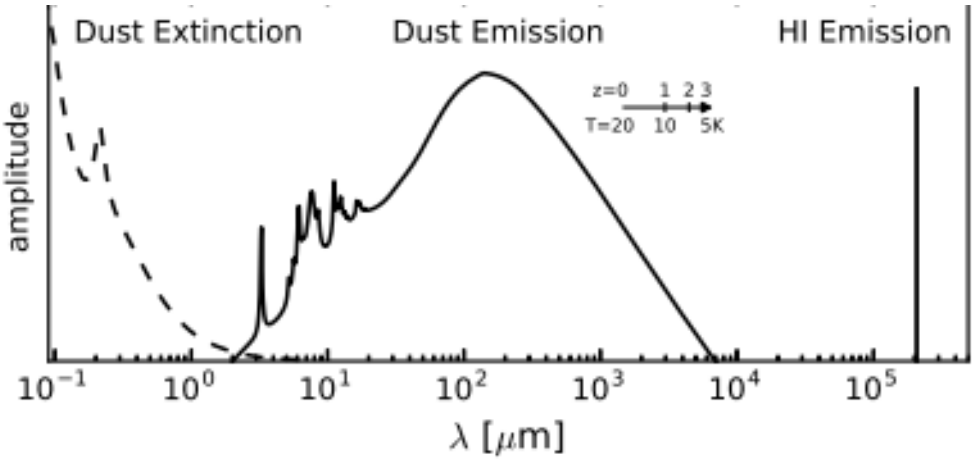

FIGURE 1.4: The impact of dust emission (solid line; Weingartner and Draine 2001) and extinction (dashed line; Draine et al. 2007) as a function of wavelength as presented by Chiang and Ménard 2018. The delta function of the hydrogen 21 cm emission is also shown. An arrow is drawn to show the expected shift in wavelength when emission temperature or redshift is varied.

where c is the speed of light.

Next, we consider the concept of a blackbody which is an idealised body that absorbs all incident radiation, regardless of frequency or angle of incidence. Furthermore, a blackbody will emit radiation in the same manner and will do so isotropically according to Planck's law where only T has any impact in the resulting emission spectrum.

Planck's law can be expressed by imagining a box that surrounds a portion of the interstellar medium and whose walls are maintained at a constant temperature, T. In these conditions, thermal equilibrium has been established and the radiation energy density is given as

$$u_\nu = \frac{8\pi h\nu^3/c^3}{\exp(h\nu/k_B T) - 1} \tag{1.4}$$

Because the radiation will be isotropic with the specific intensity I_ν direction-independent, we may refer back to equation 1.3 and solve the integral to find,

$$u_\nu \equiv \frac{4\pi}{c} B_\nu \tag{1.5}$$

where we have substituted B_ν for I_ν for the case of a blackbody with SI units of W sr^{-1} m^{-2} Hz^{-1}. This may be plugged into the left side of equation 1.4 and solved for B_ν which must be a

function of temperature T to find,

$$B_\nu(T) = \frac{2\pi h\nu^3/c^2}{\exp(h\nu/k_B T) - 1} \tag{1.6}$$

Dust grains are not perfect blackbodies but rather they are considered "quasi-blackbody-like" or "grey-bodies" and radiate instead as modified blackbodies with wavelength/frequency dependent emissivity (measure of ability to emit radiation) of less than one, especially for the submillimetre region. This dust opacity for long wavelengths is usually given as a power law $\kappa \propto \nu^\beta$ (Hildebrand, 1983) with $\beta = 1 - 2$. In Chapter 4, it will be beneficial to convert B_ν into Janskys using 1 Jy = 10^{-26} W m^{-2} Hz^{-1}. Initially, the amount of dust material compared to gas mass was thought to be around a factor of 100 and was referred to as the gas-to-dust ratio R (Draine et al., 2007). It has continued to be used throughout the literature for calculating various properties of molecular clumps within the ISM in an attempt to compensate for the amount of reddening and extinction that may be present in observations. More recently, it was confirmed that R is correlated with metallicity which is known to vary across the Galactic plane (e.g. Elia et al. 2013, 2017; König et al. 2017). Observations of the Galactic chemical evolution of dust support this connection and propose that R should increase with decreasing metallicity (Dwek, 1998; Mattsson and Andersen, 2012; Hirashita and Harada, 2017). The same correlation was also observed for disks of nearby galaxies (Sandstrom et al., 2013). Twarog et al. 1997 analysed a sample of open clusters and found that the Galactic metallicity gradient can be described via two zones, an Inner and an Outer, separated by a step-like discontinuity around the position of the solar circle ($R_{\rm GC} \sim 8.5$ kpc). Thus, the Outer Galactic regions ($R_{\rm GC} > 8.5$ kpc) will have systematically lower metallicities and higher gas-to-dust ratios compared to the Inner Galaxy. Lépine et al. 2011 and Eden et al. 2012 further suggested that the variation may be caused by entry shocks of material at the co-rotation radius, confirming the boundary and a shift in environmental conditions at the position of the solar circle. Giannetti et al. 2017 used observations of the optically thin C^{18}O(2-1) transition for 23 massive and dense star-forming regions at $R_{\rm GC} > 14$ kpc to determine the approximate gradient by which R increased as a function of $R_{\rm GC}$ (see Figure 1.5). They determined that the gas-to-dust ratio was dependent on radius, increasing via[1]:

$$\log(R) = \left(0.087^{+0.045}_{-0.025} \pm 0.007\right) R_{\rm GC} + \left(1.44^{-0.45}_{+0.21} \pm 0.03\right) \tag{1.7}$$

[1]In the original paper, Giannetti's equation uses γ instead of R. We have rewritten the formula here to remain consistent with our nomenclature.

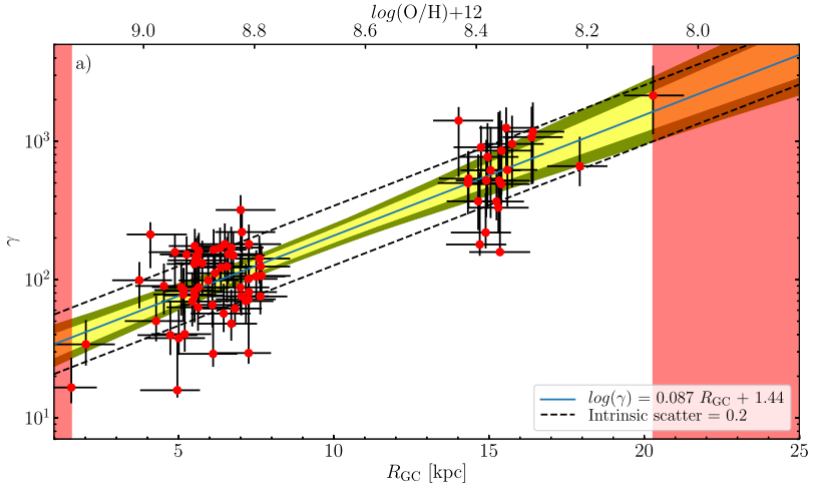

FIGURE 1.5: Observations of the $C^{18}O$(2-1) transition for 23 massive and dense star forming regions (Giannetti et al., 2017) for the Galactic gas-to-dust ratio as a function of R_{GC}. The derived law is shown in the lower right corner of the plot. Note that the value γ shown here is equivalent to our value R seen throughout the work of this text.

Equations 1.4, 1.6, and 1.7 will be vital in the following chapters to understand the environments of compact H II regions. Both Planck's formula and the equation for blackbody radiation are suitable for the conditions found within the molecular clouds that serve as the stellar nurseries for star formation.

1.2 An Introduction to Star Formation

The earliest stages of star formation occur while the young stellar object (YSO) is still deeply embedded within a dense cloud of dust and gas (Garay et al., 2004). These clouds range in size from the smallest Bok Globules ($n_{\text{cloud}} < 10^4\,\text{cm}^{-3}$, size $< 0.1\,\text{pc}$, $M_{\text{cloud}} < 10\,M_\odot$, $T < 10\,\text{K}$) to giant molecular clouds or GMCs ($n_{\text{cloud}} > 10^2\,\text{cm}^{-2}$, size $> 50\,\text{pc}$, $M_{\text{cloud}} > 10^5\,M_\odot$, $T > 15\,\text{K}$) (Stahler and Palla, 2004). For the purposes of this dissertation, we will refer to the clumpy substructures within these clouds as molecular clumps that describe the regions where the fragmented collapses occur and eventually lead to star formation. These clumps will have parsec-scale diameters that are significantly smaller than the hundreds of parsecs across for molecular clouds. They will also be much more dense in comparison.

Shu et al. 1987 describes the 'standard theory of star formation' as when stars are formed via an 'inside-out collapse' of a singular isothermal sphere. Star formation begins when the molecular system starts to fragment and the resulting cores will continue to collapse under their own gravity.

Before this occurs, however, the system (which may also describe a cloud collapsing into a clump, or a clump to a fragment, or a fragment mass/core into a star, etc) is in a state of hydrostatic equilibrium. At first, there is neither expansion nor collapse as the overall inward and outward forces balance out. Once some event triggers the initial collapse, we are able to describe the process via a simple equation of motion.

If we assume that there is a spherically symmetrical system with mass M and radius R, then we may focus on a thin shell of material that may be defined to be distance r away from the centre. The shell will be of infinitesimal thickness dr and the gas density within is ρ. It follows that the mass of the shell will be $dm = 4\pi r^2 \rho\, dr$. The shell will be subject to two primary forces with the first being gravity. Let m be the mass of the material inside of the shell or interior to radius r. Then $\rho\, dr$ is the mass of the shell per the cross sectional area. According to Newton's law, the gravitational force per unit area on the shell becomes,

$$F_g = -\frac{Gm}{r^2}\rho\, dr \tag{1.8}$$

where G is Newton's gravitational constant and the minus sign indicates that the direction of the force is towards the centre of the cloud.

The second force acting on the shell of material will be gas pressure. We are assuming that in this situation some net gas pressure exists that is opposite in direction to the force of gravity. The pressure may vary depending on the position chosen within the molecular cloud. If the pressure at the interior part of the shell is $P(r)$ (with direction away from the centre) and the pressure at the top of it is $P(r + dr)$ (with direction towards the centre), then the net pressure force per unit area that the shell feels is,

$$F_p = P(r) - P(r + dr) \tag{1.9}$$

In the limit that $dr \to 0$, the net pressure per unit area may be written as,

$$\frac{dP}{dr} = \lim_{dr \to 0} \frac{P(r + dr) - P(r)}{dr} \tag{1.10}$$

Subbing into equation 1.9 gives,

$$F_p = -\frac{dP}{dr}dr \tag{1.11}$$

Now, according to Newton's second law, $F_{tot} = ma$ and with the shell's mass per unit area being $\rho\, dr$, then we have,

$$(\rho\, dr)\,\ddot{r} = -\left(\frac{G\rho m}{r^2} + \frac{dP}{dr}\right) dr \tag{1.12}$$

$$\ddot{r} = -\frac{Gm}{r^2} - \frac{1}{\rho}\frac{dP}{dr} \tag{1.13}$$

Equation 1.13 gives the equation of motion that tells us how the mass shell accelerates in response to the forces acting on it. Hydrostatic equilibrium is defined as when the opposing forces are equal, thus making the acceleration zero ($\ddot{r} = 0$). Also, we can expand the shell to include the whole mass M of the cloud (or a star) with full radius R. Rearranging equation 1.13 yields the more common form of hydrostatic equilibrium,

$$\frac{1}{\rho}\frac{dP}{dr} = -\frac{GM}{R^2} \tag{1.14}$$

In order for gravity to overcome the gas pressure and allow fragmentation to occur, the affected region within the system must reach some critical mass and density. This is typically the result of some perturbation which compresses the cloud, increasing the local gas density by a relative amount. The perturbation is likely caused by outside forces or nearby objects that are capable of interacting with the surrounding environment to trigger local star formation (e.g. Roberts 1969; Sanders 1986; Springel et al. 2005). Events such as a nearby supernova will trigger a shockwave that travels through the interstellar medium affecting the local gas density. In an environment with spherical symmetry acted upon by outside forces such that the local gas density will temporarily increase, the critical mass, or Jeans mass, as a such that gravity dominates may be given by,

$$M_J \equiv \frac{4\pi}{3}\rho\lambda_J^3 \tag{1.15}$$

where ρ is the original density of the gas (before the shockwave) and λ_J is the necessary perturbation length or Jean's length. This value relates to the compression factor of the gas which in turn increases the local density to the critical amount. The Jean's length may be written as,

$$\lambda_J = \left(\frac{5 k_B T}{2\pi(\gamma - 1)\mu m_H \rho G} \right)^{\frac{1}{2}} \tag{1.16}$$

where k_B is Boltzman's constant, T is the gas temperature, μ is the mean molecular weight as discussed earlier ($\mu = 1$ for pure neutral hydrogen; $\mu = 0.5$ for fully ionised hydrogen), m_H is the hydrogen mass, and G is the gravitational constant.

Inside a molecular clump and after reaching the critical Jeans mass that will tip the scales of hydrostatic equilibrium, a young stellar object (YSO) begins to coalesce within the core, accumulating matter at a well defined rate. This rate can be calculated via the free-fall time.

The free-fall time is defined as the timescale for the collapse if gravity was the sole force involved. From Shu et al. 1987,

$$t_{ff} = \left(\frac{3\pi}{32 G \rho} \right)^{\frac{1}{2}} = (3.4 \text{ x } 10^7) n^{-\frac{1}{2}} \text{ [yr]} \tag{1.17}$$

with G and ρ as defined previously and n as the number density. Typical values suggest $n \geq 50$ cm^{-3} resulting in a limit of $t_{ff} \leq 5$ x 10^6 yrs (Shu et al., 1987).

In the general model of star formation, the YSO continues to grow in mass as more and more material falls onto it. Its rotation increases with mass, eventually forcing the collapse outwards and creating a more slowly rotating extended spherical envelope. Matter from the envelope falls onto the growing protostar and heats it. When the protostar reaches a temperature of approximately 2000 K, the H_2 dissociates into atomic form. The protostar continues to acquire mass from the surrounding envelope, spinning more and more rapidly. Conservation of angular momentum results in the in-falling material being forced into a circumstellar disk. While it is in the process of collapsing, the protostar is called a T-Tauri star. These are pre-main-sequence stars that are less than ten million years old. T-Tauri stars will continue to evolve along their respective Hyashi tracks which are dictated by their initial mass and luminosity (see Figure 1.6) and highlight the path the star will travel before arriving on the main sequence. When the

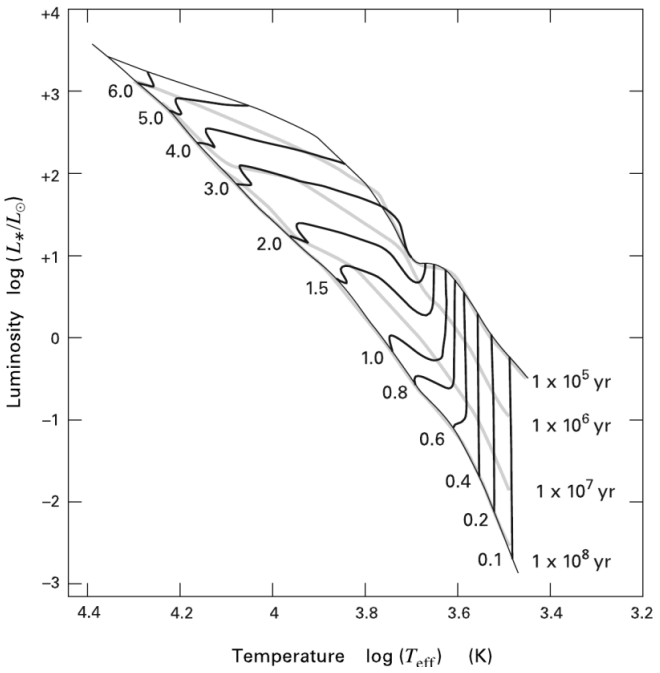

FIGURE 1.6: The various Hayashi Tracks or pre-main sequence paths that a star can take to reach the main sequence depending on its initial mass. The numbers listed on the right give an approximation of the time it takes for the protostar to reach the main sequence. (Stahler and Palla, 2004).

inner temperature of the core reaches 10^6 K, hydrogen burning begins, hydrostatic equilibrium is restored via the radiation pressure emitted by nuclear fusion and the star reaches the main sequence. Any remaining material in the envelope of the star is either accreted or dispersed by bipolar outflows and stellar winds in an effort to remove excess angular momentum from the system. The disks will likewise either disperse or themselves fragment into smaller bodies forming the basis for primordial solar systems.

1.3 The Problems with Massive Star Formation

A star's early evolutionary processes can easily be traced on a traditional Hertzsprung-Russell (HR) diagram. An HR diagram traditionally shows a scatter plot of stars illustrating the relationship between their spectral type or effective temperature versus their absolute magnitude or luminosity. Different regions of the diagram will be populated by different groups of stars depending on their current age and initial properties. A single star will move around the plot as it ages. Figure 1.7 shows the path for an average 1 $M_\odot$ star as it moves along the pre-main sequence to the main sequence. When it is no longer able to sustain itself through nuclear fusion

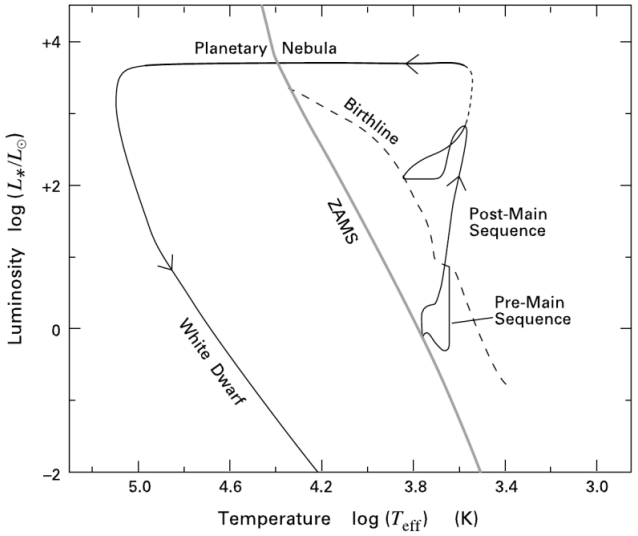

FIGURE 1.7: The path of a $1\,M_\odot$ star across the Hertzsprung-Russell diagram as it evolves. A protostellar object forms on the birthline and begins to accrete mass. Eventually, nuclear fusion begins in the core and hydrostatic equilibrium is restored. The star arrives on the main sequence, in this case, on the zero age main sequence line. The star goes through a series of expansions and contractions as fuel is depleted and equilibrium becomes harder to maintain. Eventually, the star throws off its outer layers in a rapid expansion and reaches the planetary nebula stage. These layers drift away and the star contracts into a white dwarf where electron degeneracy pressure is enough to counteract the force of gravity. (Stahler and Palla, 2004)

at the core, it will transition onto the red giant branch where hydrogen burning is happening in the outer shell. The next phase occurs when the core begins burning helium and the star moves to the horizontal branch. Eventually, layers of shell burning develop and the star evolves onto the asymptotic giant branch. A temperature gradient develops pushing the outer layers of the star out to larger radii. Eventually, all fusion ceases, the outer layers are blown off as the core collapses and finally ends as a white dwarf which is held up against its own gravity by electron degeneracy pressure. However, stars of varying initial masses will follow different evolutionary processes and their paths across the HR diagram may look very different particularly during the beginning and end of their lifetimes. As seen from Figure 1.6, the more massive stars have higher luminosities and temperatures than their lower mass counterparts, shifting up towards the top left corner of the diagram. They will also burn through their supply of hydrogen much more quickly, leaving the MS long before stars of lower mass. Stellar formation and evolution is usually discussed in terms of three distinct mass categories – low mass stars ($0.1 \leq M_* < 2M_\odot$), intermediate mass stars ($2 \leq M_* \leq 8M_\odot$), and massive stars ($M_* > 8M_\odot$) (Martins, 1996).

A measure of the evolution of a protostar to its arrival on the main sequence can be given by a timescale that defines the amount of time needed for the interior of a given star with mass

M_* to reach the required core temperatures sufficient for nuclear fusion. This is known as the Kelvin-Helmholtz timescale,

$$t_{KH} \approx \frac{GM_*^2}{R_* L_*} \text{ [yr]} \tag{1.18}$$

where R_* is the stellar radius and L_* is the stellar luminosity.

For most low to intermediate mass stars, we find that $t_{KH} > t_{ff}$ and these stars have finished their accretion phase by the time they reach the main sequence. However, for a typical massive OB star with an average mass around 40 $M_\odot$, then $t_{KH} \approx 5$ x 10^4 years and $t_{KH} < t_{ff}$, implying that massive stars can continue to accrete matter even after they have reached the main sequence and begin hydrogen burning (e.g. Kuiper et al. 2010). A major question is how the gravitational collapse is able to continue despite the resulting radiation pressure that should theoretically halt or slow it (Davies et al., 2011; Wolfire and Cassinelli, 1987). Despite this, we have observed stars of close to 150 $M_\odot$ (implying starting masses near ~300 $M_\odot$; Crowther et al. 2010). How are such stars possible?

There are currently three leading theories for the possible formation of massive stars. The first model was put forward by Shu et al. (1987) and essentially follows a scaled-up version of the inside-out theory. The 'monolithic collapse model' suggests that when the MYSO reaches the initial accretion phase, the resulting circumstellar disk continues to supply material to the protostar but at much faster rates than in the low mass model. This would imply that massive cores directly evolve into massive stars (McKee and Tan, 2003). Limitations to this model include the plausibility of high enough accretion rates over the relatively short timescales involved (e.g. 10^{-3} $M_\odot$ yr^{-1} over 10^5 yr; McKee and Tan 2003) which do not take into account feedback in the form of radiation pressure that may limit the mass accumulation as soon as as M_* reaches roughly 10 $M_\odot$, and also the low likelihood of massive molecular cores collapsing into a single star without fragmenting (Bonnell et al., 2004).

The 'competitive accretion model' proposed by Bonnell et al. 1997 derives from the observation that most massive stars seem to form within clusters. Stellar cores form within a molecular cloud and compete for accretion material from the surrounding reservoir of gas. The most massive stars tend to be found at the centres of these clusters where most of the gas and dust supply are also found, leading to mass segregation. Therefore the protostar's position within the cluster will dictate its final mass (Bonnell et al., 2004). However, it is possible that mass segregation is

only an observational effect. Our view of such clusters may be incomplete due to overcrowding towards the core and our assumption skewed by thinking that all clusters are mass segregated (Ascenso et al., 2009).

The final model for massive star formation relies on stellar mergers (Bonnell et al., 1998). The 'mergers model' relates to competitive accretion by suggesting that collisions between massive stars may be occurring within the densest regions of star forming clusters to form even more massive stars. However, this model assumes that massive stars already exist within the cluster and in such numbers that the necessary collisions are likely to occur at a high rate. There has been no observational evidence to support such high density populations and this particular theory has been largely discredited (Zinnecker and Yorke (2007)).

Current studies (e.g. Tan et al. 2014; Zinnecker and Yorke 2007; Benincasa et al. 2019; Barnes et al. 2019; Fujita et al. 2019) suggest that the most realistic model is most likely to involve components of both monolithic collapse and competitive accretion. Hindering any theory, is the fact that massive star formation is rare. This rarity means that detected massive stars tend to be at large distances and thus require high angular resolutions in order to study them at any point in their evolutionary process. We can see the origins of their scarcity by examining the Initial Mass Function (IMF).

The IMF is an equation that attempts to define the distribution of stellar masses formed in a particular cloud. It is generally understood that there will be some variation according to local environmental conditions but the IMF also seeks to quantify the reason that massive stars are so much more rare than their lower mass counterparts. Salpeter 1955 was the first to show that the number of stars for a certain mass interval can be approximated by a power law such that,

$$\xi(M_*) \sim (M_*/M_\odot)^{-\alpha} \tag{1.19}$$

where $\alpha \approx 2.35$ and is known as the Salpeter value for stars with $0.4 < M_*/M_\odot < 10$. Later studies adjusted the value of α for different mass values based on observations, leading to the currently accepted form as presented in investigations such as Kroupa 2002 and Chabrier 2003,

$$\xi(m) = C\,(M_*/M_\odot)^{-1.2} \;\rightarrow\; 0.1 < M_*/M_\odot < 1.0 \tag{1.20}$$

$$\xi(m) = C\,(M_*/M_\odot)^{-2.7} \;\rightarrow\; 1.0 \leq M_*/M_\odot < 10 \tag{1.21}$$

$$\xi(m) = C\,(M_*/M_\odot)^{-2.3} \;\rightarrow\; 10 < M_*/M_\odot \tag{1.22}$$

with C some constant that is unique for each mass interval and determined by observational results. When these equations are applied to the approximate volume of the solar neighbourhood, we find that roughly half of all stars produced will have $M_* \geq 0.2\,\mathrm{M}_\odot$, only 12% have $M_* \geq 1.0\,\mathrm{M}_\odot$, and 0.3% with $M_* \geq 10\,\mathrm{M}_\odot$.

Though we still do not fully understand the theory behind massive star formation, there are certain tracers we have found to detect regions of massive star formation. Studying the properties and local environments of these may help us to peel back the obscuring layers and understand the physical processes that are occurring underneath.

1.4 Tracing Massive Star Formation via Compact H II Regions

Massive star formation is difficult to observe directly as the actual sites of massive star formation are deeply embedded within molecular cloud cores that are themselves surrounded by thick layers of dust. Direct observation attempts can suffer from visual extinctions of greater than 100 magnitudes (Bally and Zinnecker, 2005). They evolve very quickly with lifetimes of up to $10^6 - 10^7$ years and much of this time is spent embedded within the H II region. Fortunately, these stars have a noticeable effect on their surrounding environments, particularly in the radio and infrared regimes (Menten et al., 2005; van der Tak and Menten, 2005). For the scope of this dissertation, I will focus on one of the most prominent tracers that indicates either ongoing or recent massive star formation - the compact H II regions.

Compact H II regions show up as bubbles of ionised molecular gas within a clump as a direct result of massive star formation occurring within their depths (Wood and Churchwell, 1989). Their strong emission in the radio thermal continuum and far-infrared make H II regions a valuable tool for tracing Galactic massive star formation (Wood and Churchwell, 1989; Kurtz et al., 2016; Walsh et al., 1998). They are the precursors to the more widely known extended H II regions like the Orion Nebula as discussed in Section 1.1. Recall that an H II region is formed when a YSO reaches sufficient temperature to emit UV-radiation, ionising the surrounding gas and producing

a small ultra-compact region (UC; diameter, $d < 0.1$ pc) of photoionised hydrogen within the host molecular clump. As the YSO evolves, its UV output increases, expanding the boundaries of the H II region so that it may now be defined as compact ($d < 0.5$ pc), classical ($d \sim 10$ pc), or extended ($d > 10$ pc) (Kurtz, 2005). The surrounding dust grains are heated and become visible in the far-infrared. The initial production of Lyman photons causes the H II region to rapidly expand and then slow as the ionisation front moves through the ISM. At some point the rate of ionisation is balanced by the rate of recombination and the expansion stops. As the number of ionising photons emitted increases, so does the temperature. A pressure gradient develops between the hot ionised gas and the surrounding cool ISM, driving another expansion of the H II region. A Lyman continuum flux may be derived from the free-free or Bremsstrahlung emission emitted by the hydrogen that directly correlates with the YSO's observed luminosity.

For this work, we focus on the compact and ultracompact H II regions (hereafter, UC H II regions). The advantage of UC H II regions is that they are the most visible manifestation of recent star formation ($\sim 10^5$ yrs; Kurtz et al. (2000)). Direct radio observations are able to give estimates of the luminosities of the corresponding embedded stellar object. Because of this, many studies have attempted to catalogue the number of UC H II regions in the Milky Way in order to trace Galactic star formation. Early catalogues of H II regions selected candidates based on their mid- or far-infrared colours (e.g. Wood and Churchwell 1989; Kurtz et al. 2016; Walsh et al. 1998). However, this method also identified other infrared-bright objects such as planetary nebulae and intermediate mass YSOs, leading to confusion in the catalogues and bias in any derived models (Ramesh and Sridharan, 1997). The rise of wide area radio surveys prompted a new wave of attempts to separate the similarly-coloured sources through multi-wavelength inspection (Becker et al., 1990; Zoonematkermani et al., 1990; Becker et al., 1994; Giveon et al., 2005; Murphy et al., 2010; Hindson et al., 2012) but many of these were carried out in snapshot mode, limiting UV-coverage and causing some H II regions to be falsely identified as bright compact components of more extended emission (Kurtz et al., 2000; Kim and Koo, 2000; Ellingsen et al., 2005).

With the completion of latter surveys such as CORNISH (Hoare et al., 2012) and the RMS catalogue (Lumsden et al., 2002), there has been significant progress in creating a reliable model for confirming and identifying bona-fide UC H II regions. Urquhart et al. 2013b was one of the first to utilize this method which follows a multi-wavelength approach and cross-references images from submillimetre, radio, and far- to mid-infrared datasets to look for key features expected in UC H II regions. The regions could be recognised from the coincidence of the submillimetre and radio contours embedded in regions of strong dust emission and if they met three primary

criteria: (1) they should have radio spectra consistent with thermal free-free continuum, (2) they are clearly associated with thermal infrared emission from the heated dust within the ionised nebula, and (3) they show signs of being embedded within the molecular clump. With additional new surveys becoming available in previously uncharted regions of the Milky Way (e.g. SASSy; Thompson et al. 2007; see Chapter 3), the multi-wavelength method for confirming H II regions gives a highly reliable and straightforward approach for mapping and identifying regions of massive star formation across the Galactic plane.

1.5 Star Formation on Galactic Scales

A significant population of massive stars can impact the physical and chemical structure of a whole galaxy (Kennicutt, 2005; Zinnecker and Yorke, 2007). Massive stars dominate the total observed flux and luminosity of a galaxy. On a smaller scale, they have significant impact on their local environments due to strong outflows, stellar winds, optical/UV-radiation, and eventual supernova explosions, affecting the surrounding supply of molecular gas and potentially triggering or quenching any nearby star formation.

Krumholz and Bonnell 2007 was the first to point out that even a $1\,M_\odot$ star accreting at the relatively high rates (with initial peak values at an order of magnitude around $10^4\,M_\odot\,yr^{-1}$; Smith 2014) expected for the dense environments where massive star formation is likely to occur, could generate strong enough radiation to raise the surrounding gas temperature by a few Kelvin at distances of up to ~1000 AU. The ability of the surrounding gas to fragment and begin to collapse into prestellar objects is dependent on this "fragment mass" being roughly the same as the Jeans' mass. As seen in equations 1.15 and 1.16, M_J will vary with the gas temperature as $\sim T^{3/2}$. Thus, this effect will raise the minimum mass required in order for the surrounding gas to also fragment and begin star formation. Additional radiation-hydrodynamic simulations (e.g. Krumholz and Bonnell 2007; Krumholz et al. 2011) confirm this result. Galactic evolutionary models that ignore feedback will disagree with real world observations and will likely form stars too early since the surrounding temperatures of the ISM are not being adjusted as necessary. Information from accurate observations may be fed back into such simulations in order to best understand the properties of these massive stars and how they interact with their local environment. The conditions of the local interstellar medium that will most affect star formation are metallicity and the gas-to-dust ratio. These factors must be taken into account when deriving and tracing any trends in massive star formation within a host galaxy. Understanding how massive stars form,

especially the rate and efficiency of that formation as a function of R_{GC} to account for changing environmental conditions, is essential to calculating the impact and evolution of these feedback events.

Attempts to compile such a diverse sample include the all-sky WISE-based catalogue from Anderson et al. 2014 in conjunction with the ongoing Galactic H II Region Discovery Survey (HRDS; Bania et al. 2010). The catalogue consists of over 8,000 Galactic H II regions and H II region candidates selected via their characteristic mid-infrared morphologies with the HRDS used to follow up on candidate sources to detect hydrogen radio recombination lines and to confirm their status as a bona-fide H II region. However, the catalogue focuses on later-stage H II regions or those that we consider to be extended or classical regions. HRDS uses the Green Bank Telescope (GBT) which has a FWHM beam size of 82″ at 9 GHz (3 cm). This is too large to accurately sample and identify the UC H II regions with expected sizes of approximately 1.5-20″ and is not sufficient for our purposes of tracing recent massive star formation via these more compact sources. Other WISE-based studies continue to use infrared colour selection methods (e.g. Marton et al. 2016; Izumi et al. 2017) but remain similarly sensitive to resolution and colour selection issues. Additional attempts that use partial pre-existing H II region catalogues (e.g. Eden et al. 2015; Vutisalchavakul et al. 2016) suffer from the same problems as earlier infrared-based catalogues, including false sources and having large uncertainties. Few of these studies show a sample that provides complete Galactic coverage for larger values of R_{GC}. Ragan et al. 2016 presented a star forming fraction (SFF) derived from Hi-GAL data at 70 μm to show this value as a proxy for the massive star formation rate. They derived a decreasing trend with R_{GC} at a rate of 0.026 ± 0.002 per kpc, but only for a limited range in the Inner Galaxy of $3.1 - 8.6$ kpc. Ragan et al. 2016 labelled this result somewhat surprising given the dense gas mass fraction having been observed to be constant in the Inner Galaxy and suggested that the SFF may be weakly dependent on one or more large-scale physical properties of the Galaxy, such as metallicity, pressure or other internal properties that the molecular clouds may have inherited from their environment. This reinforces our conviction that massive star formation requires further investigation in the Outer Galaxy local conditions. Wouterloot et al. 1988 attempted to push the search for UC H II regions to $R_{GC} = 14 - 20$ kpc using a set of defined far-infrared colour criteria to select likely IRAS candidates and search for H_2O masers (another tracer of star formation); however, with a beam size of 4.7′ at 100 μm, the IRAS catalogue has too much confusion to identify and classify such compact objects with any significant level of confidence (Neugebauer et al., 1984).

The most massive stars will account for the majority of a galaxy's observed luminosity and they contribute significant feedback and enrichment processes to their surrounding environment as discussed earlier. Any galactic evolution model requires an accurate star formation rate that can properly account for these processes. It must also take into account the effects of low and intermediate mass stars which form the bulk of the galaxy's mass but are harder to detect. This is where a reliable IMF becomes critical for examining the effects of various stellar populations on the overall galactic star formation. The Milky Way becomes an ideal landscape for studying the earliest stages of massive star formation due to its uniquely high resolution observations of individual star forming regions across the Galactic plane which are often difficult to fully resolve in other nearby galaxies and almost impossible for those with higher redshift, even with the capabilities of modern telescopes such as ALMA (Longmore et al., 2014). The high-resolution data from various Galactic based surveys can provide a template for use in calibrating evolutionary models (e.g. Bolatto et al. 2008; Kruijssen and Longmore 2013). Longmore et al. 2015 showed that the environments of stars in massive stellar clusters are analogous to those of stars forming in galaxies with redshift of $z = 1 - 3$. The key parameters (e.g. gas pressure, surface density, and velocity dispersion) were also found to have similar values in both settings. Local conditions will determine the local star formation rates (SFR) and efficiencies (SFE) which can later be applied to extragalactic models to better match observations.

Schmidt (1959) first proposed that the SFR of any galaxy would be related to the gas surface surface density via the power law,

$$\Sigma_{SFR} = \mathrm{A}\, \Sigma_{gas}^{N} \tag{1.23}$$

where A is the absolute SFE, Σ_{SFR} is the SFR surface density in $\mathrm{M}_{\odot}\ \mathrm{yr}^{-1}\ \mathrm{kpc}^{-2}$, N is the power law value, and Σ_{gas} is the ISM gas surface density in $\mathrm{M}_{\odot}\ \mathrm{pc}^{-2}$. Through observations, Kennicutt et al. 1989 showed that star-forming galaxies follow this equation with $N = 1.4 \pm 0.15$; this form is known as the Schmidt-Kennicutt Law.

When nearby star-forming galaxies are plotted alongside this solution, there is still a large amount of scatter, particularly for targets with larger gas surface densities. The Milky Way is our best solution to calibrate the rule for calculating SFRs. Krumholz et al. 2011 have already begun searching for an improved relation by directly comparing Galactic objects against extragalactic ones. Figure 1.8 shows the trends between the Galactic and nearby extragalactic sources.

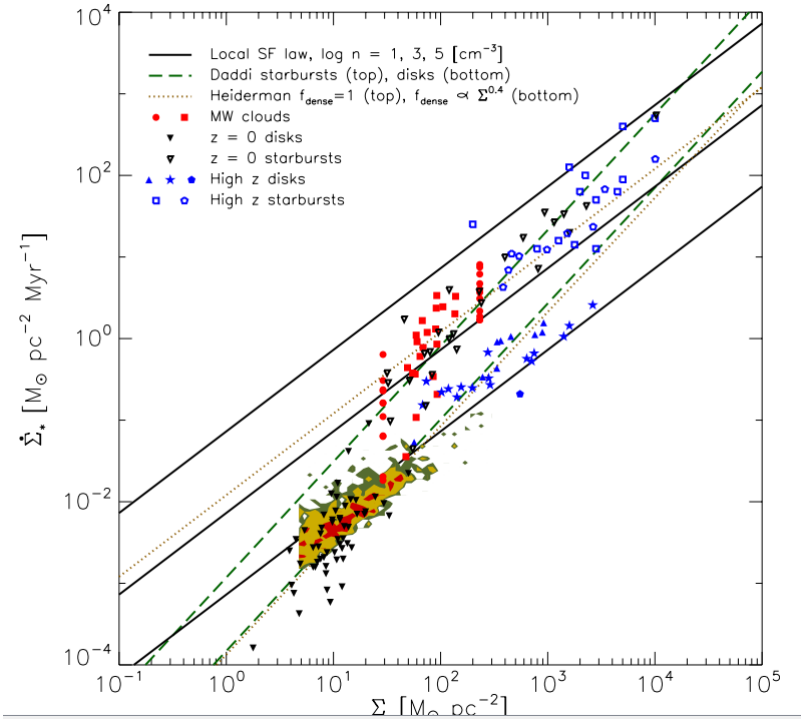

FIGURE 1.8: Refining the Schmidt-Kennicutt relation for Galactic and nearby extragalactic sources. (From Krumholz et al. 2011)

Galactic surveys targeting UC H II regions offer high resolution studies of nearby star-forming environments that allow us to constrain the IMF and better understand the underlying physical processes that govern star formation both within our home Galaxy and without.

.

1.6 Project Goals

The primary goal of this dissertation is to compile a reliable catalogue of UC H II regions that will cover the largest extent across the Galactic plane to date in order to best statistically sample massive star forming regions across the disk. We will use this catalogue to examine any variation in the massive SFRs and SFEs as a function of R_{GC} which may also indicate a dependence, if any, on local environmental conditions. To begin, we will start with the catalogues produced by Urquhart et al. 2013b, 2014d. These studies constitute a sub-sample representing the Inner Galaxy. The SCUBA-2 Ambitious Sky Survey (SASSy; Thompson et al. 2007), offers an Outer Galaxy submillimetre survey comparable to the observations used in those previous catalogues (ATLASGAL; see Chapter 2) in both overall angular resolution and sensitivity. The addition

of the SASSy dataset will be able to provide a more complete sample of objects, extending the coverage in $R_{\rm GC}$ from the original $2-8$ kpc to a new range of $2-12$ kpc with scattered individual sources reaching distances of 20 kpc.

Over the course of this work, we also reduced the SASSy data to generate the final catalogue and produce scripts that reliably show whether or not sources qualify as UC H II regions.

In Chapter 2, we review the surveys used throughout this work with Chapter 3 detailing the data reduction methods for SASSy as well as its resulting Outer Galaxy submillimetre source catalogue. Chapter 4 will focus on the multi-wavelength matching that generated a Galactic-wide UC H II catalogue and its ramifications for massive star formation on the Galactic scale. In Chapter 5, we follow up with results from later VLA observations to determine whether any additional sites of massive star formation could be detected for previously non-surveyed Galactic longitudes. Finally, in Chapter 6, we summarise and present our conclusions.

Chapter 2

Surveys

The following chapter describes the surveys that provided necessary datasets for this study. They consist of the submillimetre, radio, and infrared regimes necessary for the matching process. The breakdown in Galactic longitudes for each is shown in Figure 2.1.

2.1 Submillimetre Regime

Submillimetre wavelengths may be used to trace the cold dust emission emitted by molecular clumps that are usually home to massive star formation (refer back to Section 1.1 for our usage of the terms, cloud and clump). These regions are affected by large extinction values due to the presence of dust such that near infrared and optical surveys are unable to penetrate their depths and provide only limited surface information. In this regime, the continuum is optically thin, allowing us to see all of the dust present and by observing submillimetre flux values across the clump, we get a picture of the properties for the interior's local environment just before and during initial star formation processes.

2.1.1 ATLASGAL

The ATLASGAL survey was the first systematic submillimetre survey of the Galactic plane, covering $300° \leq l \leq 60°$ and $|b| \leq 1.5°$, but was later extended to include $280° \leq l \leq 300°$ with $2° \leq b \leq 1°$ to account for the warp of the Galactic disk (Schuller et al., 2009; Csengeri et al., 2014). The survey used the Large APEX Bolometer Camera which consists of 295 bolometers

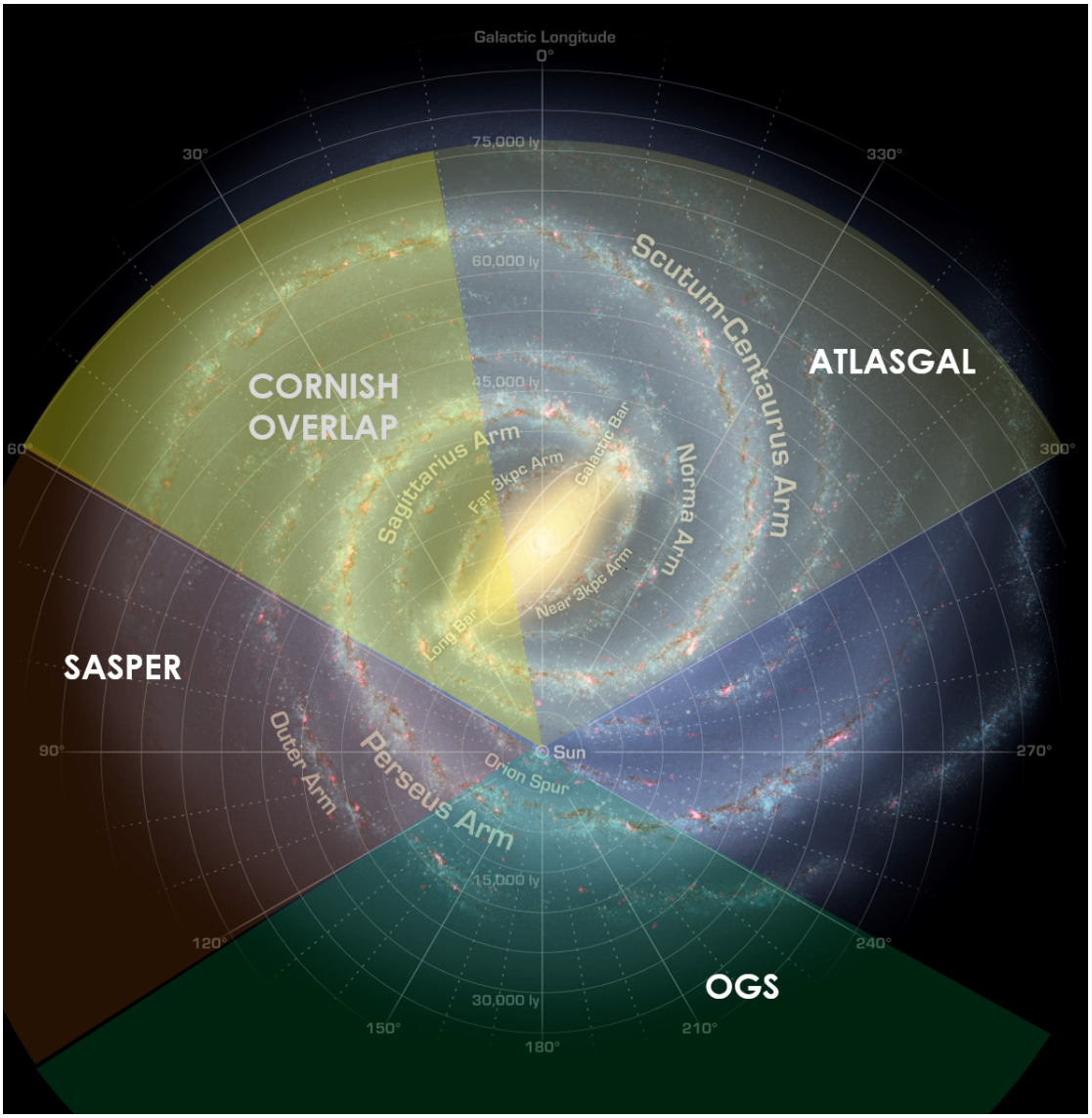

FIGURE 2.1: A schematic of the Milky Way showing the Galactic coverage of surveys relevant to this work. ATLASGAL is indicated by the gold shading, whereas the two components of SASSy ('SASPER' and 'OGS'; refer to Chapter 3 for details) are shown in red and green, respectively. The CORNISH region which overlaps ATLASGAL from $10^\circ \leq l \leq 60^\circ$ is also shown. RMS covers the full Galactic range from $10^\circ \leq l \leq 350^\circ$ though it is not shown here so as to avoid cluttering the image. The background image is an artist's impression of the Galactic plane and includes generic points of reference such as larger spiral arms and their names, location of the Sun, and the Galactic bar (Artist: Robert Hurt). To remain consistent with work by Urquhart et al. 2013b and Urquhart et al. 2014d, we adopt the value of $R_{GC} = 8.5$ kpc for the distance of the Sun from the Galactic Centre and radius of the solar circle.

observing at 870 μm or 345 GHz (Siringo et al., 2009). For this particular wavelength, the telescope has a beam size of 19.2″ at full-width-half-maximum (FWHM) and a positional accuracy of 4″ (Schuller et al., 2009). Contreras et al. 2013 used the source extraction algorithm SExtractor (Bertin and Arnouts, 1996) to produce an initial compact source catalogue of 6,774 sources for the central region of the survey area ($330^\circ \leq l \leq 21^\circ$). The full ATLASGAL compact source catalogue (CSC; Contreras et al. 2013; Urquhart et al. 2014a) consists of ~10,000 sources and is 97% complete for sources above 5σ and > 99% complete above 7σ. The results from the survey have provided a complete census of dense dust clumps within the Inner Galaxy including all potential massive star-forming clumps with masses greater than 1,000 $M_\odot$ out to a heliocentric distance of ~20 kpc (Urquhart et al., 2014a) and assuming the standard IMF and a typical SFE of 30% (Lada and Lada, 2003). The radial velocities of the molecular clumps have been measured from molecular line observations (e.g., CO, NH_3, CS). These are readily available for many of the ATLASGAL clumps from a number of Galactic plane surveys (e.g. MGPS, Burton et al. 2013; ThrUMMS, Barnes et al. 2015; SEDIGISM, Schuller et al. 2017; COHRS, Dempsey et al. 2013b; CHIMPS, Rigby et al. 2016) and also from large targeted observational programmes towards selected samples (e.g. MALT90, Jackson et al. 2013; RMS, Urquhart et al. 2007b, 2008a, 2011, 2014d; BGPS, Dunham et al. 2011) as well as dedicated ATLASGAL follow-up observations (e.g., Wienen et al. 2012; Csengeri et al. 2017; Urquhart et al. 2018).

The results of ATLASGAL have provided a detailed view of the distribution of cold dense gas across most of the northern and southern Galactic plane. A vital component of the survey mission was to complement observations from Planck and Herschel satellites (e.g. Ragan et al. 2012; Nguyên Luong et al. 2011; Zavagno et al. 2010) by providing a complete census of cold and massive GMCs where massive star formation is expected to be occurring. It has proved to be a valuable link to examine the large scale structures based on their local environmental conditions within the ISM. Following efforts continue to mine the database to study compact H II regions (Urquhart et al., 2013b, 2018; Xu et al., 2019), methanol masers (Urquhart et al., 2013a; Paulson and Pandian, 2017; Billington et al., 2019) individual sites of massive star formation and their properties (Immer et al., 2012; Boley et al., 2012; Paron et al., 2012; Gennaro et al., 2012; Li et al., 2012)), and dust properties (e.g. Kainulainen et al. 2011; Yuan et al. 2017). Urquhart et al. 2014d found that the vast majority of detected clumps (~88%) are capable of forming a massive star. They noted that clump mass is independent of evolution, suggesting clumps form with the majority of their mass in-situ. The statistical lifetime (or the average lifetime for clumps binned into a set range of mass values) of the quiescent stage is expected to be $\sim 5 \times 10^4$ years

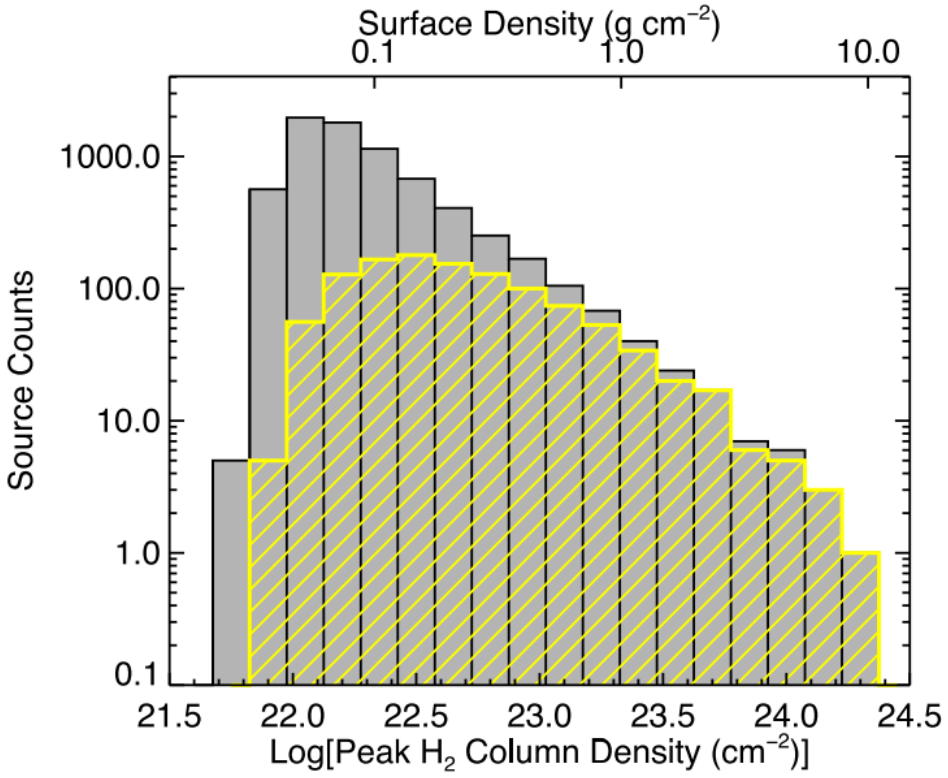

FIGURE 2.2: Peak N_{H_2} distribution for complete ATLASGAL source catalogue (grey) and known tracers of massive star formation (yellow). Bin size is 0.15 dex (Urquhart et al., 2014d). The plot shows a strong connection between clumps with the highest peak column densities to be nearly 100% associated with massive star formation for clumps with log $N_{H_2} > 23$.

for clumps of ~1000 $M_\odot$, decreasing to $\sim 1 \times 10^4$yr for clump masses of > 10000 $M_\odot$. They also found a strong correlation between the fraction of massive clumps with tracers of massive star formation and a favoured range of peak column densities (See Figure 2.2). This fraction is initially small at low column densities but reaches 100% for clumps with column density above 10^{23} cm^{-2}. They were unable to detect any currently known clumps above that value that were not already associated with massive star formation. Their conclusion was that the clumps form rapidly and are very unstable at the beginning, thus allowing star formation to quickly ensue. This result forms the foundation for the work that will be presented in this thesis where we have complemented the Inner Galaxy ATLASGAL H II regions with data from SASSy sources in the Outer Galaxy in order to better understand the distribution of massive star formation across the entire Galactic Plane. This sample and the significance for massive star formation on the Galactic scale is presented in Chapter 4. However, we noticed that several SASSy clumps (~ 100) with column densities above the 10^{23} cm^{-2} critical value had no RMS counterparts and no known tracers of massive star formation could be found in the literature for these targets. Motivated by

the findings of Urquhart et al. 2014d, we acquired follow-up observations for the SASSy clumps in question using the Very Large Array (VLA). The results are presented in Chapter 5.

2.1.2 SASSy

The SCUBA-2 Ambitious Sky Survey (SASSy) utilised the James Clerk Maxwell Telescope (JCMT) to observe the Outer Galaxy at 850 μm, with an angular resolution of 17″ (Dempsey et al., 2013a). The results of this survey are currently being prepared for publication (Thompson et al. in prep.). It was designed to fully exploit SCUBA-2's fast mapping capability and to form a long wavelength counterpart to Herschel's PACS and SPIRE (Poglitsch et al., 2008; Griffin et al., 2008), via the targeting of cold, early-stage objects (Thompson et al., 2007). It covered ~500 deg^2 of the sky visible from Mauna Kea down to a 1σ noise level of ~30 mJy beam^{-1}. It was the first ground-based submillimetre survey to target specifically the Outer Galaxy. As such, it may be used as a beneficial complement to ATLASGAL, possessing similar beam size and sensitivity limits.

Further details on the data reduction of the SASSy survey and its catalogue are discussed in Chapter 3.

2.2 Radio & Infrared Regimes

The next two necessary components for classifying the bona-fide compact and UC H II regions are radio and infrared datasets. For our purposes, we chose to use the RMS database as described below because it included both current radio and infrared measurements for nearly all sources. It is also comparable to the CORNISH survey used by Urquhart et al. 2013b. The following sections highlight the main attributes of RMS and CORNISH.

2.2.1 RMS

The Red MSX Survey (RMS)[1] provides a Galactic sample of massive young stellar candidates identified from the MSX satellite catalogue (Price et al., 2001) by comparing their mid-infrared colours to those of objects already identified as confirmed MYSOs and H II regions (Lumsden

[1] `http://rms.leeds.ac.uk/cgi-bin/public/RMS_DATABASE.cgi`

et al., 2002). It covers the majority of the Galactic plane with $10^\circ \leq l \leq 350^\circ$ and $|b| \leq 5^\circ$, purposely avoiding longitudes near the Galactic centre to circumvent problems with source confusion as a result of crowded positions and sources whose kinematic distances cannot be constrained. Though initially selected via these colours, the database has been continuously added to and refined by a programme of multi-wavelength observations, including radio continuum, molecular line, and mid-infrared observations (Hoare et al., 2005; Urquhart et al., 2007b, 2008b,a, 2009; Mottram et al., 2007; Lumsden et al., 2013). This process resulted in a catalogue containing MYSOs, H II regions, evolved stars, planetary nebulae, and nearby low-mass YSOs. Lumsden et al. 2013 classified each of these objects according to their 3-colour images provided by GLIMPSE (Benjamin et al., 2003), WISE (Wright et al., 2010), or Hi-GAL (Molinari et al., 2010) surveys, as available, and the radio contours from counterparts identified in the follow-up observations. Approximately 1,700 massive YSOs and H II regions have been identified to date with radial velocities and distances available for 90% of the objects (Urquhart et al., 2014d). An analysis from Lumsden et al. 2013 shows that RMS is more than 90% complete for the massive protostellar population within the adopted selection boundaries with a positional accuracy of the exciting source of better than 2″.

The RMS is an ideal sampling of star forming regions across the Galactic plane and at various stages. It has been used to trace Galactic structure (e.g Moore et al. 2012), examine the statistical impact of triggered star formation (e.g. Thompson et al. 2012), and to also test accretion models for massive star formation (Davies et al., 2011). It's combination of high resolution radio and infrared data make it an excellent starting point to catalogue the initial phases of massive star formation (e.g. Caswell et al. 2010; Contreras et al. 2013; Molinari et al. 2010) and we exploit this attribute for cross-matching the RMS identified UC H II regions in the Outer Galaxy with SASSy submillimetre clumps.

2.2.2 CORNISH

The CORNISH survey was used by Urquhart et al. 2013b as a radio-counterpart to the overlapping area with ATLASGAL. CORNISH mapped 5 GHz radio continuum emission in the northern Galactic plane for $10^\circ \leq l \leq 60^\circ$ and $|b| \leq 1^\circ$. It was designed to identify UC H II regions across the Galactic disk (Hoare et al., 2012) and to give a radio counterpart to arcsecond-resolution infrared surveys (e.g. UKIDSS, GLIMPSE, and MIPSGAL). CORNISH used the VLA to resolve radio emission on angular scales between 1.5-20″. The rms noise level of the images is better

than 0.4 mJy beam^{-1}, which is sufficient to detect free-free emission from an optically thin H II region around a B0 star on the other side of the Galaxy (Urquhart et al., 2013b). The CORNISH catalogue contains 2,637 sources above a 7σ intensity cut-off (Purcell et al., 2013).

Urquhart et al. 2013b cross-matched 870 μm submillimetre observations from ATLASGAL with 5 GHz CORNISH radio data and GLIMPSE mid-infrared 3-colour images (Schuller et al. 2009; Hoare et al. 2012; Benjamin et al. 2003, respectively). UC H II regions were identified and confirmed as previously discussed in Chapter 1. Within the overlapping area of these surveys ($10^\circ \leq l \leq 60^\circ$, $|b| \leq 1^\circ$), Urquhart et al. 2013b were able to identify and confirm 213 bona-fide UC H II regions embedded within 170 clumps. Kinematic distances were derived for each clump (except where parallax distances were available) and used to estimate clump mass, clump size, Lyman continuum flux, and diameter for each embedded H II region. Cesaroni et al. 2015 performed a similar analysis with HI-GAL (Molinari et al., 2010) and CORNISH, finding a comparable number of 230 UC H II regions (with $10^\circ \leq l \leq 65^\circ$, $|b| \leq 1^\circ$). However, due to the limited l range in CORNISH, these results are incomplete at larger values of galactocentric radii ($R_{GC} > 8$ kpc). CORNISH objects within this longitudinal area may also include sources up to a heliocentric distance of D$\sim$ 20 kpc, which limits the number of detections that can occur past a certain point and affects completeness limits (refer to Figure 2.1).

In the following chapter, we introduce the SASSy survey and give the necessary details of the data reduction process that resulted in the catalogue of Outer Galaxy submillimetre molecular clumps that will be matched with the RMS UC H II regions.

Chapter 3

SASSy: An ATLASGAL Complement for the Outer Galaxy

3.1 Introduction to SASSy

The SCUBA-2 Ambitious Sky Survey (SASSy) is currently the widest area 850 μm survey to be carried out from the ground. It forms an ideal counterpart to ATLASGAL by supplementing the ATLASGAL Inner Galaxy coverage with an Outer Galaxy focused survey area. It possesses similar beam size and sensitivity limits to ATLASGAL (refer to Chapter 2), and further identifies free-free radio-continuum emission that may indicate compact and UC H II regions or other possible tracers of massive star formation with $R_{\rm GC} > 8.5$ kpc.

The survey covered $\sim 500\,\mathrm{deg}^2$ of the sky visible from the James Clerk Maxwell Telescope (JCMT) down to a 1σ noise level of 30 mJy beam^{-1}. It was also able to observe in Grade 4 weather, giving the survey flexibility for scheduled observing. SASSy was split into two parts: SASSy-Perseus and SASSy-Outer-Galaxy-Survey (hereafter, SASPER and OGS, respectively; see Figure 3.1). SASPER was designed as an extension to the original science verification data when it was announced that Hi-Gal (Molinari et al., 2010) would be increasing its coverage to include the $60^\circ \leq l \leq 120^\circ$ region, i.e. the Perseus arm (also visible in Figure 3.1). It was concluded with 100% completion, covering $\sim$100 deg^2 at a nominal depth of 25 mJy beam^{-1}. The catalogue for SASPER consists of 1372 individual sources. The analysis of the SASPER dataset was done by Gaius Manser and we used similar methods and procedures to supplement the initial catalogue with OGS.

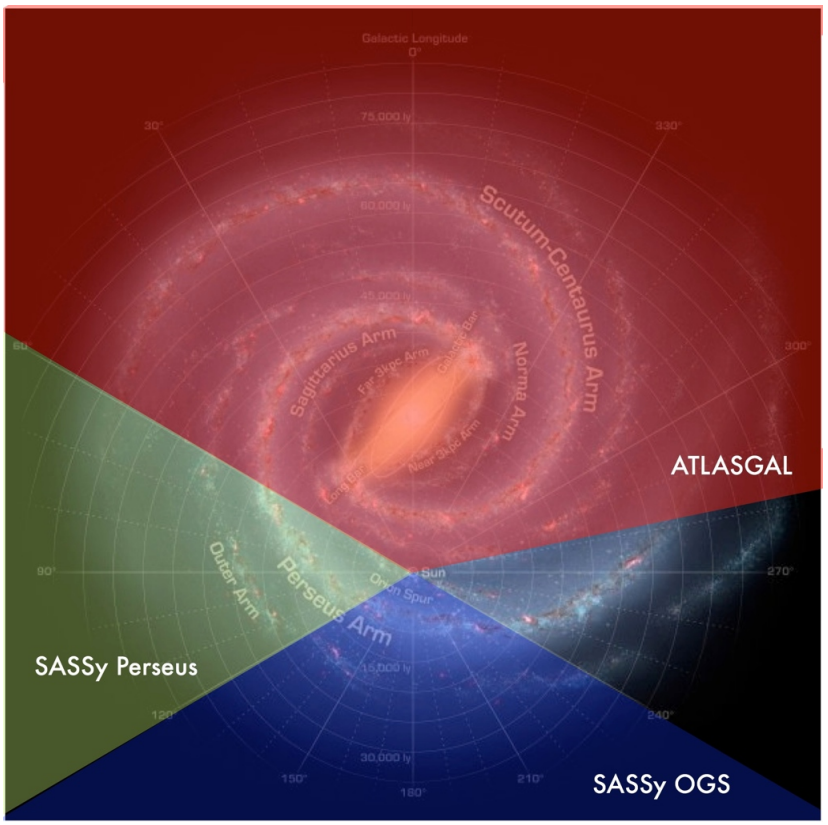

FIGURE 3.1: Coverage of SASSy-Perseus and OGS regions. ATLASGAL is also displayed for reference. See text for further details. Image credit: Mark Thompson.

OGS covered most of the remaining Galactic regions with $120° \leq l \leq 240°$. The OGS data was vital for this work as it shows the massive molecular clumps that are likely host to the UC H II regions and sites of massive star formation for $R_{GC} > 8.5$ kpc. This chapter details the steps for the reduction of the OGS data and the final catalogue for its corresponding Outer Galaxy sources. A paper is currently planned for publication in 2020 to present the full SASSy catalogue and survey analysis (Thompson et al. in prep.). The following sections provide more detail on the individual parts of SASSy. In Section 3.2, we discuss the specifics of SCUBA-2 which was the primary instrument used for the observations. Section 3.3 reviews the steps for the data reduction process and the resulting OGS catalogue is presented in Section 3.4.

3.2 SCUBA-2

The Submillimetre Common User Bolometer Array-2 (SCUBA-2) is a bolometer camera consisting of 10,000 pixels. Its two arrays may operate simultaneously in the atmospheric windows of 450 and 850 μm. Each array is further made up of four sub-arrays (Holland et al. 2013).

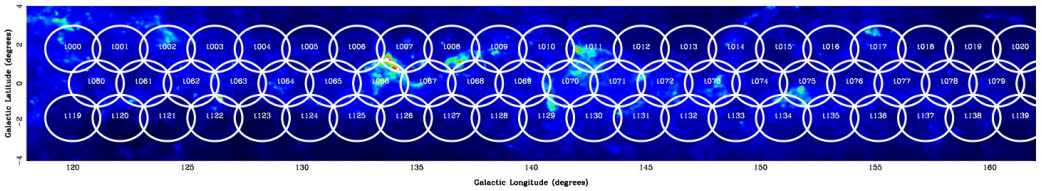

FIGURE 3.2: A sample SASSy pointing map shows the mapping scheme and coverage for OGS across the sky. Tiles were eventually stitched together during the analysis into 20° chunks. Each PONG is 2° across. The maps are overlaid on a 353 GHz emission image of the Galactic plane from the Planck Surveyor. (Thompson et al., 2007)

For the purpose of this work, we focused on the 850 μm window as it is comparable with the ATLASGAL catalogue at 870 μm.

SCUBA-2 has two observing modes: DAISY and PONG. These modes offer a choice for scanning patterns when mapping large sky areas based on the desired degree of extended emission. SASPER and OGS were carried out using PONG maps due to the ability to quickly map the full sky. To ensure an even sky background, 3-5 PONG maps would be made for a single observation position with the instrument rotated by a small amount each time. This creates a circular pattern with a diameter equal to the desired size. SASPER PONG maps possessed diameters of 1° across while OGS which had more area to cover, utilised PONGs that were 2°.

Figure 3.2 from Thompson et al. 2007 shows a sample of how the sky was divided for SCUBA-2 PONG mapping. The OGS observation areas or 'tiles' are shown as overlapping circles throughout the plot and each are labelled with an identification number. These would cover approximately the same region and area as each PONG during observations. Multiple observations for each respective tile would later be summed together to ensure consistent sky background and later cleaned and smoothed before extracting any sources (See Section 3.3). The background image is from 353 GHz emission maps of the Galactic plane from the Planck Surveyor. In this way, the full region of SASSy could be surveyed effectively and individual calibrated tiles could easily be cross-referenced with areas of known star formation or other bright components of Galactic structure.

3.3 Data Reduction

The data reduction for SASSy followed the standard SCUBA-2 data reduction procedures outlined in the cookbook provided by JCMT. The details of that procedure for the case of the OGS are given below.

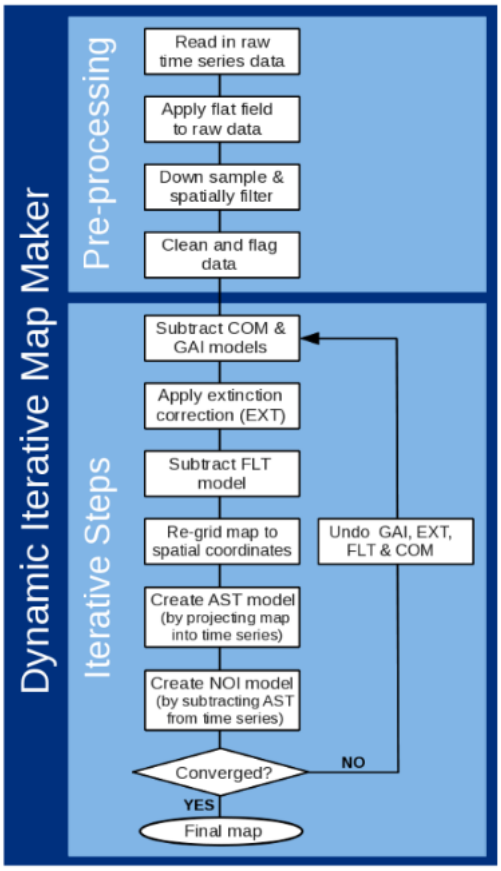

FIGURE 3.3: `MAKEMAP` steps for reducing raw observations into usable maps of specified S/N. From Chapin et al. 2013

3.3.1 Sky Maps & Mosaicking

The relevant raw SASSy data files were extracted from project codes MJLSY01, MJLSY02, and MJLSY14B (P.I.: M. A. Thompson). The raw time series observations for each tile were combined to produce corresponding sky-gridded maps with the `SMURF` package command `MAKEMAP`[1] in the `STARLINK` sofware (Currie et al., 2014) using the resources of the STRI cluster at the University of Hertfordshire.[2]

The purpose of `MAKEMAP` is to take the time series data of the bolometer array that is moving across the sky and convert signal to the appropriate pixel mapped onto the corresponding sky coordinates. The total signal obtained is a culmination of signal from several different sources. There is the atmospheric extinction, the astronomical signal (which varies with time as the telescope moves across the sky), the uncorrelated white noise generated by bolometer running temperatures, some unique signal input from each respective bolometer, the common mode

[1] http://adsabs.harvard.edu/abs/2013MNRAS.430.2545C
[2] http://stri-cluster.herts.ac.uk/

signal, and low-frequency noise. Each of these sources are modelled by `MAKEMAP` and iteratively solved to find the best solutions such that the extinction and noise components are subsequently removed in decreasing order of magnitude so that only the astronomical signal and some residual noise remain. The overall step-by-step iteration is shown in Figure 3.3 and begins with initial cleaning and down-sampling where the raw data is concatenated into a single time series for each sub-array, flat-fielded, and bolometers with unusually high noise levels are flagged and excluded from further processing. The data is then ready for the first round of iterative solutions.

The solutions that `MAKEMAP` delivers will be impacted by a configuration file supplied by the user. The file with its associated parameters and values that we chose to use for OGS (and SASPER) is provided in Table 3.1. The values were selected as a result of many hours of testing and comparing results with the JCMT Plane Survey (JPS; Eden et al. 2017) which also utilised SCUBA-2 for mapping 850μm continuum emission in the Galactic plane but only for the longitude range of $l = 7 - 63°$. The similarities in the surveys, despite targeting different areas of the Galaxy, made JPS an ideal counterpart for estimating the correct parameters for the `MAKEMAP` solutions.

During the iterative steps, `MAKEMAP` uses the given parameters to estimate the best models for each component. The components are the common-mode signal (COM), the gains that scale each bolometer to the common-mode (GAI), an extinction correction (EXT), a filter model for removing low frequencies (FLT), the astronomical signal (AST), and the residual noise (NOI). Their relative positions within the `MAKEMAP` solutions are shown in Figure 3.3. The models are subsequently subtracted from the time-series data and the remaining values are binned into a sky map. Convergence is checked against the parameters given in the configuration file and is achieved either when the requested number of iterations has been reached or when the mean change in the map pixel values is less than the specified fraction of the standard deviation (`maptol`). If neither of these requirements are met, `MAKEMAP` continues to model, solve, and remove the associated signal components.

Some maps continued to show signs of large structure or poor quality modelling even after the maximum number of iterations specified. Examples of such markers include data chunking (subject to computer memory and size of data which may lead to too few passes through each data point), an unusual number of iterations, a too small percentage of bolometers being used, and fake 'blooms' of emission. Blooming, visible as the white spot on the left side of the sample OGS tile in Figure 3.4, is caused when artificial flux is created as a result of the various

TABLE 3.1: `MAKEMAP` Configuration Parameters for OGS `PONGs`. For tiles where extended structure was present, we added a final line with `com.perarray = 1` to the file.

Parameter	Value	Description
`numiter`	-100	a negative implies this value is the max. no. of iterations that will be performed
`flt.fil_edge_largescale`	480	largest scale size to be retained by FLT model
`flagslow`	300	threshold for too slow slew velocity such that sources buried in 1f noise
`maptol`	0.01	comparison value between previous and subsequent map; specifies when to stop iterations
`noi.box_size`	-15	no. of time slices used to determine noise levels; negative denotes units in seconds.
`ast.zero_snr`	3	reduces spurious large scale structure in final map within regions of low S/N; SNR mask value
`ast.zero_snrlo`	2	allows to increase size of SNR masks without introducing noise or forming 'bowls' around sources
`flt.filt_edge_largescale_last`	100	largest scale size to be kept by FLT model
`ast.skip`	5	skip subtraction of astronomical signal between iterations allowing for SNR masks to be made first
`flt.zero_snr`	5	speeds up convergences and reduces ringing by removing high SNR pixels
`flt.zero_snrlo`	3	speeds up convergences and reduces ringing by increasing size of SNR mask.
`noi.box_type`	1	determines how noise in each box is found via a Fourier Transform
`flt.ring_box1`	0.5	controls flagging of symbols that suffer from ringing
`flt.filt_order`	4	indicates shape of filter
`com.sig_limit`	5	if bolometer's standard deviation exceeds this limit times the RMS, those time slices are rejected
`ast.zero_notlast`	1	allows flux to be present in masked areas of final map

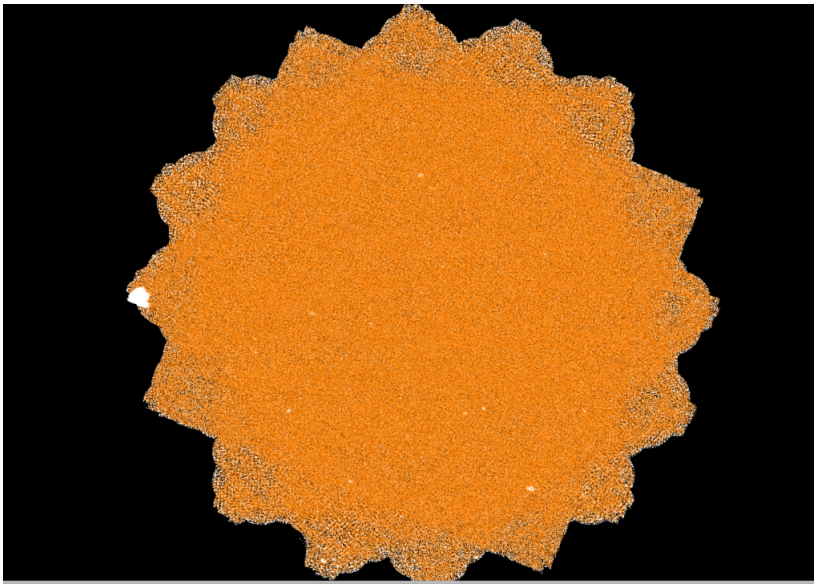

FIGURE 3.4: A example of artificial flux or 'blooms' from one of the OGS tiles. Visible as the white spot on the left side of the image. These could usually be removed by examining the original observation files and removing one image that was of noticeably poorer quality than the rest.

sub-arrays not being represented well by a single common mode. Problem tiles were noted and usually traced back to a bad observation that could be removed from the dataset. For 5 individual tiles, we were unable to generate appropriate solutions and the resulting maps had a number of artificial emission and substructures regardless of the number of iterations undergone. For these tiles, we sought advice from JCMT staff (Harriet Parsons, private communication) who informed us that this was common when the tiles were centred around extended structures and background intensities, causing one sub-array to be much noisier than the others. In this case, the configuration file could be adapted to include the parameter, `com.perarray = 1`, which would adjust for the additional noise component.

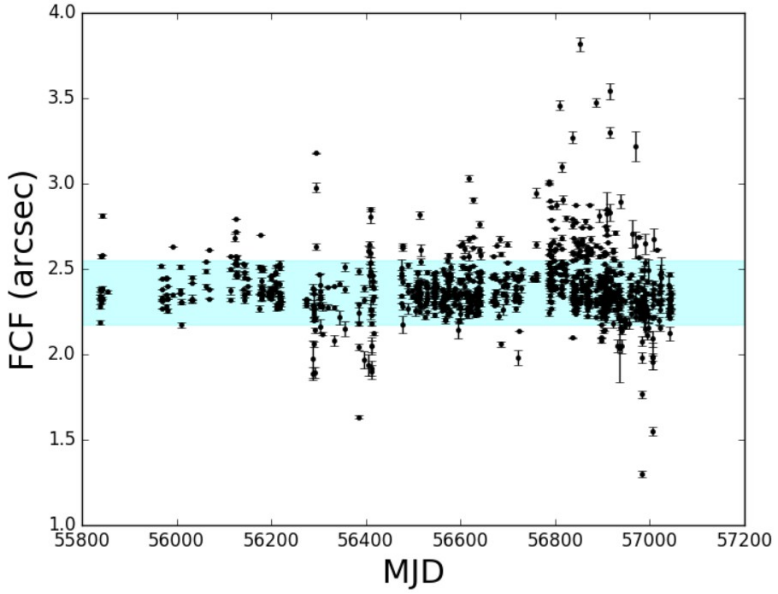

FIGURE 3.5: Calibrator check for mean Flux Correction Factor (FCF) according to Julian Date. The upward trend towards the end of survey time is due to a switch to daytime observing. The blue band is centred at the mean FCF of 2.36 Jy/pW/arcsec^2 with a standard deviation of 0.19 which is within the uncertainty of the standard value 2.34 ± 0.08.

The final tile maps were stitched together to form 20° wide mosaic regions (compared to 10° in SASPER) using `WCSMOSAIC`.

3.3.2 Flux Calibration

`MAKEMAP` produces images in units of pico-Watts (pW). In order to convert this to Jy arcsec^{-1}, some conversion factor is required. During the observations, standard calibrators with known correction values were observed each night for this purpose. We plotted the mean flux correction factor (FCF) of each calibrator source versus Julian date for each night that SASSy observed. The results are shown in Figure 3.5. The upward trend seen towards the end of the observations is a result of switching to daytime observations as part of the JCMT extended ops program. The centre of the blue band designates a mean FCF value of 2.36 Jy/pW/arcsec^2. It has a standard deviation of 0.19. The default FCF for SCUBA-2 observations as given by Dempsey et al. 2013a, is 2.34 ± 0.08 Jy/pW/arcsec^2 for the 850 μm window. This is within the region of uncertainty for our derived value and we chose to proceed using the standard FCF. The mosaics were calibrated by applying the `PICARD` recipe `CALIBRATE_SCUBA2_DATA` which generated new maps in units of mJy arcsec^{-1}. The final calibrated map for $l = 120 - 140°$ in OGS is shown in Figure 3.6.

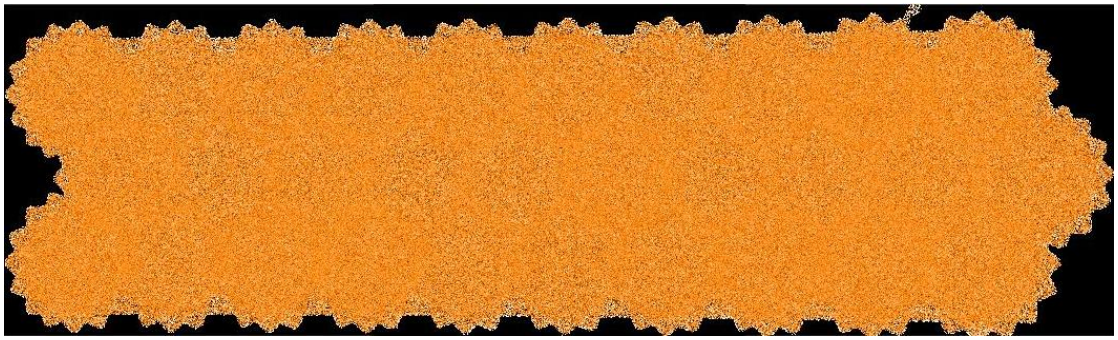

FIGURE 3.6: Calibrated mosaic for region $l = 120 - 140°$in OGS using the standard flux correction factor of 2.34 ± 0.08 Jy/pW/arcsec^2. Note that the sources will be difficult to see by eye in these maps, hence the following steps in Section 3.3.3.

3.3.3 FELLWALKER Source Extraction & Clump Masks

Next, we utilised MAKESNR to generate the signal to noise maps for each mosaic. To distinguish the individual sources, we used the FellWalker algorithm by Berry 2014. This source identification algorithm is available as part of the CUPID[3] package (Berry, 2007). FellWalker attempts to define the peaks and size of objects in an image based on local gradients (see Table 3.2 for specific parameter values). These values were also chosen as a result of the similarities between OGS and JPS as previously discussed in Section 3.3.1). We extracted sources based on their signal-to-noise values, initially choosing a 3σ threshold. This was later adjusted to 5σ after comparison with the SASPER catalogue. The resulting sources and their associated properties are shown for a subset of source in Table 3.3. The full catalogue is provided in Appendix A.1.

FELLWALKER was selected over other source extraction because it is less likely to split large clumps, thereby creating false sources. As we will be especially interested in the most massive clumps undergoing massive star formation, this is a useful characteristic. Berry2015 also showed that FELLWALKER is robust against a wide choice of input parameters, unlike other commonly used tools such as CLUMPFIND and GAUSSCLUMPS (Watson, 2010). To determine the flux densities of each source, FellWalker essentially uses aperture photometry (Eden et al., 2017). The aperture size and shape is set by the number and distribution of contiguous pixels above the set detection threshold, thus resulting in a loss of signal for outside of this aperture size and below the threshold. Dempsey et al. 2013a has shown the the wings of the JCMT beam contain significant power and because this effective aperture is SNR-dependent, the loss of signal can be significant for fainter sources. This phenomena can be corrected for by measuring the JCMT beam shape when observing either Neptune or Uranus during the observations and reducing the

[3]http://www.starlink.ac.uk/cupid

TABLE 3.2: FELLWALKER Configuration Parameters for OGS source extraction.

Parameter	*Value*	*Description*
ALLOWEDGE	0	reject clumps if they touch the edge of the data array
CLEANITER	5	no. of times to replace each clump index by most common value among neighbours
FWHMBEAM	1	Full Width Half Max of Beam in pixels
MINPIX	12	lowest no. of pixels a clump can contain
MINDIP	1.2*RMS	if dip below two adjacent peaks is less than value, peaks considered part of same clump
MAXJUMP	3	extent of neighbourhood about local max check for higher pixel values
MINHEIGHT	3	min peak value required for clump
NOISE	1.3	specifies the noise threshold per pixel

TABLE 3.3: A subset of sources for the OGS catalogue. The columns provided include the official SASSy name, object coordinates in galactic coordinates as well as right ascension and declination, the effective radius in parsecs, the aperture corrected integrated flux in Jy, the flux error, and finally the value for the aperture correction. See Appendix A.1 for the full catalogue.

SASSy Name	l	b	RA (2000)	Dec (2000)	R_{eff} [pc]	F_{int} [Jy]	error [Jy]	Ap Cor
JCMTLYS J022704.00+615219.4	133.95	1.06	02:27:04.00	+61:52:19.4	67.44	58.75	3.52	1.10
JCMTLYS J022541.53+62554.8	133.72	1.22	02:25:41.53	+62:05:54.8	74.30	79.25	4.76	1.08
JCMTLYS J022530.97+62633.8	133.69	1.22	02:25:30.97	+62:06:33.8	50.22	31.06	1.86	1.05
JCMTLYS J022529.43+62554.3	133.69	1.21	02:25:29.43	+62:05:54.3	47.09	33.05	1.98	1.04
JCMTLYS J003646.61+632858.8	121.30	0.66	00:36:46.61	+63:28:58.8	42.52	11.16	0.67	1.03
JCMTLYS J022553.46+62411.2	133.75	1.20	02:25:53.46	+62:04:11.2	32.65	6.44	0.39	1.01
JCMTLYS J03131.73+602921.1	138.29	1.56	03:01:31.73	+60:29:21.1	42.71	9.42	0.57	1.03
JCMTLYS J012331.82+614840.9	126.71	-0.82	01:23:31.82	+61:48:40.9	40.39	4.95	0.30	1.02
JCMTLYS J02806.90+60464.7	132.16	-0.72	02:08:06.90	+60:46:04.7	26.89	2.82	0.17	0.98
JCMTLYS J03321.16+60286.9	138.50	1.65	03:03:21.16	+60:28:06.9	30.27	3.84	0.23	1.00
JCMTLYS J022807.97+612957.5	134.20	0.76	02:28:07.97	+61:29:57.5	24.50	2.52	0.15	0.97

data in the same manner as the rest of the observations. An aperture correction can be obtained from the percentage of total flux measured around the planets in increasing circular apertures. The calculated aperture corrections for each OGS source are also included in Table 3.3.

3.4 An Outer Galaxy Catalogue

OGS produced 1766 clumps sources above a 5σ threshold. Combined with the 1375 sources found in SASPER, the total number of SASSy sources is 3141.

The resulting catalogue includes all sources found in OGS as well as their associated integrated flux (aperture corrected), effective radius, flux errors, and the aperture correction values for each target. The aperture correction is a scale factor that ensures that the total flux is being observed for an appropriately comparable aperture size. Dempsey et al. 2013a modelled the SCUBA-2 measured flux for a range of aperture sizes to determine the appropriate correction such that the majority of the flux was detected without going over 100% (Figure 3.7). The total fluxes of the individual sources determined by FELLWALKER are multiplied by this scale factor to produce the

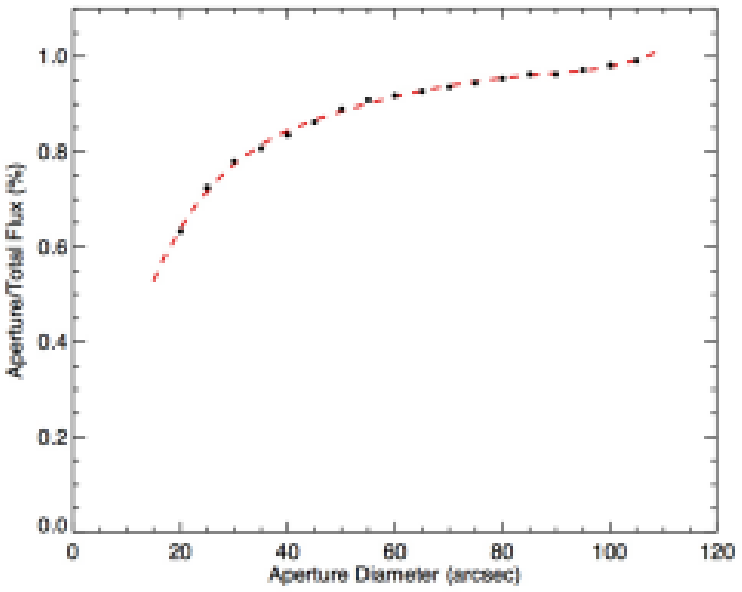

FIGURE 3.7: Aperture corrections determined by Dempsey et al. 2013a. These values are applied to the flux values calculated by `FELLWALKER`.

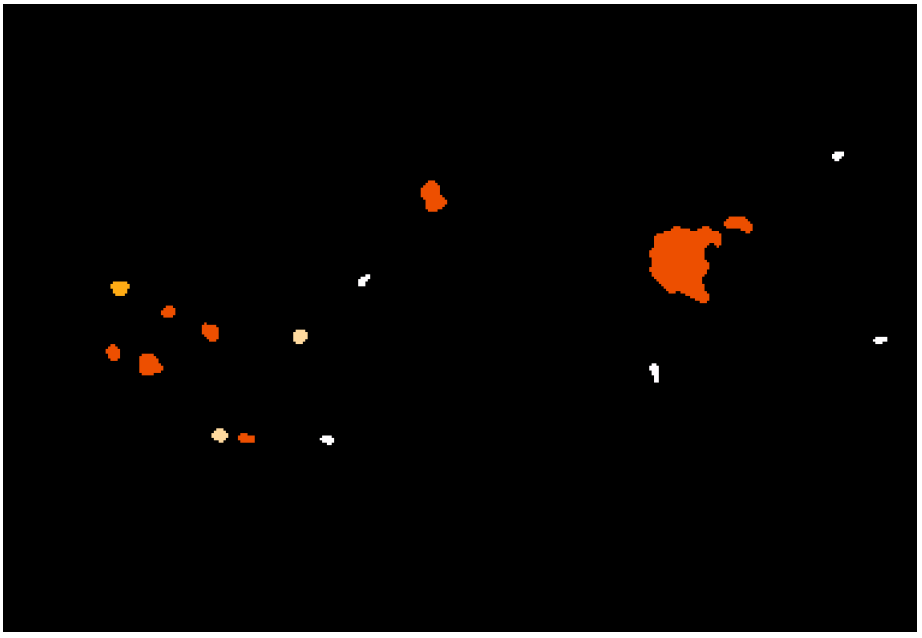

FIGURE 3.8: Sample clump masks from $l = 200 - 220°$showing evidence of a star forming complex.

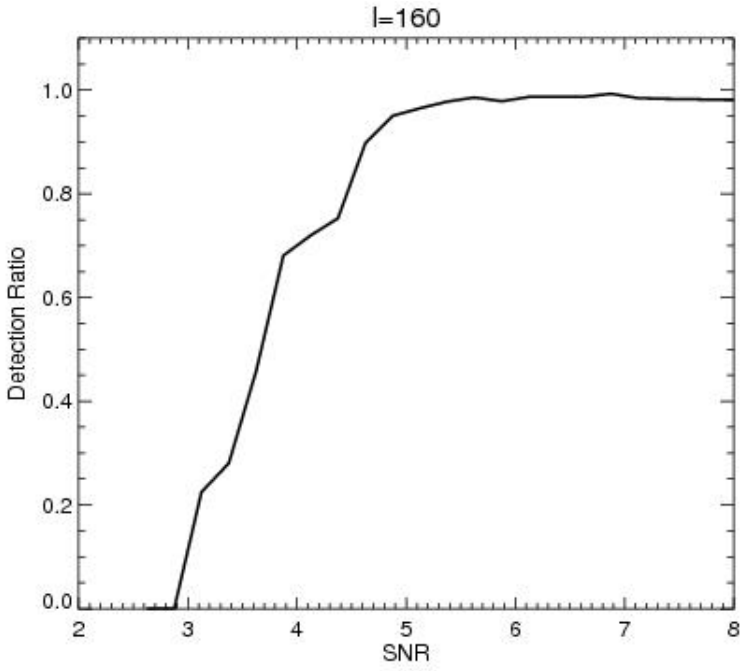

FIGURE 3.9: Completeness testing via the generation of 10,000 fake sources in OGS maps and extracted using the same `FellWalker` parameters as detailed in Table 3.2. The results show that SASSy is 99% complete for sources above 5σ. Credit: David Eden.

final flux values. Signal-to-Noise masks were also generated to indicate the position and scope of each source in a separate image (see example in Figure 3.8). Each clump mask was given an identification number for easy reference during later matching to other catalogues.

To ensure that our catalogue would be comparable to ATLASGAL, we ran a completeness check to determine the sensitivity and limits of SASSy. A region of SASSy was selected for comparison and maps containing fake sources ($\sim$ 10% of the true number) were generated. The fake sources had a set size of 7 pixels FWHM, and a uniform distribution of 1-15σ (David Eden, private communication). The fake sources were then added to the original emission map and extracted using the same `FellWalker` parameters as the original SASSy reduction. These steps were repeated until 10,000 fake sources had been added to the original map. The resulting histogram for peak flux of the real sources as well as the fake sources as compared with the true sources extracted from the original map is shown in Figure 3.9. This result for the $l = 160 - 180^{\circ}$ region shows that SASSy has 99% completeness for sources above 5σ making it an ideal counterpart to ATLASGAL which possesses 97% completeness above the 5σ threshold (see Chapter 2). The similarities of ATLASGAL and SASSy allow us to safely utilise their source catalogues as representative of molecular clumps hosting massive star formation in the Inner and Outer Galaxy, respectively. In the following chapter, we continue with the matching of the submillimetre clumps

to their respective radio counterparts: the UC H II regions.

Chapter 4

A Galactic Census of UC H II Regions

The classification of a bona-fide UC H II region relies on examining the alignment of radio, infrared, and submillimetre data. Several studies have used this technique to classify radio emission, including Urquhart et al. 2009, 2013b, Thompson et al. 2006, Hindson et al. 2012, and Purcell et al. 2013 but current catalogues remain restricted in their Galactic coverage and/or introduce bias via false H II regions (see Chapter 1). By using the coincidence of the submillimetre data for the SASSy survey covering ($60^\circ \leq l \leq 240^\circ$) and ATLASGAL ($280^\circ \leq l \leq 60^\circ$) with peaks in the radio and correlation with strong mid-infrared emission available in RMS ($10^\circ \leq l \leq 350^\circ$), we seek to compile the widest coverage catalogue to date with only the confirmed and bona-fide UC H II regions. The UC H II regions will help us to trace any trends in massive star formation across the Galactic plane for a range of galactocentric radius larger than any continuous study has attempted before. In this manner, we can examine the effects between the Inner and Outer Galaxy regions to determine if galactocentric radial-dependent properties such as metallicity or the gas-to-dust mass ratio have any bearing on massive star formation on Galactic scales.

4.1 Cross-Survey Matching & Catalogue Construction

Our compilation is based on ATLASGAL and SASSy submillimetre datasets with ATLASGAL primarily representing the Inner Galaxy and SASSy, the Outer Galaxy. However, we must first confirm that the two surveys have similar source reliability even though each used a different method for source extraction during the data reduction. In addition to the final source lists,

ATLASGAL and SASSy produced clump mask images marking the extent and location of each detected clump source. To ensure consistency between the survey results, we compared their clump-finding methods. As described in Section 2, ATLASGAL identified clumps using the source extraction algorithm `SExtractor` whereas SASSy used `FellWalker`. We selected an area around the W3 star-forming complex and ran both algorithms using the `SExtractor` parameters given in Contreras et al. 2013. After excluding sources with fewer than 12 pixels, `FellWalker` found 46 sources while `SExtractor` produced 47 sources. The algorithms yielded overall similar results with similar flux densities and only minor variations in pinpointing the centre of a source and in how they distinguished partially blended sources.

We examined the RMS database which includes radio and associated infrared data for a large majority of its objects. Lumsden et al. 2013 had utilised follow-up 5 GHz radio observations from multiple studies to match each source with either GLIMPSE 3.6, 4.5, and 8.0 μm, MIPSGAL 24 and 70 μm, WISE 3.4, 4.6, 12, and 22 μm, or Hi-GAL 70, 160, 250, 350, 500 μm data as available (Benjamin et al. 2003; Carey et al. 2009; Wright et al. 2010; Molinari et al. 2010; respectively). Each MYSO candidate was then classified according to a manual inspection of the results. Comments regarding the reasoning for each classification decision were recorded in the database (see footnote link provided in Chapter 2). The follow-up radio observations were completed with ATCA and the VLA, which was also used in the CORNISH survey. Both CORNISH and the follow-up observations are sensitive to radio emission from angular scales of up to 20″. RMS currently contains over 5,000 objects across the Galactic plane but only ~900 are classified as H II regions which includes both compact and extended sources.

These radio sources were matched with their corresponding submillimetre host clump using positional matching methods. A Python code was written that adopted RMS confirmed H II regions and their galactic coordinate positions and then searched for each of these sources within the appropriate longitudinal range of submillimetre clump mask images which had already been converted into the appropriate sky coordinates system. If a source was found within a clump, the RMS coordinates were returned along with the clump identification number. In the mask images, the pixels between the clumps are given `NULL` values so that any non-matches were passed over and considered outside the clumps. For ATLASGAL sources, we adopted the matches found by Urquhart et al. 2013b and Urquhart et al. 2014d who used similar methods by applying the CORNISH coordinates to `SExtractor` identified ATLASGAL clumps. Next, archival infrared data was inspected. The 3-colour image of the source overlaid with radio and submillimetre contours could be used to confirm proper coincidence and characteristics of an UC H II region

(Urquhart et al., 2013b). RMS H II regions have already been cross-checked against infrared datasets and so only the positional matching for associated ATLASGAL and SASSy clumps remained to confirm the final sample of UC H II regions.

During this procedure, sources are eliminated as UC H II regions if they show signs of the radio emission being outside of or not embedded in a host clump and/or if further inspection of the RMS database revealed that there was no associated dust emission. Of the 900 H II regions listed in RMS, 751 are located in the area of the ATLASGAL survey ($280^\circ \leq l \leq 60^\circ$), with 301 of these lying in the CORNISH region ($10^\circ \leq l \leq 60^\circ$). Urquhart et al. 2013b identified 213 UC H II regions from ATLASGAL-CORNISH matching. Urquhart et al. 2014d matched counterparts between ATLASGAL and RMS sources and found an additional 239 sources. Of these, 49 were located in the CORNISH area that had not been detected previously. We have examined these objects and find that the majority appear to have peak fluxes below the CORNISH sensitivity limit of ~2.7 mJy. Others may have only been detected later as a result of flux variability. Kalcheva et al. 2018 has estimated that ~5% of all H II regions are affected by this trait. The remaining few sources (~5) have flux differences of only a few mJy from the CORNISH sensitivity limits which may be a result of differences between data reduction and/or calibration techniques among the various surveys. Lastly, in the SASSy region ($60^\circ \leq l \leq 240^\circ$), RMS lists 124 H II regions and we identified 84 matches with a SASSy counterpart. Overall, the final catalogue consists of 536 H II regions associated with 445 molecular host clumps covering the Galactic plane with $280^\circ \leq l \leq 240^\circ$ and more than doubling the initial sample size from Urquhart et al. 2013b. We note that there are a relatively small number of matches identified for the SASSy-OGS region but further examination showed that very few of the potential RMS matches in this area had existing radio data.

We are not concerned with the possibility of chance alignments of Galactic dust emission with extragalactic background sources, planetary nebulae, or radio emission from more extended H II regions as these objects were already re-classified as non-H II regions and excluded during the RMS classifications made using follow-up observations.

4.1.1 Distances

Reliable distance estimates are essential for examining the physical properties of the UC H II regions and their host clumps. Maser parallax and spectroscopic distances are the preferred methods as these tend to be more reliable. In our catalogue, we found 20 sources known

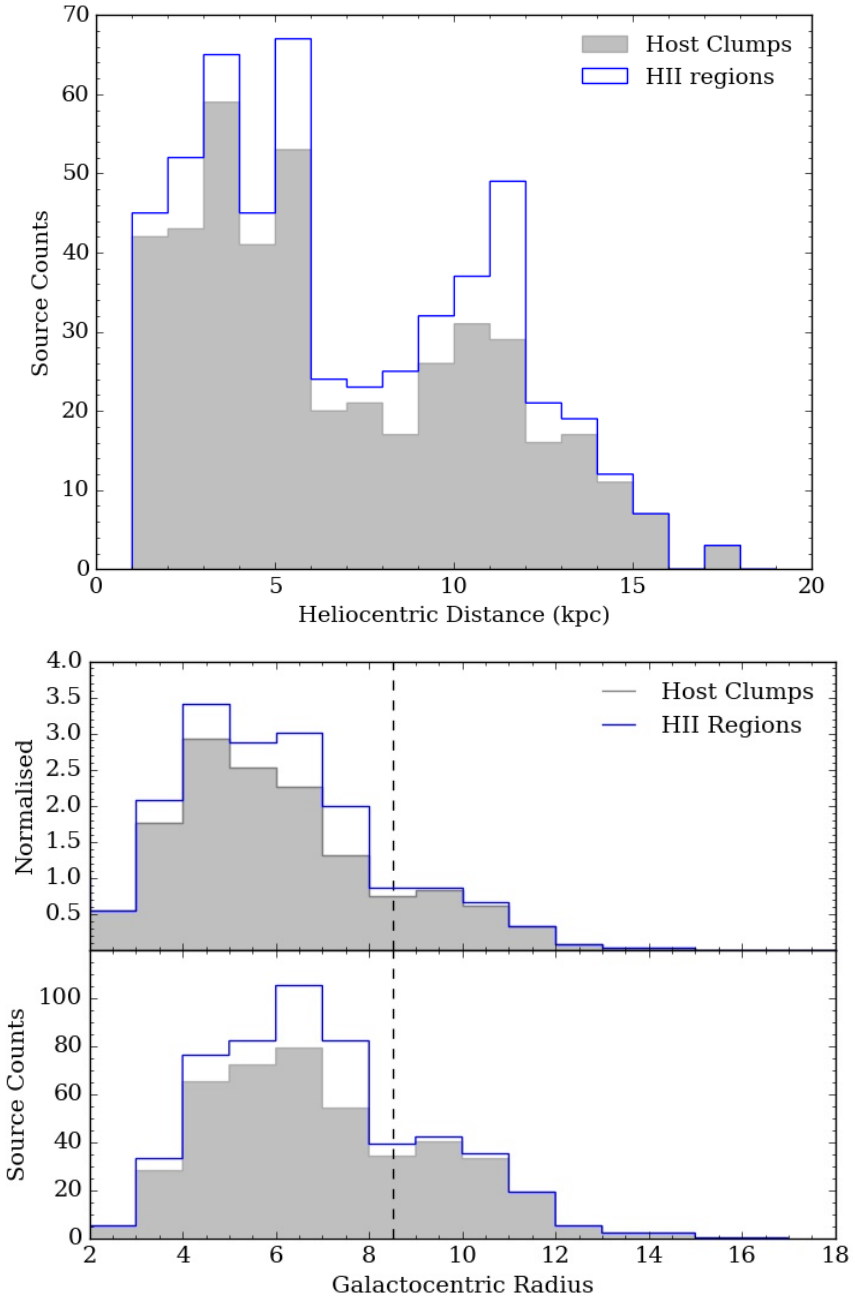

FIGURE 4.1: Distance distributions of host clumps (grey) and their embedded UC H II regions (blue). The upper panel depicts heliocentric distance and shows a relatively complete distribution of distances between 1 and 20 kpc away. This plot is included for direct comparison with the original sample from Urquhart et al. 2013b. The lower panel presents the distribution for galactocentric radius for source counts and normalised source counts by area. The normalised distribution is included to better represent the parts of the Galactic plane that were actually surveyed. The vertical dashed line at R_{GC} = 8.5 kpc represents the location of the sun and the corresponding solar circle which we will use as the boundary between the Inner Galaxy and the Outer Galaxy. On average, the Outer Galaxy will have lower metallicities and higher gas-to-dust ratios when compared to the Inner Galaxy.

to be associated with the Cygnus X region located at an average distance D = 1.4 kpc and R_{GC} = 8.36 kpc (Urquhart et al., 2014b) for which well known parallax information is available and thus their associated uncertainties will be very small compared to the rest of the sample (Rygl et al., 2012).

The remaining sources in our catalogue have kinematic distances. It is important to stress we have chosen to use the updated distance and galactocentric radii values provided by Urquhart et al. 2018 which recalculated kinematic distances for many ATLASGAL clump sources (see distance reference flags included in Table 4.1). Despite the corrections, the radial velocity measurements tend to have a general uncertainty of ±10 km s^{-1} due to systematic errors from streaming motions (Reid et al., 2009). This corresponds to a kinematic distance error of ~0.6-1 kpc. For the SASSy sources, we adopt the distance listed for the corresponding radio source in the RMS catalogue which draws on various references and follow-up studies to provide values for each source (see Urquhart et al. 2007a, 2008a, 2014d and references therein). These values are subject to similar overall distance errors as those found in ATLASGAL. Of the 445 total host clumps, we were unable to determine distances for 6 of them (correlating with 7 H II regions) due to radial velocities not being available in RMS or other literature.

Figure 4.1 shows the complete distribution of distances for both the host massive star forming clumps (grey) and UC H II regions (blue). The upper panel shows the distribution in terms of heliocentric distances with the sample of star forming regions possessing distances ranging from ~ 1 to 20 kpc and is included for direct comparison with Figure 13 in Urquhart et al. 2013b. There are evident peaks in massive star forming clumps around 3, 5, and 12 kpc where there is a higher density of UC H II regions present per clumps. Urquhart et al. 2013b pointed out that these distances roughly coincide with the tangent points of the Galactic spiral arms and the distance between the peaks is larger than the assumed distance errors of ±1 kpc which also describes the approximate average width of a spiral arm (Reid et al., 2009). In the lower panel of Figure 4.1, the sources are re-plotted in terms of galactocentric radius for both a regular distribution of source counts as well as a distribution normalised by area observed. The location of the sun at R_{GC} = 8.5 kpc is illustrated as a vertical dashed line. The sample is dominated by Inner Galaxy sources (~75%) with 334 clumps and 420 H II regions having $R_{GC} \leq 8.5$ kpc. In the Outer Galaxy, the catalogue includes 105 clumps and 109 H II regions. The normalised distribution will better represent the longitudinal limits of the Galactic plane surveys. It shows that the Inner Galaxy is well-sampled while the Outer Galaxy remains more limited by current survey ranges. This is also visible in Figure 4.2 which displays the UC H II regions overlaid on

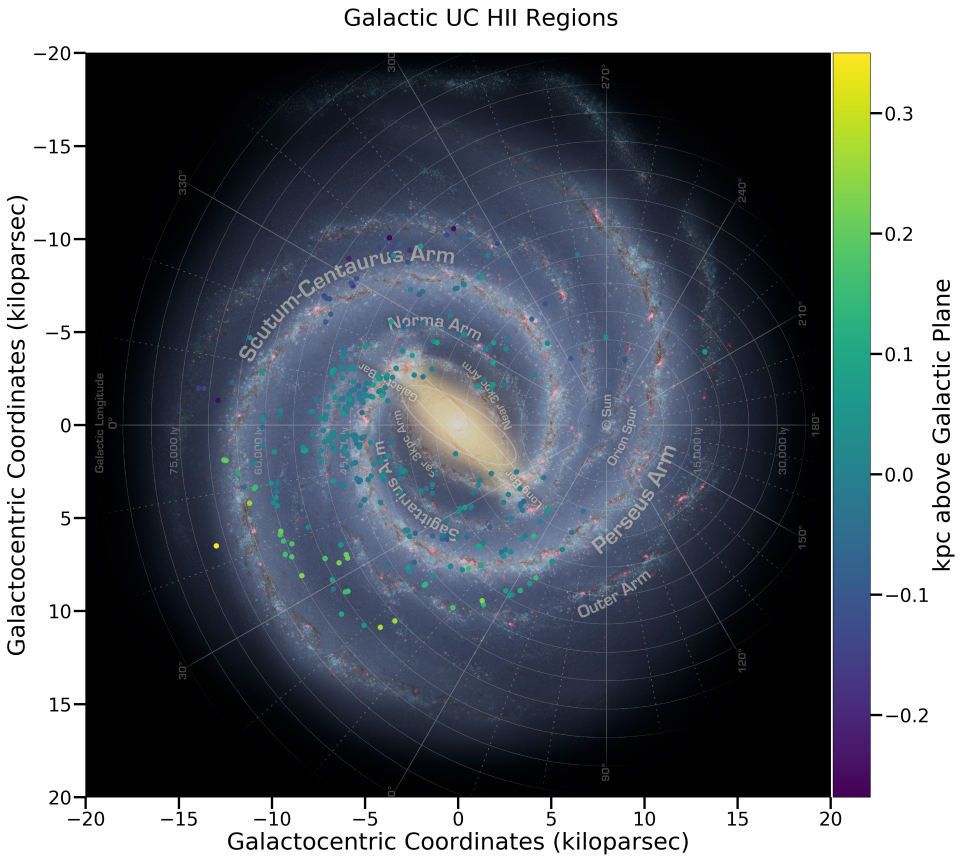

FIGURE 4.2: The UC H II regions are plotted over an artistic portrayal of the Milky Way (Artist, Robert Hurt). Note that for this image, the location of the Sun is on the right side. The map illustrates the positions of the high number of ATLASGAL-RMS matched sources which well-sample the Inner Galaxy. The Outer Galaxy shows fair coverage of the Perseus arm for the SASPER-RMS matched sources. However, the remainder of the Outer Galaxy remains sparse to the limited RMS data available for this region.

the Milky Way. The colours indicates the height in kpc of each above the Galactic plane. (Note that for this image, the Sun is positioned to the right of the image). This map clearly shows the complete sampling of Inner Galaxy clumps thanks to the longitudinal ranges available for both ATLASGAL and RMS. However, the Outer Galaxy (with the exception of the Perseus arm region thanks to SASPER) remains sparse, despite the additional sources that are visible, many of which are not included in previous studies. These limits in the Outer Galaxy are mainly a result of the lack of available matches for this region that currently exist in the RMS catalogue. We will address this issue later in Chapter 5.

In the following sections, we will examine how the properties of these clumps and their embedded UC H II regions vary as a function of galactocentric radius. We will investigate any trends that

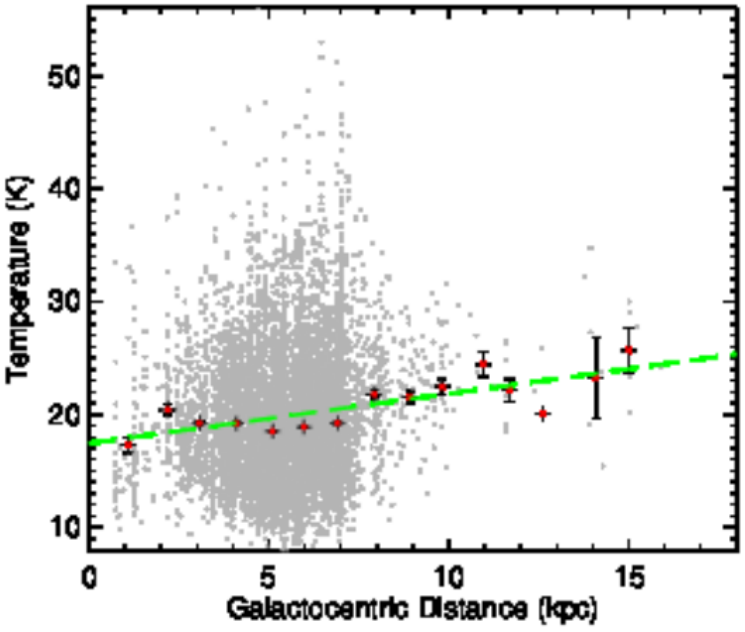

FIGURE 4.3: From Figure 12 of Urquhart et al. 2018 which shows the measured dust temperatures for the full ATLASGAL catalogue as a function of galactocentric radius. The red filled circles portray the average dust temperature with error bars represented by the standard error in the mean. These are averaged in bins of width 1 kpc. The dashed green line shows the results of a linear fit to the data. The averages illustrate a gradual increase in dust temperature with galactocentric radius.

appear, in particular how SFRs and SFEs are affected when viewing the relatively denser and higher metallicity Inner Galaxy versus the sparser, lower metallicity regions of the Outer Galaxy. The inclusion of SASSy data ensures that the sample is investigated out to a galactocentric radius of 12 kpc with additional clumps scattered out to 15 kpc or up to nearly twice the solar radius.

4.1.2 Dust Temperatures

The clump properties for sources adopted from Urquhart et al. 2013b and Urquhart et al. 2014d were initially calculated using a uniform dust temperature of $T_{\rm dust}$ = 20 K across the Galactic plane. However, Urquhart et al. 2018 also obtained individual dust temperatures for each ATLASGAL source, showing that temperatures tend to increase by ~5 K for galactocentric radius between 5 and 15 kpc (see red points indicating average dust temperatures in Figure 4.3 from Urquhart et al. 2018). Due to the amount of scatter present in their data, and the fact that no dust temperatures are currently available for the SASSy clumps, we decided to adopt the average dust temperature from those calculated by Urquhart et al. 2018 and find a mean value of $T_{\rm dust}$ = 27 K. We will use this value to calculate all corresponding clump and H II region

TABLE 4.1: Derived clump properties of the host molecular clumps. The first column gives Submillimetre Name (*AGAL* for ATLASGAL objects; *JCMTLSY* for SASSy) with superscripts denoting publication clump source was adopted from: [1]Urquhart et al. 2013b; [2]Urquhart et al. 2014d; [3]Thompson et. al. in prep. The remaining columns include: Complex that clump belongs to (if any); H II Region Density; Radial Velocity; Heliocentric Distance; galactocentric Radius; Flag denoting source of adopted distance information ([1]Urquhart et al. 2018; [2]Urquhart et al. 2013b; [3]Urquhart et al. 2014d; [4]Adopted from RMS database); Effective Radius of clump; Peak and Integrated submillimetre fluxes; Gas-to-dust Ratio Value with Giannetti et al. 2015 correction; Column Density; Corrected Column Density; Clump Mass; Corrected Clump Mass. Full table available in Appendix B.1. (All log values are based 10.)

Submm Name	Complex	H II	v_{lsr} [km s^{-1}]	D [kpc]	R_{GC} [kpc]	Flag	Radius [pc]	Peak Flux [Jy beam^{-1}]	Int Flux [Jy]	R	Log N_{H_2} [cm^{-2}]	Log N_{H_2} [corr] [cm^{-2}]	Log M [M$_\odot$]	Log M [corr] [M$_\odot$]
[1]AGAL010.299−00.147	W31-North	1	12.8	3.5	4.9	1	2.77	7.67	54.18	73.5	19.13	19	3.38	3.25
[1]AGAL010.321−00.257	W31-South	1	32.2	3	5.4	1	2.48	2.39	14.93	81.25	18.62	18.53	2.69	2.6
[1]AGAL010.472+00.027	–	2	66.7	8.5	1.6	1	5.54	35.01	88.12	37.95	19.79	19.37	4.36	3.94
[1]AGAL037.819+00.412	–	2	18	12.3	7.7	1	3.58	2.94	7.57	128.8	18.71	18.82	3.62	3.73
[1]AGAL037.867−00.601	–	1	50.7	10	6.2	2	1	1.67	5.05	95.37	18.47	18.45	3.26	3.24
[1]AGAL037.874−00.399	–	1	60.8	9.7	6	1	4.4	5.37	18.45	91.62	18.97	18.94	3.8	3.76
[1]AGAL038.646−00.226	–	1	69.2	4.7	5.7	2	0.53	0.84	2.86	86.28	18.17	18.11	2.36	2.3
[1]AGAL038.652+00.087	–	1	-36.5	14.6	9.6	1	2.38	0.77	3.62	188.45	18.13	18.41	3.45	3.72
[2]AGAL346.076−00.056	–	1	-83.9	10.2	2.9	1	5.1	2.38	11.57	49.24	18.62	18.31	3.64	3.33
[2]AGAL346.232−00.321	–	1	-11.5	14.98	7.02	3	1.31	0.78	2.65	112.39	18.14	18.19	3.33	3.39
[2]AGAL347.304+00.014	–	1	-8.9	1.4	7	1	0.16	0.69	1.68	111.94	18.08	18.13	1.08	1.13
[3]JCMTLSY J073538.53−184855.1	–	1	46.8	3.5	10.8	4	0.95	0.27	15.38	239.66	17.7	18.08	2.81	3.19
[3]JCMTLSY J074451.83−240744.3	–	1	66.8	5.4	12	4	2.33	2.52	179.97	304.79	18.67	19.16	4.26	4.74
[3]JCMTLSY J194815.31+280727.4	–	1	-55.3	11.7	11	4	2.19	0.54	0.53	249.46	18	18.4	2.4	2.8
[3]JCMTLSY J194914.48+265010.9	–	1	–	–	–	–	–	0.68	2.39	–	18.1	–	–	–
[3]JCMTLSY J195803.01+314407.3	–	1	-65.5	11.7	11.6	4	2.08	0.33	0.32	281.32	17.79	18.24	2.18	2.63
[3]JCMTLSY J200137.46+333527.5	–	1	-22.9	7.4	9.1	4	3.75	0.54	2.28	170.49	18	18.24	2.64	2.87
[3]JCMTLSY J200145.71+333244.3	–	1	-25.2	7.6	9.2	4	7.8	12.68	47.43	173.94	19.37	19.62	3.98	4.22
[3]JCMTLSY J203900.97+421931.5	–	2	-2.4	1.2	8.3	4	1.52	18.33	143.38	145.24	19.53	19.7	2.85	3.02
[3]JCMTLSY J203901.27+422203.6	–	1	-3.8	1.4	8.3	4	1.09	10.32	50.6	145.24	19.29	19.45	2.54	2.7
[3]JCMTLSY J203925.53+411959.2	–	1	-2	1.4	8.3	4	0.81	1.08	7.28	145.24	18.31	18.47	1.69	1.86
[3]JCMTLSY J204233.19+425645.6	–	1	-4.1	1.4	8.3	4	0.57	1.05	3.33	145.24	18.29	18.46	1.35	1.52
[3]JCMTLSY J205413.82+445408.8	–	1	-35.8	5.5	9.6	4	2.82	1.88	6.02	188.45	18.55	18.82	2.8	3.07

properties as presented in the following sections, with the caveat that if the temperature should actually increase as a function of radius, then we may be overestimating the masses for clumps at higher galactocentric radii.

4.2 Clump Properties

In the following section, we present the physical properties of the molecular clumps which host the sample of UC H II regions. All calculations are based on the distances and temperature assumption described previously. The clump properties for a selection of sources are listed in Table 4.1 with the full catalogue available in Appendix B. The results are also summarised with a series of histograms displaying the data as two subsets representing Inner and Outer Galaxy sources. The Inner Galaxy is normally defined as those sources that have $R_{GC} < 8.5$ and Outer Galaxy sources will have R_{GC} above this value. However, due to the ±1 kpc distance error, we exclude 64 sources within the range of uncertainty. Thus, the figures below display the definite Inner Galaxy sources with $2 \leq R_{GC} < 7.5$ kpc while definite Outer Galaxy sources have $R_{GC} > 9.5$ kpc. We also exclude an additional 6 clumps whose distances could not be obtained. The host molecular clumps are likely to be forming protoclusters of YSOs. The most massive

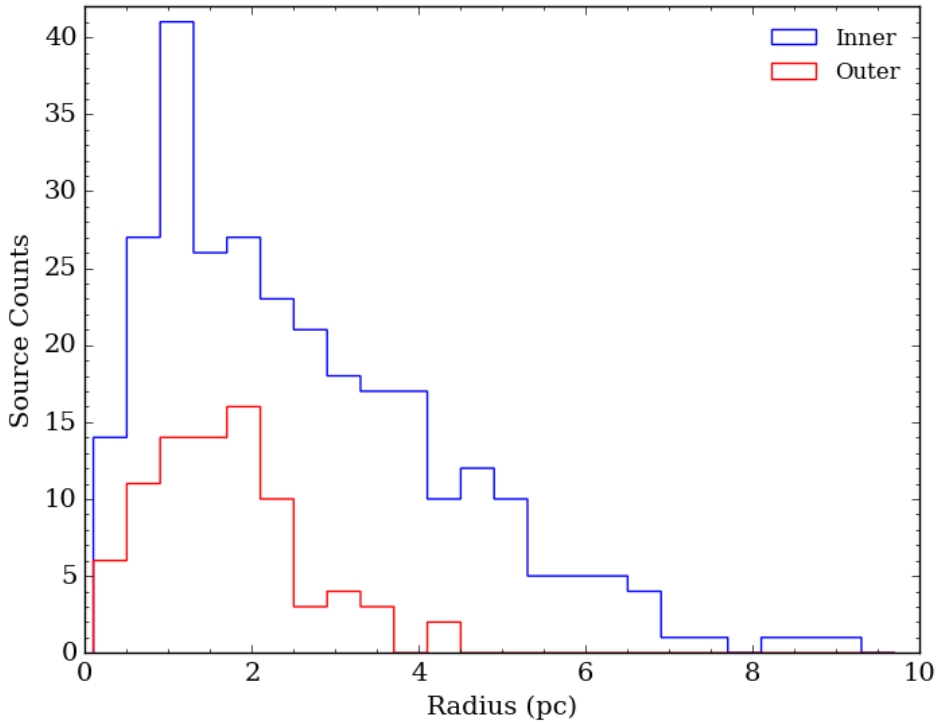

FIGURE 4.4: The distribution of Inner (blue) vs Outer (red) Galaxy sources of effective radii for each clump associated with at least one H II region. Both samples show a peak between 1-2 pc with the Outer Galaxy sources tending towards 2 pc. The Inner Galaxy sources cover a larger range of radii with clumps measuring up to 9 pc while the larger Outer Galaxy clumps cut off around 4 pc. See text for further details. Bin size is 0.4 pc.

members of these protoclusters will be responsible for the majority of the observed bolometric luminosity and Lyman continuum flux.

4.2.1 Clump Radius

Effective radii were derived from source areas observed by corresponding submillimetre data. The approximation as originally presented by Rosolowsky et al. 2010 is

$$R_{eff} = \sqrt{A/\pi} \tag{4.1}$$

where A is the area of the clump. For sources with a known distance, the results were converted to a physical size. The resulting distributions are shown in Figure 4.4 for 289 Inner Galaxy sources (blue) and 83 Outer Galaxy sources (red). Overall, the subsets are similar with peaks between 1-2 pc. However, the larger Inner Galactic sample covers a wider range of radii with sources falling between 0.13 and 12.09 pc while the Outer sources are found in the more limited

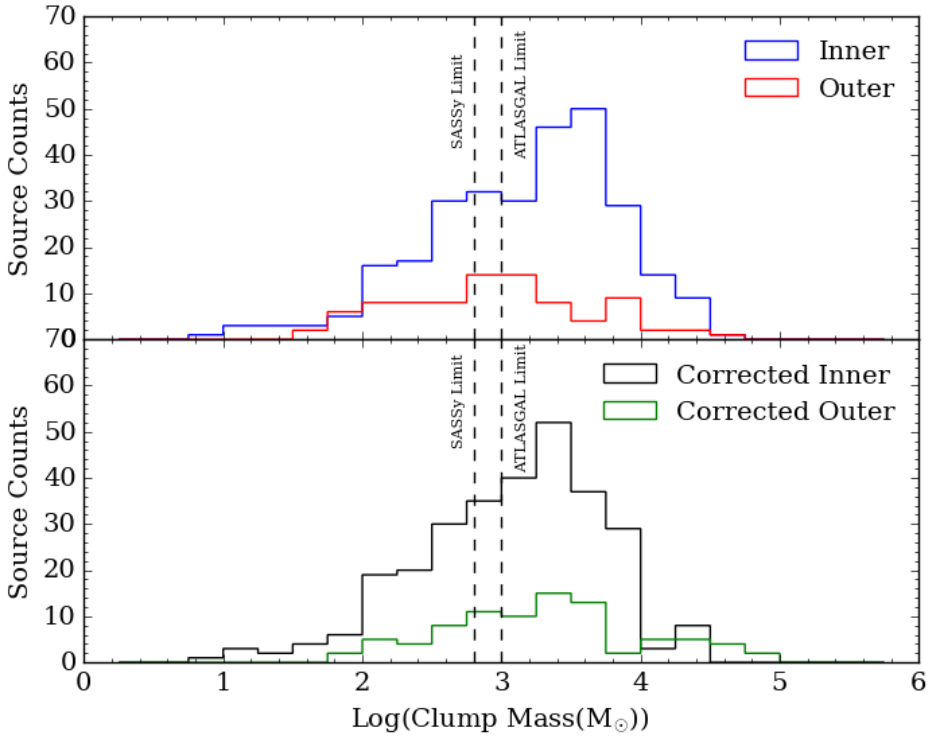

FIGURE 4.5: Upper panel: Distribution of clump masses for Inner and Outer Galaxy sources assuming R = 100. Peaks for Inner and Outer Galaxy subsets are offset, with Inner Galaxy clumps having overall higher masses. Lower panel: Distribution of clump mass after corrections have been made for R with respect to each source's R_{GC}. By the nature of equation (3), Inner Galaxy sources will not be significantly impacted. However, the corrections for Outer Galaxy sources will affect the resulting mass values more dramatically. The peak for Outer Galaxy sources now shifts to higher mass values with the Inner Galaxy subset shifting only a small amount towards lower values. The mass limits for ATLASGAL and SASSy are depicted via the dashed horizontal lines at 10^3 and $10^{2.8}$ $M_\odot$, respectively. Bin size is 0.25 dex.

0.3-4.37 pc range. The average Inner Galaxy clump size is 2.7 pc with a median value of 2.3 pc. The average Outer Galaxy clump is smaller at 1.67 pc and a median of 1.58 pc. This corresponds with the overall closer distances for the SASSy sources which will result in identifying a larger number of smaller sources whose counterparts would not be as readily detected by ATLASGAL. These differences are confirmed via a Kolmogorov-Smirnov test (KS-test) which gives a p-value $\ll 0.001$. Thus, we are able to confidently (within 3σ) reject the hypothesis that the two subsets are drawn from the same parent sample.

4.2.2 Clump Mass

For this work, we will use the mass formula from Hildebrand 1983 which assumes that the submillimetre emission is optically thin and represented by a single dust temperature. Assuming

that the total clump mass is proportional to the total flux density integrated over the source, the equation is

$$M_{\rm clump} = \frac{D^2 S_\nu R}{B_\nu(T_{\rm dust})\kappa_\nu} \tag{4.2}$$

where S_ν is the integrated submillimetre flux in Jy, D is the heliocentric distance in kpc, R is the gas-to-dust mass ratio assumed to be 100 (Draine et al., 2007), B_ν is the Planck function (with $T_{\rm dust}$ = 27 K) which has a value of 7.14×10^{10} Jy/steradian, and κ_ν is the dust absorption coefficient. When these values are inserted into the mass equation, the clump mass can be calculated in terms of solar masses.

Overall, the Planck function is non-linear (See Chapter 1) which can contribute an error of a factor of 2 or 3 in the derived values. We must also recall our assumption that the Galactic disk may be approximated by a uniform dust temperature which may result in us overestimating the clump masses. For the ATLASGAL sources, κ_ν is taken as 1.85 cm^2 g^{-1} (or 3.86×10^{-10} kpc^2 M$_\odot^{-1}$) as derived by Schuller et al. 2009 by interpolating 870 μm from table 1, column 5 of Ossenkopf and Henning 1994. Similarly, we use a value of 1.87 cm^2 g^{-1} (3.90×10^{-10} kpc^2 M$_\odot^{-1}$) for the SASSy 850 μm sources .

The results are shown in the top panel of Figure 4.5. However, it is unlikely this gas-to-dust ratio remains constant throughout the Galaxy. In fact, in the Outer Galaxy, the metallicity and average disk surface density begin to substantially decrease as previously discussed in Chapter 1. In the lower panel of Figure 4.5, we have calculated the ATLASGAL and SASSy clump masses using the corrections found by Giannetti et al. 2015 as given by equation (1.7). Both values are included in Table 4.1. The completeness limits for ATLASGAL and SASSy are also shown at 10^3 M$_\odot$ and $10^{2.8}$ M$_\odot$, respectively. The ATLASGAL limit was adopted from Urquhart et al. 2013b while the representative value for SASSy was estimated by measuring the background rms value of each image and averaging together to represent a flux uncertainty for the full SASSy region. This value was inserted into equation (4.2) along with the maximum observed distance (8 kpc) of a matched SASSy-RMS source to derive the corresponding mass completeness limit.

In the Inner and Outer Galaxy subsets, there are 289 and 86 clumps, respectively. When the gas-to-dust corrections are applied to the mass calculations, we notice an overall shift towards lower values for the Inner Galaxy subset and an opposite shift apparent in the Outer Galaxy sample. Inner Galaxy uncorrected masses peak around 3.8 dex with an average value of 3.14 dex

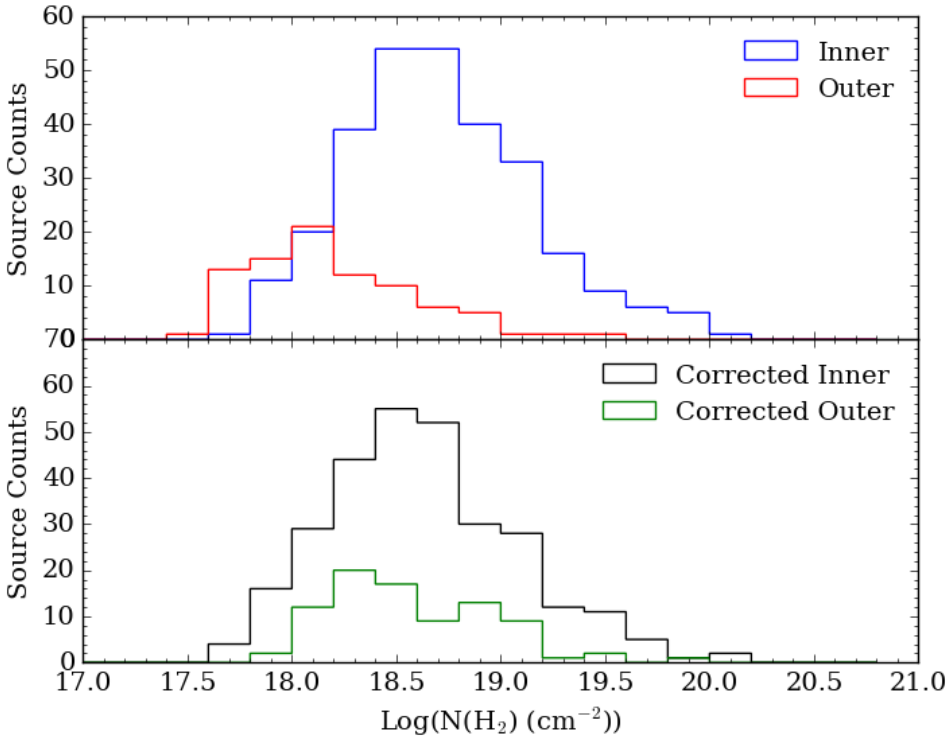

FIGURE 4.6: Upper Panel: Column densities calculated with R = 100. Outer Galaxy sources dominate the lower range of values while Inner Galaxy sources have overall higher values. Lower Panel: Distribution of sources with corrected values of R. Inner and Outer Galaxy subsets align better in peak, and range, with Outer Galaxy sources increasing significantly to higher values. Bin size is 0.2 dex.

and a median of 3.27 dex. These are distinctly different from the Outer Galaxy values of 3, 2.92, 2.93 dex, respectively. With the corrected masses, both subsets show a peak around 3.5 dex. Similarly, the Inner and Outer Galaxy averages (3.06 dex vs. 3.3 dex) and median values (3.18 dex vs. 3.47 dex) also show the relative shifts of each subset.

A KS-test shows that while the Inner vs Outer Galaxy uncorrected masses have a p-value of 0.012, the corrected values possess an even lower p-value of 0.006, This result suggests that there is a < 1 % chance that our rejection of the null hypothesis is incorrect. However it remains outside the established $p \ll 0.001$ confidence level. Later, we will re-examine the clump masses as they correlate with other parameters of the star forming clumps and embedded UC H II regions to better cancel out corresponding sources of error.

TABLE 4.2: Derived H II region properties for a selection of the full sample. Columns are as follows - Radio Name (in galactic coordinates); Submillimetre Name (as previously defined); Offset between radio and submillimetre centres; Radio Peak and Integrated fluxes; Angular Diameter; Physical Diameter; Frequency of observations; Lyman continuum flux; Bolometric Luminosity; Associated Ratios as discussed in Section 6. Full table available in Appendix C.1. (All log values are base 10.)

Radio Name	Submm Name	Offset [']	Peak Flux [mJy beam^{-1}]	Int Flux [mJy]	d [']	d [pc]	Freq [GHz]	Log N_{Ly} [photons s^{-1}]	Log L_{bol} [$L_\odot$]	Log L_{bol}/M	Log L_{bol}/M_{corr}	Log N_{Ly}/M	Log N_{Ly}/M_{corr}
[1]G010.3009−00.1477	AGAL010.299−00.147	5.2	56.37	631.39	5.2	0.09	5	47.84	5.17	1.79	1.92	44.46	44.59
[1]G010.3204−00.2586	AGAL010.321−00.257	4.1	14.61	18.2	–	–	5	46.17	–	–	–	43.48	43.57
[1]G010.4736+00.0274	AGAL010.472+00.027	3.9	12.3	19.3	1.4	0.06	5	47.1	5.65	1.29	1.71	42.73	43.16
[1]G010.4724+00.0275	AGAL010.472+00.027	0.8	22.34	38.43	1.7	0.07	5	47.4	5.65	1.29	1.71	43.03	43.45
[1]G010.6240−00.3813	AGAL010.624−00.384	10.6	38.23	71.65	1.4	0.03	5	47.21	5.72	1.69	1.94	43.18	43.43
[1]G010.6218−00.3848	AGAL010.624−00.384	8.5	16.81	37.06	1.7	0.04	5	46.92	5.72	1.69	1.94	42.9	43.14
[2]G031.0709+00.0508	AGAL031.071+00.049	4.52	8.3	248.6	–	–	5	47.21	3.76	1.9	1.92	45.35	45.37
[1]G031.1596+00.0448	AGAL031.158+00.047	12.4	18.7	23.83	–	–	5	46.19	3.27	0.9	0.92	43.82	43.84
[1]G031.1590+00.0465	AGAL031.158+00.047	6.4	3.89	7.04	1.4	0.02	5	45.66	3.27	0.9	0.92	43.29	43.31
[1]G031.2435−00.1103	AGAL031.243−00.111	4.1	133.77	353.06	2.2	0.14	5	48.72	5.28	1.6	1.53	45.04	44.97
[2]G302.0218+00.2539	AGAL302.021+00.251	11.9	47.89	59.48	0.81	0.02	4.8	46.99	3.92	1.2	1.14	44.27	44.22
[2]G302.1525−00.9485	AGAL302.149−00.949	11.73	5.66	39.17	6.52	0.35	4.8	47.64	4.52	1.41	1.13	44.52	44.24
[2]G302.4868−00.0315	AGAL302.486−00.031	4.42	10.18	23.41	2.67	0.04	4.8	46.33	3.73	1.21	1.15	43.81	43.74
[2]G303.1173−00.9714	AGAL303.118−00.972	3.19	192.9	411.8	2.45	0.02	4.8	46.98	3.03	1.62	1.52	45.57	45.47
[2]G303.5351−00.5971	AGAL303.536−00.597	3.08	5.04	8.68	2.05	0.1	4.8	46.93	4.03	0.82	0.59	43.72	43.49
[2]G303.9976+00.2801	AGAL303.999+00.279	6.85	6.56	33.04	4.97	0.28	4.8	47.6	4.23	1.35	1.06	44.73	44.43
[3]G064.1528+01.2817	JCMTLSY J194815.31+280727.4	5.03	12.6	25.7	–	–	5	47.5	4.3	1.9	1.5	45.1	44.7
[3]G111.1919−00.7965	JCMTLSY J231545.69+595239.3	7.05	–	1.1	–	–	5	45.26	3.76	2.2	1.83	43.7	43.33
[3]G111.2824−00.6639B	JCMTLSY J231603.89+600153.8	4.47	6.5	90.8	–	–	5	47	4.37	1.38	1.06	44.01	43.69

4.2.3 Column Density

Column densities (in units of cm^{-2}) are derived from the peak submillimetre flux of the clumps using the definition

$$N_{H_2} = \frac{S_\nu R}{B_\nu(T_{dust})\Omega\kappa_\nu\mu m_H} \tag{4.3}$$

where Ω is the beam solid angle in steradians, μ is the mean molecular weight of the gas which we assume to be 2.8 (Kauffmann et al., 2008), m_H is the mass of a hydrogen atom in grams, and κ_ν and R are as defined previously (using the original units of cm^2 g^{-1} for κ_ν). Once more, we assume $T_{dust} = 27$ K and use $B_\nu = 7.14 \times 10^{10}$ Jy/steradian. The distribution of column densities is shown in Figure 4.6 where the upper panel uses $R = 100$ and the lower panel shows the values obtained using the Gianetti corrections.

Both the Inner and Outer Galaxy subsets have an approximate range of ~17.5-20 dex. After the R corrections, the Inner Galaxy peak shifts from 18.75 to 18 dex, with the Outer Galaxy peak also moving to ~18.5 dex from 18 dex. The Inner Galaxy pre-correction values for the median and mean column densities are 18.68 dex and 18.71 dex while the Outer Galaxy has corresponding stats of 18.12 dex and 18.19 dex. After the corrections, the Inner Galaxy median and mean become 18.58 dex and 18.63 dex with the Outer Galaxy similarly shifting to 18.49 and 18.57 dex. A KS-test gives a p-value of 0.04 which does not allow us to reject the null hypothesis.

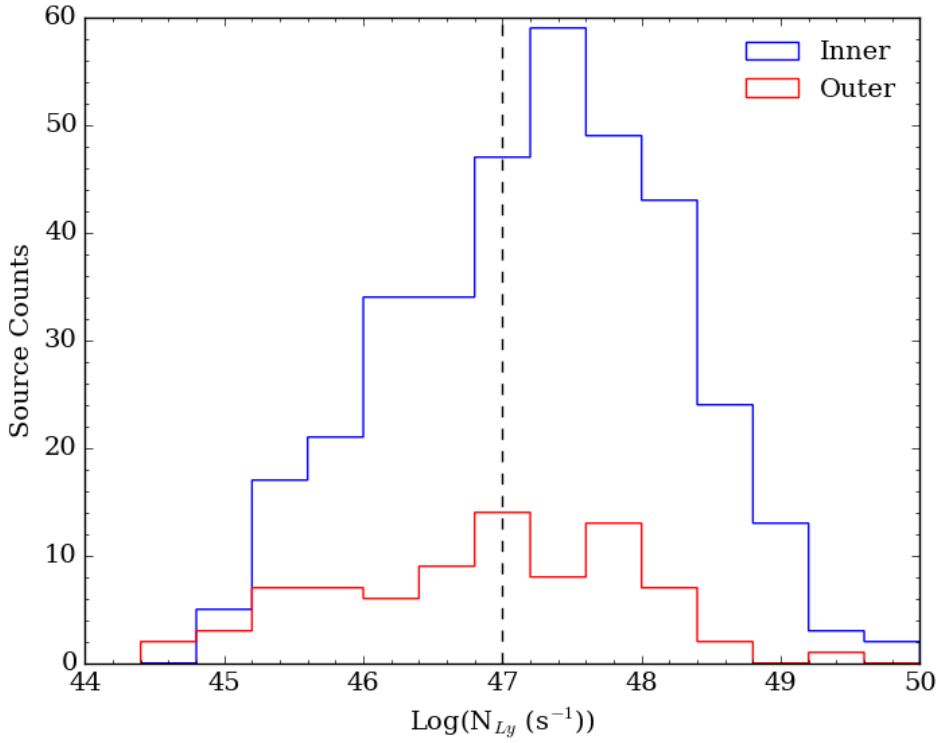

FIGURE 4.7: Lyman continuum flux distribution for Inner (blue) and Outer Galaxy H II regions. The VLA completeness limit at 10^{47} photons s^{-1} is shown as the vertical dashed line. The Outer Galaxy sources show a much flatter distribution when compared to the Inner Galaxy subset which peaks near the completeness limit. Bin size is 0.4 dex.

4.3 H II Region Properties

We now examine the properties of the embedded UC H II regions using radio measurements obtained from CORNISH or the RMS database. Once more, we present the number distributions of these parameters with regards to Inner and Outer Galaxy subsets. A selection of UC H II regions is given in Table 4.2. The full catalogue is available in Appendix C.

4.3.1 Lyman Continuum Flux

For a massive star, one can derive the Lyman continuum flux from the radio continuum using the following equation originally presented by Carpenter et al. (1990).

$$N_{\rm Ly} = 9 \times 10^{43} \left(\frac{S_\nu}{\rm mJy}\right)\left(\frac{D}{\rm kpc}\right)^2 \left(\frac{\nu}{5\,\rm GHz}\right)^{0.1} \text{photon s}^{-1} \tag{4.4}$$

where S_ν is the integrated radio flux measured at a frequency ν and D is the heliocentric distance. We assume that the UC H II regions are optically thin and that the calculations will significantly underestimate the Lyman continuum flux for more compact H II regions which will be optically thick at $\nu = 5$ GHz. The typical Lyman continuum flux error is ~20%, taking into account the 10% errors in both distance and the average flux measurement from RMS.

Figure 4.7 shows the distribution of fluxes for the 350 Inner (blue) and 81 Outer (red) Galaxy sources. Radio observations for both CORNISH and RMS data were obtained with either VLA or ATCA, giving a consistent completeness limit of $\sim 10^{47}$ photons s^{-1}. Both subsets have a similar range and peak near this value, although the Outer Galaxy sources have a flatter distribution. The medians for both subsets also fall near the limit at 47.29 dex for the Inner Galaxy and 46.95 dex for the Outer Galaxy as do the mean values of 47.24 dex and 46.79 dex, respectively. A KS-test yields a p-value of 0.017. In this case, we are unable to reject the null hypothesis that the H II regions are derived from the same parent distribution. This fact will be relevant for further discussion.

4.3.2 H II Region Size

Physical sizes for the UC H II regions of each subset are given in Figure 4.8. The Outer Galaxy sample has a much smaller range falling between 0.1 and 0.5 pc in diameter, while Inner Galaxy sources have an upper limit closer to 1 pc. Nonetheless, both samples show most H II regions falling within the compact and UC limits, as expected. The dashed vertical lines represent the arbitrary size limits usually assigned to UC, compact, and classical H II regions. Both Inner and Outer Galaxy sources have a mean and median value around 0.1pc. The Inner Galaxy outliers with $d > 0.5$ pc appear to be objects that had the highest angular sizes and also fell near to the distance error cutoff limits around $R_{GC} = 8.5 \pm 1$ kpc. These objects will suffer the most from the associated distance uncertainties, thus skewing calculations for the physical diameter. All sources fall well below the maximum accepted 1 pc limit and may be regarded as 'compact' sources. Associated uncertainties will be dominated by the distance errors. A KS-test gives a p-value result of $p \ll 0.001$ and the null hypothesis may once again be rejected.

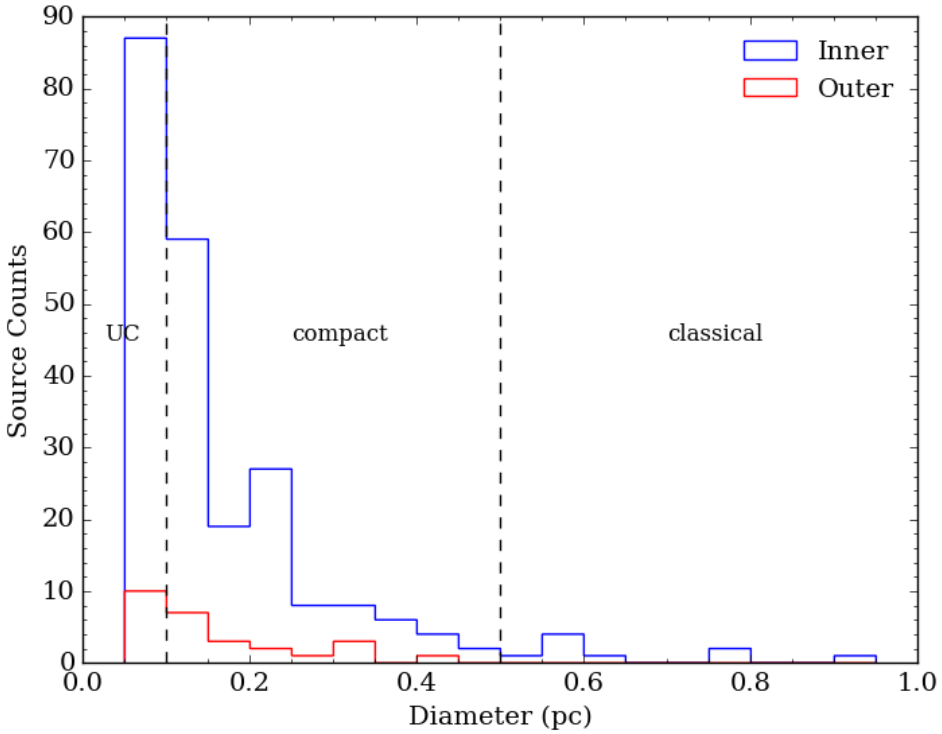

FIGURE 4.8: Distribution for diameter sizes of H II regions. Vertical lines represent the cut-offs for UC, compact, and classical H II regions normally used in the literature. Though these limits are not firmly set, the majority of sources in both samples fall within the most compact areas limits indicating that we are indeed tracing regions of very recent massive star formation. The Outer Galaxy subset is substantially smaller due to the lack of radio information in that region of the Galaxy and we were unable to obtain major and minor axis measurements for a larger portion H II regions associated with SASSy sources. Bin size is 0.05 pc.

4.3.3 Bolometric Luminosity

The use of RMS allows us to include the estimated bolometric luminosities of each source (Mottram et al., 2011b,a). The RMS survey is complete to a few 10^4 $L_\odot$ for the population of mid-infrared-selected H II regions and MYSOs sample. Urquhart et al. 2013b noted that this made it well matched to comparisons with CORNISH and we extend that comparison with our additional collection of H II regions.

In Figure 4.9, the Inner Galaxy sources cover a wider range with ~2-6.5 dex while the Outer Galaxy subset is more limited between 3-6 dex. These correspond with the limits of 10^3 $L_\odot$ for a B3 star and 10^6 $L_\odot$ for an O3 star, respectively (Martins et al., 2005). The Inner Galaxy sample peaks at 5 dex but the Outer Galaxy peak is closer to ~4.3 dex. The median and average luminosity values for the Inner Galaxy are identified to both be around 4.6 dex while the Outer Galaxy values fall near 4.3 dex. The same trend appears for average and median values with Outer Galaxy sources having average luminosities of 4.22 dex vs. the Inner Galaxy's 4.62 dex and an

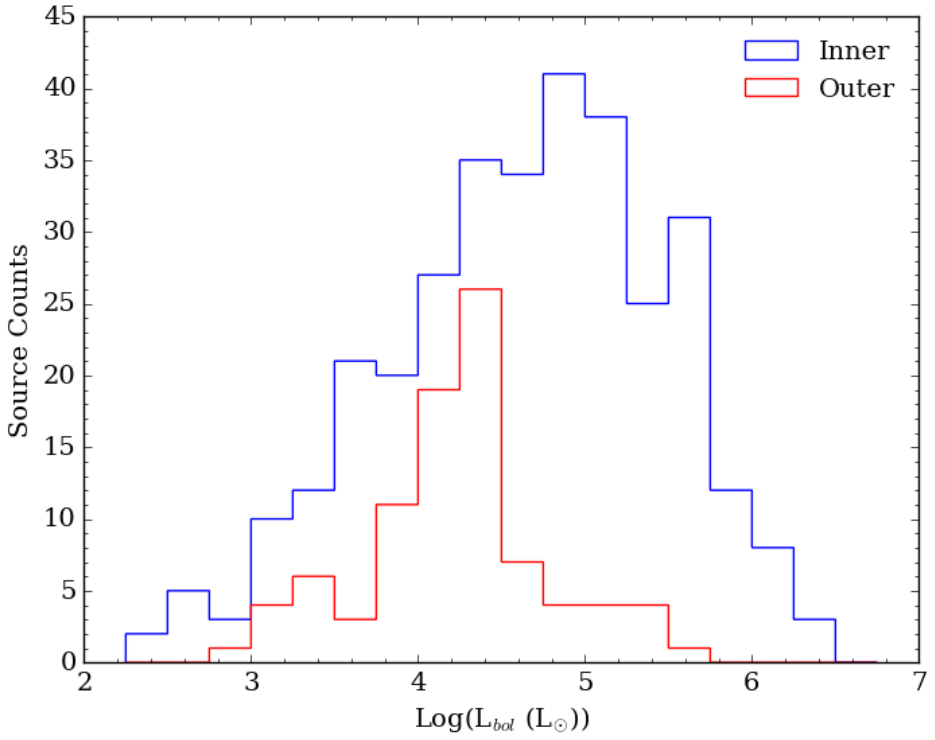

FIGURE 4.9: Bolometric luminosities for both subsets were adopted from the RMS catalogue. Though they share similar ranges, the peak of the Outer Galaxy sources is shifted towards lower luminosities, whereas the Inner Galaxy sources have overall higher values. See text for further details. Bin size is 0.25 dex.

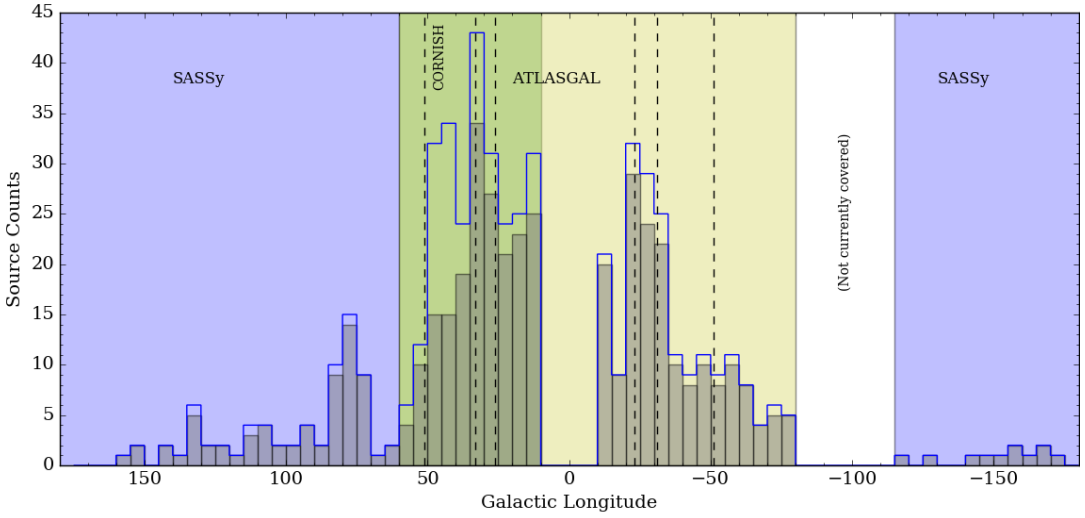

FIGURE 4.10: The distribution in Galactic longitude for the complete sample. Host clumps are shown as the filled histogram with H II regions as the blue line. The background has been shaded according to the submillimetre survey which studied the corresponding longitudinal range. CORNISH has also been highlighted to illustrate the scope of the original catalogue. The inclusion of the rest of ATLASGAL and the more recent SASSy data greatly increase the area covered. Peaks can be observed where particularly intense regions of star formation have a high multiplicity of H II regions per host clump. Vertical dashed lines indicate mean tangent points for spiral arms for reference within survey area as compiled by Vallee and P. 2014. Bin size is 5 degrees.

Outer Galaxy median at 4.26 vs. the Inner Galaxy median of 4.73 dex. A KS-test conclusively rejects the null hypothesis with $p \ll 0.001$. The fluxes used to estimate the luminosities are effectively clump-averaged values and thus, are a measure of the total luminosity of the embedded YSOs. In reality, it will not be a single star embedded within the H II region but several with the most massive star being a few subclasses later than expected. Typical errors for these values are approximately 34% (Mottram et al., 2011a).

4.4 Discussion

The supplementary UC H II regions have more than doubled the sample size of the original ATLASGAL-CORNISH study. With an additional 323 H II regions and 275 host clumps, the total UC H II region catalogue now includes 536 UC H II regions associated with 445 molecular clumps. These cover a wide range of Galactic longitudes encompassing ~80% of the Galactic plane. The farthest object is nearly 20 kpc away from the Sun and we have extended the sample to include sources out to $R_{GC} \sim 15$ kpc, allowing us to examine any trends in massive star formation across a more complete scope of Galactic plane variation.

4.4.1 Galactic Distribution

Figure 4.10 shows the Galactic longitude distribution of the full catalogue. Host clumps are plotted as the filled grey histogram and the embedded H II regions are shown as the blue line. The addition of the remaining ATLASGAL and SASSy regions allows the total sample to cover the majority of the Galactic plane with the exceptions of $-120^\circ \leq l \leq -80^\circ$ for which there are currently no equivalent submillimetre observations, and the Galactic centre ($-10^\circ \leq l \leq 10^\circ$) that we have avoided due to source confusion. Peaks in the number of H II regions per clump are clearly seen, indicating areas of intense star formation. These correspond to well known star forming complexes. For example, the effects from W43, W51, and W49A are visible within $30^\circ \leq l \leq 50^\circ$ (Eden et al., 2017; Urquhart et al., 2014d).

Figure 4.11 shows the distribution in Galactic latitude. ATLASGAL observed sources with $|b| < 1.5^\circ$ while the SASSy range included those with $|b| < 2^\circ$. In the Inner Galaxy, star formation appears to be mostly restricted to the Galactic plane with a skew towards negative latitudes due to the Sun's position as well as from the observed warp in the Galactic plane. The Outer Galaxy shows a broader distribution. This is in part due to the fact that the molecular disk

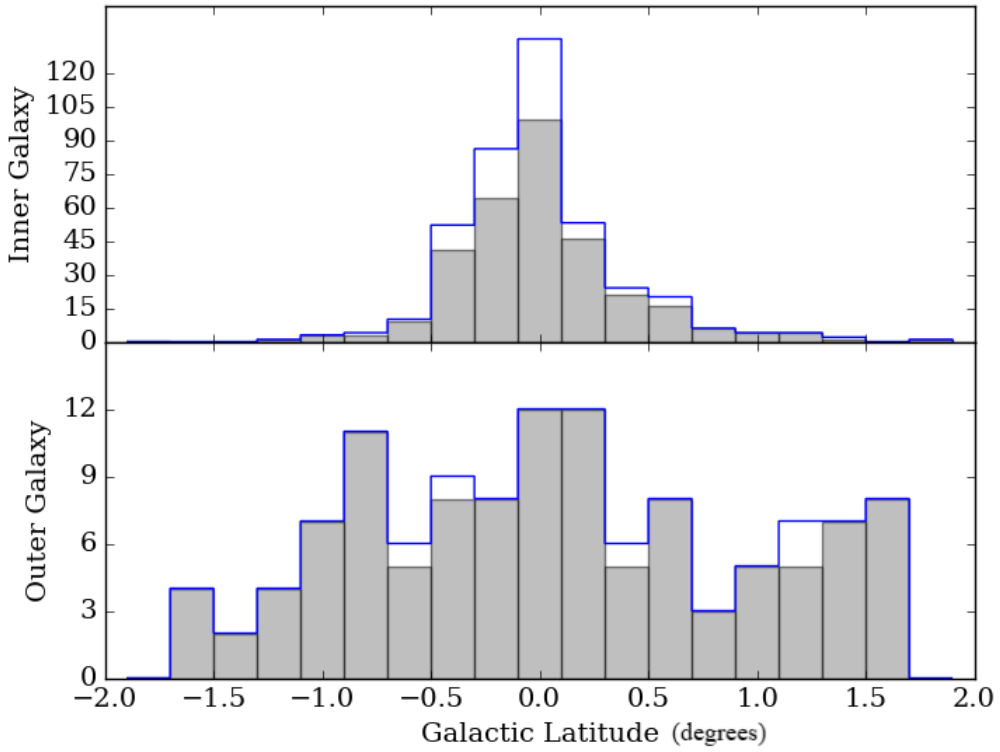

FIGURE 4.11: Distribution for star forming clumps (grey filled) and embedded H II regions (blue line) of the complete sample. The upper panel illustrates the distribution for sources with $R_{GC} < 8.5$ and the lower panel shows the same for sources with $R_{GC} > 8.5$. The broader distribution of the Outer Galaxy is in part due to the flare in the molecular disk with increasing radius also from projection, with closer sources such as those found in SASSy having higher observed angles than the ATLASGAL sources observed at much farther distances. Bin size is 0.2 degrees.

flares out with galactocentric radius (Wouterloot et al., 1990) and also the overall closer SASSy sources will have larger ranges of latitudes observed than the more distant ATLASGAL sources.

4.4.2 Galactic Trends

4.4.2.1 Clump Mass & Lyman Continuum Flux

In Figure 4.12, we examine the relationship between clump mass and galactocentric radius. The estimation of clump masses relies heavily on accurate distance measurements and we must be cautious of the completeness limits associated with each survey to ensure that any trends we may observe are not a result of the Malmquist bias. ATLASGAL observed across the Inner Galaxy mid-plane covering $280° \leq l \leq 60°$, while SASSy was directed away from the centre and examined the overall closer regions of the Perseus arm and nearby Outer Galaxy which includes $60° \leq l \leq 240°$ (see Figure 2.1). We determined their respective sensitivity limits by considering

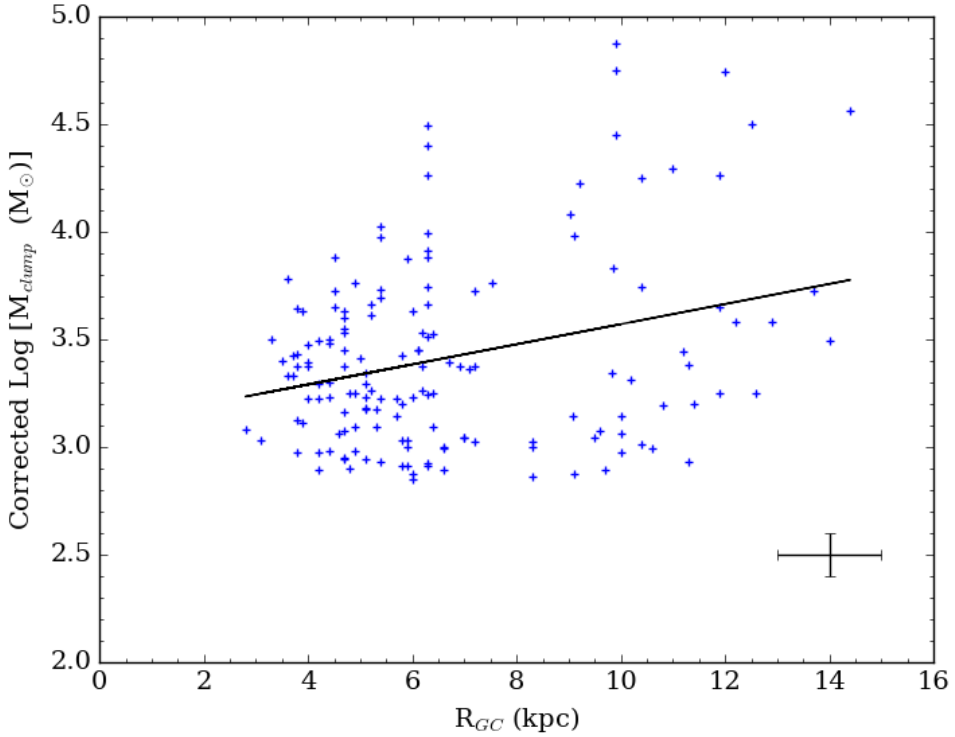

FIGURE 4.12: Corrected masses of host star forming clumps as a function of galactocentric radius. We have applied a uniform mass cutoff limit of $10^{2.85}$ $M_\odot$ and removed sources with $D > 8$ kpc. An unweighted linear approximate fitted to the data suggests that the data is relatively flat with slope of 0.05 ± 0.01. See text for details.

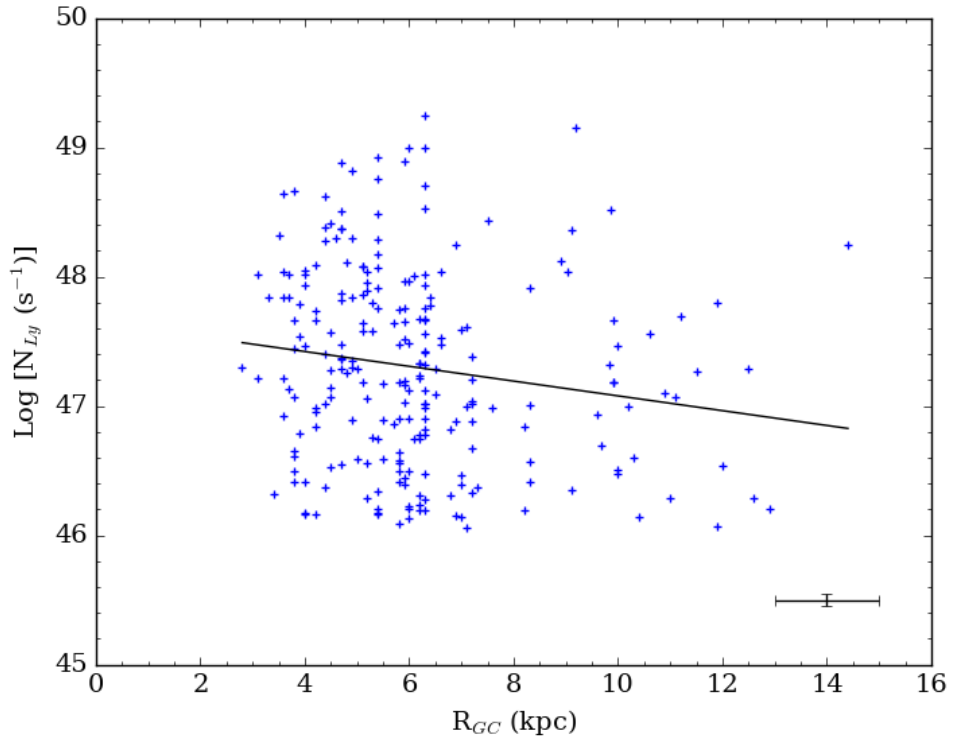

FIGURE 4.13: The relationship of Lyman continuum flux to galactocentric radius of UC H II regions above the flux completeness limit of $10^{46.06}$ photons s^{-1} and with $D > 8$ kpc.

a hypothetical source at a distance of 8 kpc. At this range, ATLASGAL is complete for all Inner Galaxy sources ($R_{GC} \approx 2-8$ kpc) and SASSy is complete for the Outer radii ($R_{GC} \approx 8-15$ kpc). Using a significance level of 5σ and adopting the average rms values for each survey, we calculated mass completeness limits of $10^{2.85}$ $M_\odot$ and $10^{2.48}$ $M_\odot$ for ATLASGAL and SASSY, respectively. For consistency, we used the higher of these values and removed any sources that fell below $10^{2.85}$ $M_\odot$. We also removed sources with heliocentric distance $D > 8$ kpc since we will not be able to detect a complete distribution in masses beyond this boundary. In the end, we are left with 154 clumps, ranging from $\sim 10^3$ to 10^5 $M_\odot$ (using corrections from Giannetti et al. 2015 as previously discussed) across $R_{GC} = 2-15$ kpc. Representative error bars are given in the lower right corner of Figure 4.12.

We also calculated the equivalent completeness limits for the Lyman continuum fluxes. Once more, we consider a source at the maximum distance (8 kpc) and use the mean rms values as found in the RMS radio follow-up and CORNISH survey papers (Urquhart et al. 2007b; Urquhart et al. 2009; Purcell et al. 2013). The same 5σ significance level is applied. We find Lyman flux cutoffs at $10^{45.93}$ and $10^{46.06}$ photons s^{-1} for RMS and CORNISH data, respectively. We again implemented the higher limit of $10^{46.06}$ photons s^{-1} as well as the distance cutoff limit for sources with $D > 8$ kpc. The results are plotted as a function of R_{GC} in Figure 4.13 for 238 UC H II regions.

Both Figures 4.12 and 4.13 contain a great deal of scatter in the data, particular with sources in the Outer Galaxy. In the case of Lyman flux, the Inner Galaxy sources are significantly scattered, as well. To better interpret the data, we included trendlines representing the unweighted least squares linear regression fits for each dataset. In Figure 4.12, clump mass appears to increase with increasing R_{GC} but has a relatively flat slope of $+0.05 \pm 0.01$ kpc^{-1}. We recall that our use of a single average dust temperature for all sources ($T_{dust} = 27$ K) may result in overestimating clump masses at higher radii. Indeed, a Spearman rank test gives a correlation of 0.123 with a high p-value of 0.11. We determine that the recorded slope is consistent with being flat and conclude that there is no correlation between clump mass with galactocentric radius. In Figure 4.13, we observe an overall decrease in Lyman flux but with another shallow slope of -0.06 ± 0.02 kpc^{-1} and there is a large amount of scatter present. The scatter is likely a result from using the optically thin assumption for all H II regions which would underestimate the Lyman continuum flux for the most compact regions that are optically thick at $\nu = 5$ GHz. A Spearman test gives a correlation of -0.078 with another high p-value of 0.22. We conclude that there is no significant correlation between Lyman continuum flux with galactocentric radius. In the next step, we will

examine the distance-independent variables of $N_{\rm Ly}/M$ and $L_{\rm bol}/M$ and how their corresponding trends correlate with previous studies.

4.4.2.2 A Proxy for Star Formation Efficiency & Related Quantities

By examining the Lyman flux and the luminosity of the H II regions per unit mass, we are able to remove the distance dependence. As such, $N_{\rm Ly}/M$ will serve as a proxy for the massive star formation efficiency while $L_{\rm bol}/M$ will represent the overall star formation efficiency in massive star forming clumps but includes both the low and high mass stars. This gives us the added benefit of being able to study the whole catalogue as we no longer have to eliminate sources due to completeness limits.

These distance-independent parameters are shown in Figures 4.14 and 4.15 with colours indicating heliocentric distance in kpc. Although Figure 4.14 shows a mostly flat trend, the Outer Galaxy sources tend to be overall closer in distance and there is a high degree of scatter caused by farther away ATLASGAL sources. For the 518 H II regions plotted, we estimate a gradient of 0.001 ± 0.04 and a a Spearman test gives a correlation number of -0.075 with p-value of 0.24 which remains well above our desired confidence level and thus shows no significant correlation. This may indicate inconsistency in ATLASGAL sensitivity limits compared to SASSy. If this is the case and taken with the high degree of scatter, it is likely that the gradient of the trendline would be pulled downwards and massive star formation efficiency may likely decrease with increasing galactocentric radius. Figure 4.15 shows a clear downward trend suggesting that overall star formation efficiencies are lower in the Outer Galaxy than in the Inner Galaxy. Figure 4.15 yields a slope of -0.1 ± 0.008 kpc^{-1} and this decline over $R_{\rm GC}$ can be confirmed with the Spearman rank test giving a correlation of -0.258 with a p-value $\ll 0.001$. Thus, we conclude that the overall star formation efficiency for massive star forming clumps is decreasing and is lower in the Outer Galaxy.

While there has been little previous investigation into these exact quantities as a function of galactocentric radius, Lada et al. 2010 previously showed that star formation was observed to be closely correlated with dense gas. The decline in overall star formation efficiency seen in Figure 4.15 is mirrored in the results by Roman-Duval et al. 2016 who traced the ratio of dense (^{13}CO-emitting) gas surface density to the total (^{12}CO + ^{13}CO) gas surface density and found an average gradient of $-0.06\,$kpc^{-1} over $3 \leq R_{\rm GC} \leq 8\,$kpc. A decreasing trend is also seen in Nakanishi and Sofue 2006 who plotted the molecular gas surface density as a

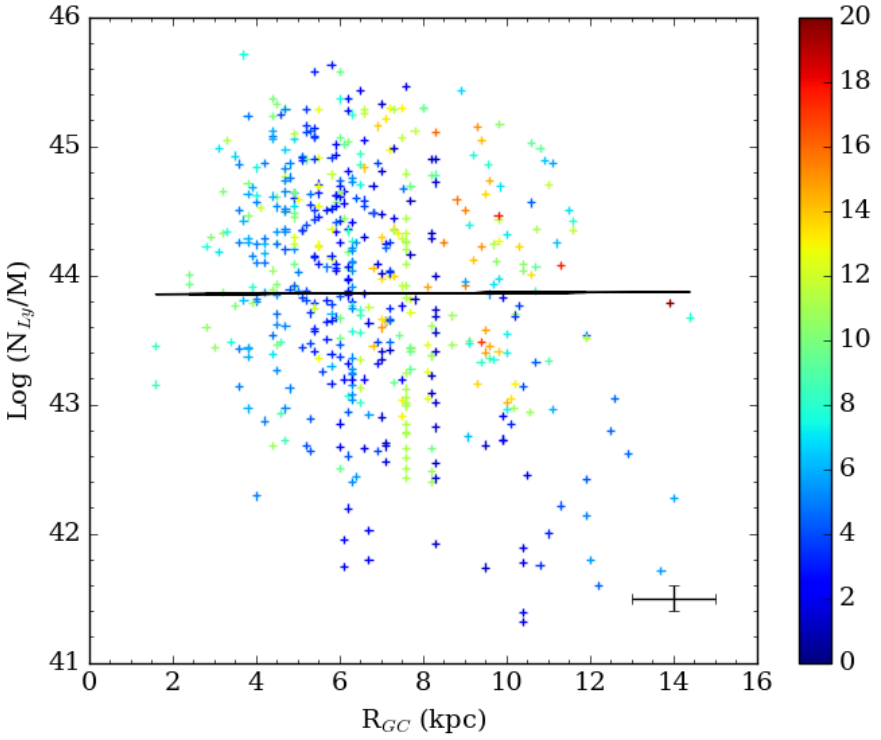

FIGURE 4.14: The Lyman continuum flux or rate of UV-photon output per unit mass serves as a proxy for the star formation efficiency of the most massive stars. By focusing on this relation, we are able to examine the entire sample of UC H II regions because the shared reliance of N_{Ly} and M on D^2 cancels out to create a distance-independent value. However, we have still colour-coded the H II regions according to heliocentric distance (kpc) to determine if sensitivity limits may be creeping into the results. When this is plotted as a function of galactocentric radius, we observe a flat trend but the scatter presents a high degree of uncertainty. We also notice that the higher R_{GC} sources tend to have overall closer heliocentric distances. If ATLASGAL is not complete for lower masses and given the high degree of scatter already present, it is possible that these Outer Galaxy sources may succeed in pulling the gradient of the trendline downwards. See text for details.

function of galactocentric radius and found a noticeable decline, dropping steeply just beyond the solar neighbourhood or the start of the Outer Galaxy by our previous definition. The same was observed in the nearby galaxy NGC 6946 by Schruba et al. 2011. Misiriotis et al. 2006 presented an estimate of the surface density of the star formation rate which declined steeply past $R_{GC} = 5$ kpc though the data was acquired from older COBE observations of extended H II regions (Boggess et al., 1992). Finally, Ragan et al. 2016 defined a star forming fraction (SFF) as the ratio of Hi-GAL objects associated with a 70 μm component with the total catalogue of Hi-GAL sources. The SFF may be considered as the fraction of dense clumps with embedded YSOs. They derived a mean SFF in the Galactic disk ($3.1 < R_{GC} < 8.6$ kpc) of 25% that declined with R_{GC} at a rate of -0.026 ± 0.002 kpc^{-1}. However, a few other studies have found no change in the dense gas between the Inner and Outer Galaxy, including Battisti and Heyer 2013 who defined a dense gas mass fraction as the ratio of the mass traced by submillimetre dust

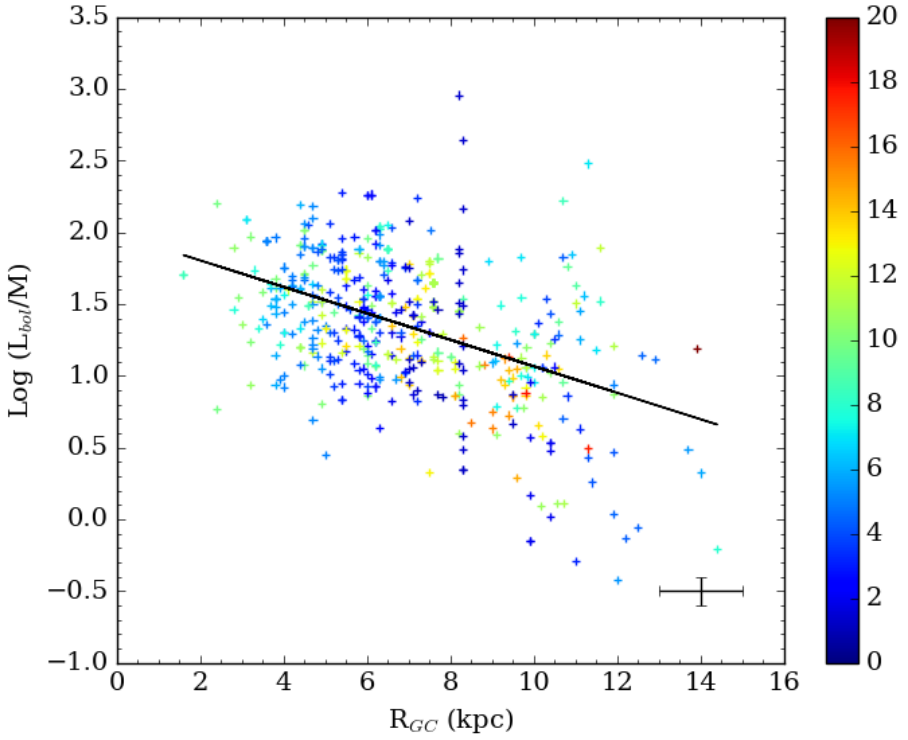

FIGURE 4.15: The relation $L_{\rm bol}/M$ serves as a proxy for overall star formation efficiency. By plotting this value as a function of galactocentric radius, we observe a downward trend where star formation appears to be less efficient in the Outer Galaxy than in the Inner Galaxy. This agrees with Figure 4.14 which shows the trend for star formation efficiency of only the massive stars.

emission to the mass of the parent cloud traced by ^{13}CO. They found no dependence on $R_{\rm GC}$ but were limited to a range over $3 \leq R_{\rm GC} \leq 8$ kpc. Eden et al. 2012 also observed the ratio between clump to cloud mass to determine a clump formation efficiency and found no difference between the inter-arm and spiral-arm region along the selected line of sight ($37.83° \leq l \leq 42.50°$) which translates to a galactocentric range of $4 \leq R_{\rm GC} \leq 8.5$ kpc. It must be noted that all of these studies are primarily restricted to the Inner Galaxy and show very subtle trends which are only apparent with large samples (e.g. Roman-Duval et al. 2016) or large $R_{\rm GC}$ range.

Overall, we see a flat trend with increasing $R_{\rm GC}$ for the amount of massive stars per unit clump mass and a downward trend for overall stars per unit clump mass (in the massive star forming clumps) although only the latter is confirmed as a significant result. This drop in the overall star formation efficiency combined with a flat trend in the massive star formation efficiency may imply a shift in the initial mass function (IMF) towards a lesser fraction of lower mass stars in the Outer Galaxy. However, we are unable to draw any robust conclusions because we only see a statistically significant trend in the overall star formation efficiency or $\rm L_{bol}/M$. The remaining

quantities contain too much scatter to confidently identify any trends and would require further investigation in order to determine the effects if any on the IMF.

4.5 Summary & Conclusions

In summary, we have used the methods of Urquhart et al. 2013b and Urquhart et al. 2014d and incorporated Outer Galaxy data from SASSy to compile a sample of compact and UC H II regions that covers the Galactic plane from $280^\circ \leq l \leq 240^\circ$. These massive star forming regions have been identified via cross-matching and coincidence of infrared, radio, and submillimetre data with ATLASGAL providing the bulk of Inner Galaxy molecular clumps while SASSy encompassed the Outer Galaxy. The complete catalogue totals 536 UC H II regions associated with 445 host clumps. From this catalogue, we are able to state that while Inner Galaxy clumps are similar to their Outer Galaxy counterparts, this is not the case for the UC H II regions as the 2-sample Kolmogorov-Smirnov test indicates that the two subsets are drawn from two different parent samples. Similarly, with the Spearman rank test, we can confirm a significant correlation for L_{bol}/M with galactocentric radius but this is not the case when examining (N_{Ly}/M). In conclusion, we conclude that the overall star formation efficiency is lower in the Outer Galaxy than in the Inner Galaxy. The massive star formation efficiency likely remains constant but there is too much scatter to acquire a statistically significant result. However, if a uniform gradient could be confirmed, it would lead to interesting results on the Galactic IMF as massive star formation would appear to cease after a certain distance. This result would be of great importance for studies that examine the formation and evolution of nearby galaxies and assume an unchanging IMF throughout the galactic disks.

Chapter 5

Searching for New UC H II Regions in the Outer Galaxy

5.1 The Galactic Distribution of Massive Star Formation

The SASSy submillimetre clump catalogue contains 3138 sources (Chapter 3). However, in Chapter 4, we noticed a significant number of the OGS sources did not match with an existing RMS radio counterpart (> 1000). The decision was made to investigate the lack of UC H II regions in the Outer Galaxy as represented by little currently available survey data. Unlike CORNISH in the Inner Galaxy, there are no continuous radio coverage surveys at these limits and even RMS pulls from multiple radio surveys to fill in the various parts of the Galactic plane (Chapter 2).

In Figure 5.1, we show the surface distribution of our UC H II region sample as a function of galactocentric radius. We binned the regions into circular annuli of width 1 kpc. Then, the number of objects located at each radial position was normalised by the area observed for each corresponding annulus. From the results shown in Chapter 4, we successfully filled in a significant number of sources with $R_{\rm GC} > 8.5$ kpc and supplemented the previous catalogues obtained for the Inner Galaxy. The small overall number densities for sources in annuli above 12 kpc correspond to those with higher Poisson errors. We see a clear distinction in the number of sources available for the Inner Galaxy versus the Outer Galaxy which is visible on this plot as beginning near $R_{\rm GC} \approx 8$ kpc.

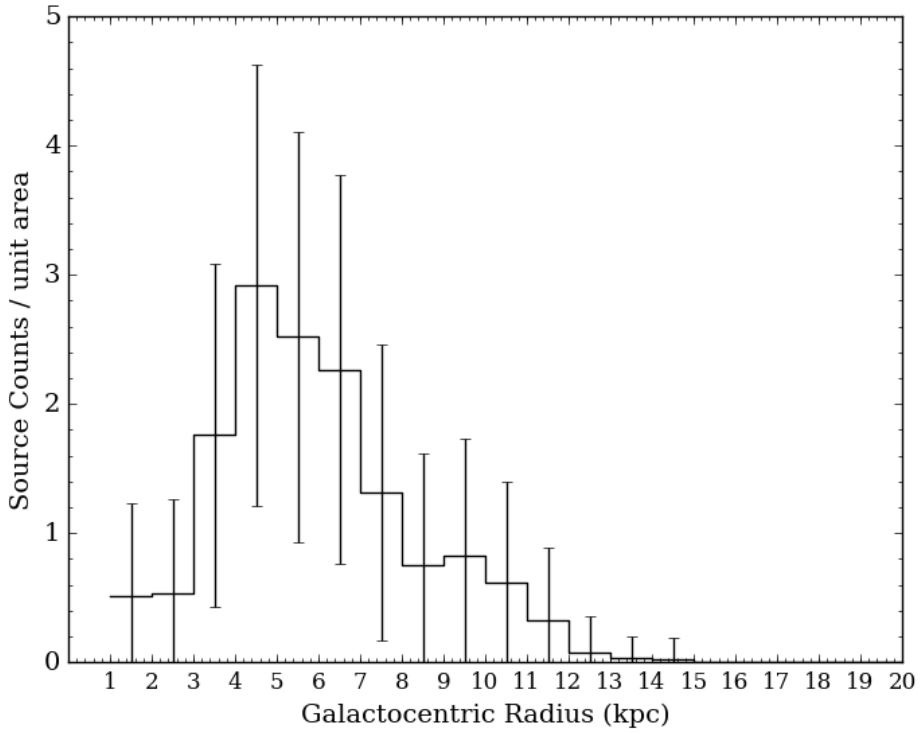

FIGURE 5.1: Surface distribution of UC H II regions from the catalogue sorted into bins with width of 1 kpc. Each bin has also been normalised by the area of the corresponding annulus that was observed. Error bars were calculated using Poisson errors. There is an abrupt change in the number of massive star forming sites known in the Inner Galaxy versus those in the Outer Galaxy.

The profile shape from our distribution is nearly identical to results from Palla and Stahler 2008 who compiled observations of pulsars, supernova remnants, and extended H II regions to trace star formation rates per unit area as a function of galactocentric radius across the plane (see Figure 5.2). All three datasets show a similar increase between $2 \leq R_{GC} \leq 4$ kpc with a peak near 4-5 kpc (i.e. the controversial 'molecular ring' as discussed in Chapter 1). Star formation then proceeds to fall off with sharp drops at 7-8 kpc and 12-13 kpc. These patterns remain consistent with the results seen in our UC H II regions. The dashed and continuous lines are produced by Cavichia et al. 2013 for SFR models with and without radial gas flows, respectively. All three independent and uniquely approached studies appear to agree that the star formation rate should drop in the Outer Galaxy, just past the boundary of the solar circle.

However, the amount of area that remains unobserved in the Outer Galaxy as well as the number of SASSy submillimetre clumps detected in that region leads us to ask whether or not all of the massive star forming sites beyond 8.5 kpc have been observed? Is it possible that we are missing a significant sample? Would it be possible to confirm that those remote areas are indeed empty of relevant massive star formation and this is a real effect? Current attempts have used

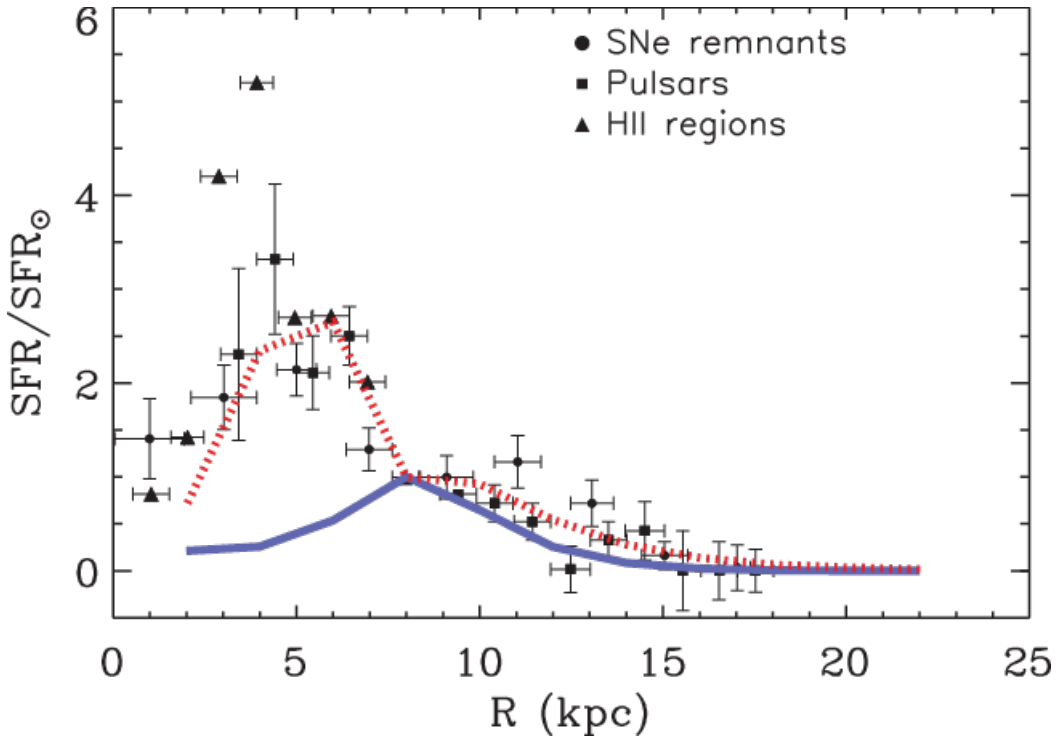

FIGURE 5.2: Star formation rate per unit area for the Galaxy as a function of galactocentric radius, normalised to the solar rate. The data points for the supernova remnants, pulsars and H II regions come from Palla and Stahler 2008 while dashed and continuous line represent SFR models with and without radial gas flows, respectively as produced by Cavichia et al. 2013.

the WISE catalogue in order to pick out star forming regions and calculate their corresponding star formations rates and efficiencies (e.g. Vutisalchavakul et al. 2016; Armentrout et al. 2017; Izumi et al. 2017); however, these are not complete for the compact and ultracompact objects as we previously noted in Chapter 1.

5.2 A Proposal

The SASSy submillimetre clump catalogue which we discussed in detail in Chapter 3, contains 3141 sources. However, during the matching procedures, we noticed a significant number of these did not match with any existing RMS radio counterpart. In Chapter 2, we referred to studies by Urquhart et al. 2013b and Urquhart et al. 2014d that claimed that the clumps with the highest column densities were also the most likely to host massive star formation and these clumps could often be observed to include various tracers such as the compact H II regions (Figure 2.2). They had shown that beyond a column density of $\sim 10^{23}$ cm^{-2}, ~100% of ATLASGAL clump sources were found to be associated with massive star formation. Motivated, we examined the SASSy clumps and calculated corresponding column densities for the full submillimetre catalogue. We

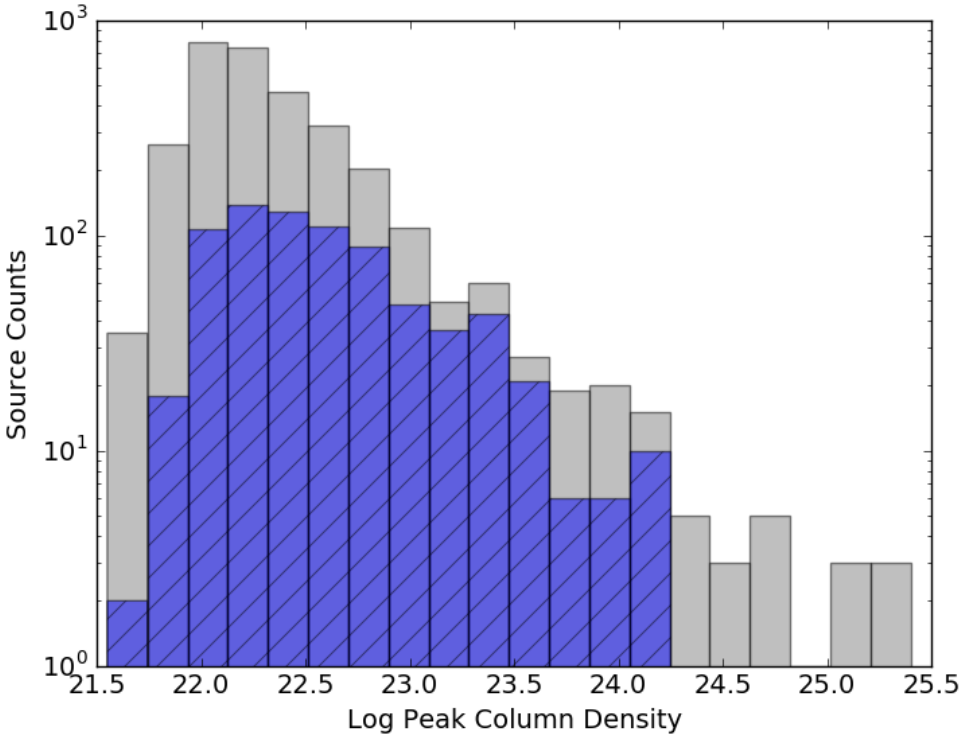

FIGURE 5.3: Column densities of SASSy submillimetre clump catalogue containing over 3,000 sources (grey). Previously observed clumps with known tracers of massive star formation are also shown in overlaid distribution (blue). A number of high column density SASSy clumps which should host massive star formation appear to be empty of any known tracers. Bin size is 20 dex.

reconsidered the RMS catalogue and extracted a subset that included all known potential tracers of massive star formation. For the sake of completeness, we counted the compact H II regions as well as masers, extended H II regions, and intermediate mass YSOs. We matched this subset of known tracers against SASSy using similar matching techniques as described in Chapter 4. We also examined the available literature for any additional known radio star formation tracers within the SASSy region. This second subset included sources from the Methanol Multibeam Survey (MMB) (Green et al., 2007) and from the YSO catalogue compiled by Marton et al. 2016 from ALLWISE data (Wright et al., 2010). Figure 5.3 shows the the whole catalogue of SASSy source clumps (grey) and overplotted by the number distribution of those clumps that contained at least one matching radio counterpart tracer (blue). A large percentage of the higher column density SASSy clumps above 10^{23} cm^{-2} do not possess a match with currently known tracers. If the claim that higher column density clumps are nearly 100% found to be associated with star formation is true (Urquhart et al., 2014d), then we would expect to find radio counterparts for all of the $\sim$ 100 clumps in question. However, we found little to no radio observations for this part of the Galaxy. This suggests that we may be missing additional UC H II regions for the Outer

Galaxy and that our sample is not yet complete.

For the final steps of this research project, we submitted a proposal to the VLA to observe 200 SASSy clumps of the highest column densities and with no currently known radio counterparts. Our goal was to determine whether or not we could detect the free-free emission from a compact H II region which would indicate ongoing star formation. 200 Outer Galaxy sources would significantly impact Figures 4.14 and Figure 4.15, allowing us to conclude with confidence whether or not massive star formation efficiency, like the overall star formation efficiency, is also lower in the Outer Galaxy. Combined with increased interest in the astronomical community for finding new star forming regions in the Outer Galaxy, any confirmed H II regions (or alternatively, any non-detections) will prove vital for confirming and fine-tuning future Galactic evolutionary and star formation history models.

5.3 Observations

We initially selected 177 SASSy clumps with log $N_{H_2} \geq 24$ to target, searching for radio counterparts embedded in the clump thus potentially indicating ongoing massive star formation. We selected this value to achieve a uniform column density sampling of the potential star-forming clumps and Figure 5.3 illustrates a noticeable drop-off at this point. For the actual observations, we were able to increase this number to 200 sources (with log $N_{H_2} > 22$) when we were granted a higher priority time than expected and could gain more on-target time by consolidating the overhead calibration times via more continuous observation blocks

The data were acquired in August 2017 while the VLA was in C-configuration. C is well-suited to filling in these supposed "missing regions of star formation." We used the C-band receiver at 6 GHz as our goal was to match the CORNISH sensitivity at 0.4 mJy beam^{-1}. We matched this sensitivity limit by using an on-source integration time of 5 minutes. We requested the 3-bit sampler be set up to observe in wideband mode covering 4-8 GHz with 2 MHz channels, thus allowing us to search the thermal radio continuum for free-free emission from H II regions. The H II regions will only be a few arcseconds across which is suitable for the high resolution available in VLA C-configuration (FWHM~3.5″). We also requested to simultaneously observe the 6.7 GHz line, with the 8-bit sampler (standard dump time) and a bandwidth of 8 MHz and 4096 channels. This setup would allow us to return to the data in the future to search for methanol masers.

TABLE 5.1: List of VLA calibrators used during data reduction and their intents.

Calibrator	*Intent*
3C48	Flux
J0319+4130	Bandpass
J0228+6721	Phase
J0349+4609	Phase
J0359+5057	Phase
J0555+3948	Phase
J0559+2353	Phase
J0632+1022	Phase
J0725-0054	Phase
J0730-1141	Phase
J0735-1735	Phase

5.4 Continuum Data Reduction

We reduced the continuum observations as per the NRAO VLA CASA pipeline (version 5.1.2) with additional flagging of bad data points as needed. In general, the pipeline began by loading the dataset into a CASA measurement set and first applying Hanning smoothing. Hanning smoothing reduces the Gibbs phenomenon which is when RFI or other bright sources produce strong narrow line emission features which spill over into adjacent spectral channels ('ringing'). The data is then flagged for the first time which clears the dataset of shadowed antenna, antennas not on source, absolute zero values sometimes produced by the correlators, quacking (beginning and end of each scan), noisy channel edges and sub-bands, and any known RFI signatures in the observing frequency range.

When the observations are first set up, each target field is assigned an intent. This is particularly important for calibrating the data by identifying the flux density, bandpass, and phase calibrators. We selected our calibrators from the list provided by NRAO and by their position with respect to our SASSy clumps. They are listed in Table 5.1. After the initial flagging, a model is prepared for later flux density calibration by examining the flux calibrator intent-marked field. For our purposes, we chose 3C48 and generated calibration tables as well as plots of amplitude versus UV-distance per spectral window. Next, pre-determined calibration tables are generated for the dataset that will determine corrections for antenna positions, gain curves, atmospheric opacities, and requantizer gains as necessary.

The pipeline applied all the previously derived calibration tables to estimate the first round of delays and bandpass solutions (gain and phase). This was followed by another round of flagging for additional RFI and other outliers. The pipeline continued to refine the bandpass and phase

TABLE 5.2: `tclean` Parameters for Imaging VLA Data

Parameter	*Value*	*Description*
`niter`	10000	Max number of iterations
`threshold`	10mJy	stopping threshold for peak residual across all image planes
`specmode`	mfs	continuum imaging with one output image channel
`deconvolver`	mtmfs	Multi-term (Multi-Scale) Multi-freq synthesis
`nterms`	2	computer spectral index
`smallscalebias`	0.9	bias scales towards compact point-like sources
`weighting`	briggs	values multiplied by weight before accumulated on uv-grid
`robust`	0.5	weighting parameter ideal for sensitivity to HII regions
`imagesize`	[200,200]	200 pixels by 200 pixels
`pblimit`	0.2	PB gain limit at which to cut off normalisations

solutions with additional iterations and alternating stages of deriving the calibration solutions with further flagging. Finally the solutions were applied to the full dataset and we could begin cleaning the sources to produce images and search for any confirmed detections.

5.4.1 Imaging

The images were generated using the CASA command `tclean` which makes images from derived visibilities and reconstructs a sky model. It may be run interactively to manual select regions of interest to clean against. We ran the command on each field that represented a SASSy submillimetre clump source, using parameters selected to best detect point-like compact objects and a limited degree of extended emission. We selected a background sky threshold value of 10 mJy in order to obtain similar sensitivities to surveys in the Inner Galaxy (see Section 5.3). Descriptions of the `tclean` parameters used and their values are given in Table 5.2.

5.5 Results & Summary

The final cleaned images were cropped to postage stamp image sizes of 1.5′ by 1.5′. On top of these, the contours from the corresponding SASSy submillimetre clumps were overlaid and the results examined for complementary sources. Of the 200 SASSy clumps targeted by the VLA, we were able to identify 7 with a positive radio source at 6 GHz. These positive detections are shown in Figure 5.4.

We present the positive detections along with their background rms values, as well as their derived R_{GC} as available from the literature in Table 5.3. SASSy derived integrated submillemetre fluxes

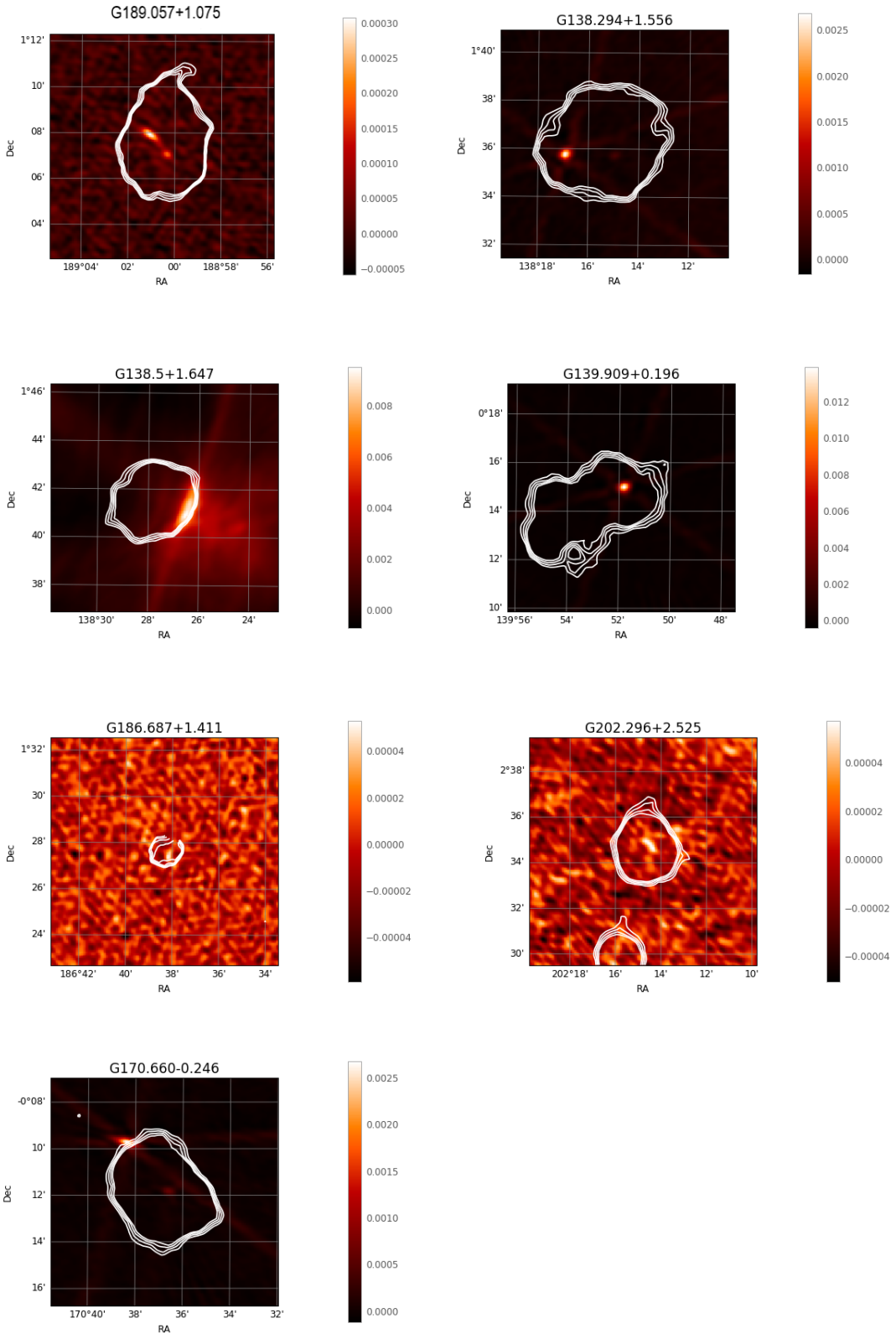

FIGURE 5.4: SASSy submillimetre clumps are shown as white contours overlaid on positive radio detections identified in VLA observations. Positive detection indicates that the radio source was located anywhere within the SASSy clump. Postage stamps are 0.15° by 0.15°. VLA images are in mJy. Contours begin at 5σ.

TABLE 5.3: SASSy targets with a confirmed radio source associated with the clump boundaries. SASSy name is given in galactic coordinates in column 1. Right ascension and declination are given as well as the measured background RMS for each source. Galactocentric radius values are listed as available with references [1] Bronfman et al. 1996 and [2] Anderson et al. 2014; see text for details. Associated OGS Catalogue integrated fluxes and column densities are also included.

Target	*RA* (2000)	*Dec* (2000)	*RMS* [mJy]	R_{GC} [kpc]	*OGS* F_{int} [mJy]	*Log* N_{H_2}
G186.687+1.411	06:06:07.01	+23.52.13.10	0.01	–	2.4	22.8
G202.296+2.525	06:40:58.40	+10.36.50.90	0.01	10.79[1]	2.52	22.8
G170.660-0.246	05:20:22.18	+36.37.56.30	0.03	–	6.67	23.2
G189.057+1.075	06:09:49.81	+21.38.09.40	0.02	10.54[1]	3.77	23.0
G138.294+1.556	03:01:31.24	+60.29.18.90	0.03	–	9.42	23.4
G138.500+1.647	03:03:20.44	+60.28.06.30	0.34	10.81[1]	3.86	23.0
G139.909+0.196	03:07:23.79	+58.30.46.10	0.15	10.82[1]/12.8[2]	4.83	23.1

TABLE 5.4: Subset of SASSy targets that did not have a confirmed radio source associated with the clump boundaries. Column notes are as given in previous table. Image notes are also provided in the final column. Full table is available in Appendix D.

Target	*RA* (2000)	*Dec* (2000)	*RMS* [mJy]	*Upper Limit* [mJy]	*Image Notes*
G176.423-0.399	05:35:15.01	+31.45.21.50	0.01	0.04	noise
G177.503+3.180	05:52:20.89	+32.42.44.00	0.02	0.04	noise
G179.179+1.162	05:48:14.14	+30.14.25.30	0.04	0.13	sidelobes
G179.219+2.222	05:52:33.26	+30.44.57.00	0.02	0.06	sidelobes
G179.409+1.834	05:51:27.31	+30.23.15.50	0.01	0.04	neighbouring source
G180.115+3.236	05:58:43.13	+30.29.04.20	0.02	0.05	neighbouring source
G182.445+3.132	06:03:34.53	+28.24.34.80	0.02	0.05	noise
G183.125+2.574	06:02:52.99	+27.32.35.90	0.01	0.03	noise
G179.982-0.712	05:42:48.42	+28.34.41.90	0.04	0.11	sidelobes

and column densities have also been provided. For the remaining 193 sources, we were unable to confidently identity a radio source within the boundary of the SASSy clumps. A large subset of these observations produced only noise but others were afflicted by large sidelobes from nearby sources or neighbouring objects, limiting our ability to suitably clean the images down to the desired thresholds. In these instances, we measured the background rms of each image and calculated the upper flux limit for each respective target region for 3σ. We present these values for all 193 non-detections in Table 5.4. The full table is provided in Appendix D.1. These interfering sources impacts approximately 58% of the sources. However, only 19% were within one arcminute of the targeted position ("neighbouring source"). Future analysis could lead to removing these sources from the images by calculated sky values for the full image and subtracting the interfering emission. However, the associated rms values calculated for these corresponding sources remain very low with an average around 0.4 mJy. This corresponds to an upper flux limit of 0.11 mJy which is well below the values expected for UC H II regions.

The positive detections were all associated with SASSy sources that had column densities

$\geq 10^{23}$, which agrees with the results from Urquhart et al. 2014d. These detections show that there are additional sites of massive star formation residing in the Outer Galaxy, but not enough to disprove the results we saw in Chapter 4. The overall L_{bol}/M will still diminish with increasing galactocentric radius. However, some of the negative detection targets also had high column densities which did not appear to be associated with massive star formation. It is likely that these regions could be further examined to find other tracers of massive star formation such as methanol masers. Methanol masers that feature strong emission at 6.7 GHz have been found to be almost ubiquitously associated with massive star forming clumps (e.g. Fontani et al. 2007, 2010; Urquhart et al. 2013a, 2014c). With the observations occurring during the VLA's C-configuration and utilising the C-band, it would be possible to subtract the continuum emission to search for spectral emission signatures of the methanol masers that are sufficiently bright enough to be be detected amid neighbouring luminous sources. However, as highlighted in Chapter 4, we focus on the UC II regions as our primary tracers of massive star formation and maser detection is beyond scope of this thesis, although it presents a promising follow-up project for confirming our results for Galactic scales in the future.

Chapter 6

Conclusions

The scientist's task is to find ways to try to disprove things that seem to make sense.

- Terry Prachett, Author

Over the course of this investigation, we have compiled the largest Galactic census of bona-fide UC H II regions to date, spanning Galactic longitudes of $280^\circ \leq l \leq 240^\circ$. In addition, the catalogue also samples UC H II regions at a range of galactocentric radius with $2 \leq R_{\rm GC} \leq 12$ kpc. This unique feature allowed us to compare subsets for Inner and Outer Galaxy sources using the solar circle at $R_{\rm GC} = R_0 = 8.5$ kpc as our boundary. The final catalogue consists of 536 UC H II regions associated with 445 host clumps. We have also contributed to the reduction of the SASSy survey which provides the first wide-area continuous submillimetre source catalogue for the Outer Galaxy. For the OGS component of this survey ($60 \leq l \leq 240^\circ$), we identified and generated flux densities for 1766 sources. The SASSy catalogue will be widely useful in the field of Galactic astronomy and for examining cold dust emission especially for use alongside the expected full Hi-GAL data release.

We examined the impact of our UC H II catalogue on Galactic scale massive star formation trends between the Inner and Outer Galaxy and drew the following conclusions:

- We compiled or calculated the host clump properties (size, mass, column density). We found that clump sizes between the Inner and Outer Galaxy samples tend to be drawn from different parent populations as confirmed by the 2-sample Kolmogorov-Smirnov test. We also notice that while the mass corrected comparisons using Giannetti et al. 2015 tend to give much lower p-values for clump mass and column density between the two samples

than the uncorrected versions, these values are not quite low enough to reject the null hypthesis with a significant level of confidence.

- We calculated the H II regions properties (size, Lyman flux) and compiled their bolometric luminosities. By the KS-test, we found that were were able to reject the null hypothesis for the comparisons of size and bolometric luminosity but not for the Lyman flux.

- We plotted the clump mass and Lyman continuum flux as a function of galactocentric radius finding that mass tended to increase with increasing $R_{\rm GC}$ while Lyman flux decreased, although the results could not be proven as significant due to the large degree of scatter and error in the data.

- We removed the distance errors by also plotting the massive star formation efficiency or number of massive stars per unit mass ($\rm N_{Ly}/M$) and the overall star formation efficiency or total number of stars per unit mass (Lbol/M) as a function of $R_{\rm GC}$. However, to compensate for any remaining completeness limits, we coloured each point by its heliocentric distance. By the Spearman rank test, we confirmed a significant correlation for $\rm L_{bol}/M$ with Galactocentric radius.

- We conclude that the overall star formation efficiency is lower in the Outer Galaxy than in the Inner Galaxy, since it will scale with L_{bol}/M which yields the combined output luminosities of both massive and low-intermediate mass stars per unit mass

We further investigated 200 Outer Galaxy submillimetre clumps that had no known radio counterparts or other tracers of star formation by submitting a proposal to the VLA in C-configuration that was 100% completed in August 2017. The results of the data reduction yielded 7 confirmed radio detections associated with SASSy molecular clumps which we identified and imaged. For the remaining 193 non-detections, we measured background RMS values such that we could place a 3σ upper flux limit on the images and the associated SASSy clump regions. The results showed that high column density molecular clumps continue to be associated with massive star formation even in the Outer Galaxy, indicating that there is no difference in massive star formation between the Inner and Outer Galactic regions despite the drastic environmental changes such as metallicity and the gas-to-dust ratio that have been proven to vary with galactocentric radius. This suggests that something else drives massive star formation that is not as evident in low or intermediate mass star formation. Future work will investigate this result and continue to more finely tune detailed models of massive star formation for the Galactic plane. The Milky Way

becomes the optimal template for testing evolutionary models. It's diverse range of environments mimicking those of nearby spiral galaxies. In our home Galaxy, it is here that we can examine the biggest and brightest individual stars whose counterparts shine out from the the grand forest of galaxies roaming the Universe.

Appendix A

OGS Submillimetre Source Catalogue

SASSy Name	*l*	*b*	*RA* (2000)	*Dec* (2000)	Rad_{eff} [Jy]	F_{int} [Jy]	*error* [Correction	*Aperture*
JCMTLYS J022704.00+615219.4	133.95	1.06	02:27:04.00	+61:52:19.4	67.44	58.75	3.52	1.10
JCMTLYS J022541.53+62554.8	133.72	1.22	02:25:41.53	+62:05:54.8	74.30	79.25	4.76	1.08
JCMTLYS J022530.97+62633.8	133.69	1.22	02:25:30.97	+62:06:33.8	50.22	31.06	1.86	1.05
JCMTLYS J022529.43+62554.3	133.69	1.21	02:25:29.43	+62:05:54.3	47.09	33.05	1.98	1.04
JCMTLYS J003646.61+632858.8	121.30	0.66	00:36:46.61	+63:28:58.8	42.52	11.16	0.67	1.03
JCMTLYS J022553.46+62411.2	133.75	1.20	02:25:53.46	+62:04:11.2	32.65	6.44	0.39	1.01
JCMTLYS J03131.73+602921.1	138.29	1.56	03:01:31.73	+60:29:21.1	42.71	9.42	0.57	1.03
JCMTLYS J012331.82+614840.9	126.71	-0.82	01:23:31.82	+61:48:40.9	40.39	4.95	0.30	1.02
JCMTLYS J02806.90+60464.7	132.16	-0.72	02:08:06.90	+60:46:04.7	26.89	2.82	0.17	0.98
JCMTLYS J03321.16+60286.9	138.50	1.65	03:03:21.16	+60:28:06.9	30.27	3.84	0.23	1.00
JCMTLYS J022807.97+612957.5	134.20	0.76	02:28:07.97	+61:29:57.5	24.50	2.52	0.15	0.97
JCMTLYS J03724.70+583045.6	139.91	0.20	03:07:24.70	+58:30:45.6	42.21	6.85	0.41	1.03
JCMTLYS J022805.14+612919.6	134.20	0.75	02:28:05.14	+61:29:19.6	30.52	4.58	0.28	1.00
JCMTLYS J003713.08+64413.8	121.38	1.24	00:37:13.08	+64:04:13.8	20.99	1.24	0.07	0.94
JCMTLYS J022804.48+612748.5	134.21	0.73	02:28:04.48	+61:27:48.5	36.37	3.80	0.23	1.01
JCMTLYS J022808.05+612714.1	134.22	0.72	02:28:08.05	+61:27:14.1	19.51	1.15	0.07	0.92
JCMTLYS J022811.44+612939.1	134.21	0.76	02:28:11.44	+61:29:39.1	25.02	2.17	0.13	0.97

Table A.1 continued from previous page

SASSy Name	*l*	*b*	*RA* (2000)	*Dec* (2000)	$Rad_{\rm eff}$ pc	$F_{\rm int}$ Jy	*error* Jy	*Aperture* Correction
JCMTLYS J022713.96+615320.4	133.96	1.09	02:27:13.96	+61:53:20.4	27.07	2.40	0.14	0.99
JCMTLYS J002605.89+645414	120.25	2.16	00:26:05.89	+64:54:14.0	20.93	1.52	0.09	0.94
JCMTLYS J022901.58+613329.1	134.28	0.86	02:29:01.58	+61:33:29.1	21.72	1.56	0.09	0.95
JCMTLYS J03727.74+583024.2	139.92	0.19	03:07:27.74	+58:30:24.2	19.51	1.54	0.09	0.92
JCMTLYS J025009.02+615952.6	136.38	2.27	02:50:09.02	+61:59:52.6	22.44	1.46	0.09	0.95
JCMTLYS J023448.05+614637	134.83	1.32	02:34:48.05	+61:46:37.0	25.03	1.79	0.11	0.97
JCMTLYS J022649.82+615749.5	133.89	1.14	02:26:49.82	+61:57:49.5	20.15	1.01	0.06	0.93
JCMTLYS J001425.69+642838.7	118.96	1.89	00:14:25.69	+64:28:38.7	23.51	1.63	0.10	0.96
JCMTLYS J004716.82+62510.2	122.45	-0.78	00:47:16.82	+62:05:10.2	19.17	0.72	0.04	0.92
JCMTLYS J022800.46+612844.3	134.19	0.74	02:28:00.46	+61:28:44.3	21.91	1.11	0.07	0.95
JCMTLYS J01750.74+652122.6	124.64	2.54	01:07:50.74	+65:21:22.6	18.29	1.20	0.07	0.90
JCMTLYS J025819.33+603545.9	137.90	1.46	02:58:19.33	+60:35:45.9	10.06	1.54	0.09	0.71
JCMTLYS J024904.00+604315.1	136.83	1.06	02:49:04.00	+60:43:15.1	19.28	0.90	0.05	0.92
JCMTLYS J022806.27+612842	134.21	0.74	02:28:06.27	+61:28:42.0	13.71	0.63	0.04	0.81
JCMTLYS J024328.31+625711.2	135.28	2.80	02:43:28.31	+62:57:11.2	13.32	0.85	0.05	0.80
JCMTLYS J022814.19+613026.2	134.21	0.77	02:28:14.19	+61:30:26.2	25.18	1.24	0.07	0.97
JCMTLYS J011636.59+645040.5	125.60	2.10	01:16:36.59	+64:50:40.5	15.85	0.57	0.03	0.86

Table A.1 continued from previous page

SASSy Name	*l*	*b*	*RA* (2000)	*Dec* (2000)	$Rad_{\rm eff}$ pc	$F_{\rm int}$ Jy	*error* Jy	*Aperture* Correction
JCMTLYS J002837.50+652747.4	120.56	2.70	00:28:37.50	+65:27:47.4	12.78	0.39	0.02	0.79
JCMTLYS J012313.11+614958.7	126.67	-0.81	01:23:13.11	+61:49:58.7	20.76	0.53	0.03	0.94
JCMTLYS J012338.77+614822.6	126.73	-0.83	01:23:38.77	+61:48:22.6	22.56	0.76	0.05	0.95
JCMTLYS J015624.55+602919.6	130.85	-1.38	01:56:24.55	+60:29:19.6	10.78	0.51	0.03	0.73
JCMTLYS J022600.90+62224.1	133.77	1.18	02:26:00.90	+62:02:24.1	11.90	0.37	0.02	0.77
JCMTLYS J011648.21+644543.9	125.63	2.02	01:16:48.21	+64:45:43.9	13.34	0.38	0.02	0.80
JCMTLYS J012317.82+614738	126.69	-0.85	01:23:17.82	+61:47:38.0	13.06	0.32	0.02	0.80
JCMTLYS J012337.04+61490.9	126.72	-0.82	01:23:37.04	+61:49:00.9	18.17	0.49	0.03	0.90
JCMTLYS J001818.19+615753.7	119.05	-0.66	00:18:18.19	+61:57:53.7	6.09	1.23	0.07	0.55
JCMTLYS J005959.17+593455.2	124.02	-3.27	00:59:59.17	+59:34:55.2	10.06	1.58	0.09	0.71
JCMTLYS J004054.02+63454.6	121.74	0.23	00:40:54.02	+63:04:54.6	14.93	0.37	0.02	0.84
JCMTLYS J022526.75+615623.6	133.75	1.06	02:25:26.75	+61:56:23.6	14.67	0.34	0.02	0.84
JCMTLYS J003704.07+632759.6	121.33	0.64	00:37:04.07	+63:27:59.6	9.72	0.22	0.01	0.70
JCMTLYS J025501.72+603546	137.54	1.28	02:55:01.72	+60:35:46.0	14.53	0.35	0.02	0.83
JCMTLYS J002929.26+652716.8	120.65	2.68	00:29:29.26	+65:27:16.8	13.85	0.39	0.02	0.82
JCMTLYS J022603.04+62830.9	133.74	1.27	02:26:03.04	+62:08:30.9	16.76	0.43	0.03	0.88
JCMTLYS J013423.28+611753.1	128.07	-1.14	01:34:23.28	+61:17:53.1	10.79	0.74	0.04	0.73

Table A.1 continued from previous page

SASSy Name	*l*	*b*	*RA* (2000)	*Dec* (2000)	$Rad_{\rm eff}$ pc	$F_{\rm int}$ Jy	*error* Jy	*Aperture* Correction
JCMTLYS J022559.68+62833.8	133.73	1.27	02:25:59.68	+62:08:33.8	18.04	0.53	0.03	0.90
JCMTLYS J022825.43+613220.6	134.22	0.81	02:28:25.43	+61:32:20.6	13.51	0.29	0.02	0.81
JCMTLYS J022801.86+612624.8	134.21	0.70	02:28:01.86	+61:26:24.8	17.39	0.49	0.03	0.89
JCMTLYS J024154.76+593613.7	136.50	-0.33	02:41:54.76	+59:36:13.7	13.93	0.31	0.02	0.82
JCMTLYS J031204.53+57186.4	141.06	-0.54	03:12:04.53	+57:18:06.4	6.10	0.50	0.03	0.55
JCMTLYS J022659.10+615452.2	133.92	1.10	02:26:59.10	+61:54:52.2	14.92	0.39	0.02	0.84
JCMTLYS J022806.20+613030.3	134.19	0.77	02:28:06.20	+61:30:30.3	14.89	0.37	0.02	0.84
JCMTLYS J022652.97+583610.4	135.11	-1.99	02:26:52.97	+58:36:10.4	8.77	0.29	0.02	0.66
JCMTLYS J021805.72+602544.6	133.43	-0.66	02:18:05.72	+60:25:44.6	8.58	0.25	0.01	0.65
JCMTLYS J023949.93+565144.6	137.37	-2.94	02:39:49.93	+56:51:44.6	10.18	5.16	0.31	0.71
JCMTLYS J03135.70+602840.9	138.31	1.55	03:01:35.70	+60:28:40.9	11.82	0.31	0.02	0.76
JCMTLYS J022719.02+615513.6	133.96	1.12	02:27:19.02	+61:55:13.6	13.82	0.32	0.02	0.82
JCMTLYS J031516.70+581159.2	140.96	0.45	03:15:16.70	+58:11:59.2	7.16	0.27	0.02	0.60
JCMTLYS J022539.10+62715.6	133.70	1.24	02:25:39.10	+62:07:15.6	12.55	0.25	0.02	0.78
JCMTLYS J01149.53+594054.8	124.24	-3.16	01:01:49.53	+59:40:54.8	6.70	0.22	0.01	0.58
JCMTLYS J03300.97+602824.7	138.46	1.63	03:03:00.97	+60:28:24.7	18.37	0.61	0.04	0.90
JCMTLYS J024716.70+603053.3	136.72	0.78	02:47:16.70	+60:30:53.3	12.18	0.20	0.01	0.77

Table A.1 continued from previous page

SASSy Name	*l*	*b*	*RA* (2000)	*Dec* (2000)	$Rad_{\rm eff}$ pc	$F_{\rm int}$ Jy	*error* Jy	*Aperture* Correction
JCMTLYS J022459.63+6256.9	133.64	1.18	02:24:59.63	+62:05:06.9	14.68	0.32	0.02	0.84
JCMTLYS J024728.49+605952.8	136.53	1.23	02:47:28.49	+60:59:52.8	9.79	0.20	0.01	0.70
JCMTLYS J03809.48+57451.9	140.71	-0.99	03:08:09.48	+57:04:51.9	6.66	0.40	0.02	0.57
JCMTLYS J03021.97+56403.7	139.98	-1.87	03:00:21.97	+56:40:03.7	5.54	0.77	0.05	0.52
JCMTLYS J022520.85+62453.9	133.68	1.19	02:25:20.85	+62:04:53.9	10.50	0.21	0.01	0.72
JCMTLYS J024947.85+604217.2	136.92	1.09	02:49:47.85	+60:42:17.2	13.72	0.27	0.02	0.81
JCMTLYS J002125.93+614930.8	119.40	-0.84	00:21:25.93	+61:49:30.8	11.21	0.35	0.02	0.74
JCMTLYS J005957.47+615256.8	123.94	-0.97	00:59:57.47	+61:52:56.8	9.67	0.19	0.01	0.69
JCMTLYS J011752.77+642714.3	125.78	1.73	01:17:52.77	+64:27:14.3	9.50	0.19	0.01	0.69
JCMTLYS J024020.54+58584.3	136.58	-0.99	02:40:20.54	+58:58:04.3	9.64	0.15	0.01	0.69
JCMTLYS J022622.20+62435.4	133.80	1.22	02:26:22.20	+62:04:35.4	13.26	0.28	0.02	0.80
JCMTLYS J013004.40+65370.2	126.91	3.04	01:30:04.40	+65:37:00.2	8.37	0.45	0.03	0.65
JCMTLYS J03325.94+602840.9	138.51	1.66	03:03:25.94	+60:28:40.9	11.38	0.21	0.01	0.75
JCMTLYS J012044.16+612616.7	126.43	-1.23	01:20:44.16	+61:26:16.7	11.35	0.18	0.01	0.75
JCMTLYS J031444.81+574520.6	141.13	0.04	03:14:44.81	+57:45:20.6	5.70	0.29	0.02	0.53
JCMTLYS J024933.99+604831.3	136.85	1.17	02:49:33.99	+60:48:31.3	11.75	0.21	0.01	0.76
JCMTLYS J03741.85+57236.1	140.68	-1.06	03:07:41.85	+57:02:36.1	6.30	1.58	0.09	0.56

Table A.1 continued from previous page

SASSy Name	*l*	*b*	*RA* (2000)	*Dec* (2000)	$Rad_{\rm eff}$ pc	$F_{\rm int}$ Jy	*error* Jy	*Aperture* Correction
JCMTLYS J001510.51+604533.3	118.52	-1.80	00:15:10.51	+60:45:33.3	6.95	0.38	0.02	0.59
JCMTLYS J005824.50+631857.6	123.71	0.45	00:58:24.50	+63:18:57.6	7.35	0.23	0.01	0.60
JCMTLYS J022648.56+62333.5	133.85	1.23	02:26:48.56	+62:03:33.5	16.03	0.42	0.03	0.86
JCMTLYS J015022.84+65612.6	129.09	2.94	01:50:22.84	+65:06:12.6	7.43	3.97	0.24	0.61
JCMTLYS J003658.13+632755.4	121.32	0.64	00:36:58.13	+63:27:55.4	9.72	0.17	0.01	0.70
JCMTLYS J005141.16+654630.2	122.96	2.90	00:51:41.16	+65:46:30.2	6.96	0.36	0.02	0.59
JCMTLYS J014548.08+59533.7	129.71	-2.27	01:45:48.08	+59:53:03.7	8.57	0.95	0.06	0.65
JCMTLYS J022621.15+6249.1	133.80	1.22	02:26:21.15	+62:04:09.1	15.95	0.38	0.02	0.86
JCMTLYS J012554.79+594259.2	127.27	-2.86	01:25:54.79	+59:42:59.2	12.23	16.26	0.98	0.77
JCMTLYS J022623.14+58559.8	135.23	-2.49	02:26:23.14	+58:05:59.8	6.96	0.18	0.01	0.59
JCMTLYS J022502.92+62859.1	133.63	1.24	02:25:02.92	+62:08:59.1	11.23	0.22	0.01	0.75
JCMTLYS J025813.38+622031.5	137.07	3.00	02:58:13.38	+62:20:31.5	10.73	0.46	0.03	0.73
JCMTLYS J023817.44+565248.9	137.17	-3.01	02:38:17.44	+56:52:48.9	8.61	4.57	0.27	0.66
JCMTLYS J015748.87+644040.2	129.96	2.72	01:57:48.87	+64:40:40.2	5.96	0.10	0.01	0.54
JCMTLYS J012329.24+615338.4	126.70	-0.74	01:23:29.24	+61:53:38.4	13.69	0.24	0.01	0.81
JCMTLYS J023705.54+594340.2	135.89	-0.46	02:37:05.54	+59:43:40.2	11.28	0.28	0.02	0.75
JCMTLYS J022622.78+61542.1	133.86	1.06	02:26:22.78	+61:54:02.1	11.45	0.19	0.01	0.75

Table A.1 continued from previous page

SASSy Name	*l*	*b*	*RA* (2000)	*Dec* (2000)	$Rad_{\rm eff}$ pc	$F_{\rm int}$ Jy	*error* Jy	*Aperture* Correction
JCMTLYS J022520.33+62437.1	133.69	1.18	02:25:20.33	+62:04:37.1	6.88	0.10	0.01	0.58
JCMTLYS J025354.81+58950.4	138.52	-0.95	02:53:54.81	+58:09:50.4	8.69	0.11	0.01	0.66
JCMTLYS J025131.05+62849.8	136.46	2.47	02:51:31.05	+62:08:49.8	8.99	0.11	0.01	0.67
JCMTLYS J015720.97+58538.5	131.37	-2.90	01:57:20.97	+58:53:08.5	10.47	7.47	0.45	0.72
JCMTLYS J025001.68+604144.7	136.95	1.09	02:50:01.68	+60:41:44.7	10.62	0.16	0.01	0.73
JCMTLYS J022800.49+612555.7	134.21	0.69	02:28:00.49	+61:25:55.7	13.89	0.24	0.01	0.82
JCMTLYS J015630.38+591227.2	131.19	-2.62	01:56:30.38	+59:12:27.2	5.90	0.24	0.01	0.54
JCMTLYS J004956.34+654346.1	122.78	2.86	00:49:56.34	+65:43:46.1	11.08	0.30	0.02	0.74
JCMTLYS J012755.24+61406.2	127.25	-0.90	01:27:55.24	+61:40:06.2	7.65	0.10	0.01	0.62
JCMTLYS J003816.63+63638.5	121.44	0.28	00:38:16.63	+63:06:38.5	9.71	0.19	0.01	0.70
JCMTLYS J024929.85+604731.7	136.85	1.15	02:49:29.85	+60:47:31.7	8.68	0.15	0.01	0.66
JCMTLYS J012833.72+654130	126.74	3.10	01:28:33.72	+65:41:30.0	9.76	0.40	0.02	0.70
JCMTLYS J013542.55+6362	127.91	0.66	01:35:42.55	+63:06:02.0	9.87	0.14	0.01	0.70
JCMTLYS J003005.19+654755.5	120.74	3.02	00:30:05.19	+65:47:55.5	6.55	0.49	0.03	0.57
JCMTLYS J002739.77+653030.6	120.47	2.75	00:27:39.77	+65:30:30.6	9.42	0.18	0.01	0.69
JCMTLYS J022556.26+61587.1	133.79	1.11	02:25:56.26	+61:58:07.1	10.24	0.15	0.01	0.71
JCMTLYS J031529.46+581136.3	140.99	0.46	03:15:29.46	+58:11:36.3	7.00	0.31	0.02	0.59

Table A.1 continued from previous page

SASSy Name	*l*	*b*	*RA* (2000)	*Dec* (2000)	$Rad_{\rm eff}$ pc	$F_{\rm int}$ Jy	*error* Jy	*Aperture* Correction
JCMTLYS J014105.01+592226	129.23	-2.89	01:41:05.01	+59:22:26.0	11.32	0.51	0.03	0.75
JCMTLYS J022753.68+613225.4	134.16	0.79	02:27:53.68	+61:32:25.4	8.24	0.11	0.01	0.64
JCMTLYS J004736.65+595433.7	122.45	-2.96	00:47:36.65	+59:54:33.7	10.09	0.33	0.02	0.71
JCMTLYS J031445.96+57458	141.13	0.04	03:14:45.96	+57:45:08.0	8.21	0.45	0.03	0.64
JCMTLYS J005135.42+614012.1	122.95	-1.20	00:51:35.42	+61:40:12.1	6.95	0.08	0.00	0.59
JCMTLYS J022718.11+615525	133.96	1.12	02:27:18.11	+61:55:25.0	8.25	0.14	0.01	0.64
JCMTLYS J023203.80+594822.1	135.28	-0.63	02:32:03.80	+59:48:22.1	5.77	0.09	0.01	0.53
JCMTLYS J011414.97+653025.4	125.30	2.74	01:14:14.97	+65:30:25.4	8.74	0.34	0.02	0.66
JCMTLYS J001729.14+614345.6	118.92	-0.88	00:17:29.14	+61:43:45.6	6.54	0.36	0.02	0.57
JCMTLYS J031157.55+592645.9	139.95	1.30	03:11:57.55	+59:26:45.9	7.71	0.23	0.01	0.62
JCMTLYS J03624.15+594938.9	139.15	1.27	03:06:24.15	+59:49:38.9	6.77	0.08	0.01	0.58
JCMTLYS J03939.95+571949.9	140.76	-0.68	03:09:39.95	+57:19:49.9	6.66	0.79	0.05	0.57
JCMTLYS J031500.02+58234.1	140.83	0.59	03:15:00.02	+58:23:04.1	5.51	0.25	0.01	0.52
JCMTLYS J01722.11+65568.6	124.56	3.11	01:07:22.11	+65:56:08.6	7.53	1.01	0.06	0.61
JCMTLYS J02317.78+614119.5	131.34	0.00	02:03:17.78	+61:41:19.5	6.57	0.07	0.00	0.57
JCMTLYS J025553.45+603736.1	137.62	1.35	02:55:53.45	+60:37:36.1	12.70	0.16	0.01	0.79
JCMTLYS J022659.83+61546.6	133.93	1.09	02:26:59.83	+61:54:06.6	15.01	0.23	0.01	0.84

Table A.1 continued from previous page

SASSy Name	*l*	*b*	*RA* (2000)	*Dec* (2000)	$Rad_{\rm eff}$ pc	$F_{\rm int}$ Jy	*error* Jy	*Aperture* Correction
JCMTLYS J031455.57+574313	141.17	0.02	03:14:55.57	+57:43:13.0	6.64	0.46	0.03	0.57
JCMTLYS J004840.62+595649.6	122.59	-2.92	00:48:40.62	+59:56:49.6	6.06	0.15	0.01	0.55
JCMTLYS J005105.74+60028.2	122.89	-2.86	00:51:05.74	+60:00:28.2	7.52	0.24	0.01	0.61
JCMTLYS J022716.96+615712.5	133.94	1.15	02:27:16.96	+61:57:12.5	10.61	0.16	0.01	0.73
JCMTLYS J01055.83+624931.4	124.02	-0.03	01:00:55.83	+62:49:31.4	10.92	0.21	0.01	0.74
JCMTLYS J03806.48+57424.6	140.71	-1.00	03:08:06.48	+57:04:24.6	6.84	0.36	0.02	0.58
JCMTLYS J014507.99+60352.1	129.59	-2.11	01:45:07.99	+60:03:52.1	6.61	0.10	0.01	0.57
JCMTLYS J01909.04+611838.4	125.06	-1.49	01:09:09.04	+61:18:38.4	7.32	0.06	0.00	0.60
JCMTLYS J025146.85+555924.2	139.24	-3.02	02:51:46.85	+55:59:24.2	7.08	0.32	0.02	0.59
JCMTLYS J002659.83+65328.2	120.40	2.78	00:26:59.83	+65:32:08.2	10.01	0.19	0.01	0.71
JCMTLYS J024511.08+604938.3	136.36	0.96	02:45:11.08	+60:49:38.3	8.71	0.13	0.01	0.66
JCMTLYS J022556.44+621018.8	133.72	1.30	02:25:56.44	+62:10:18.8	9.59	0.14	0.01	0.69
JCMTLYS J031226.72+572434.4	141.04	-0.42	03:12:26.72	+57:24:34.4	6.99	0.34	0.02	0.59
JCMTLYS J03908.86+571658.2	140.73	-0.75	03:09:08.86	+57:16:58.2	6.11	1.97	0.12	0.55
JCMTLYS J02359.41+581434.8	132.38	-3.29	02:03:59.41	+58:14:34.8	6.50	0.57	0.03	0.57
JCMTLYS J031211.22+572027	141.05	-0.49	03:12:11.22	+57:20:27.0	6.10	0.21	0.01	0.55
JCMTLYS J03907.46+591144.2	139.76	0.90	03:09:07.46	+59:11:44.2	6.18	0.09	0.01	0.55

Table A.1 continued from previous page

SASSy Name	*l*	*b*	*RA* (2000)	*Dec* (2000)	$Rad_{\rm eff}$ pc	$F_{\rm int}$ Jy	*error* Jy	*Aperture* Correction
JCMTLYS J025446.09+555657.6	139.63	-2.87	02:54:46.09	+55:56:57.6	6.35	0.23	0.01	0.56
JCMTLYS J014521.02+60649.3	129.61	-2.06	01:45:21.02	+60:06:49.3	5.95	0.06	0.00	0.54
JCMTLYS J022141.11+61544.1	133.62	0.11	02:21:41.11	+61:05:44.1	11.80	0.31	0.02	0.76
JCMTLYS J024328.45+581512.7	137.24	-1.47	02:43:28.45	+58:15:12.7	5.68	0.06	0.00	0.53
JCMTLYS J024057.93+57256.6	137.44	-2.71	02:40:57.93	+57:02:56.6	9.16	0.37	0.02	0.68
JCMTLYS J021323.87+581359.4	133.57	-2.94	02:13:23.87	+58:13:59.4	6.46	0.45	0.03	0.57
JCMTLYS J025216.36+60314.3	137.48	0.64	02:52:16.36	+60:03:14.3	13.19	0.28	0.02	0.80
JCMTLYS J013928.68+64541.5	128.00	2.50	01:39:28.68	+64:54:01.5	6.67	0.08	0.01	0.57
JCMTLYS J031219.92+572214.3	141.05	-0.46	03:12:19.92	+57:22:14.3	6.10	0.21	0.01	0.55
JCMTLYS J005732.48+605424.8	123.67	-1.96	00:57:32.48	+60:54:24.8	6.06	0.07	0.00	0.55
JCMTLYS J014338.10+643611.1	128.49	2.30	01:43:38.10	+64:36:11.1	6.66	0.09	0.01	0.57
JCMTLYS J031207.84+572020.5	141.04	-0.50	03:12:07.84	+57:20:20.5	6.64	0.48	0.03	0.57
JCMTLYS J025153.52+6073.3	137.41	0.68	02:51:53.52	+60:07:03.3	10.34	0.21	0.01	0.72
JCMTLYS J025236.42+604514	137.20	1.28	02:52:36.42	+60:45:14.0	7.24	0.10	0.01	0.60
JCMTLYS J015127.05+63218.9	129.60	1.26	01:51:27.05	+63:21:08.9	6.63	0.07	0.00	0.57
JCMTLYS J022031.79+632441	132.71	2.24	02:20:31.79	+63:24:41.0	6.10	0.11	0.01	0.55
JCMTLYS J031208.19+572027.4	141.04	-0.50	03:12:08.19	+57:20:27.4	9.27	0.72	0.04	0.68

Table A.1 continued from previous page

SASSy Name	*l*	*b*	*RA* (2000)	*Dec* (2000)	$Rad_{\rm eff}$ pc	$F_{\rm int}$ Jy	*error* Jy	*Aperture* Correction
JCMTLYS J022559.76+615820.2	133.79	1.11	02:25:59.76	+61:58:20.2	11.68	0.18	0.01	0.76
JCMTLYS J021227.89+633711.2	131.79	2.15	02:12:27.89	+63:37:11.2	7.33	0.12	0.01	0.60
JCMTLYS J022113.49+635247.8	132.62	2.71	02:21:13.49	+63:52:47.8	6.53	0.11	0.01	0.57
JCMTLYS J005736.89+594349.9	123.71	-3.13	00:57:36.89	+59:43:49.9	7.31	0.42	0.03	0.60
JCMTLYS J03301.53+602845.6	138.46	1.64	03:03:01.53	+60:28:45.6	5.64	0.08	0.00	0.53
JCMTLYS J012212.96+593622.9	126.82	-3.03	01:22:12.96	+59:36:22.9	7.07	0.45	0.03	0.59
JCMTLYS J025152.51+565628.3	138.83	-2.17	02:51:52.51	+56:56:28.3	5.81	0.07	0.00	0.53
JCMTLYS J002258.01+622636.2	119.65	-0.25	00:22:58.01	+62:26:36.2	7.75	2.30	0.14	0.62
JCMTLYS J014908.14+601536.8	130.03	-1.81	01:49:08.14	+60:15:36.8	6.60	0.12	0.01	0.57
JCMTLYS J03723.92+583123.4	139.90	0.21	03:07:23.92	+58:31:23.4	6.90	0.10	0.01	0.58
JCMTLYS J021255.95+583925.1	133.38	-2.55	02:12:55.95	+58:39:25.1	5.83	0.08	0.00	0.54
JCMTLYS J014652.08+6080.8	129.79	-2.00	01:46:52.08	+60:08:00.8	6.60	0.10	0.01	0.57
JCMTLYS J03747.52+57319.6	140.68	-1.04	03:07:47.52	+57:03:19.6	6.30	0.15	0.01	0.56
JCMTLYS J015352.22+585037.1	130.95	-3.05	01:53:52.22	+58:50:37.1	9.26	0.40	0.02	0.68
JCMTLYS J025114.55+555455.4	139.20	-3.12	02:51:14.55	+55:54:55.4	7.08	0.30	0.02	0.59
JCMTLYS J022727.96+615538.9	133.97	1.13	02:27:27.96	+61:55:38.9	9.84	0.17	0.01	0.70
JCMTLYS J023926.80+59952.2	136.39	-0.86	02:39:26.80	+59:09:52.2	6.92	0.08	0.00	0.59

Table A.1 continued from previous page

SASSy Name	*l*	*b*	*RA* (2000)	*Dec* (2000)	$Rad_{\rm eff}$ pc	$F_{\rm int}$ Jy	*error* Jy	*Aperture* Correction
JCMTLYS J02414.36+635333.9	130.84	2.14	02:04:14.36	+63:53:33.9	6.16	0.07	0.00	0.55
JCMTLYS J03029.17+59138.5	138.79	0.38	03:00:29.17	+59:13:08.5	6.43	0.05	0.00	0.56
JCMTLYS J024849.67+56457.7	138.83	-3.12	02:48:49.67	+56:04:57.7	12.01	69.17	4.15	0.77
JCMTLYS J002953.31+593826.8	120.21	-3.12	00:29:53.31	+59:38:26.8	9.22	1.22	0.07	0.68
JCMTLYS J02738.90+644910.9	130.93	3.14	02:07:38.90	+64:49:10.9	6.98	0.21	0.01	0.59
JCMTLYS J014759.34+593734.5	130.03	-2.46	01:47:59.34	+59:37:34.5	6.99	0.10	0.01	0.59
JCMTLYS J03121.08+582016.6	139.30	-0.34	03:01:21.08	+58:20:16.6	6.39	0.10	0.01	0.56
JCMTLYS J023604.60+615730.1	134.90	1.54	02:36:04.60	+61:57:30.1	9.91	0.21	0.01	0.70
JCMTLYS J02437.65+645631.4	130.58	3.16	02:04:37.65	+64:56:31.4	9.03	1.04	0.06	0.67
JCMTLYS J022622.51+62332.8	133.81	1.21	02:26:22.51	+62:03:32.8	6.68	0.09	0.01	0.58
JCMTLYS J03819.84+585347.8	139.82	0.59	03:08:19.84	+58:53:47.8	7.40	0.10	0.01	0.61
JCMTLYS J013839.98+642836	127.99	2.07	01:38:39.98	+64:28:36.0	7.08	0.10	0.01	0.59
JCMTLYS J013257.09+59843.6	128.24	-3.30	01:32:57.09	+59:08:43.6	6.83	0.33	0.02	0.58
JCMTLYS J021549.27+602132.5	133.19	-0.82	02:15:49.27	+60:21:32.5	8.74	0.11	0.01	0.66
JCMTLYS J013008.63+653855.7	126.91	3.08	01:30:08.63	+65:38:55.7	8.37	3.43	0.21	0.65
JCMTLYS J001835.24+614537.1	119.06	-0.86	00:18:35.24	+61:45:37.1	7.74	0.19	0.01	0.62
JCMTLYS J005322.23+625057	123.15	-0.02	00:53:22.23	+62:50:57.0	8.27	0.12	0.01	0.64

Table A.1 continued from previous page

SASSy Name	*l*	*b*	*RA* (2000)	*Dec* (2000)	$Rad_{\rm eff}$ pc	$F_{\rm int}$ Jy	*error* Jy	*Aperture* Correction
JCMTLYS J02543.35+633127.1	131.10	1.84	02:05:43.35	+63:31:27.1	8.06	0.09	0.01	0.63
JCMTLYS J013109.06+631319.3	127.39	0.69	01:31:09.06	+63:13:19.3	6.03	0.08	0.01	0.55
JCMTLYS J013751.42+621335.5	128.31	-0.16	01:37:51.42	+62:13:35.5	6.66	0.06	0.00	0.57
JCMTLYS J005401.21+603815.4	123.25	-2.23	00:54:01.21	+60:38:15.4	7.52	0.09	0.01	0.61
JCMTLYS J003953.49+613223.4	121.56	-1.30	00:39:53.49	+61:32:23.4	7.36	0.09	0.01	0.60
JCMTLYS J03921.05+59340.3	139.85	0.80	03:09:21.05	+59:03:40.3	6.55	0.08	0.01	0.57
JCMTLYS J02146.56+644548.5	130.34	2.91	02:01:46.56	+64:45:48.5	5.95	0.08	0.00	0.54
JCMTLYS J032738.66+584658.4	142.00	1.82	03:27:38.66	+58:46:58.4	38.75	8.51	0.51	1.02
JCMTLYS J03131.70+602921.5	138.29	1.56	03:01:31.70	+60:29:21.5	43.58	9.49	0.57	1.03
JCMTLYS J03321.10+60286.9	138.50	1.65	03:03:21.10	+60:28:06.9	31.35	3.86	0.23	1.00
JCMTLYS J03723.81+583050	139.91	0.20	03:07:23.81	+58:30:50.0	33.31	4.83	0.29	1.01
JCMTLYS J043620.96+511254.4	154.35	2.61	04:36:20.96	+51:12:54.4	30.49	4.46	0.27	1.00
JCMTLYS J035524.11+564156.1	146.21	2.39	03:55:24.11	+56:41:56.1	11.81	2.58	0.15	0.76
JCMTLYS J03727.04+583031.9	139.92	0.20	03:07:27.04	+58:30:31.9	33.48	3.57	0.21	1.01
JCMTLYS J032724.02+584338.1	142.01	1.76	03:27:24.02	+58:43:38.1	18.65	1.12	0.07	0.91
JCMTLYS J041104.61+511022	151.60	-0.24	04:11:04.61	+51:10:22.0	25.09	1.36	0.08	0.97
JCMTLYS J035929.78+505750.9	150.38	-1.60	03:59:29.78	+50:57:50.9	10.72	0.61	0.04	0.73

Table A.1 continued from previous page

SASSy Name	*l*	*b*	*RA* (2000)	*Dec* (2000)	$Rad_{\rm eff}$ pc	$F_{\rm int}$ Jy	*error* Jy	*Aperture* Correction
JCMTLYS J042226.09+515045.7	152.40	1.48	04:22:26.09	+51:50:45.7	16.04	0.74	0.04	0.86
JCMTLYS J042550.53+46429.2	156.90	-2.17	04:25:50.53	+46:04:29.2	17.51	0.70	0.04	0.89
JCMTLYS J042231.08+515034.4	152.41	1.48	04:22:31.08	+51:50:34.4	20.68	0.94	0.06	0.93
JCMTLYS J04402.32+512242.1	150.64	-0.82	04:04:02.32	+51:22:42.1	13.67	0.36	0.02	0.81
JCMTLYS J032730.99+581922.6	142.24	1.43	03:27:30.99	+58:19:22.6	18.33	0.87	0.05	0.90
JCMTLYS J045139.84+45357.2	160.27	0.85	04:51:39.84	+45:35:07.2	13.98	0.38	0.02	0.82
JCMTLYS J045139.24+453534.1	160.26	0.85	04:51:39.24	+45:35:34.1	15.01	0.44	0.03	0.84
JCMTLYS J043251.71+455916.5	157.81	-1.35	04:32:51.71	+45:59:16.5	8.63	0.95	0.06	0.66
JCMTLYS J041011.61+505955.4	151.61	-0.46	04:10:11.61	+50:59:55.4	15.17	0.47	0.03	0.85
JCMTLYS J035612.25+51140.5	149.81	-1.73	03:56:12.25	+51:14:00.5	9.70	1.03	0.06	0.70
JCMTLYS J03035.78+55756.2	140.74	-3.21	03:00:35.78	+55:07:56.2	9.36	0.69	0.04	0.68
JCMTLYS J035531.29+564631.1	146.18	2.45	03:55:31.29	+56:46:31.1	8.99	0.56	0.03	0.67
JCMTLYS J044019.52+472311.2	157.63	0.54	04:40:19.52	+47:23:11.2	11.64	0.26	0.02	0.76
JCMTLYS J04235.53+5034.3	151.35	-1.97	04:02:35.53	+50:03:04.3	8.29	0.87	0.05	0.64
JCMTLYS J045825.25+47549.7	159.19	3.20	04:58:25.25	+47:54:09.7	7.81	0.55	0.03	0.62
JCMTLYS J04527.11+49397.2	151.96	-1.96	04:05:27.11	+49:39:07.2	11.10	0.24	0.01	0.74
JCMTLYS J045056.24+452746.9	160.28	0.67	04:50:56.24	+45:27:46.9	8.30	0.30	0.02	0.64

Table A.1 continued from previous page

SASSy Name	*l*	*b*	*RA* (2000)	*Dec* (2000)	$Rad_{\rm eff}$ pc	$F_{\rm int}$ Jy	*error* Jy	*Aperture* Correction
JCMTLYS J032739.91+584548.1	142.01	1.80	03:27:39.91	+58:45:48.1	15.10	0.39	0.02	0.84
JCMTLYS J03135.67+602841.3	138.31	1.55	03:01:35.67	+60:28:41.3	12.20	0.30	0.02	0.77
JCMTLYS J04026.55+511034	150.35	-1.35	04:00:26.55	+51:10:34.0	9.68	1.16	0.07	0.69
JCMTLYS J043616.60+51820.2	154.40	2.55	04:36:16.60	+51:08:20.2	13.37	0.47	0.03	0.80
JCMTLYS J034308.45+514115.1	147.94	-2.65	03:43:08.45	+51:41:15.1	7.75	0.53	0.03	0.62
JCMTLYS J031346.05+54717.4	142.90	-3.14	03:13:46.05	+54:07:17.4	6.27	0.38	0.02	0.56
JCMTLYS J034225.30+513224.3	147.94	-2.83	03:42:25.30	+51:32:24.3	6.39	0.52	0.03	0.56
JCMTLYS J033007.21+52498.5	145.66	-2.91	03:30:07.21	+52:49:08.5	10.92	36.20	2.17	0.74
JCMTLYS J04223.72+50750	151.27	-1.93	04:02:23.72	+50:07:50.0	6.50	0.12	0.01	0.57
JCMTLYS J042015.60+4941.5	154.11	-0.74	04:20:15.60	+49:04:01.5	5.98	0.09	0.01	0.54
JCMTLYS J035606.59+495416.5	150.65	-2.76	03:56:06.59	+49:54:16.5	7.29	0.14	0.01	0.60
JCMTLYS J03300.96+602826.2	138.46	1.63	03:03:00.96	+60:28:26.2	20.03	0.65	0.04	0.93
JCMTLYS J032451.55+545732.2	143.81	-1.57	03:24:51.55	+54:57:32.2	16.69	0.38	0.02	0.88
JCMTLYS J041932.74+525813.5	151.29	1.96	04:19:32.74	+52:58:13.5	14.40	0.37	0.02	0.83
JCMTLYS J04631.26+555719.5	147.86	2.83	04:06:31.26	+55:57:19.5	9.67	0.67	0.04	0.69
JCMTLYS J044026.98+502835.5	155.33	2.60	04:40:26.98	+50:28:35.5	12.79	0.30	0.02	0.79
JCMTLYS J04330.59+51143	150.68	-0.99	04:03:30.59	+51:14:03.0	7.84	0.15	0.01	0.62

Table A.1 continued from previous page

SASSy Name	*l*	*b*	*RA* (2000)	*Dec* (2000)	$Rad_{\rm eff}$ pc	$F_{\rm int}$ Jy	*error* Jy	*Aperture* Correction
JCMTLYS J04717.47+474559.3	153.45	-3.16	04:07:17.47	+47:45:59.3	6.40	1.84	0.11	0.56
JCMTLYS J025501.87+603545.8	137.54	1.28	02:55:01.87	+60:35:45.8	10.83	0.35	0.02	0.73
JCMTLYS J04005.89+505917.3	150.43	-1.52	04:00:05.89	+50:59:17.3	8.65	0.25	0.02	0.66
JCMTLYS J04940.41+501332.3	152.08	-1.08	04:09:40.41	+50:13:32.3	6.48	0.08	0.00	0.57
JCMTLYS J043617.54+51125.3	154.35	2.59	04:36:17.54	+51:12:05.3	14.91	0.59	0.04	0.84
JCMTLYS J041952.21+4695.5	156.12	-2.86	04:19:52.21	+46:09:05.5	10.40	5.52	0.33	0.72
JCMTLYS J043710.00+484624.5	156.25	1.07	04:37:10.00	+48:46:24.5	8.18	0.16	0.01	0.64
JCMTLYS J035623.51+51542.7	149.92	-1.82	03:56:23.51	+51:05:42.7	9.12	2.03	0.12	0.67
JCMTLYS J035439.16+57463.5	145.45	3.14	03:54:39.16	+57:46:03.5	6.04	0.53	0.03	0.55
JCMTLYS J04231.33+492814.3	151.72	-2.41	04:02:31.33	+49:28:14.3	6.06	0.10	0.01	0.55
JCMTLYS J033201.89+554217.8	144.24	-0.38	03:32:01.89	+55:42:17.8	6.50	0.09	0.01	0.57
JCMTLYS J03435.44+5507.2	141.31	-3.05	03:04:35.44	+55:00:07.2	6.06	0.49	0.03	0.55
JCMTLYS J032220.84+581721.6	141.70	1.03	03:22:20.84	+58:17:21.6	9.09	0.10	0.01	0.67
JCMTLYS J04428.74+494215.3	151.81	-2.03	04:04:28.74	+49:42:15.3	6.68	0.11	0.01	0.58
JCMTLYS J044426.55+501740.7	155.89	2.96	04:44:26.55	+50:17:40.7	5.69	0.35	0.02	0.53
JCMTLYS J045244.54+484725.2	157.91	3.02	04:52:44.54	+48:47:25.2	8.21	0.46	0.03	0.64
JCMTLYS J034651.42+52126.3	148.18	-2.03	03:46:51.42	+52:01:26.3	7.92	0.42	0.03	0.63

Table A.1 continued from previous page

SASSy Name	*l*	*b*	*RA* (2000)	*Dec* (2000)	$Rad_{\rm eff}$ pc	$F_{\rm int}$ Jy	*error* Jy	*Aperture* Correction
JCMTLYS J044152.47+47742.3	158.00	0.56	04:41:52.47	+47:07:42.3	9.80	27.90	1.67	0.70
JCMTLYS J04552.11+493510.5	152.05	-1.97	04:05:52.11	+49:35:10.5	6.47	0.09	0.01	0.57
JCMTLYS J04209.24+511121.8	150.55	-1.16	04:02:09.24	+51:11:21.8	7.13	0.10	0.01	0.59
JCMTLYS J03153.25+57846.6	139.94	-1.35	03:01:53.25	+57:08:46.6	7.74	0.11	0.01	0.62
JCMTLYS J03325.94+602841	138.51	1.66	03:03:25.94	+60:28:41.0	11.23	0.20	0.01	0.75
JCMTLYS J045311.81+485418.3	157.87	3.16	04:53:11.81	+48:54:18.3	12.61	13.72	0.82	0.78
JCMTLYS J041012.02+55055	148.89	2.49	04:10:12.02	+55:00:55.0	13.52	0.31	0.02	0.81
JCMTLYS J031253.81+54540.9	142.81	-3.23	03:12:53.81	+54:05:40.9	6.70	0.27	0.02	0.58
JCMTLYS J04420.48+512339.9	150.67	-0.78	04:04:20.48	+51:23:39.9	12.87	0.20	0.01	0.79
JCMTLYS J04118.07+49423.8	151.42	-2.37	04:01:18.07	+49:42:03.8	6.07	0.17	0.01	0.55
JCMTLYS J034451.92+574338.5	144.45	2.29	03:44:51.92	+57:43:38.5	8.05	0.14	0.01	0.63
JCMTLYS J045245.61+483836.2	158.02	2.93	04:52:45.61	+48:38:36.2	7.75	0.96	0.06	0.62
JCMTLYS J032728.06+585350.7	141.92	1.90	03:27:28.06	+58:53:50.7	11.57	0.23	0.01	0.76
JCMTLYS J035626.22+51216.4	149.96	-1.86	03:56:26.22	+51:02:16.4	8.51	0.62	0.04	0.65
JCMTLYS J05035.78+471049.7	159.99	3.05	05:00:35.78	+47:10:49.7	6.63	0.43	0.03	0.57
JCMTLYS J041101.07+47468.9	153.91	-2.73	04:11:01.07	+47:46:08.9	8.29	0.45	0.03	0.64
JCMTLYS J043550.59+515443.7	153.78	3.02	04:35:50.59	+51:54:43.7	8.18	0.35	0.02	0.64

Table A.1 continued from previous page

SASSy Name	*l*	*b*	*RA* (2000)	*Dec* (2000)	$Rad_{\rm eff}$ pc	$F_{\rm int}$ Jy	*error* Jy	*Aperture* Correction
JCMTLYS J044219.86+475057	157.51	1.10	04:42:19.86	+47:50:57.0	5.62	0.09	0.01	0.53
JCMTLYS J025513.84+56637.9	139.61	-2.70	02:55:13.84	+56:06:37.9	9.68	1.66	0.10	0.69
JCMTLYS J043642.40+462253.4	157.97	-0.60	04:36:42.40	+46:22:53.4	6.20	0.07	0.00	0.55
JCMTLYS J031817.11+54530.9	143.48	-2.81	03:18:17.11	+54:05:30.9	6.49	0.14	0.01	0.57
JCMTLYS J041931.67+525829.4	151.29	1.96	04:19:31.67	+52:58:29.4	12.53	0.26	0.02	0.78
JCMTLYS J045628.49+481714.1	158.69	3.19	04:56:28.49	+48:17:14.1	6.35	0.37	0.02	0.56
JCMTLYS J044911.53+494621.9	156.78	3.20	04:49:11.53	+49:46:21.9	10.97	18.31	1.10	0.74
JCMTLYS J031333.96+542631.1	142.71	-2.88	03:13:33.96	+54:26:31.1	6.05	0.09	0.01	0.55
JCMTLYS J043541.34+512546.4	154.12	2.68	04:35:41.34	+51:25:46.4	6.40	0.15	0.01	0.56
JCMTLYS J043221.04+463935.7	157.25	-0.96	04:32:21.04	+46:39:35.7	6.23	0.07	0.00	0.55
JCMTLYS J034424.17+583355.3	143.89	2.92	03:44:24.17	+58:33:55.3	7.33	0.33	0.02	0.60
JCMTLYS J05002.85+462349.7	160.55	2.49	05:00:02.85	+46:23:49.7	6.05	0.30	0.02	0.55
JCMTLYS J03846.51+55142.4	141.82	-2.73	03:08:46.51	+55:01:42.4	8.73	0.46	0.03	0.66
JCMTLYS J044308.49+505019.4	155.34	3.16	04:43:08.49	+50:50:19.4	7.27	0.34	0.02	0.60
JCMTLYS J044420.99+472041.9	158.11	1.02	04:44:20.99	+47:20:41.9	6.20	0.07	0.00	0.55
JCMTLYS J031353.39+54721.9	142.92	-3.13	03:13:53.39	+54:07:21.9	8.87	1.02	0.06	0.67
JCMTLYS J031043.30+542532.9	142.36	-3.11	03:10:43.30	+54:25:32.9	9.49	1.85	0.11	0.69

Table A.1 continued from previous page

SASSy Name	*l*	*b*	*RA* (2000)	*Dec* (2000)	$Rad_{\rm eff}$ pc	$F_{\rm int}$ Jy	*error* Jy	*Aperture* Correction
JCMTLYS J044052.01+4762.5	157.91	0.42	04:40:52.01	+47:06:02.5	7.28	0.07	0.00	0.60
JCMTLYS J041346.72+491140.4	153.26	-1.38	04:13:46.72	+49:11:40.4	5.79	0.11	0.01	0.53
JCMTLYS J032907.78+58475.4	142.16	1.93	03:29:07.78	+58:47:05.4	8.77	0.27	0.02	0.66
JCMTLYS J043932.53+47616.8	157.75	0.25	04:39:32.53	+47:06:16.8	7.61	0.08	0.00	0.62
JCMTLYS J043842.52+461010.7	158.36	-0.48	04:38:42.52	+46:10:10.7	5.57	0.08	0.00	0.52
JCMTLYS J043850.74+463646	158.04	-0.17	04:38:50.74	+46:36:46.0	6.75	0.08	0.00	0.58
JCMTLYS J044317.92+50516.9	155.35	3.19	04:43:17.92	+50:51:06.9	8.24	0.46	0.03	0.64
JCMTLYS J043607.28+515724.4	153.77	3.08	04:36:07.28	+51:57:24.4	6.42	7.56	0.45	0.56
JCMTLYS J041757.51+495528.7	153.25	-0.39	04:17:57.51	+49:55:28.7	7.72	0.10	0.01	0.62
JCMTLYS J031859.41+53546.7	143.67	-2.92	03:18:59.41	+53:54:06.7	6.48	0.28	0.02	0.57
JCMTLYS J034610.38+5237.1	148.08	-2.08	03:46:10.38	+52:03:07.1	7.57	0.23	0.01	0.61
JCMTLYS J031137.49+54947.1	142.61	-3.26	03:11:37.49	+54:09:47.1	7.68	0.56	0.03	0.62
JCMTLYS J041400.51+472629	154.50	-2.63	04:14:00.51	+47:26:29.0	6.93	0.13	0.01	0.59
JCMTLYS J035530.10+49371	150.76	-3.04	03:55:30.10	+49:37:01.0	8.61	0.62	0.04	0.66
JCMTLYS J03638.53+551334.9	141.45	-2.71	03:06:38.53	+55:13:34.9	8.90	0.53	0.03	0.67
JCMTLYS J031019.91+543520	142.23	-2.99	03:10:19.91	+54:35:20.0	6.50	0.21	0.01	0.57
JCMTLYS J044232.91+461748	158.70	0.10	04:42:32.91	+46:17:48.0	5.76	0.07	0.00	0.53

Table A.1 continued from previous page

SASSy Name	*l*	*b*	*RA* (2000)	*Dec* (2000)	$Rad_{\rm eff}$ pc	$F_{\rm int}$ Jy	*error* Jy	*Aperture* Correction
JCMTLYS J031838.82+535840.9	143.59	-2.88	03:18:38.82	+53:58:40.9	6.70	0.41	0.02	0.58
JCMTLYS J04939.91+494337.4	152.41	-1.45	04:09:39.91	+49:43:37.4	7.58	0.18	0.01	0.61
JCMTLYS J045250.00+484524	157.94	3.01	04:52:50.00	+48:45:24.0	6.58	0.78	0.05	0.57
JCMTLYS J044013.73+471129.3	157.77	0.39	04:40:13.73	+47:11:29.3	6.40	0.08	0.00	0.56
JCMTLYS J035629.31+514212.4	149.54	-1.34	03:56:29.31	+51:42:12.4	6.57	0.56	0.03	0.57
JCMTLYS J035810.44+57106.2	146.20	2.99	03:58:10.44	+57:10:06.2	6.25	0.53	0.03	0.56
JCMTLYS J044330.43+472424.7	157.97	0.95	04:43:30.43	+47:24:24.7	6.76	0.06	0.00	0.58
JCMTLYS J044050.77+454724.4	158.89	-0.46	04:40:50.77	+45:47:24.4	5.54	0.05	0.00	0.52
JCMTLYS J041107.46+51850.4	151.62	-0.25	04:11:07.46	+51:08:50.4	10.16	0.20	0.01	0.71
JCMTLYS J041832.30+53261.5	150.86	2.19	04:18:32.30	+53:26:01.5	13.08	0.28	0.02	0.80
JCMTLYS J035823.33+512931	149.90	-1.31	03:58:23.33	+51:29:31.0	6.76	0.16	0.01	0.58
JCMTLYS J041110.67+51855.9	151.62	-0.24	04:11:10.67	+51:08:55.9	15.43	0.34	0.02	0.85
JCMTLYS J032555.68+581530.1	142.11	1.26	03:25:55.68	+58:15:30.1	6.75	0.08	0.00	0.58
JCMTLYS J03321.55+582941.2	139.46	-0.08	03:03:21.55	+58:29:41.2	7.17	0.10	0.01	0.60
JCMTLYS J044640.18+454722.9	159.55	0.31	04:46:40.18	+45:47:22.9	6.11	0.05	0.00	0.55
JCMTLYS J034226.05+585835.2	143.44	3.09	03:42:26.05	+58:58:35.2	8.07	0.98	0.06	0.63
JCMTLYS J041945.20+502124.5	153.15	0.12	04:19:45.20	+50:21:24.5	6.64	0.05	0.00	0.57

Table A.1 continued from previous page

SASSy Name	*l*	*b*	*RA* (2000)	*Dec* (2000)	$Rad_{\rm eff}$ pc	$F_{\rm int}$ Jy	*error* Jy	*Aperture* Correction
JCMTLYS J034329.74+584110.4	143.73	2.94	03:43:29.74	+58:41:10.4	7.33	0.65	0.04	0.60
JCMTLYS J043907.26+485540.6	156.35	1.41	04:39:07.26	+48:55:40.6	9.83	0.15	0.01	0.70
JCMTLYS J045804.87+455940.1	160.65	1.98	04:58:04.87	+45:59:40.1	8.54	2.33	0.14	0.65
JCMTLYS J044312.78+475925.1	157.50	1.30	04:43:12.78	+47:59:25.1	7.63	0.10	0.01	0.62
JCMTLYS J03726.48+55404	141.33	-2.27	03:07:26.48	+55:40:04.0	6.94	0.13	0.01	0.59
JCMTLYS J04728.07+482333.3	153.05	-2.68	04:07:28.07	+48:23:33.3	6.81	0.18	0.01	0.58
JCMTLYS J042636.75+523348.1	152.33	2.44	04:26:36.75	+52:33:48.1	5.84	0.08	0.00	0.54
JCMTLYS J032829.29+58354.3	142.20	1.72	03:28:29.29	+58:35:04.3	6.54	0.09	0.01	0.57
JCMTLYS J042402.78+51333.6	153.13	1.10	04:24:02.78	+51:03:33.6	6.03	0.07	0.00	0.55
JCMTLYS J031328.16+612924.2	139.05	3.15	03:13:28.16	+61:29:24.2	6.77	0.35	0.02	0.58
JCMTLYS J033917.78+555935.9	144.89	0.45	03:39:17.78	+55:59:35.9	14.33	0.19	0.01	0.83
JCMTLYS J031016.37+565038.2	141.08	-1.05	03:10:16.37	+56:50:38.2	13.71	0.27	0.02	0.81
JCMTLYS J043916.79+465539.4	157.86	0.10	04:39:16.79	+46:55:39.4	6.58	0.07	0.00	0.57
JCMTLYS J042323.68+492843.7	154.19	-0.08	04:23:23.68	+49:28:43.7	6.59	0.09	0.01	0.57
JCMTLYS J04201.28+50431.3	151.26	-2.01	04:02:01.28	+50:04:31.3	10.66	0.16	0.01	0.73
JCMTLYS J041619.56+48315.6	154.36	-1.92	04:16:19.56	+48:03:15.6	7.12	0.11	0.01	0.59
JCMTLYS J03637.22+551055.2	141.47	-2.75	03:06:37.22	+55:10:55.2	7.33	0.45	0.03	0.60

Table A.1 continued from previous page

SASSy Name	*l*	*b*	*RA* (2000)	*Dec* (2000)	$Rad_{\rm eff}$ pc	$F_{\rm int}$ Jy	*error* Jy	*Aperture* Correction
JCMTLYS J04255.71+51522.3	150.70	-1.15	04:02:55.71	+51:05:22.3	6.93	0.12	0.01	0.59
JCMTLYS J044026.17+472244.4	157.65	0.55	04:40:26.17	+47:22:44.4	10.77	0.15	0.01	0.73
JCMTLYS J033122.44+594831.5	141.81	2.93	03:31:22.44	+59:48:31.5	8.93	5.08	0.30	0.67
JCMTLYS J032011.04+543325.5	143.47	-2.27	03:20:11.04	+54:33:25.5	9.19	0.14	0.01	0.68
JCMTLYS J041440.38+47564.2	154.24	-2.19	04:14:40.38	+47:56:04.2	7.13	0.17	0.01	0.59
JCMTLYS J035608.89+502115.3	150.37	-2.41	03:56:08.89	+50:21:15.3	9.24	0.16	0.01	0.68
JCMTLYS J041113.36+473536.3	154.05	-2.84	04:11:13.36	+47:35:36.3	6.57	0.52	0.03	0.57
JCMTLYS J033150.83+571233.8	143.35	0.84	03:31:50.83	+57:12:33.8	6.94	0.09	0.01	0.59
JCMTLYS J033147.63+583929.4	142.51	2.02	03:31:47.63	+58:39:29.4	6.31	0.12	0.01	0.56
JCMTLYS J043729.09+505927	154.63	2.59	04:37:29.09	+50:59:27.0	6.58	0.08	0.00	0.57
JCMTLYS J033629.50+522746	146.65	-2.64	03:36:29.50	+52:27:46.0	7.24	0.14	0.01	0.60
JCMTLYS J033914.98+513811.3	147.48	-3.05	03:39:14.98	+51:38:11.3	7.75	0.43	0.03	0.62
JCMTLYS J033140.41+573741.4	143.09	1.17	03:31:40.41	+57:37:41.4	6.07	0.10	0.01	0.55
JCMTLYS J042041.44+49629.7	154.14	-0.66	04:20:41.44	+49:06:29.7	6.78	0.08	0.00	0.58
JCMTLYS J044406.87+464826.2	158.49	0.64	04:44:06.87	+46:48:26.2	5.98	0.06	0.00	0.54
JCMTLYS J045040.11+485858.6	157.54	2.88	04:50:40.11	+48:58:58.6	6.23	0.09	0.01	0.55
JCMTLYS J05026.09+47826.2	160.00	3.00	05:00:26.09	+47:08:26.2	8.73	0.88	0.05	0.66

Table A.1 continued from previous page

SASSy Name	*l*	*b*	*RA* (2000)	*Dec* (2000)	$Rad_{\rm eff}$ pc	$F_{\rm int}$ Jy	*error* Jy	*Aperture* Correction
JCMTLYS J025016.43+555250.7	139.10	-3.22	02:50:16.43	+55:52:50.7	8.24	2.41	0.14	0.64
JCMTLYS J034048.14+59111.9	143.15	3.13	03:40:48.14	+59:11:01.9	9.96	0.74	0.04	0.70
JCMTLYS J025542.06+59029.8	138.34	-0.09	02:55:42.06	+59:00:29.8	7.75	0.24	0.01	0.62
JCMTLYS J043347.71+47178.3	156.96	-0.35	04:33:47.71	+47:17:08.3	6.05	0.06	0.00	0.55
JCMTLYS J044217.98+51012	155.13	3.17	04:42:17.98	+51:00:12.0	5.73	0.16	0.01	0.53
JCMTLYS J042101.01+504328.5	153.03	0.53	04:21:01.01	+50:43:28.5	6.45	0.08	0.00	0.56
JCMTLYS J04723.01+49588	151.98	-1.52	04:07:23.01	+49:58:08.0	6.27	0.10	0.01	0.56
JCMTLYS J024234.73+565747.2	137.67	-2.69	02:42:34.73	+56:57:47.2	8.42	0.24	0.01	0.65
JCMTLYS J04740.54+515111.5	150.75	-0.09	04:07:40.54	+51:51:11.5	6.54	0.09	0.01	0.57
JCMTLYS J045258.39+485942.2	157.77	3.18	04:52:58.39	+48:59:42.2	7.29	0.99	0.06	0.60
JCMTLYS J043650.58+505329.8	154.64	2.45	04:36:50.58	+50:53:29.8	9.02	0.15	0.01	0.67
JCMTLYS J043841.19+502610.5	155.17	2.36	04:38:41.19	+50:26:10.5	5.73	0.09	0.01	0.53
JCMTLYS J035826.32+493554.2	151.14	-2.75	03:58:26.32	+49:35:54.2	7.45	1.30	0.08	0.61
JCMTLYS J033149.24+553239.9	144.30	-0.53	03:31:49.24	+55:32:39.9	8.39	0.11	0.01	0.65
JCMTLYS J043107.36+522724.9	152.89	2.86	04:31:07.36	+52:27:24.9	6.46	0.09	0.01	0.57
JCMTLYS J034245.21+513511.2	147.95	-2.77	03:42:45.21	+51:35:11.2	5.95	0.44	0.03	0.54
JCMTLYS J042533.57+534319.3	151.39	3.13	04:25:33.57	+53:43:19.3	8.15	14.10	0.85	0.64

Table A.1 continued from previous page

SASSy Name	*l*	*b*	*RA* (2000)	*Dec* (2000)	$Rad_{\rm eff}$ pc	$F_{\rm int}$ Jy	*error* Jy	*Aperture* Correction
JCMTLYS J041031.81+495843.5	152.34	-1.17	04:10:31.81	+49:58:43.5	8.25	0.37	0.02	0.64
JCMTLYS J035851.24+511234.9	150.14	-1.48	03:58:51.24	+51:12:34.9	7.85	0.13	0.01	0.63
JCMTLYS J044456.07+463227.6	158.79	0.57	04:44:56.07	+46:32:27.6	6.15	0.08	0.00	0.55
JCMTLYS J032923.42+554248.9	143.92	-0.58	03:29:23.42	+55:42:48.9	6.06	0.10	0.01	0.55
JCMTLYS J042338.69+504130.3	153.35	0.80	04:23:38.69	+50:41:30.3	5.80	0.07	0.00	0.53
JCMTLYS J04357.59+494428	151.72	-2.06	04:03:57.59	+49:44:28.0	6.28	0.11	0.01	0.56
JCMTLYS J03811.21+57459.7	140.71	-0.99	03:08:11.21	+57:04:59.7	6.75	0.10	0.01	0.58
JCMTLYS J042759.98+445319	158.02	-2.73	04:27:59.98	+44:53:19.0	6.17	0.17	0.01	0.55
JCMTLYS J042334.58+47565	155.30	-1.15	04:23:34.58	+47:56:05.0	7.08	0.11	0.01	0.59
JCMTLYS J044536.70+494425.5	156.43	2.74	04:45:36.70	+49:44:25.5	7.03	0.18	0.01	0.59
JCMTLYS J045216.14+481511.1	158.27	2.62	04:52:16.14	+48:15:11.1	8.75	0.24	0.01	0.66
JCMTLYS J035643.56+522937.5	149.06	-0.72	03:56:43.56	+52:29:37.5	7.18	0.11	0.01	0.60
JCMTLYS J033517.51+573148.2	143.54	1.37	03:35:17.51	+57:31:48.2	6.07	0.10	0.01	0.55
JCMTLYS J044424.29+501950.6	155.86	2.98	04:44:24.29	+50:19:50.6	7.74	0.31	0.02	0.62
JCMTLYS J043642.56+47504.7	156.89	0.38	04:36:42.56	+47:50:04.7	6.26	0.06	0.00	0.56
JCMTLYS J032015.96+554156.9	142.86	-1.30	03:20:15.96	+55:41:56.9	7.52	0.13	0.01	0.61
JCMTLYS J033735.65+514251.3	147.23	-3.14	03:37:35.65	+51:42:51.3	5.97	1.57	0.09	0.54

Table A.1 continued from previous page

SASSy Name	*l*	*b*	*RA* (2000)	*Dec* (2000)	$Rad_{\rm eff}$ pc	$F_{\rm int}$ Jy	*error* Jy	*Aperture* Correction
JCMTLYS J04203.91+492259.2	151.72	-2.53	04:02:03.91	+49:22:59.2	5.84	0.08	0.01	0.54
JCMTLYS J04403.40+504237	151.09	-1.32	04:04:03.40	+50:42:37.0	7.29	0.14	0.01	0.60
JCMTLYS J03902.91+55233	141.84	-2.70	03:09:02.91	+55:02:33.0	8.06	0.26	0.02	0.63
JCMTLYS J043655.60+462033.9	158.02	-0.59	04:36:55.60	+46:20:33.9	7.58	0.07	0.00	0.61
JCMTLYS J042318.28+502751.1	153.47	0.60	04:23:18.28	+50:27:51.1	6.43	0.08	0.01	0.56
JCMTLYS J043907.44+464848	157.92	0.00	04:39:07.44	+46:48:48.0	7.44	0.11	0.01	0.61
JCMTLYS J04748.44+505035.3	151.44	-0.83	04:07:48.44	+50:50:35.3	7.97	0.07	0.00	0.63
JCMTLYS J024508.45+581331.8	137.45	-1.40	02:45:08.45	+58:13:31.8	9.09	0.33	0.02	0.67
JCMTLYS J04533.72+484723.7	152.55	-2.59	04:05:33.72	+48:47:23.7	6.64	0.17	0.01	0.57
JCMTLYS J04900.12+47429.9	153.70	-3.01	04:09:00.12	+47:42:09.9	11.74	1.38	0.08	0.76
JCMTLYS J035736.38+514839.6	149.60	-1.15	03:57:36.38	+51:48:39.6	6.77	0.10	0.01	0.58
JCMTLYS J042831.27+475651.7	155.87	-0.55	04:28:31.27	+47:56:51.7	5.90	0.08	0.00	0.54
JCMTLYS J045946.95+463342.8	160.39	2.56	04:59:46.95	+46:33:42.8	6.77	0.27	0.02	0.58
JCMTLYS J03317.64+561248.3	140.56	-2.08	03:03:17.64	+56:12:48.3	6.74	0.14	0.01	0.58
JCMTLYS J035615.04+535219.1	148.12	0.29	03:56:15.04	+53:52:19.1	10.48	0.19	0.01	0.72
JCMTLYS J04658.70+51921.1	151.13	-0.68	04:06:58.70	+51:09:21.1	8.31	0.14	0.01	0.64
JCMTLYS J044233.93+453029.1	159.30	-0.42	04:42:33.93	+45:30:29.1	6.31	0.05	0.00	0.56

Table A.1 continued from previous page

SASSy Name	*l*	*b*	*RA* (2000)	*Dec* (2000)	$Rad_{\rm eff}$ pc	$F_{\rm int}$ Jy	*error* Jy	*Aperture* Correction
JCMTLYS J04217.49+51558.4	150.62	-1.21	04:02:17.49	+51:05:58.4	9.24	0.19	0.01	0.68
JCMTLYS J044055.92+464222	158.21	0.16	04:40:55.92	+46:42:22.0	6.19	0.06	0.00	0.55
JCMTLYS J035831.43+502852.4	150.57	-2.07	03:58:31.43	+50:28:52.4	5.88	0.12	0.01	0.54
JCMTLYS J044208.61+485219.9	156.72	1.75	04:42:08.61	+48:52:19.9	6.47	0.11	0.01	0.57
JCMTLYS J042229.63+505655.9	153.04	0.85	04:22:29.63	+50:56:55.9	7.39	0.10	0.01	0.61
JCMTLYS J034227.65+582622	143.77	2.67	03:42:27.65	+58:26:22.0	6.06	0.16	0.01	0.55
JCMTLYS J033815.08+51494.5	147.25	-3.00	03:38:15.08	+51:49:04.5	9.79	1.05	0.06	0.70
JCMTLYS J044554.52+49819.8	156.92	2.39	04:45:54.52	+49:08:19.8	6.26	0.10	0.01	0.56
JCMTLYS J044429.62+493134.8	156.47	2.46	04:44:29.62	+49:31:34.8	5.67	0.06	0.00	0.53
JCMTLYS J044211.86+46931.2	158.76	-0.04	04:42:11.86	+46:09:31.2	5.76	0.07	0.00	0.53
JCMTLYS J043430.78+492638.8	155.46	1.20	04:34:30.78	+49:26:38.8	7.60	0.10	0.01	0.61
JCMTLYS J032731.02+58449.2	142.01	1.77	03:27:31.02	+58:44:09.2	13.50	0.19	0.01	0.81
JCMTLYS J04315.32+494812.5	151.59	-2.09	04:03:15.32	+49:48:12.5	6.07	0.08	0.00	0.55
JCMTLYS J044333.99+451136.7	159.65	-0.49	04:43:33.99	+45:11:36.7	6.10	0.05	0.00	0.55
JCMTLYS J033143.62+524546.7	145.89	-2.81	03:31:43.62	+52:45:46.7	6.66	0.68	0.04	0.57
JCMTLYS J041207.10+47738.8	154.48	-3.08	04:12:07.10	+47:07:38.8	7.62	0.31	0.02	0.62
JCMTLYS J044234.50+505258.8	155.25	3.12	04:42:34.50	+50:52:58.8	8.25	0.25	0.02	0.64

Table A.1 continued from previous page

SASSy Name	*l*	*b*	*RA* (2000)	*Dec* (2000)	$Rad_{\rm eff}$ pc	$F_{\rm int}$ Jy	*error* Jy	*Aperture* Correction
JCMTLYS J043650.19+431259.6	160.33	-2.70	04:36:50.19	+43:12:59.6	7.54	0.36	0.02	0.61
JCMTLYS J04015.51+571144	146.40	3.19	04:00:15.51	+57:11:44.0	8.67	0.32	0.02	0.66
JCMTLYS J03849.20+545959	141.84	-2.75	03:08:49.20	+54:59:59.0	7.33	0.31	0.02	0.60
JCMTLYS J034202.47+585118.2	143.47	2.96	03:42:02.47	+58:51:18.2	6.73	0.31	0.02	0.58
JCMTLYS J042219.57+472648.6	155.50	-1.64	04:22:19.57	+47:26:48.6	6.32	0.12	0.01	0.56
JCMTLYS J031116.80+542015.1	142.48	-3.14	03:11:16.80	+54:20:15.1	7.31	4.51	0.27	0.60
JCMTLYS J044839.40+492228	157.03	2.88	04:48:39.40	+49:22:28.0	6.45	0.10	0.01	0.56
JCMTLYS J04449.66+51272.9	150.69	-0.69	04:04:49.66	+51:27:02.9	9.10	0.14	0.01	0.67
JCMTLYS J045632.12+481559.5	158.71	3.18	04:56:32.12	+48:15:59.5	6.89	0.55	0.03	0.58
JCMTLYS J04817.49+475928.2	153.42	-2.88	04:08:17.49	+47:59:28.2	6.40	0.14	0.01	0.56
JCMTLYS J033306.81+59410.8	142.42	2.46	03:33:06.81	+59:04:10.8	7.73	0.09	0.01	0.62
JCMTLYS J035738.02+505336.2	150.20	-1.85	03:57:38.02	+50:53:36.2	6.54	0.09	0.01	0.57
JCMTLYS J045158.47+482951.9	158.05	2.74	04:51:58.47	+48:29:51.9	7.27	0.18	0.01	0.60
JCMTLYS J04705.66+481328.5	153.11	-2.84	04:07:05.66	+48:13:28.5	6.42	0.14	0.01	0.56
JCMTLYS J044454.57+501124.4	156.01	2.95	04:44:54.57	+50:11:24.4	10.10	2.79	0.17	0.71
JCMTLYS J03521.72+574923.2	140.02	-0.54	03:05:21.72	+57:49:23.2	7.37	0.09	0.01	0.61
JCMTLYS J035858.03+51120.9	150.16	-1.48	03:58:58.03	+51:12:00.9	7.14	0.12	0.01	0.60

Table A.1 continued from previous page

SASSy Name	*l*	*b*	*RA* (2000)	*Dec* (2000)	$Rad_{\rm eff}$ pc	$F_{\rm int}$ Jy	*error* Jy	*Aperture* Correction
JCMTLYS J031405.10+54618.1	142.95	-3.13	03:14:05.10	+54:06:18.1	6.91	0.70	0.04	0.59
JCMTLYS J045354.11+44424.6	161.69	0.20	04:53:54.11	+44:04:24.6	5.97	0.18	0.01	0.54
JCMTLYS J042808.34+501657.3	154.14	1.02	04:28:08.34	+50:16:57.3	5.99	0.05	0.00	0.54
JCMTLYS J042007.76+49165.4	153.96	-0.61	04:20:07.76	+49:16:05.4	6.40	0.08	0.00	0.56
JCMTLYS J031823.82+54258.4	143.52	-2.84	03:18:23.82	+54:02:58.4	9.33	0.38	0.02	0.68
JCMTLYS J043453.40+462117.6	157.78	-0.84	04:34:53.40	+46:21:17.6	5.59	0.04	0.00	0.52
JCMTLYS J035503.44+503253.3	150.11	-2.37	03:55:03.44	+50:32:53.3	7.84	0.14	0.01	0.62
JCMTLYS J042333.70+484631.7	154.70	-0.56	04:23:33.70	+48:46:31.7	6.37	0.08	0.00	0.56
JCMTLYS J043552.92+515351.9	153.79	3.02	04:35:52.92	+51:53:51.9	5.78	0.38	0.02	0.53
JCMTLYS J04856.30+50931	152.03	-1.21	04:08:56.30	+50:09:31.0	5.84	0.10	0.01	0.54
JCMTLYS J043823.45+451513.5	159.00	-1.13	04:38:23.45	+45:15:13.5	6.13	0.07	0.00	0.55
JCMTLYS J034213.30+51324.6	147.91	-2.86	03:42:13.30	+51:32:04.6	7.20	0.96	0.06	0.60
JCMTLYS J042510.17+513030.1	152.94	1.54	04:25:10.17	+51:30:30.1	7.91	0.11	0.01	0.63
JCMTLYS J033320.57+553018.9	144.50	-0.43	03:33:20.57	+55:30:18.9	6.71	0.08	0.00	0.58
JCMTLYS J044158.48+45404.3	159.11	-0.39	04:41:58.48	+45:40:04.3	8.25	0.09	0.01	0.64
JCMTLYS J043553.65+515423.8	153.79	3.02	04:35:53.65	+51:54:23.8	7.35	0.61	0.04	0.60
JCMTLYS J03844.87+5536.1	141.80	-2.71	03:08:44.87	+55:03:06.1	8.40	0.46	0.03	0.65

Table A.1 continued from previous page

SASSy Name	*l*	*b*	*RA* (2000)	*Dec* (2000)	$Rad_{\rm eff}$ pc	$F_{\rm int}$ Jy	*error* Jy	*Aperture* Correction
JCMTLYS J035412.51+511716	149.53	-1.89	03:54:12.51	+51:17:16.0	9.85	2.49	0.15	0.70
JCMTLYS J044123.74+445745	159.57	-0.93	04:41:23.74	+44:57:45.0	6.29	0.05	0.00	0.56
JCMTLYS J035417.54+502749.9	150.07	-2.52	03:54:17.54	+50:27:49.9	7.67	0.15	0.01	0.62
JCMTLYS J03632.77+55037.6	141.55	-2.90	03:06:32.77	+55:00:37.6	6.06	0.30	0.02	0.55
JCMTLYS J042800.11+473237.2	156.10	-0.89	04:28:00.11	+47:32:37.2	5.67	0.07	0.00	0.53
JCMTLYS J044706.53+462312.6	159.15	0.76	04:47:06.53	+46:23:12.6	5.74	0.06	0.00	0.53
JCMTLYS J025745.39+553523	140.17	-3.00	02:57:45.39	+55:35:23.0	8.74	0.41	0.02	0.66
JCMTLYS J044114.80+472127.4	157.76	0.63	04:41:14.80	+47:21:27.4	7.61	0.09	0.01	0.62
JCMTLYS J031058.86+542528	142.40	-3.09	03:10:58.86	+54:25:28.0	9.04	7.18	0.43	0.67
JCMTLYS J043735.63+464949.6	157.74	-0.18	04:37:35.63	+46:49:49.6	6.21	0.08	0.00	0.55
JCMTLYS J032713.48+591816	141.66	2.22	03:27:13.48	+59:18:16.0	8.10	0.10	0.01	0.64
JCMTLYS J053047.84+334757.8	174.20	-0.07	05:30:47.84	+33:47:57.8	54.38	20.21	1.21	1.07
JCMTLYS J053912.13+354553.9	173.48	2.44	05:39:12.13	+35:45:53.9	46.76	20.47	1.23	1.04
JCMTLYS J052022.27+363757.5	170.66	-0.25	05:20:22.27	+36:37:57.5	32.25	6.67	0.40	1.00
JCMTLYS J054053.51+354150.9	173.72	2.70	05:40:53.51	+35:41:50.9	46.74	14.86	0.89	1.04
JCMTLYS J053910.83+354514.2	173.49	2.43	05:39:10.83	+35:45:14.2	25.69	3.80	0.23	0.98
JCMTLYS J053908.53+354645.8	173.46	2.44	05:39:08.53	+35:46:45.8	23.52	2.36	0.14	0.96

Table A.1 continued from previous page

SASSy Name	*l*	*b*	*RA* (2000)	*Dec* (2000)	$Rad_{\rm eff}$ pc	$F_{\rm int}$ Jy	*error* Jy	*Aperture* Correction
JCMTLYS J054131.03+354926	173.68	2.87	05:41:31.03	+35:49:26.0	26.41	2.96	0.18	0.98
JCMTLYS J051252.71+404144.5	166.50	0.92	05:12:52.71	+40:41:44.5	13.06	0.65	0.04	0.80
JCMTLYS J054130.83+35505.1	173.67	2.88	05:41:30.83	+35:50:05.1	26.11	2.58	0.15	0.98
JCMTLYS J053752.65+3205.7	176.52	0.20	05:37:52.65	+32:00:05.7	24.56	2.58	0.15	0.97
JCMTLYS J054107.39+354935	173.63	2.81	05:41:07.39	+35:49:35.0	19.43	1.30	0.08	0.92
JCMTLYS J053801.30+355818	173.18	2.35	05:38:01.30	+35:58:18.0	23.95	1.79	0.11	0.97
JCMTLYS J051713.84+392221.8	168.06	0.82	05:17:13.84	+39:22:21.8	14.96	0.76	0.05	0.84
JCMTLYS J054100.41+354927.1	173.62	2.79	05:41:00.41	+35:49:27.1	20.22	1.17	0.07	0.93
JCMTLYS J054814.28+301425.3	179.18	1.16	05:48:14.28	+30:14:25.3	9.51	1.57	0.09	0.69
JCMTLYS J053800.65+355859.3	173.17	2.36	05:38:00.65	+35:58:59.3	26.40	2.68	0.16	0.98
JCMTLYS J053928.06+354045.9	173.58	2.44	05:39:28.06	+35:40:45.9	30.50	2.60	0.16	1.00
JCMTLYS J054122.86+35528.6	173.63	2.87	05:41:22.86	+35:52:08.6	16.53	1.00	0.06	0.87
JCMTLYS J053342.11+371444.9	171.64	2.31	05:33:42.11	+37:14:44.9	18.12	0.68	0.04	0.90
JCMTLYS J054100.65+354836	173.64	2.78	05:41:00.65	+35:48:36.0	18.18	0.81	0.05	0.90
JCMTLYS J052848.15+342337.7	173.48	-0.09	05:28:48.15	+34:23:37.7	16.38	0.66	0.04	0.87
JCMTLYS J054053.40+353828.1	173.77	2.67	05:40:53.40	+35:38:28.1	17.21	0.79	0.05	0.89
JCMTLYS J054129.27+354855.8	173.68	2.86	05:41:29.27	+35:48:55.8	20.59	1.12	0.07	0.93

Table A.1 continued from previous page

SASSy Name	*l*	*b*	*RA* (2000)	*Dec* (2000)	$Rad_{\rm eff}$ pc	$F_{\rm int}$ Jy	*error* Jy	*Aperture* Correction
JCMTLYS J054053.25+354041.3	173.73	2.69	05:40:53.25	+35:40:41.3	19.35	0.92	0.06	0.92
JCMTLYS J053237.10+31379.7	176.23	-0.94	05:32:37.10	+31:37:09.7	8.66	0.33	0.02	0.66
JCMTLYS J054111.25+35502.5	173.63	2.82	05:41:11.25	+35:50:02.5	16.14	0.61	0.04	0.87
JCMTLYS J053752.95+315933.2	176.52	0.20	05:37:52.95	+31:59:33.2	14.47	0.83	0.05	0.83
JCMTLYS J052425.49+363638.6	171.14	0.41	05:24:25.49	+36:36:38.6	7.32	0.14	0.01	0.60
JCMTLYS J045139.81+45356.5	160.27	0.85	04:51:39.81	+45:35:06.5	15.32	0.38	0.02	0.85
JCMTLYS J045139.24+453534.6	160.26	0.85	04:51:39.24	+45:35:34.6	15.87	0.43	0.03	0.86
JCMTLYS J053020.78+31127.9	176.47	-1.68	05:30:20.78	+31:01:27.9	12.71	0.48	0.03	0.79
JCMTLYS J053651.94+361051.2	172.87	2.27	05:36:51.94	+36:10:51.2	19.12	0.73	0.04	0.91
JCMTLYS J053356.15+372350.5	171.53	2.43	05:33:56.15	+37:23:50.5	18.13	0.49	0.03	0.90
JCMTLYS J043832.93+43155.9	160.51	-2.45	04:38:32.93	+43:15:05.9	7.34	0.55	0.03	0.60
JCMTLYS J053358.50+372420.6	171.53	2.44	05:33:58.50	+37:24:20.6	22.42	0.65	0.04	0.95
JCMTLYS J055234.64+304643.2	179.20	2.24	05:52:34.64	+30:46:43.2	10.35	0.67	0.04	0.72
JCMTLYS J054149.67+341253.9	175.08	2.08	05:41:49.67	+34:12:53.9	5.76	0.12	0.01	0.53
JCMTLYS J053515.22+314522.9	176.42	-0.40	05:35:15.22	+31:45:22.9	8.36	0.55	0.03	0.65
JCMTLYS J044821.26+48129.8	157.90	2.09	04:48:21.26	+48:12:09.8	7.94	1.10	0.07	0.63
JCMTLYS J052632.12+405954.2	167.73	3.21	05:26:32.12	+40:59:54.2	10.66	1.90	0.11	0.73

Table A.1 continued from previous page

SASSy Name	*l*	*b*	*RA* (2000)	*Dec* (2000)	$Rad_{\rm eff}$ pc	$F_{\rm int}$ Jy	*error* Jy	*Aperture* Correction
JCMTLYS J054105.93+355213.7	173.59	2.83	05:41:05.93	+35:52:13.7	15.14	0.52	0.03	0.85
JCMTLYS J054128.06+354917.5	173.67	2.86	05:41:28.06	+35:49:17.5	8.98	0.23	0.01	0.67
JCMTLYS J054106.21+35508.5	173.62	2.81	05:41:06.21	+35:50:08.5	15.64	0.55	0.03	0.86
JCMTLYS J05418.04+431255.4	163.53	1.14	05:04:18.04	+43:12:55.4	8.26	0.12	0.01	0.64
JCMTLYS J052631.38+41017.1	167.73	3.21	05:26:31.38	+41:00:17.1	11.04	0.60	0.04	0.74
JCMTLYS J054045.93+354816.5	173.61	2.73	05:40:45.93	+35:48:16.5	13.79	0.35	0.02	0.82
JCMTLYS J051422.56+434935.6	164.12	2.97	05:14:22.56	+43:49:35.6	7.71	0.42	0.03	0.62
JCMTLYS J051919.96+411148.3	166.80	2.20	05:19:19.96	+41:11:48.3	21.53	0.70	0.04	0.94
JCMTLYS J052642.15+4112	167.73	3.24	05:26:42.15	+41:01:02.0	10.39	2.34	0.14	0.72
JCMTLYS J053654.00+361033.7	172.88	2.27	05:36:54.00	+36:10:33.7	15.13	0.37	0.02	0.85
JCMTLYS J045809.79+425959.2	163.01	0.13	04:58:09.79	+42:59:59.2	6.08	0.09	0.01	0.55
JCMTLYS J044336.37+423753.1	161.59	-2.16	04:43:36.37	+42:37:53.1	6.74	0.18	0.01	0.58
JCMTLYS J045824.63+383116.8	166.55	-2.62	04:58:24.63	+38:31:16.8	6.66	0.19	0.01	0.57
JCMTLYS J05528.86+39355.5	166.55	-0.88	05:05:28.86	+39:35:05.5	8.67	0.36	0.02	0.66
JCMTLYS J044539.07+425523	161.61	-1.69	04:45:39.07	+42:55:23.0	11.68	0.33	0.02	0.76
JCMTLYS J05805.87+45954.9	162.38	2.86	05:08:05.87	+45:09:54.9	10.27	2.59	0.16	0.71
JCMTLYS J05923.06+404428	166.07	0.41	05:09:23.06	+40:44:28.0	9.76	0.41	0.02	0.70

Table A.1 continued from previous page

SASSy Name	*l*	*b*	*RA* (2000)	*Dec* (2000)	$Rad_{\rm eff}$ pc	$F_{\rm int}$ Jy	*error* Jy	*Aperture* Correction
JCMTLYS J05536.79+403452.5	165.77	-0.26	05:05:36.79	+40:34:52.5	8.20	0.48	0.03	0.64
JCMTLYS J052919.41+363243.4	171.74	1.19	05:29:19.41	+36:32:43.4	6.53	0.09	0.01	0.57
JCMTLYS J05821.50+45941.7	162.41	2.90	05:08:21.50	+45:09:41.7	9.55	0.93	0.06	0.69
JCMTLYS J052914.34+342242.8	173.54	-0.02	05:29:14.34	+34:22:42.8	16.38	0.33	0.02	0.87
JCMTLYS J053847.88+304115.9	177.73	-0.33	05:38:47.88	+30:41:15.9	15.54	0.44	0.03	0.85
JCMTLYS J051959.99+415015.8	166.35	2.67	05:19:59.99	+41:50:15.8	6.69	0.19	0.01	0.58
JCMTLYS J055227.79+304510.6	179.21	2.21	05:52:27.79	+30:45:10.6	12.91	0.85	0.05	0.79
JCMTLYS J053034.18+385645.9	169.87	2.72	05:30:34.18	+38:56:45.9	6.17	0.10	0.01	0.55
JCMTLYS J044633.23+424519.7	161.85	-1.67	04:46:33.23	+42:45:19.7	15.45	0.50	0.03	0.85
JCMTLYS J054248.76+283447.3	179.98	-0.71	05:42:48.76	+28:34:47.3	7.17	0.58	0.04	0.60
JCMTLYS J044505.99+425543.7	161.54	-1.76	04:45:05.99	+42:55:43.7	7.35	0.18	0.01	0.60
JCMTLYS J053258.90+38411.9	170.35	2.97	05:32:58.90	+38:41:01.9	7.54	0.45	0.03	0.61
JCMTLYS J053654.91+36107.1	172.89	2.27	05:36:54.91	+36:10:07.1	8.11	0.13	0.01	0.64
JCMTLYS J05352.23+372259.1	168.11	-2.47	05:03:52.23	+37:22:59.1	6.62	0.11	0.01	0.57
JCMTLYS J051712.25+392152	168.07	0.81	05:17:12.25	+39:21:52.0	11.15	0.18	0.01	0.74
JCMTLYS J053801.12+355739.5	173.19	2.35	05:38:01.12	+35:57:39.5	15.52	0.52	0.03	0.85
JCMTLYS J044403.94+415615.3	162.17	-2.55	04:44:03.94	+41:56:15.3	9.06	0.31	0.02	0.67

Table A.1 continued from previous page

SASSy Name	*l*	*b*	*RA* (2000)	*Dec* (2000)	$Rad_{\rm eff}$ pc	$F_{\rm int}$ Jy	*error* Jy	*Aperture* Correction
JCMTLYS J044511.29+425537.3	161.56	-1.75	04:45:11.29	+42:55:37.3	8.92	0.25	0.02	0.67
JCMTLYS J044109.10+42020.7	161.76	-2.92	04:41:09.10	+42:00:20.7	17.48	1.24	0.07	0.89
JCMTLYS J045116.33+422347.3	162.68	-1.24	04:51:16.33	+42:23:47.3	8.42	0.12	0.01	0.65
JCMTLYS J052449.43+412343	167.22	3.16	05:24:49.43	+41:23:43.0	7.27	0.68	0.04	0.60
JCMTLYS J044633.51+42225	162.14	-1.92	04:46:33.51	+42:22:05.0	26.73	1.29	0.08	0.98
JCMTLYS J053533.66+324654.2	175.60	0.21	05:35:33.66	+32:46:54.2	6.93	0.07	0.00	0.59
JCMTLYS J054054.36+354949.5	173.61	2.77	05:40:54.36	+35:49:49.5	11.53	0.27	0.02	0.75
JCMTLYS J05746.93+453042.3	162.07	3.02	05:07:46.93	+45:30:42.3	7.74	5.91	0.35	0.62
JCMTLYS J051320.55+39852.2	167.81	0.08	05:13:20.55	+39:08:52.2	8.80	0.17	0.01	0.66
JCMTLYS J043833.99+43814.4	160.60	-2.52	04:38:33.99	+43:08:14.4	6.74	0.11	0.01	0.58
JCMTLYS J052025.38+363832	170.66	-0.23	05:20:25.38	+36:38:32.0	6.57	0.10	0.01	0.57
JCMTLYS J054543.25+301311.1	178.92	0.69	05:45:43.25	+30:13:11.1	5.58	0.15	0.01	0.52
JCMTLYS J052018.32+424349.6	165.64	3.22	05:20:18.32	+42:43:49.6	6.04	0.25	0.02	0.55
JCMTLYS J05854.63+445829.9	162.62	2.86	05:08:54.63	+44:58:29.9	7.55	0.25	0.01	0.61
JCMTLYS J044342.82+434557.4	160.74	-1.41	04:43:42.82	+43:45:57.4	11.69	0.27	0.02	0.76
JCMTLYS J055127.26+302319	179.41	1.83	05:51:27.26	+30:23:19.0	5.55	0.59	0.04	0.52
JCMTLYS J052014.62+423924.7	165.70	3.17	05:20:14.62	+42:39:24.7	9.33	0.37	0.02	0.68

Table A.1 continued from previous page

SASSy Name	*l*	*b*	*RA* (2000)	*Dec* (2000)	$Rad_{\rm eff}$ pc	$F_{\rm int}$ Jy	*error* Jy	*Aperture* Correction
JCMTLYS J053347.88+325347.7	175.30	-0.04	05:33:47.88	+32:53:47.7	7.81	0.08	0.00	0.62
JCMTLYS J051326.10+37273.6	169.19	-0.90	05:13:26.10	+37:27:03.6	13.92	0.27	0.02	0.82
JCMTLYS J055234.12+304535.4	179.21	2.23	05:52:34.12	+30:45:35.4	9.63	0.53	0.03	0.69
JCMTLYS J051401.11+433431.8	164.29	2.78	05:14:01.11	+43:34:31.8	6.07	0.17	0.01	0.55
JCMTLYS J052839.21+342354	173.46	-0.11	05:28:39.21	+34:23:54.0	12.81	0.26	0.02	0.79
JCMTLYS J054836.35+301028.3	179.28	1.20	05:48:36.35	+30:10:28.3	6.36	0.17	0.01	0.56
JCMTLYS J044533.55+425838	161.56	-1.67	04:45:33.55	+42:58:38.0	9.54	0.20	0.01	0.69
JCMTLYS J052042.99+414156.2	166.54	2.70	05:20:42.99	+41:41:56.2	8.85	0.21	0.01	0.66
JCMTLYS J044450.52+42211.8	161.95	-2.17	04:44:50.52	+42:21:01.8	7.34	0.18	0.01	0.60
JCMTLYS J044038.75+42167.2	161.50	-2.81	04:40:38.75	+42:16:07.2	9.81	0.24	0.01	0.70
JCMTLYS J054103.90+354956.9	173.62	2.80	05:41:03.90	+35:49:56.9	8.69	0.18	0.01	0.66
JCMTLYS J054712.71+303610.9	178.76	1.16	05:47:12.71	+30:36:10.9	11.49	0.27	0.02	0.75
JCMTLYS J044132.18+43219.7	160.80	-1.97	04:41:32.18	+43:21:09.7	10.53	0.24	0.01	0.72
JCMTLYS J055337.85+321353.7	178.06	3.17	05:53:37.85	+32:13:53.7	7.31	0.34	0.02	0.60
JCMTLYS J044635.20+424516.9	161.85	-1.67	04:46:35.20	+42:45:16.9	6.74	0.15	0.01	0.58
JCMTLYS J053049.64+312116.9	176.25	-1.41	05:30:49.64	+31:21:16.9	5.69	0.09	0.01	0.53
JCMTLYS J052443.80+301737.1	176.40	-3.09	05:24:43.80	+30:17:37.1	6.29	0.44	0.03	0.56

Table A.1 continued from previous page

SASSy Name	*l*	*b*	*RA* (2000)	*Dec* (2000)	$Rad_{\rm eff}$ pc	$F_{\rm int}$ Jy	*error* Jy	*Aperture* Correction
JCMTLYS J043721.97+43159.1	160.37	-2.61	04:37:21.97	+43:15:09.1	10.52	0.32	0.02	0.72
JCMTLYS J054729.84+294221.2	179.55	0.75	05:47:29.84	+29:42:21.2	5.75	0.11	0.01	0.53
JCMTLYS J045110.69+422157.7	162.69	-1.27	04:51:10.69	+42:21:57.7	12.61	0.20	0.01	0.78
JCMTLYS J052142.71+341127.8	172.82	-1.41	05:21:42.71	+34:11:27.8	7.42	0.21	0.01	0.61
JCMTLYS J044343.67+434511	160.76	-1.41	04:43:43.67	+43:45:11.0	10.40	0.22	0.01	0.72
JCMTLYS J044508.00+42552.4	161.56	-1.76	04:45:08.00	+42:55:02.4	6.74	0.13	0.01	0.58
JCMTLYS J05043.73+365923.3	168.04	-3.20	05:00:43.73	+36:59:23.3	7.39	0.45	0.03	0.61
JCMTLYS J053612.22+38642.4	171.17	3.19	05:36:12.22	+38:06:42.4	5.90	0.19	0.01	0.54
JCMTLYS J052902.86+335921.8	173.84	-0.27	05:29:02.86	+33:59:21.8	6.64	0.06	0.00	0.57
JCMTLYS J053035.03+394324.7	169.22	3.15	05:30:35.03	+39:43:24.7	7.21	0.41	0.02	0.60
JCMTLYS J053349.04+33318.2	174.78	0.30	05:33:49.04	+33:31:08.2	6.40	0.10	0.01	0.56
JCMTLYS J051901.38+36126.8	170.86	-0.72	05:19:01.38	+36:12:06.8	8.36	0.10	0.01	0.65
JCMTLYS J053518.96+38951.7	171.03	3.07	05:35:18.96	+38:09:51.7	7.14	0.43	0.03	0.60
JCMTLYS J053626.69+311746.3	176.95	-0.43	05:36:26.69	+31:17:46.3	10.66	0.26	0.02	0.73
JCMTLYS J044544.20+425546.2	161.62	-1.67	04:45:44.20	+42:55:46.2	12.50	0.31	0.02	0.78
JCMTLYS J044244.24+414828.5	162.11	-2.82	04:42:44.24	+41:48:28.5	10.23	0.43	0.03	0.71
JCMTLYS J052007.36+414942.9	166.37	2.68	05:20:07.36	+41:49:42.9	9.75	0.27	0.02	0.70

Table A.1 continued from previous page

SASSy Name	*l*	*b*	*RA* (2000)	*Dec* (2000)	$Rad_{\rm eff}$ pc	$F_{\rm int}$ Jy	*error* Jy	*Aperture* Correction
JCMTLYS J043922.05+423416.5	161.12	-2.79	04:39:22.05	+42:34:16.5	13.98	0.35	0.02	0.82
JCMTLYS J051916.67+411152.2	166.79	2.19	05:19:16.67	+41:11:52.2	9.60	0.14	0.01	0.69
JCMTLYS J052904.71+343921.9	173.29	0.11	05:29:04.71	+34:39:21.9	6.86	0.09	0.01	0.58
JCMTLYS J053301.31+38426	170.34	2.98	05:33:01.31	+38:42:06.0	7.54	1.74	0.10	0.61
JCMTLYS J052627.75+405640.6	167.77	3.17	05:26:27.75	+40:56:40.6	7.44	0.32	0.02	0.61
JCMTLYS J054926.51+301838	179.25	1.42	05:49:26.51	+30:18:38.0	5.56	0.21	0.01	0.52
JCMTLYS J051016.05+403937.6	166.24	0.50	05:10:16.05	+40:39:37.6	13.39	0.30	0.02	0.81
JCMTLYS J053445.41+373636.4	171.44	2.68	05:34:45.41	+37:36:36.4	7.50	0.12	0.01	0.61
JCMTLYS J053631.41+332252.4	175.20	0.70	05:36:31.41	+33:22:52.4	6.58	0.08	0.00	0.57
JCMTLYS J053240.77+381545.5	170.67	2.69	05:32:40.77	+38:15:45.5	5.92	0.13	0.01	0.54
JCMTLYS J05232.13+38252.5	167.13	-2.04	05:02:32.13	+38:25:02.5	6.65	0.09	0.01	0.57
JCMTLYS J052015.36+424011.5	165.69	3.18	05:20:15.36	+42:40:11.5	6.70	0.85	0.05	0.58
JCMTLYS J045415.42+383419.3	166.00	-3.22	04:54:15.42	+38:34:19.3	7.45	0.43	0.03	0.61
JCMTLYS J053011.84+395332.2	169.04	3.18	05:30:11.84	+39:53:32.2	7.40	0.64	0.04	0.61
JCMTLYS J044216.90+43125.1	161.13	-2.09	04:42:16.90	+43:01:25.1	8.08	0.16	0.01	0.63
JCMTLYS J052942.15+372412.9	171.07	1.73	05:29:42.15	+37:24:12.9	6.76	0.07	0.00	0.58
JCMTLYS J052736.87+403128.4	168.24	3.11	05:27:36.87	+40:31:28.4	7.79	2.08	0.12	0.62

Table A.1 continued from previous page

SASSy Name	*l*	*b*	*RA* (2000)	*Dec* (2000)	$Rad_{\rm eff}$ pc	$F_{\rm int}$ Jy	*error* Jy	*Aperture* Correction
JCMTLYS J044401.83+421421	161.94	-2.36	04:44:01.83	+42:14:21.0	11.54	0.29	0.02	0.75
JCMTLYS J054126.36+355241.8	173.62	2.89	05:41:26.36	+35:52:41.8	11.41	0.27	0.02	0.75
JCMTLYS J052951.16+385749.7	169.78	2.61	05:29:51.16	+38:57:49.7	6.17	0.11	0.01	0.55
JCMTLYS J05429.21+36747.7	169.18	-3.13	05:04:29.21	+36:07:47.7	8.55	1.77	0.11	0.65
JCMTLYS J052730.13+395126.1	168.78	2.73	05:27:30.13	+39:51:26.1	6.63	0.26	0.02	0.57
JCMTLYS J044244.74+414814.8	162.11	-2.83	04:42:44.74	+41:48:14.8	13.55	0.72	0.04	0.81
JCMTLYS J052754.45+36736.6	171.93	0.72	05:27:54.45	+36:07:36.6	5.88	0.06	0.00	0.54
JCMTLYS J051306.46+423927	164.94	2.10	05:13:06.46	+42:39:27.0	6.51	0.08	0.00	0.57
JCMTLYS J054029.48+334746.9	175.29	1.62	05:40:29.48	+33:47:46.9	6.77	0.08	0.01	0.58
JCMTLYS J044546.37+425629.7	161.61	-1.66	04:45:46.37	+42:56:29.7	9.23	0.23	0.01	0.68
JCMTLYS J053949.86+3680.3	173.23	2.75	05:39:49.86	+36:08:00.3	8.41	0.14	0.01	0.65
JCMTLYS J054057.24+35517.7	173.59	2.79	05:40:57.24	+35:51:07.7	6.65	0.10	0.01	0.57
JCMTLYS J044041.48+421619.5	161.51	-2.80	04:40:41.48	+42:16:19.5	12.13	0.32	0.02	0.77
JCMTLYS J055122.49+302245.7	179.41	1.82	05:51:22.49	+30:22:45.7	5.96	0.32	0.02	0.54
JCMTLYS J044521.35+432758.5	161.17	-1.38	04:45:21.35	+43:27:58.5	7.91	0.21	0.01	0.63
JCMTLYS J054420.19+282424.8	-179.70	-0.52	05:44:20.19	+28:24:24.8	5.70	0.69	0.04	0.53
JCMTLYS J052334.16+314638	175.03	-2.46	05:23:34.16	+31:46:38.0	5.74	0.11	0.01	0.53

Table A.1 continued from previous page

SASSy Name	*l*	*b*	*RA* (2000)	*Dec* (2000)	$Rad_{\rm eff}$ pc	$F_{\rm int}$ Jy	*error* Jy	*Aperture* Correction
JCMTLYS J052735.29+403533.8	168.18	3.15	05:27:35.29	+40:35:33.8	5.99	0.24	0.01	0.54
JCMTLYS J044212.85+432245.1	160.86	-1.86	04:42:12.85	+43:22:45.1	8.43	0.17	0.01	0.65
JCMTLYS J053029.06+343226.5	173.54	0.28	05:30:29.06	+34:32:26.5	6.46	0.08	0.00	0.57
JCMTLYS J051324.37+37271.1	169.19	-0.91	05:13:24.37	+37:27:01.1	9.91	0.16	0.01	0.70
JCMTLYS J045120.74+422652.9	162.65	-1.19	04:51:20.74	+42:26:52.9	8.75	0.11	0.01	0.66
JCMTLYS J053809.49+36313.8	172.73	2.67	05:38:09.49	+36:31:03.8	11.70	0.32	0.02	0.76
JCMTLYS J054309.72+31113.1	177.95	0.64	05:43:09.72	+31:01:13.1	6.24	0.09	0.01	0.56
JCMTLYS J044223.19+4212.9	161.90	-2.74	04:42:23.19	+42:01:02.9	11.53	0.35	0.02	0.75
JCMTLYS J052756.01+303457.9	176.55	-2.35	05:27:56.01	+30:34:57.9	6.29	0.10	0.01	0.56
JCMTLYS J053228.35+341347.2	174.03	0.46	05:32:28.35	+34:13:47.2	5.80	0.08	0.00	0.53
JCMTLYS J052452.17+41223.7	167.25	3.15	05:24:52.17	+41:22:03.7	7.27	0.62	0.04	0.60
JCMTLYS J054637.59+33834.4	176.52	2.37	05:46:37.59	+33:08:34.4	5.91	0.07	0.00	0.54
JCMTLYS J054026.85+343220.6	174.65	2.01	05:40:26.85	+34:32:20.6	7.17	0.10	0.01	0.60
JCMTLYS J053901.90+364048.2	172.69	2.90	05:39:01.90	+36:40:48.2	7.08	1.97	0.12	0.59
JCMTLYS J043921.68+42350.6	161.11	-2.78	04:39:21.68	+42:35:00.6	8.75	0.26	0.02	0.66
JCMTLYS J044524.92+415847.5	162.30	-2.34	04:45:24.92	+41:58:47.5	11.66	0.29	0.02	0.76
JCMTLYS J043744.22+424719	160.76	-2.87	04:37:44.22	+42:47:19.0	6.94	0.22	0.01	0.59

Table A.1 continued from previous page

SASSy Name	*l*	*b*	*RA* (2000)	*Dec* (2000)	$Rad_{\rm eff}$ pc	$F_{\rm int}$ Jy	*error* Jy	*Aperture* Correction
JCMTLYS J044456.87+431948.3	161.22	-1.52	04:44:56.87	+43:19:48.3	7.73	0.18	0.01	0.62
JCMTLYS J05932.68+391444.2	167.29	-0.46	05:09:32.68	+39:14:44.2	6.87	0.07	0.00	0.58
JCMTLYS J053657.55+324952.5	175.71	0.48	05:36:57.55	+32:49:52.5	6.36	0.07	0.00	0.56
JCMTLYS J053641.21+314742.4	176.55	-0.12	05:36:41.21	+31:47:42.4	5.90	0.13	0.01	0.54
JCMTLYS J044631.41+422232.5	162.13	-1.92	04:46:31.41	+42:22:32.5	19.71	0.65	0.04	0.92
JCMTLYS J053006.51+395426.1	169.02	3.17	05:30:06.51	+39:54:26.1	8.91	5.46	0.33	0.67
JCMTLYS J053336.32+344353.1	173.74	0.92	05:33:36.32	+34:43:53.1	6.24	0.08	0.00	0.56
JCMTLYS J054858.84+323647.8	177.23	2.52	05:48:58.84	+32:36:47.8	6.28	0.10	0.01	0.56
JCMTLYS J051214.15+443537.5	163.28	3.11	05:12:14.15	+44:35:37.5	7.54	0.26	0.02	0.61
JCMTLYS J054639.31+294513.1	179.42	0.62	05:46:39.31	+29:45:13.1	6.53	0.11	0.01	0.57
JCMTLYS J053744.73+32039.4	176.49	0.18	05:37:44.73	+32:00:39.4	9.73	0.24	0.01	0.70
JCMTLYS J045317.30+40930.9	164.65	-2.36	04:53:17.30	+40:09:30.9	7.30	0.10	0.01	0.60
JCMTLYS J053749.82+365714.6	172.32	2.84	05:37:49.82	+36:57:14.6	6.51	0.11	0.01	0.57
JCMTLYS J051957.06+38105	169.35	0.56	05:19:57.06	+38:10:05.0	7.20	0.08	0.00	0.60
JCMTLYS J053233.06+38147.6	170.68	2.65	05:32:33.06	+38:14:07.6	9.00	0.19	0.01	0.67
JCMTLYS J044106.68+42034.3	161.75	-2.92	04:41:06.68	+42:00:34.3	17.15	1.07	0.06	0.88
JCMTLYS J05026.27+47827.2	160.00	3.00	05:00:26.27	+47:08:27.2	8.79	0.51	0.03	0.66

Table A.1 continued from previous page

SASSy Name	*l*	*b*	*RA* (2000)	*Dec* (2000)	$Rad_{\rm eff}$ pc	$F_{\rm int}$ Jy	*error* Jy	*Aperture* Correction
JCMTLYS J054125.12+355315.5	173.61	2.89	05:41:25.12	+35:53:15.5	8.39	0.21	0.01	0.65
JCMTLYS J044541.40+425549.2	161.61	-1.68	04:45:41.40	+42:55:49.2	15.27	0.48	0.03	0.85
JCMTLYS J05919.76+435314.5	163.54	2.28	05:09:19.76	+43:53:14.5	8.26	0.10	0.01	0.64
JCMTLYS J044541.08+425723.3	161.59	-1.66	04:45:41.08	+42:57:23.3	7.91	0.17	0.01	0.63
JCMTLYS J044414.07+432334.5	161.09	-1.58	04:44:14.07	+43:23:34.5	8.77	0.18	0.01	0.66
JCMTLYS J05238.16+424110.9	163.76	0.58	05:02:38.16	+42:41:10.9	6.07	0.07	0.00	0.55
JCMTLYS J052042.88+414247.9	166.52	2.71	05:20:42.88	+41:42:47.9	6.69	0.20	0.01	0.58
JCMTLYS J044506.68+425620.6	161.54	-1.75	04:45:06.68	+42:56:20.6	8.60	0.17	0.01	0.65
JCMTLYS J05739.99+374734.8	168.24	-1.62	05:07:39.99	+37:47:34.8	7.03	0.09	0.01	0.59
JCMTLYS J053307.00+355431.6	172.69	1.48	05:33:07.00	+35:54:31.6	6.89	0.07	0.00	0.58
JCMTLYS J053220.20+39226.4	169.98	3.06	05:32:20.20	+39:02:26.4	6.59	0.25	0.01	0.57
JCMTLYS J055133.44+313743.2	178.35	2.49	05:51:33.44	+31:37:43.2	6.22	0.09	0.01	0.55
JCMTLYS J044455.48+42563.1	161.52	-1.78	04:44:55.48	+42:56:03.1	6.74	0.13	0.01	0.58
JCMTLYS J052909.61+331421.7	174.48	-0.66	05:29:09.61	+33:14:21.7	6.41	0.07	0.00	0.56
JCMTLYS J054102.34+361220.5	173.30	2.99	05:41:02.34	+36:12:20.5	7.58	0.25	0.02	0.61
JCMTLYS J054428.67+312826.8	177.71	1.11	05:44:28.67	+31:28:26.8	5.64	0.06	0.00	0.53
JCMTLYS J053219.15+38451	170.78	2.53	05:32:19.15	+38:04:51.0	7.52	0.31	0.02	0.61

Table A.1 continued from previous page

SASSy Name	*l*	*b*	*RA* (2000)	*Dec* (2000)	$Rad_{\rm eff}$ pc	$F_{\rm int}$ Jy	*error* Jy	*Aperture* Correction
JCMTLYS J052838.43+361211.9	171.95	0.89	05:28:38.43	+36:12:11.9	5.88	0.06	0.00	0.54
JCMTLYS J052625.67+405034.7	167.85	3.10	05:26:25.67	+40:50:34.7	6.22	0.38	0.02	0.55
JCMTLYS J054648.45+331516.4	176.44	2.46	05:46:48.45	+33:15:16.4	5.91	0.09	0.01	0.54
JCMTLYS J053144.94+364048.2	171.90	1.67	05:31:44.94	+36:40:48.2	6.53	0.09	0.01	0.57
JCMTLYS J05030.21+472448.1	159.79	3.18	05:00:30.21	+47:24:48.1	8.79	0.65	0.04	0.66
JCMTLYS J053847.44+334319.2	175.16	1.28	05:38:47.44	+33:43:19.2	6.58	0.09	0.01	0.57
JCMTLYS J054820.35+324912.8	176.98	2.51	05:48:20.35	+32:49:12.8	6.29	0.10	0.01	0.56
JCMTLYS J053200.76+332923.2	174.60	-0.03	05:32:00.76	+33:29:23.2	6.41	0.08	0.00	0.56
JCMTLYS J044506.06+425449.8	161.55	-1.77	04:45:06.06	+42:54:49.8	7.54	0.17	0.01	0.61
JCMTLYS J045741.27+383826.3	166.37	-2.65	04:57:41.27	+38:38:26.3	6.66	0.18	0.01	0.57
JCMTLYS J052633.97+341318.2	173.36	-0.57	05:26:33.97	+34:13:18.2	6.66	0.08	0.00	0.57
JCMTLYS J044631.60+42453	161.85	-1.68	04:46:31.60	+42:45:03.0	9.38	0.21	0.01	0.68
JCMTLYS J044659.99+42112.6	162.34	-1.98	04:46:59.99	+42:11:02.6	8.75	0.12	0.01	0.66
JCMTLYS J052305.11+401923.5	167.92	2.29	05:23:05.11	+40:19:23.5	10.39	0.15	0.01	0.72
JCMTLYS J044400.55+425023	161.48	-1.97	04:44:00.55	+42:50:23.0	6.74	0.14	0.01	0.58
JCMTLYS J052050.58+382855.9	169.19	0.89	05:20:50.58	+38:28:55.9	6.82	0.08	0.00	0.58
JCMTLYS J054404.34+321410.7	177.01	1.44	05:44:04.34	+32:14:10.7	6.29	0.09	0.01	0.56

Table A.1 continued from previous page

SASSy Name	*l*	*b*	*RA* (2000)	*Dec* (2000)	$Rad_{\rm eff}$ pc	$F_{\rm int}$ Jy	*error* Jy	*Aperture* Correction
JCMTLYS J052832.32+322735.6	175.06	-1.20	05:28:32.32	+32:27:35.6	7.13	0.07	0.00	0.59
JCMTLYS J044222.37+415836.5	161.93	-2.76	04:42:22.37	+41:58:36.5	11.77	0.48	0.03	0.76
JCMTLYS J051342.81+441840.6	163.66	3.16	05:13:42.81	+44:18:40.6	6.94	4.69	0.28	0.59
JCMTLYS J054541.30+301429.4	178.89	0.69	05:45:41.30	+30:14:29.4	6.19	0.11	0.01	0.55
JCMTLYS J053025.59+381620.6	170.42	2.33	05:30:25.59	+38:16:20.6	6.58	0.10	0.01	0.57
JCMTLYS J052217.23+402422.5	167.77	2.21	05:22:17.23	+40:24:22.5	7.63	0.11	0.01	0.62
JCMTLYS J044401.25+473251.5	157.92	1.11	04:44:01.25	+47:32:51.5	7.37	0.66	0.04	0.61
JCMTLYS J044524.77+415733.1	162.32	-2.35	04:45:24.77	+41:57:33.1	6.94	0.14	0.01	0.59
JCMTLYS J052447.07+412520.9	167.20	3.17	05:24:47.07	+41:25:20.9	6.88	0.55	0.03	0.58
JCMTLYS J054607.52+34310.9	175.29	2.99	05:46:07.52	+34:31:00.9	7.13	0.25	0.02	0.60
JCMTLYS J044031.28+41567.9	161.74	-3.05	04:40:31.28	+41:56:07.9	8.41	0.58	0.04	0.65
JCMTLYS J054054.35+354311.8	173.70	2.71	05:40:54.35	+35:43:11.8	6.45	0.11	0.01	0.56
JCMTLYS J044438.05+41754.2	162.85	-3.00	04:44:38.05	+41:07:54.2	8.05	0.28	0.02	0.63
JCMTLYS J044240.87+414448.3	162.15	-2.87	04:42:40.87	+41:44:48.3	8.06	0.29	0.02	0.63
JCMTLYS J044310.57+43108.7	161.13	-1.87	04:43:10.57	+43:10:08.7	6.95	0.13	0.01	0.59
JCMTLYS J053606.05+34613.3	174.54	1.02	05:36:06.05	+34:06:13.3	9.88	0.12	0.01	0.70
JCMTLYS J044402.33+43059.2	161.35	-1.85	04:44:02.33	+43:00:59.2	6.95	0.16	0.01	0.59

Table A.1 continued from previous page

SASSy Name	*l*	*b*	*RA* (2000)	*Dec* (2000)	$Rad_{\rm eff}$ pc	$F_{\rm int}$ Jy	*error* Jy	*Aperture* Correction
JCMTLYS J044131.40+421547.4	161.61	-2.69	04:41:31.40	+42:15:47.4	8.74	0.21	0.01	0.66
JCMTLYS J044343.99+434532.7	160.75	-1.41	04:43:43.99	+43:45:32.7	7.36	0.14	0.01	0.60
JCMTLYS J052710.86+323826	174.75	-1.34	05:27:10.86	+32:38:26.0	6.59	0.10	0.01	0.57
JCMTLYS J052959.16+395444.1	169.00	3.15	05:29:59.16	+39:54:44.1	6.19	0.31	0.02	0.55
JCMTLYS J054127.52+3143.9	177.71	0.35	05:41:27.52	+31:04:03.9	6.63	0.10	0.01	0.57
JCMTLYS J044659.38+431829.2	161.48	-1.25	04:46:59.38	+43:18:29.2	6.53	0.10	0.01	0.57
JCMTLYS J053951.91+313858	177.04	0.37	05:39:51.91	+31:38:58.0	7.37	0.15	0.01	0.61
JCMTLYS J051115.47+383622.3	168.01	-0.57	05:11:15.47	+38:36:22.3	6.22	0.08	0.00	0.55
JCMTLYS J051320.84+39811.9	167.82	0.07	05:13:20.84	+39:08:11.9	6.86	0.10	0.01	0.58
JCMTLYS J053018.20+385523.5	169.86	2.66	05:30:18.20	+38:55:23.5	7.74	0.11	0.01	0.62
JCMTLYS J054246.59+313531.4	177.42	0.87	05:42:46.59	+31:35:31.4	5.65	0.06	0.00	0.53
JCMTLYS J053632.28+334541.9	174.88	0.91	05:36:32.28	+33:45:41.9	8.16	0.09	0.01	0.64
JCMTLYS J054151.62+305247.9	177.92	0.33	05:41:51.62	+30:52:47.9	7.80	0.10	0.01	0.62
JCMTLYS J054705.17+33422.4	176.63	2.42	05:47:05.17	+33:04:22.4	7.40	0.10	0.01	0.61
JCMTLYS J053010.40+325820.3	174.82	-0.63	05:30:10.40	+32:58:20.3	6.97	0.09	0.01	0.59
JCMTLYS J045904.43+453958.2	161.02	1.91	04:59:04.43	+45:39:58.2	7.75	0.11	0.01	0.62
JCMTLYS J051911.72+383410.3	168.94	0.67	05:19:11.72	+38:34:10.3	7.03	0.07	0.00	0.59

Table A.1 continued from previous page

SASSy Name	*l*	*b*	*RA* (2000)	*Dec* (2000)	$Rad_{\rm eff}$ pc	$F_{\rm int}$ Jy	*error* Jy	*Aperture* Correction
JCMTLYS J053800.17+373251.5	171.84	3.19	05:38:00.17	+37:32:51.5	7.48	0.21	0.01	0.61
JCMTLYS J053654.14+361015.7	172.89	2.27	05:36:54.14	+36:10:15.7	7.61	0.12	0.01	0.62
JCMTLYS J05416.43+39251.8	166.84	-1.39	05:04:16.43	+39:02:51.8	6.45	0.10	0.01	0.56
JCMTLYS J045754.12+383413.6	166.45	-2.66	04:57:54.12	+38:34:13.6	6.66	0.82	0.05	0.57
JCMTLYS J044137.63+421526.3	161.63	-2.68	04:41:37.63	+42:15:26.3	9.37	0.23	0.01	0.68
JCMTLYS J053019.49+345123.8	173.26	0.43	05:30:19.49	+34:51:23.8	6.26	0.07	0.00	0.56
JCMTLYS J052654.50+391239.1	169.26	2.27	05:26:54.50	+39:12:39.1	5.96	0.09	0.01	0.54
JCMTLYS J045109.76+422224.3	162.69	-1.27	04:51:09.76	+42:22:24.3	6.74	0.09	0.01	0.58
JCMTLYS J054127.07+332142.9	175.76	1.56	05:41:27.07	+33:21:42.9	6.36	0.10	0.01	0.56
JCMTLYS J054425.16+28378.2	-179.87	-0.39	05:44:25.16	+28:37:08.2	6.11	0.29	0.02	0.55
JCMTLYS J051140.62+423353.9	164.86	1.84	05:11:40.62	+42:33:53.9	8.23	0.10	0.01	0.64
JCMTLYS J044348.10+414612.2	162.26	-2.70	04:43:48.10	+41:46:12.2	14.46	1.16	0.07	0.83
JCMTLYS J052246.16+303859.7	175.87	-3.24	05:22:46.16	+30:38:59.7	8.35	0.85	0.05	0.65
JCMTLYS J053308.09+383228.4	170.49	2.92	05:33:08.09	+38:32:28.4	6.58	0.22	0.01	0.57
JCMTLYS J053117.32+34223.2	173.78	0.33	05:31:17.32	+34:22:03.2	7.02	0.07	0.00	0.59
JCMTLYS J05438.36+4583.6	162.04	2.35	05:04:38.36	+45:08:03.6	6.97	0.09	0.01	0.59
JCMTLYS J055231.61+304410.3	179.23	2.21	05:52:31.61	+30:44:10.3	8.01	0.72	0.04	0.63

Table A.1 continued from previous page

SASSy Name	*l*	*b*	*RA* (2000)	*Dec* (2000)	$Rad_{\rm eff}$ pc	$F_{\rm int}$ Jy	*error* Jy	*Aperture* Correction
JCMTLYS J054851.84+2941.6	-179.74	0.67	05:48:51.84	+29:04:01.6	6.29	0.99	0.06	0.56
JCMTLYS J05706.73+38176.9	167.78	-1.41	05:07:06.73	+38:17:06.9	6.21	0.07	0.00	0.55
JCMTLYS J053107.88+314539.3	175.94	-1.13	05:31:07.88	+31:45:39.3	5.71	0.08	0.00	0.53
JCMTLYS J044220.59+415854.5	161.93	-2.77	04:42:20.59	+41:58:54.5	11.65	0.47	0.03	0.76
JCMTLYS J055231.91+305633.4	179.05	2.32	05:52:31.91	+30:56:33.4	6.18	0.13	0.01	0.55
JCMTLYS J043906.33+425453.5	160.83	-2.60	04:39:06.33	+42:54:53.5	9.22	0.20	0.01	0.68
JCMTLYS J054602.58+283723.8	-179.68	-0.08	05:46:02.58	+28:37:23.8	6.10	0.51	0.03	0.55
JCMTLYS J053653.57+364432.4	172.40	2.57	05:36:53.57	+36:44:32.4	6.51	0.08	0.01	0.57
JCMTLYS J045113.11+422256.8	162.69	-1.25	04:51:13.11	+42:22:56.8	8.59	0.09	0.01	0.65
JCMTLYS J051845.54+41838.3	166.78	2.08	05:18:45.54	+41:08:38.3	7.47	0.11	0.01	0.61
JCMTLYS J051435.52+393257.6	167.62	0.51	05:14:35.52	+39:32:57.6	6.23	0.09	0.01	0.55
JCMTLYS J052326.69+321938.2	174.56	-2.17	05:23:26.69	+32:19:38.2	6.39	0.19	0.01	0.56
JCMTLYS J052922.35+361834.4	171.94	1.07	05:29:22.35	+36:18:34.4	5.88	0.07	0.00	0.54
JCMTLYS J055000.13+302721.1	179.19	1.60	05:50:00.13	+30:27:21.1	6.17	0.21	0.01	0.55
JCMTLYS J055233.41+30451.2	179.22	2.22	05:52:33.41	+30:45:01.2	7.71	0.83	0.05	0.62
JCMTLYS J054510.92+315230.2	177.44	1.45	05:45:10.92	+31:52:30.2	6.65	0.08	0.00	0.57
JCMTLYS J055129.53+323742.5	177.48	2.98	05:51:29.53	+32:37:42.5	9.00	0.24	0.01	0.67

Table A.1 continued from previous page

SASSy Name	*l*	*b*	*RA* (2000)	*Dec* (2000)	$Rad_{\rm eff}$ pc	$F_{\rm int}$ Jy	*error* Jy	*Aperture* Correction
JCMTLYS J05213.06+37456.1	168.15	-2.91	05:02:13.06	+37:04:56.1	6.19	0.12	0.01	0.55
JCMTLYS J052918.56+364411.3	171.58	1.29	05:29:18.56	+36:44:11.3	6.33	0.07	0.00	0.56
JCMTLYS J05235.36+39340.9	166.23	-1.33	05:02:35.36	+39:34:00.9	7.09	0.09	0.01	0.59
JCMTLYS J053710.28+36454.8	172.43	2.62	05:37:10.28	+36:45:04.8	7.09	0.07	0.00	0.59
JCMTLYS J053835.50+3600.7	173.21	2.46	05:38:35.50	+36:00:00.7	10.86	0.25	0.01	0.73
JCMTLYS J051026.09+444541.2	162.95	2.95	05:10:26.09	+44:45:41.2	7.73	0.21	0.01	0.62
JCMTLYS J053319.04+365910.2	171.81	2.10	05:33:19.04	+36:59:10.2	7.48	0.08	0.00	0.61
JCMTLYS J051916.64+411139.7	166.80	2.19	05:19:16.64	+41:11:39.7	13.47	0.24	0.01	0.81
JCMTLYS J052350.28+312546	175.35	-2.61	05:23:50.28	+31:25:46.0	5.94	0.10	0.01	0.54
JCMTLYS J05946.42+37492.7	168.47	-1.27	05:09:46.42	+37:49:02.7	8.61	0.10	0.01	0.66
JCMTLYS J054107.61+335335.8	175.28	1.79	05:41:07.61	+33:53:35.8	5.75	0.09	0.01	0.53
JCMTLYS J053524.48+38038.2	171.17	3.00	05:35:24.48	+38:00:38.2	6.55	0.25	0.01	0.57
JCMTLYS J052113.46+41445.5	166.56	2.80	05:21:13.46	+41:44:05.5	7.66	0.20	0.01	0.62
JCMTLYS J054818.33+301325.7	179.20	1.17	05:48:18.33	+30:13:25.7	6.36	0.16	0.01	0.56
JCMTLYS J052809.35+361543.9	171.85	0.84	05:28:09.35	+36:15:43.9	7.30	0.08	0.00	0.60
JCMTLYS J053352.16+304259.9	177.14	-1.21	05:33:52.16	+30:42:59.9	9.54	0.12	0.01	0.69
JCMTLYS J053334.54+363924	172.12	1.97	05:33:34.54	+36:39:24.0	5.88	0.07	0.00	0.54

Table A.1 continued from previous page

SASSy Name	*l*	*b*	*RA* (2000)	*Dec* (2000)	$Rad_{\rm eff}$ pc	$F_{\rm int}$ Jy	*error* Jy	*Aperture* Correction
JCMTLYS J043916.58+42316.7	161.49	-3.15	04:39:16.58	+42:03:16.7	10.50	5.27	0.32	0.72
JCMTLYS J043845.88+423945.7	160.98	-2.81	04:38:45.88	+42:39:45.7	6.94	0.15	0.01	0.59
JCMTLYS J052546.94+36506.3	171.11	0.76	05:25:46.94	+36:50:06.3	6.55	0.07	0.00	0.57
JCMTLYS J053005.95+324547.4	174.98	-0.76	05:30:05.95	+32:45:47.4	9.71	0.13	0.01	0.70
JCMTLYS J055220.94+324243.9	177.50	3.18	05:52:20.94	+32:42:43.9	6.83	0.58	0.03	0.58
JCMTLYS J051127.52+373136.9	168.90	-1.17	05:11:27.52	+37:31:36.9	7.02	0.09	0.01	0.59
JCMTLYS J05020.90+441514.4	162.27	1.21	05:00:20.90	+44:15:14.4	6.76	0.09	0.01	0.58
JCMTLYS J052316.70+34733.4	173.06	-1.18	05:23:16.70	+34:07:33.4	7.05	0.18	0.01	0.59
JCMTLYS J044402.97+433315.1	160.94	-1.50	04:44:02.97	+43:33:15.1	7.73	0.19	0.01	0.62
JCMTLYS J053919.50+293818.8	178.68	-0.80	05:39:19.50	+29:38:18.8	6.38	0.11	0.01	0.56
JCMTLYS J052334.46+323219	174.41	-2.03	05:23:34.46	+32:32:19.0	7.33	0.50	0.03	0.60
JCMTLYS J052858.93+353833.5	172.46	0.63	05:28:58.93	+35:38:33.5	5.86	0.07	0.00	0.54
JCMTLYS J054622.57+30297.2	178.76	0.95	05:46:22.57	+30:29:07.2	5.80	0.09	0.01	0.53
JCMTLYS J054543.16+301249.4	178.92	0.68	05:45:43.16	+30:12:49.4	5.58	0.12	0.01	0.52
JCMTLYS J043908.76+42518.4	161.45	-3.14	04:39:08.76	+42:05:18.4	6.73	0.23	0.01	0.58
JCMTLYS J051429.28+403139.1	166.82	1.07	05:14:29.28	+40:31:39.1	6.68	0.09	0.01	0.58
JCMTLYS J05753.86+40530.9	165.79	0.27	05:07:53.86	+40:53:00.9	7.30	0.08	0.00	0.60

Table A.1 continued from previous page

SASSy Name	*l*	*b*	*RA* (2000)	*Dec* (2000)	$Rad_{\rm eff}$ pc	$F_{\rm int}$ Jy	*error* Jy	*Aperture* Correction
JCMTLYS J043723.46+431646.5	160.35	-2.59	04:37:23.46	+43:16:46.5	7.90	0.19	0.01	0.63
JCMTLYS J052245.18+382651.5	169.44	1.17	05:22:45.18	+38:26:51.5	6.81	0.11	0.01	0.58
JCMTLYS J053622.37+364428.3	172.35	2.48	05:36:22.37	+36:44:28.3	6.30	0.09	0.01	0.56
JCMTLYS J044756.36+40939.8	164.00	-3.15	04:47:56.36	+40:09:39.8	7.67	0.58	0.03	0.62
JCMTLYS J052839.14+325756.2	174.65	-0.90	05:28:39.14	+32:57:56.2	7.15	0.09	0.01	0.60
JCMTLYS J061254.22+175919	-167.40	-0.05	06:12:54.22	+17:59:19.0	45.33	16.59	1.00	1.03
JCMTLYS J06853.29+213823	-171.05	0.88	06:08:53.29	+21:38:23.0	48.36	18.31	1.10	1.04
JCMTLYS J061253.58+18022.5	-167.42	-0.04	06:12:53.58	+18:00:22.5	45.33	17.70	1.06	1.03
JCMTLYS J06840.60+21314.7	-170.97	0.78	06:08:40.60	+21:31:04.7	45.87	17.44	1.05	1.04
JCMTLYS J06835.10+203911.3	-170.22	0.34	06:08:35.10	+20:39:11.3	41.49	10.88	0.65	1.02
JCMTLYS J055111.13+25468.1	-176.65	-0.58	05:51:11.13	+25:46:08.1	34.85	8.13	0.49	1.01
JCMTLYS J06907.00+215037.5	-171.21	1.03	06:09:07.00	+21:50:37.5	35.35	5.59	0.34	1.01
JCMTLYS J06949.76+213813.4	-170.94	1.08	06:09:49.76	+21:38:13.4	31.07	3.77	0.23	1.00
JCMTLYS J061436.65+134930.1	-163.55	-1.68	06:14:36.65	+13:49:30.1	29.51	4.57	0.27	1.00
JCMTLYS J061316.16+152243.2	-165.07	-1.22	06:13:16.16	+15:22:43.2	27.62	2.97	0.18	0.99
JCMTLYS J06845.82+213152.1	-170.97	0.81	06:08:45.82	+21:31:52.1	38.60	6.58	0.39	1.02
JCMTLYS J055824.71+201355.4	-171.03	-1.94	05:58:24.71	+20:13:55.4	25.09	2.33	0.14	0.97

Table A.1 continued from previous page

SASSy Name	*l*	*b*	*RA* (2000)	*Dec* (2000)	$Rad_{\rm eff}$ pc	$F_{\rm int}$ Jy	*error* Jy	*Aperture* Correction
JCMTLYS J061256.79+175832.5	-167.38	-0.05	06:12:56.79	+17:58:32.5	30.05	3.72	0.22	1.00
JCMTLYS J061503.43+19253.8	-168.08	0.91	06:15:03.43	+19:02:53.8	31.15	2.38	0.14	1.00
JCMTLYS J06840.18+20385.5	-170.20	0.35	06:08:40.18	+20:38:05.5	28.78	2.30	0.14	0.99
JCMTLYS J06853.92+202930.1	-170.05	0.33	06:08:53.92	+20:29:30.1	23.93	1.45	0.09	0.97
JCMTLYS J061051.78+202940.2	-169.83	0.73	06:10:51.78	+20:29:40.2	17.06	0.74	0.04	0.88
JCMTLYS J06921.11+20390.7	-170.13	0.50	06:09:21.11	+20:39:00.7	23.15	1.33	0.08	0.96
JCMTLYS J061256.62+175748.2	-167.37	-0.05	06:12:56.62	+17:57:48.2	22.40	1.45	0.09	0.95
JCMTLYS J06847.89+203842.5	-170.19	0.38	06:08:47.89	+20:38:42.5	21.84	1.31	0.08	0.95
JCMTLYS J06845.06+203814.3	-170.19	0.37	06:08:45.06	+20:38:14.3	22.27	1.35	0.08	0.95
JCMTLYS J061014.83+165552.8	-166.78	-1.11	06:10:14.83	+16:55:52.8	10.12	0.24	0.01	0.71
JCMTLYS J061534.52+14175.3	-163.84	-1.25	06:15:34.52	+14:17:05.3	14.24	0.68	0.04	0.83
JCMTLYS J055211.41+27026.3	-177.60	0.25	05:52:11.41	+27:00:26.3	21.43	1.52	0.09	0.94
JCMTLYS J061436.20+13494	-163.54	-1.68	06:14:36.20	+13:49:04.0	16.19	1.05	0.06	0.87
JCMTLYS J06252.87+273235.3	-176.87	2.57	06:02:52.87	+27:32:35.3	6.29	0.95	0.06	0.56
JCMTLYS J061433.32+13491.3	-163.54	-1.70	06:14:33.32	+13:49:01.3	20.78	1.46	0.09	0.94
JCMTLYS J063230.85+101843.6	-158.39	0.54	06:32:30.85	+10:18:43.6	13.09	0.61	0.04	0.80
JCMTLYS J06818.00+203636.3	-170.22	0.27	06:08:18.00	+20:36:36.3	13.70	0.47	0.03	0.81

Table A.1 continued from previous page

SASSy Name	*l*	*b*	*RA* (2000)	*Dec* (2000)	$Rad_{\rm eff}$ pc	$F_{\rm int}$ Jy	*error* Jy	*Aperture* Correction
JCMTLYS J06411.56+23732.3	-172.88	0.66	06:04:11.56	+23:07:32.3	7.04	0.19	0.01	0.59
JCMTLYS J063556.13+11022.2	-158.62	1.60	06:35:56.13	+11:00:22.2	15.66	0.67	0.04	0.86
JCMTLYS J061058.28+14932.8	-164.26	-2.29	06:10:58.28	+14:09:32.8	17.64	0.88	0.05	0.89
JCMTLYS J061051.95+203039.4	-169.84	0.74	06:10:51.95	+20:30:39.4	15.33	0.36	0.02	0.85
JCMTLYS J055343.51+241445.8	-175.05	-0.86	05:53:43.51	+24:14:45.8	10.02	0.32	0.02	0.71
JCMTLYS J063310.84+11200.2	-159.22	1.16	06:33:10.84	+11:20:00.2	6.52	0.11	0.01	0.57
JCMTLYS J061246.69+175826.4	-167.40	-0.08	06:12:46.69	+17:58:26.4	14.39	0.48	0.03	0.83
JCMTLYS J061622.99+16542.6	-165.34	-0.22	06:16:22.99	+16:05:42.6	10.63	0.60	0.04	0.73
JCMTLYS J061321.00+15248.1	-165.08	-1.19	06:13:21.00	+15:24:08.1	15.55	0.57	0.03	0.85
JCMTLYS J055240.73+253027.9	-176.25	-0.42	05:52:40.73	+25:30:27.9	7.87	0.53	0.03	0.63
JCMTLYS J054712.52+303616.1	178.75	1.16	05:47:12.52	+30:36:16.1	14.56	0.40	0.02	0.83
JCMTLYS J061027.39+164318.7	-166.57	-1.17	06:10:27.39	+16:43:18.7	11.84	0.29	0.02	0.76
JCMTLYS J06504.86+20110	-170.07	-0.68	06:05:04.86	+20:01:10.0	5.89	0.54	0.03	0.54
JCMTLYS J054940.67+23173.7	-174.69	-2.14	05:49:40.67	+23:17:03.7	12.68	0.29	0.02	0.79
JCMTLYS J062423.40+16930.4	-164.49	1.50	06:24:23.40	+16:09:30.4	6.49	0.08	0.00	0.57
JCMTLYS J061424.38+174457	-167.02	0.15	06:14:24.38	+17:44:57.0	14.35	0.35	0.02	0.83
JCMTLYS J06836.02+203518.1	-170.17	0.32	06:08:36.02	+20:35:18.1	18.66	0.58	0.03	0.91

Table A.1 continued from previous page

SASSy Name	*l*	*b*	*RA* (2000)	*Dec* (2000)	$Rad_{\rm eff}$ pc	$F_{\rm int}$ Jy	*error* Jy	*Aperture* Correction
JCMTLYS J055212.06+265935.3	-177.59	0.24	05:52:12.06	+26:59:35.3	14.58	0.57	0.03	0.83
JCMTLYS J054000.33+2560.5	-177.39	-3.08	05:40:00.33	+25:06:00.5	8.20	0.54	0.03	0.64
JCMTLYS J06843.06+203627.3	-170.17	0.35	06:08:43.06	+20:36:27.3	13.70	0.42	0.03	0.81
JCMTLYS J061253.84+175720.7	-167.37	-0.06	06:12:53.84	+17:57:20.7	19.10	0.68	0.04	0.91
JCMTLYS J06747.59+203932.6	-170.32	0.19	06:07:47.59	+20:39:32.6	15.28	0.49	0.03	0.85
JCMTLYS J063516.23+13948.1	-160.61	2.45	06:35:16.23	+13:09:48.1	6.26	0.14	0.01	0.56
JCMTLYS J055956.15+24527.6	-174.88	0.68	05:59:56.15	+24:52:07.6	8.19	0.16	0.01	0.64
JCMTLYS J06029.11+163758.1	-167.66	-3.30	06:00:29.11	+16:37:58.1	7.52	0.81	0.05	0.61
JCMTLYS J061158.04+201137.3	-169.44	0.82	06:11:58.04	+20:11:37.3	9.51	0.18	0.01	0.69
JCMTLYS J061123.73+172629	-167.09	-0.63	06:11:23.73	+17:26:29.0	17.05	0.57	0.03	0.88
JCMTLYS J061854.41+151757.3	-164.35	-0.06	06:18:54.41	+15:17:57.3	13.79	0.35	0.02	0.82
JCMTLYS J061649.30+131858.5	-162.84	-1.45	06:16:49.30	+13:18:58.5	6.19	0.10	0.01	0.55
JCMTLYS J055212.42+265918.2	-177.58	0.24	05:52:12.42	+26:59:18.2	14.19	0.50	0.03	0.82
JCMTLYS J06841.92+203611	-170.17	0.34	06:08:41.92	+20:36:11.0	11.57	0.31	0.02	0.76
JCMTLYS J061632.82+101234.6	-160.14	-2.98	06:16:32.82	+10:12:34.6	5.42	0.30	0.02	0.52
JCMTLYS J061329.97+175531.4	-167.27	0.05	06:13:29.97	+17:55:31.4	13.16	0.30	0.02	0.80
JCMTLYS J063107.16+10265.5	-158.66	0.29	06:31:07.16	+10:26:05.5	10.51	0.27	0.02	0.72

Table A.1 continued from previous page

SASSy Name	*l*	*b*	*RA* (2000)	*Dec* (2000)	$Rad_{\rm eff}$ pc	$F_{\rm int}$ Jy	*error* Jy	*Aperture* Correction
JCMTLYS J061624.56+10733.2	-160.08	-3.05	06:16:24.56	+10:07:33.2	6.88	0.25	0.02	0.58
JCMTLYS J06838.43+203550	-170.17	0.33	06:08:38.43	+20:35:50.0	11.92	0.30	0.02	0.77
JCMTLYS J063052.46+15616	-162.83	2.40	06:30:52.46	+15:06:16.0	6.21	0.15	0.01	0.55
JCMTLYS J061058.24+20712.5	-169.49	0.58	06:10:58.24	+20:07:12.5	12.63	0.20	0.01	0.79
JCMTLYS J061431.14+174523.7	-167.01	0.18	06:14:31.14	+17:45:23.7	12.01	0.27	0.02	0.77
JCMTLYS J06335.39+282437.1	-177.55	3.14	06:03:35.39	+28:24:37.1	8.91	0.85	0.05	0.67
JCMTLYS J063611.87+104010.1	-158.29	1.51	06:36:11.87	+10:40:10.1	7.10	0.39	0.02	0.59
JCMTLYS J062334.67+095629.6	-159.08	-1.58	06:23:34.67	+09:56:29.6	13.98	0.47	0.03	0.82
JCMTLYS J06834.15+16635.7	-166.25	-1.86	06:08:34.15	+16:06:35.7	6.94	0.11	0.01	0.59
JCMTLYS J061038.23+233319.3	-172.54	2.16	06:10:38.23	+23:33:19.3	7.03	0.22	0.01	0.59
JCMTLYS J061329.27+175539.5	-167.28	0.04	06:13:29.27	+17:55:39.5	8.80	0.16	0.01	0.66
JCMTLYS J063118.14+125739.6	-160.88	1.50	06:31:18.14	+12:57:39.6	5.70	0.10	0.01	0.53
JCMTLYS J062925.59+165532.7	-164.61	2.93	06:29:25.59	+16:55:32.7	8.91	2.30	0.14	0.67
JCMTLYS J061250.26+11293.8	-161.69	-3.18	06:12:50.26	+11:29:03.8	6.48	20.96	1.26	0.57
JCMTLYS J061724.32+145444.9	-164.18	-0.57	06:17:24.32	+14:54:44.9	12.05	0.32	0.02	0.77
JCMTLYS J06731.47+1610.5	-166.29	-2.13	06:07:31.47	+16:01:00.5	5.74	0.11	0.01	0.53
JCMTLYS J062058.57+204047.1	-168.86	2.91	06:20:58.57	+20:40:47.1	10.02	0.43	0.03	0.71

Table A.1 continued from previous page

SASSy Name	*l*	*b*	*RA* (2000)	*Dec* (2000)	$Rad_{\rm eff}$ pc	$F_{\rm int}$ Jy	*error* Jy	*Aperture* Correction
JCMTLYS J062540.05+13616.5	-161.64	0.35	06:25:40.05	+13:06:16.5	7.82	0.12	0.01	0.62
JCMTLYS J06213.38+23210.5	-173.30	0.38	06:02:13.38	+23:21:00.5	8.14	0.41	0.02	0.64
JCMTLYS J06857.96+20305.2	-170.05	0.35	06:08:57.96	+20:30:05.2	7.32	0.13	0.01	0.60
JCMTLYS J055726.54+18913.3	-169.34	-3.17	05:57:26.54	+18:09:13.3	6.48	0.28	0.02	0.57
JCMTLYS J063226.84+144616.6	-162.36	2.58	06:32:26.84	+14:46:16.6	13.82	0.51	0.03	0.82
JCMTLYS J061542.22+16412.1	-165.39	-0.38	06:15:42.22	+16:04:12.1	6.34	0.09	0.01	0.56
JCMTLYS J06042.02+174153.2	-168.56	-2.73	06:00:42.02	+17:41:53.2	6.46	0.23	0.01	0.57
JCMTLYS J061820.83+131857.5	-162.67	-1.12	06:18:20.83	+13:18:57.5	7.09	0.09	0.01	0.59
JCMTLYS J055124.40+21422.3	-172.58	-2.93	05:51:24.40	+21:04:22.3	8.57	1.07	0.06	0.65
JCMTLYS J055010.61+265137.9	-177.70	-0.21	05:50:10.61	+26:51:37.9	7.71	0.14	0.01	0.62
JCMTLYS J055642.97+182425.9	-169.65	-3.19	05:56:42.97	+18:24:25.9	8.89	0.52	0.03	0.67
JCMTLYS J055130.78+272855.7	-178.08	0.36	05:51:30.78	+27:28:55.7	14.50	0.27	0.02	0.83
JCMTLYS J061642.24+134356.1	-163.22	-1.28	06:16:42.24	+13:43:56.1	7.45	0.15	0.01	0.61
JCMTLYS J06828.19+203737.6	-170.21	0.31	06:08:28.19	+20:37:37.6	9.96	0.20	0.01	0.70
JCMTLYS J06034.80+24428.7	-174.11	0.41	06:00:34.80	+24:04:28.7	8.34	0.24	0.01	0.64
JCMTLYS J054355.39+325950.1	176.35	1.81	05:43:55.39	+32:59:50.1	6.97	0.46	0.03	0.59
JCMTLYS J06537.27+145645.6	-165.58	-3.05	06:05:37.27	+14:56:45.6	7.90	0.34	0.02	0.63

Table A.1 continued from previous page

SASSy Name	*l*	*b*	*RA* (2000)	*Dec* (2000)	$Rad_{\rm eff}$ pc	$F_{\rm int}$ Jy	*error* Jy	*Aperture* Correction
JCMTLYS J06607.04+235215.2	-173.31	1.41	06:06:07.04	+23:52:15.2	8.15	2.40	0.14	0.64
JCMTLYS J062645.05+09855.8	-158.02	-1.26	06:26:45.05	+09:08:55.8	5.89	0.15	0.01	0.54
JCMTLYS J06202.11+1953.8	-169.61	-1.77	06:02:02.11	+19:05:03.8	6.91	0.10	0.01	0.59
JCMTLYS J062518.46+182851.5	-166.44	2.78	06:25:18.46	+18:28:51.5	6.19	0.35	0.02	0.55
JCMTLYS J062730.02+085456.2	-157.73	-1.20	06:27:30.02	+08:54:56.2	5.87	0.30	0.02	0.54
JCMTLYS J061008.51+23514.3	-172.85	2.21	06:10:08.51	+23:51:04.3	6.84	0.12	0.01	0.58
JCMTLYS J055843.12+30294.8	-179.89	3.24	05:58:43.12	+30:29:04.8	7.56	0.72	0.04	0.61
JCMTLYS J061243.48+112059.8	-161.59	-3.27	06:12:43.48	+11:20:59.8	6.29	0.65	0.04	0.56
JCMTLYS J06105.54+163520.7	-167.55	-3.19	06:01:05.54	+16:35:20.7	8.33	0.32	0.02	0.64
JCMTLYS J062716.03+17255.7	-164.95	2.53	06:27:16.03	+17:02:55.7	5.91	0.13	0.01	0.54
JCMTLYS J053959.27+25613.5	-177.40	-3.08	05:39:59.27	+25:06:13.5	8.37	0.45	0.03	0.65
JCMTLYS J06143.81+162426.5	-167.31	-3.15	06:01:43.81	+16:24:26.5	8.00	0.37	0.02	0.63
JCMTLYS J063033.01+16252.3	-164.03	2.93	06:30:33.01	+16:25:02.3	6.65	0.24	0.01	0.57
JCMTLYS J054909.54+263126.8	-177.53	-0.58	05:49:09.54	+26:31:26.8	6.73	0.13	0.01	0.58
JCMTLYS J063226.56+144551	-162.35	2.58	06:32:26.56	+14:45:51.0	8.32	0.29	0.02	0.64
JCMTLYS J055722.55+181450.5	-169.43	-3.14	05:57:22.55	+18:14:50.5	6.49	0.43	0.03	0.57
JCMTLYS J061300.34+19620.7	-168.37	0.51	06:13:00.34	+19:06:20.7	6.68	0.09	0.01	0.58

Table A.1 continued from previous page

SASSy Name	*l*	*b*	*RA* (2000)	*Dec* (2000)	$Rad_{\rm eff}$ pc	$F_{\rm int}$ Jy	*error* Jy	*Aperture* Correction
JCMTLYS J061050.53+141023	-164.29	-2.32	06:10:50.53	+14:10:23.0	13.38	0.31	0.02	0.81
JCMTLYS J062426.83+19145.2	-167.20	2.95	06:24:26.83	+19:14:05.2	8.20	0.31	0.02	0.64
JCMTLYS J063341.35+131837.9	-160.92	2.18	06:33:41.35	+13:18:37.9	5.49	0.07	0.00	0.52
JCMTLYS J06254.07+241733.4	-174.04	0.98	06:02:54.07	+24:17:33.4	8.66	0.10	0.01	0.66
JCMTLYS J062812.58+174520.8	-165.48	3.06	06:28:12.58	+17:45:20.8	8.55	0.51	0.03	0.65
JCMTLYS J053951.04+25413.3	-177.39	-3.13	05:39:51.04	+25:04:13.3	8.70	0.56	0.03	0.66
JCMTLYS J062258.02+103737.9	-159.76	-1.39	06:22:58.02	+10:37:37.9	5.62	0.06	0.00	0.53
JCMTLYS J053812.83+252719.8	-177.91	-3.23	05:38:12.83	+25:27:19.8	7.86	0.66	0.04	0.63
JCMTLYS J06950.14+203034.3	-169.96	0.53	06:09:50.14	+20:30:34.3	8.81	0.12	0.01	0.66
JCMTLYS J063146.70+095939.9	-158.19	0.23	06:31:46.70	+09:59:39.9	6.09	0.09	0.01	0.55
JCMTLYS J06851.43+202931.7	-170.05	0.32	06:08:51.43	+20:29:31.7	10.22	0.20	0.01	0.71
JCMTLYS J061534.22+134259.4	-163.34	-1.53	06:15:34.22	+13:42:59.4	7.29	0.13	0.01	0.60
JCMTLYS J054338.81+325837.6	176.33	1.75	05:43:38.81	+32:58:37.6	7.18	0.51	0.03	0.60
JCMTLYS J063636.69+104351.2	-158.30	1.63	06:36:36.69	+10:43:51.2	5.92	0.12	0.01	0.54
JCMTLYS J061207.19+25359.5	-173.70	3.19	06:12:07.19	+25:03:59.5	6.86	0.41	0.02	0.58
JCMTLYS J055421.25+243119.9	-175.21	-0.59	05:54:21.25	+24:31:19.9	6.89	0.11	0.01	0.58
JCMTLYS J062230.94+115419.6	-160.94	-0.89	06:22:30.94	+11:54:19.6	6.09	0.07	0.00	0.55

Table A.1 continued from previous page

SASSy Name	*l*	*b*	*RA* (2000)	*Dec* (2000)	$Rad_{\rm eff}$ pc	$F_{\rm int}$ Jy	*error* Jy	*Aperture* Correction
JCMTLYS J061752.09+16741.2	-165.20	0.11	06:17:52.09	+16:07:41.2	6.33	0.06	0.00	0.56
JCMTLYS J06438.15+152636	-166.13	-3.01	06:04:38.15	+15:26:36.0	12.08	0.66	0.04	0.77
JCMTLYS J062902.16+16535.1	-164.61	2.83	06:29:02.16	+16:53:05.1	5.68	0.57	0.03	0.53
JCMTLYS J062422.98+09233.3	-158.20	-1.83	06:24:22.98	+09:02:33.3	6.26	0.13	0.01	0.56
JCMTLYS J06616.34+14259.4	-165.04	-3.17	06:06:16.34	+14:25:09.4	5.89	0.36	0.02	0.54
JCMTLYS J061707.93+103739.4	-160.44	-2.66	06:17:07.93	+10:37:39.4	5.44	0.12	0.01	0.52
JCMTLYS J06829.28+203754.3	-170.22	0.31	06:08:29.28	+20:37:54.3	13.10	0.32	0.02	0.80
JCMTLYS J055213.16+27010	-177.59	0.25	05:52:13.16	+27:00:10.0	12.60	0.34	0.02	0.78
JCMTLYS J054159.55+255152.2	-177.81	-2.30	05:41:59.55	+25:51:52.2	6.72	0.09	0.01	0.58
JCMTLYS J06255.78+204842	-171.01	-0.73	06:02:55.78	+20:48:42.0	6.77	0.10	0.01	0.58
JCMTLYS J055958.20+28420.8	-177.65	2.28	05:59:58.20	+28:04:20.8	6.74	0.10	0.01	0.58
JCMTLYS J063018.76+114249.7	-159.88	0.71	06:30:18.76	+11:42:49.7	5.84	0.09	0.01	0.54
JCMTLYS J055250.81+20543.3	-171.57	-3.13	05:52:50.81	+20:05:43.3	8.52	3.34	0.20	0.65
JCMTLYS J062728.68+171018	-165.04	2.63	06:27:28.68	+17:10:18.0	6.13	0.12	0.01	0.55
JCMTLYS J063050.10+104851.9	-159.03	0.41	06:30:50.10	+10:48:51.9	7.90	0.11	0.01	0.63
JCMTLYS J055744.98+181738.1	-169.43	-3.04	05:57:44.98	+18:17:38.1	7.25	0.19	0.01	0.60
JCMTLYS J061422.93+174320.5	-167.00	0.13	06:14:22.93	+17:43:20.5	10.64	0.19	0.01	0.73

Table A.1 continued from previous page

SASSy Name	*l*	*b*	*RA* (2000)	*Dec* (2000)	$Rad_{\rm eff}$ pc	$F_{\rm int}$ Jy	*error* Jy	*Aperture* Correction
JCMTLYS J055637.57+182342.8	-169.65	-3.22	05:56:37.57	+18:23:42.8	7.44	0.39	0.02	0.61
JCMTLYS J055234.76+271432.9	-177.76	0.44	05:52:34.76	+27:14:32.9	8.59	0.13	0.01	0.65
JCMTLYS J055331.20+265633.2	-177.39	0.47	05:53:31.20	+26:56:33.2	8.75	0.17	0.01	0.66
JCMTLYS J061850.02+171942.8	-166.15	0.88	06:18:50.02	+17:19:42.8	8.29	0.12	0.01	0.64
JCMTLYS J054035.87+25720.2	-177.34	-2.95	05:40:35.87	+25:07:20.2	6.91	0.23	0.01	0.59
JCMTLYS J062147.79+103928.1	-159.92	-1.63	06:21:47.79	+10:39:28.1	10.63	0.25	0.02	0.73
JCMTLYS J061727.92+172719.2	-166.41	0.65	06:17:27.92	+17:27:19.2	6.97	0.13	0.01	0.59
JCMTLYS J063600.76+14817.4	-161.40	3.06	06:36:00.76	+14:08:17.4	5.93	0.24	0.01	0.54
JCMTLYS J061253.56+113015.1	-161.70	-3.16	06:12:53.56	+11:30:15.1	9.16	2.36	0.14	0.68
JCMTLYS J06052.49+245114.8	-174.76	0.86	06:00:52.49	+24:51:14.8	8.52	0.12	0.01	0.65
JCMTLYS J062413.04+155527.4	-164.30	1.36	06:24:13.04	+15:55:27.4	7.37	0.11	0.01	0.61
JCMTLYS J055833.46+264957.2	-176.73	1.39	05:58:33.46	+26:49:57.2	7.70	0.12	0.01	0.62
JCMTLYS J063543.36+114811	-159.35	1.92	06:35:43.36	+11:48:11.0	5.99	0.09	0.01	0.54
JCMTLYS J061600.81+12274.9	-162.17	-2.03	06:16:00.81	+12:27:04.9	6.15	0.08	0.00	0.55
JCMTLYS J055915.05+284425.4	-178.31	2.47	05:59:15.05	+28:44:25.4	6.95	0.07	0.00	0.59
JCMTLYS J061013.96+14138.3	-164.23	-2.52	06:10:13.96	+14:01:38.3	6.82	0.14	0.01	0.58
JCMTLYS J062628.30+164231.8	-164.74	2.20	06:26:28.30	+16:42:31.8	7.23	0.15	0.01	0.60

Table A.1 continued from previous page

SASSy Name	*l*	*b*	*RA* (2000)	*Dec* (2000)	$Rad_{\rm eff}$ pc	$F_{\rm int}$ Jy	*error* Jy	*Aperture* Correction
JCMTLYS J063458.11+105459.6	-158.65	1.35	06:34:58.11	+10:54:59.6	5.76	0.09	0.01	0.53
JCMTLYS J06338.66+282147.1	-177.51	3.12	06:03:38.66	+28:21:47.1	8.07	0.25	0.01	0.63
JCMTLYS J062030.74+113447.3	-160.89	-1.48	06:20:30.74	+11:34:47.3	5.68	0.09	0.01	0.53
JCMTLYS J055337.84+321353.6	178.06	3.17	05:53:37.84	+32:13:53.6	6.98	0.30	0.02	0.59
JCMTLYS J055840.13+23522.4	-173.48	-0.46	05:58:40.13	+23:05:22.4	8.95	0.17	0.01	0.67
JCMTLYS J063341.94+142331.8	-161.88	2.68	06:33:41.94	+14:23:31.8	5.96	0.08	0.00	0.54
JCMTLYS J061051.24+233536.9	-172.55	2.23	06:10:51.24	+23:35:36.9	6.20	0.09	0.01	0.55
JCMTLYS J06742.73+265152.3	-175.76	3.18	06:07:42.73	+26:51:52.3	6.91	0.46	0.03	0.59
JCMTLYS J06233.52+205857.1	-171.20	-0.72	06:02:33.52	+20:58:57.1	7.54	0.10	0.01	0.61
JCMTLYS J054934.25+27528	-177.97	-0.21	05:49:34.25	+27:05:28.0	7.34	0.09	0.01	0.60
JCMTLYS J06842.91+203732	-170.18	0.36	06:08:42.91	+20:37:32.0	8.97	0.13	0.01	0.67
JCMTLYS J062208.40+13728.6	-162.06	-0.40	06:22:08.40	+13:07:28.6	8.43	0.18	0.01	0.65
JCMTLYS J06655.38+16433.7	-166.97	-1.91	06:06:55.38	+16:43:03.7	6.40	0.08	0.01	0.56
JCMTLYS J06408.28+191143.3	-169.46	-1.28	06:04:08.28	+19:11:43.3	6.09	0.08	0.00	0.55
JCMTLYS J06632.04+205817.4	-170.74	0.08	06:06:32.04	+20:58:17.4	6.14	0.08	0.00	0.55
JCMTLYS J06932.03+171227.4	-167.10	-1.13	06:09:32.03	+17:12:27.4	6.61	0.07	0.00	0.57
JCMTLYS J062502.85+192037.1	-167.23	3.13	06:25:02.85	+19:20:37.1	6.43	0.28	0.02	0.56

Table A.1 continued from previous page

SASSy Name	*l*	*b*	*RA* (2000)	*Dec* (2000)	$Rad_{\rm eff}$ pc	$F_{\rm int}$ Jy	*error* Jy	*Aperture* Correction
JCMTLYS J061758.34+094054.3	-159.50	-2.92	06:17:58.34	+09:40:54.3	7.47	0.14	0.01	0.61
JCMTLYS J061420.06+174218.4	-166.99	0.12	06:14:20.06	+17:42:18.4	9.35	0.15	0.01	0.68
JCMTLYS J055752.95+201719.3	-171.14	-2.02	05:57:52.95	+20:17:19.3	6.77	0.10	0.01	0.58
JCMTLYS J055839.52+231929.6	-173.68	-0.34	05:58:39.52	+23:19:29.6	6.44	0.11	0.01	0.56
JCMTLYS J062028.09+11528.1	-160.46	-1.72	06:20:28.09	+11:05:28.1	7.09	0.09	0.01	0.59
JCMTLYS J061345.19+17556.8	-167.24	0.10	06:13:45.19	+17:55:06.8	9.77	0.14	0.01	0.70
JCMTLYS J062644.85+171535	-165.20	2.52	06:26:44.85	+17:15:35.0	6.53	0.18	0.01	0.57
JCMTLYS J06400.92+155546.6	-166.63	-2.90	06:04:00.92	+15:55:46.6	7.30	0.42	0.03	0.60
JCMTLYS J06849.70+213346.4	-170.99	0.84	06:08:49.70	+21:33:46.4	15.43	0.29	0.02	0.85
JCMTLYS J054122.94+24565.2	-177.09	-2.90	05:41:22.94	+24:56:05.2	6.04	0.16	0.01	0.55
JCMTLYS J055118.20+213232.4	-173.00	-2.71	05:51:18.20	+21:32:32.4	5.96	0.18	0.01	0.54
JCMTLYS J061225.56+11580.3	-162.17	-3.03	06:12:25.56	+11:58:00.3	6.86	0.42	0.03	0.58
JCMTLYS J06919.52+203937.3	-170.15	0.50	06:09:19.52	+20:39:37.3	9.26	0.16	0.01	0.68
JCMTLYS J061254.84+12629	-162.23	-2.86	06:12:54.84	+12:06:29.0	7.36	0.19	0.01	0.61
JCMTLYS J061648.11+092539.8	-159.42	-3.30	06:16:48.11	+09:25:39.8	5.58	0.25	0.01	0.52
JCMTLYS J061609.75+16324.2	-165.75	-0.06	06:16:09.75	+16:32:04.2	7.28	0.11	0.01	0.60
JCMTLYS J055951.67+172120.2	-168.36	-3.07	05:59:51.67	+17:21:20.2	8.37	1.07	0.06	0.65

Table A.1 continued from previous page

SASSy Name	*l*	*b*	*RA* (2000)	*Dec* (2000)	$Rad_{\rm eff}$ pc	$F_{\rm int}$ Jy	*error* Jy	*Aperture* Correction
JCMTLYS J062035.74+095846.1	-159.46	-2.21	06:20:35.74	+09:58:46.1	5.98	0.08	0.01	0.54
JCMTLYS J06615.65+142554.8	-165.05	-3.16	06:06:15.65	+14:25:54.8	11.23	0.74	0.04	0.75
JCMTLYS J054723.56+21583.9	-173.83	-3.27	05:47:23.56	+21:58:03.9	7.03	0.50	0.03	0.59
JCMTLYS J063651.43+132834.7	-160.71	2.94	06:36:51.43	+13:28:34.7	5.48	0.30	0.02	0.52
JCMTLYS J063550.13+141758	-161.56	3.09	06:35:50.13	+14:17:58.0	6.86	0.28	0.02	0.58
JCMTLYS J054126.87+262935.2	-178.40	-2.07	05:41:26.87	+26:29:35.2	6.73	0.11	0.01	0.58
JCMTLYS J063018.55+155024.8	-163.54	2.62	06:30:18.55	+15:50:24.8	6.05	0.08	0.00	0.55
JCMTLYS J063224.36+134719.8	-161.49	2.12	06:32:24.36	+13:47:19.8	7.02	0.10	0.01	0.59
JCMTLYS J06024.23+16545.3	-167.90	-3.18	06:00:24.23	+16:54:05.3	5.79	0.34	0.02	0.53
JCMTLYS J062139.22+18216.4	-166.73	1.95	06:21:39.22	+18:21:06.4	6.41	0.09	0.01	0.56
JCMTLYS J054447.98+28225.2	-179.33	-0.62	05:44:47.98	+28:02:25.2	8.44	0.12	0.01	0.65
JCMTLYS J061610.49+14293.1	-163.94	-1.03	06:16:10.49	+14:29:03.1	6.45	0.07	0.00	0.56
JCMTLYS J06048.61+283744	-178.05	2.71	06:00:48.61	+28:37:44.0	7.73	0.10	0.01	0.62
JCMTLYS J062656.89+101152.7	-158.92	-0.73	06:26:56.89	+10:11:52.7	6.82	0.10	0.01	0.58
JCMTLYS J054429.08+281312.5	-179.52	-0.59	05:44:29.08	+28:13:12.5	6.31	0.09	0.01	0.56
JCMTLYS J06205.75+20914.3	-170.53	-1.23	06:02:05.75	+20:09:14.3	8.35	0.09	0.01	0.65
JCMTLYS J06825.12+17611.7	-167.14	-1.41	06:08:25.12	+17:06:11.7	7.69	0.10	0.01	0.62

Table A.1 continued from previous page

SASSy Name	*l*	*b*	*RA* (2000)	*Dec* (2000)	$Rad_{\rm eff}$ pc	$F_{\rm int}$ Jy	*error* Jy	*Aperture* Correction
JCMTLYS J061139.47+20311.2	-169.76	0.91	06:11:39.47	+20:31:01.2	10.20	0.16	0.01	0.71
JCMTLYS J061258.25+12463.5	-162.81	-2.54	06:12:58.25	+12:46:03.5	6.73	0.09	0.01	0.58
JCMTLYS J063644.91+14419.2	-161.26	3.19	06:36:44.91	+14:04:19.2	7.49	0.49	0.03	0.61
JCMTLYS J062759.96+133225.5	-161.76	1.06	06:27:59.96	+13:32:25.5	5.75	0.06	0.00	0.53
JCMTLYS J055726.46+18102	-169.35	-3.17	05:57:26.46	+18:10:02.0	6.68	0.23	0.01	0.58
JCMTLYS J06326.30+282427	-177.57	3.11	06:03:26.30	+28:24:27.0	8.08	0.30	0.02	0.63
JCMTLYS J055901.40+183443.6	-169.52	-2.64	05:59:01.40	+18:34:43.6	5.86	0.10	0.01	0.54
JCMTLYS J06033.03+16391.9	-167.67	-3.27	06:00:33.03	+16:39:01.9	7.35	0.32	0.02	0.60
JCMTLYS J06117.79+2972.8	-178.42	3.05	06:01:17.79	+29:07:02.8	7.91	0.29	0.02	0.63
JCMTLYS J061359.22+175245.4	-167.18	0.13	06:13:59.22	+17:52:45.4	10.53	0.21	0.01	0.72
JCMTLYS J061254.97+121055.6	-162.30	-2.83	06:12:54.97	+12:10:55.6	6.34	0.22	0.01	0.56
JCMTLYS J06522.51+261514.1	-175.48	2.43	06:05:22.51	+26:15:14.1	7.30	0.13	0.01	0.60
JCMTLYS J061234.09+175637.7	-167.40	-0.14	06:12:34.09	+17:56:37.7	6.43	0.09	0.01	0.56
JCMTLYS J061428.39+224718.1	-171.44	2.57	06:14:28.39	+22:47:18.1	5.94	0.08	0.00	0.54
JCMTLYS J055725.08+18759.1	-169.33	-3.19	05:57:25.08	+18:07:59.1	8.88	1.55	0.09	0.67
JCMTLYS J063200.22+16147.7	-163.52	3.06	06:32:00.22	+16:01:47.7	5.63	0.16	0.01	0.53
JCMTLYS J061358.22+113420.8	-161.64	-2.89	06:13:58.22	+11:34:20.8	5.91	0.09	0.01	0.54

Table A.1 continued from previous page

SASSy Name	*l*	*b*	*RA* (2000)	*Dec* (2000)	$Rad_{\rm eff}$ pc	$F_{\rm int}$ Jy	*error* Jy	*Aperture* Correction
JCMTLYS J062013.18+12211.8	-161.32	-1.32	06:20:13.18	+12:02:11.8	6.29	0.09	0.01	0.56
JCMTLYS J062058.13+155927.7	-164.72	0.70	06:20:58.13	+15:59:27.7	7.73	0.11	0.01	0.62
JCMTLYS J063412.21+13184.9	-160.85	2.28	06:34:12.21	+13:18:04.9	7.14	0.12	0.01	0.60
JCMTLYS J06830.52+204021	-170.25	0.34	06:08:30.52	+20:40:21.0	11.70	0.17	0.01	0.76
JCMTLYS J055535.25+28377.9	-178.61	1.71	05:55:35.25	+28:37:07.9	6.32	0.08	0.01	0.56
JCMTLYS J061140.85+20918.4	-169.44	0.74	06:11:40.85	+20:09:18.4	8.78	0.10	0.01	0.66
JCMTLYS J062953.39+10138.8	-158.44	-0.17	06:29:53.39	+10:01:38.8	5.93	0.07	0.00	0.54
JCMTLYS J055604.99+184050.4	-169.96	-3.19	05:56:04.99	+18:40:50.4	5.86	0.74	0.04	0.54
JCMTLYS J06615.39+205532.4	-170.73	0.00	06:06:15.39	+20:55:32.4	8.21	0.13	0.01	0.64
JCMTLYS J061423.37+174340.7	-167.00	0.14	06:14:23.37	+17:43:40.7	10.88	0.22	0.01	0.73
JCMTLYS J062135.48+092353.1	-158.83	-2.27	06:21:35.48	+09:23:53.1	6.80	0.10	0.01	0.58
JCMTLYS J061600.68+144526.5	-164.20	-0.94	06:16:00.68	+14:45:26.5	5.65	0.07	0.00	0.53
JCMTLYS J061850.03+115058.4	-161.32	-1.71	06:18:50.03	+11:50:58.4	5.50	0.07	0.00	0.52
JCMTLYS J061157.66+153646	-165.42	-1.39	06:11:57.66	+15:36:46.0	6.33	0.09	0.01	0.56
JCMTLYS J054222.12+235553.7	-176.11	-3.24	05:42:22.12	+23:55:53.7	10.82	70.23	4.21	0.73
JCMTLYS J061402.11+13352	-162.94	-2.17	06:14:02.11	+13:03:52.0	6.19	0.10	0.01	0.55
JCMTLYS J055944.31+174447.4	-168.71	-2.90	05:59:44.31	+17:44:47.4	8.85	1.43	0.09	0.66

Table A.1 continued from previous page

SASSy Name	*l*	*b*	*RA* (2000)	*Dec* (2000)	$Rad_{\rm eff}$ pc	$F_{\rm int}$ Jy	*error* Jy	*Aperture* Correction
JCMTLYS J061220.95+251117.1	-173.78	3.29	06:12:20.95	+25:11:17.1	8.49	1.96	0.12	0.65
JCMTLYS J06615.31+172815.9	-167.71	-1.68	06:06:15.31	+17:28:15.9	6.83	0.10	0.01	0.58
JCMTLYS J063523.98+115530.8	-159.50	1.91	06:35:23.98	+11:55:30.8	7.80	0.13	0.01	0.62
JCMTLYS J055006.71+222918.6	-173.96	-2.46	05:50:06.71	+22:29:18.6	8.13	0.13	0.01	0.64
JCMTLYS J062435.83+093034.8	-158.59	-1.56	06:24:35.83	+09:30:34.8	5.93	0.08	0.01	0.54
JCMTLYS J06742.22+223156.6	-171.97	1.08	06:07:42.22	+22:31:56.6	6.61	0.10	0.01	0.57
JCMTLYS J062614.81+16194.5	-164.42	1.97	06:26:14.81	+16:19:04.5	5.67	0.07	0.00	0.53
JCMTLYS J055944.85+171938.2	-168.35	-3.11	05:59:44.85	+17:19:38.2	7.56	0.40	0.02	0.61
JCMTLYS J06952.70+213953.6	-170.96	1.10	06:09:52.70	+21:39:53.6	11.15	0.18	0.01	0.74
JCMTLYS J06915.26+225856.4	-172.19	1.61	06:09:15.26	+22:58:56.4	6.62	0.09	0.01	0.57
JCMTLYS J061336.16+125343.1	-162.84	-2.34	06:13:36.16	+12:53:43.1	6.37	0.10	0.01	0.56
JCMTLYS J062216.66+09537.4	-158.49	-2.26	06:22:16.66	+09:05:37.4	5.33	0.09	0.01	0.51
JCMTLYS J06815.47+23460.2	-172.98	1.79	06:08:15.47	+23:46:00.2	7.79	0.08	0.01	0.62
JCMTLYS J063647.12+14638.6	-161.29	3.21	06:36:47.12	+14:06:38.6	6.11	0.33	0.02	0.55
JCMTLYS J062431.91+09141.8	-158.17	-1.80	06:24:31.91	+09:01:41.8	6.76	0.18	0.01	0.58
JCMTLYS J061330.85+222216.2	-171.18	2.18	06:13:30.85	+22:22:16.2	6.38	0.12	0.01	0.56
JCMTLYS J063104.43+09486.6	-158.10	-0.01	06:31:04.43	+09:48:06.6	5.72	0.06	0.00	0.53

Table A.1 continued from previous page

SASSy Name	*l*	*b*	*RA* (2000)	*Dec* (2000)	$Rad_{\rm eff}$ pc	$F_{\rm int}$ Jy	*error* Jy	*Aperture* Correction
JCMTLYS J062236.92+182334.4	-166.66	2.17	06:22:36.92	+18:23:34.4	6.41	0.13	0.01	0.56
JCMTLYS J055050.04+223036.2	-173.89	-2.31	05:50:50.04	+22:30:36.2	7.24	0.11	0.01	0.60
JCMTLYS J063015.55+14036.3	-161.93	1.76	06:30:15.55	+14:00:36.3	7.22	0.11	0.01	0.60
JCMTLYS J063902.53+11816.3	-158.39	2.34	06:39:02.53	+11:08:16.3	5.93	0.10	0.01	0.54
JCMTLYS J06210.20+27110.6	-176.64	2.26	06:02:10.20	+27:11:00.6	6.06	0.09	0.01	0.55
JCMTLYS J061312.12+152032.1	-165.04	-1.25	06:13:12.12	+15:20:32.1	8.65	0.13	0.01	0.66
JCMTLYS J055752.63+30048.6	-179.57	2.84	05:57:52.63	+30:00:48.6	6.97	0.11	0.01	0.59
JCMTLYS J061906.83+184328.9	-167.34	1.60	06:19:06.83	+18:43:28.9	8.96	0.13	0.01	0.67
JCMTLYS J062905.61+125814.2	-161.13	1.03	06:29:05.61	+12:58:14.2	6.11	0.08	0.00	0.55
JCMTLYS J054622.38+302911.6	178.76	0.95	05:46:22.38	+30:29:11.6	6.98	0.10	0.01	0.59
JCMTLYS J062925.05+165552.5	-164.61	2.93	06:29:25.05	+16:55:52.5	6.10	2.38	0.14	0.55
JCMTLYS J055956.13+17428.3	-168.65	-2.88	05:59:56.13	+17:42:08.3	7.04	0.19	0.01	0.59
JCMTLYS J06130.07+173153.2	-168.32	-2.64	06:01:30.07	+17:31:53.2	8.06	0.08	0.00	0.63
JCMTLYS J063501.99+131355.8	-160.70	2.43	06:35:01.99	+13:13:55.8	5.48	0.06	0.00	0.52
JCMTLYS J062956.67+164058.8	-164.33	2.93	06:29:56.67	+16:40:58.8	8.61	13.46	0.81	0.66
JCMTLYS J055611.30+26112.9	-176.44	0.60	05:56:11.30	+26:11:02.9	6.06	0.12	0.01	0.55
JCMTLYS J055704.32+183942	-169.83	-2.99	05:57:04.32	+18:39:42.0	7.45	0.25	0.01	0.61

Table A.1 continued from previous page

SASSy Name	*l*	*b*	*RA* (2000)	*Dec* (2000)	$Rad_{\rm eff}$ pc	$F_{\rm int}$ Jy	*error* Jy	*Aperture* Correction
JCMTLYS J053847.65+304117.8	177.73	-0.33	05:38:47.65	+30:41:17.8	14.74	0.56	0.03	0.84
JCMTLYS J055950.88+28950.8	-177.75	2.30	05:59:50.88	+28:09:50.8	7.90	0.12	0.01	0.63
JCMTLYS J063723.68+12435	-159.41	2.41	06:37:23.68	+12:04:35.0	6.71	0.09	0.01	0.58
JCMTLYS J055551.64+21740.7	-172.10	-2.01	05:55:51.64	+21:07:40.7	7.19	0.11	0.01	0.60
JCMTLYS J055926.70+181745.7	-169.23	-2.69	05:59:26.70	+18:17:45.7	7.07	0.12	0.01	0.59
JCMTLYS J054925.72+265237.5	-177.80	-0.35	05:49:25.72	+26:52:37.5	6.73	0.11	0.01	0.58
JCMTLYS J054144.47+321623	176.72	1.04	05:41:44.47	+32:16:23.0	6.10	0.24	0.01	0.55
JCMTLYS J06030.37+18345.7	-168.90	-2.59	06:00:30.37	+18:03:45.7	6.67	0.16	0.01	0.57
JCMTLYS J063513.15+131119.5	-160.64	2.45	06:35:13.15	+13:11:19.5	6.08	0.09	0.01	0.55
JCMTLYS J063818.91+122223.6	-159.57	2.75	06:38:18.91	+12:22:23.6	5.42	0.09	0.01	0.52
JCMTLYS J063320.19+125252.2	-160.58	1.90	06:33:20.19	+12:52:52.2	8.03	0.09	0.01	0.63
JCMTLYS J061012.10+124850.6	-163.17	-3.11	06:10:12.10	+12:48:50.6	12.09	0.59	0.04	0.77
JCMTLYS J063337.81+134545.1	-161.33	2.37	06:33:37.81	+13:45:45.1	6.67	0.11	0.01	0.57
JCMTLYS J063033.77+151511.5	-162.99	2.40	06:30:33.77	+15:15:11.5	6.02	0.09	0.01	0.54
JCMTLYS J061923.25+103042.3	-160.07	-2.22	06:19:23.25	+10:30:42.3	6.02	0.08	0.00	0.54
JCMTLYS J062600.55+165428.1	-164.97	2.20	06:26:00.55	+16:54:28.1	6.71	0.11	0.01	0.58
JCMTLYS J06209.98+17447.2	-167.85	-2.73	06:02:09.98	+17:04:47.2	8.35	0.14	0.01	0.65

Table A.1 continued from previous page

SASSy Name	*l*	*b*	*RA* (2000)	*Dec* (2000)	$Rad_{\rm eff}$ pc	$F_{\rm int}$ Jy	*error* Jy	*Aperture* Correction
JCMTLYS J06952.11+202954.5	-169.94	0.53	06:09:52.11	+20:29:54.5	14.62	0.21	0.01	0.83
JCMTLYS J054505.94+271457.7	-178.62	-0.98	05:45:05.94	+27:14:57.7	8.08	0.06	0.00	0.63
JCMTLYS J055245.81+224155.3	-173.82	-1.83	05:52:45.81	+22:41:55.3	6.21	0.06	0.00	0.55
JCMTLYS J062753.74+131555.6	-161.53	0.91	06:27:53.74	+13:15:55.6	5.53	0.08	0.00	0.52
JCMTLYS J061914.45+122319.3	-161.75	-1.37	06:19:14.45	+12:23:19.3	7.02	0.11	0.01	0.59
JCMTLYS J055957.69+23455.7	-173.32	-0.21	05:59:57.69	+23:04:55.7	6.64	0.14	0.01	0.57
JCMTLYS J055147.79+264928.2	-177.49	0.08	05:51:47.79	+26:49:28.2	6.52	0.12	0.01	0.57
JCMTLYS J061929.68+09592.9	-159.59	-2.45	06:19:29.68	+09:59:02.9	5.40	0.08	0.00	0.51
JCMTLYS J06727.13+182346.4	-168.38	-0.98	06:07:27.13	+18:23:46.4	6.47	0.07	0.00	0.57
JCMTLYS J062248.13+173742.3	-165.96	1.86	06:22:48.13	+17:37:42.3	5.96	0.11	0.01	0.54
JCMTLYS J062021.65+172916.9	-166.11	1.28	06:20:21.65	+17:29:16.9	6.38	0.12	0.01	0.56
JCMTLYS J06815.11+171821.3	-167.33	-1.35	06:08:15.11	+17:18:21.3	9.63	0.13	0.01	0.69
JCMTLYS J054946.93+2771.4	-177.97	-0.16	05:49:46.93	+27:07:01.4	9.38	0.13	0.01	0.68
JCMTLYS J062258.88+084619.7	-158.12	-2.26	06:22:58.88	+08:46:19.7	6.75	0.18	0.01	0.58
JCMTLYS J061346.95+17550.3	-167.24	0.10	06:13:46.95	+17:55:00.3	13.05	0.24	0.01	0.80
JCMTLYS J062554.44+093241.2	-158.47	-1.26	06:25:54.44	+09:32:41.2	5.92	0.07	0.00	0.54
JCMTLYS J055744.08+181622	-169.41	-3.05	05:57:44.08	+18:16:22.0	12.14	0.50	0.03	0.77

Table A.1 continued from previous page

SASSy Name	*l*	*b*	*RA* (2000)	*Dec* (2000)	$Rad_{\rm eff}$ pc	$F_{\rm int}$ Jy	*error* Jy	*Aperture* Correction
JCMTLYS J062340.29+191431.5	-167.30	2.79	06:23:40.29	+19:14:31.5	6.02	0.10	0.01	0.54
JCMTLYS J055250.52+20175.4	-171.73	-3.04	05:52:50.52	+20:17:05.4	7.34	0.20	0.01	0.60
JCMTLYS J06848.23+213321.4	-170.99	0.83	06:08:48.23	+21:33:21.4	12.20	0.21	0.01	0.77
JCMTLYS J055632.74+182256.5	-169.65	-3.24	05:56:32.74	+18:22:56.5	6.07	0.32	0.02	0.55
JCMTLYS J062657.80+164459.3	-164.72	2.33	06:26:57.80	+16:44:59.3	5.69	0.11	0.01	0.53
JCMTLYS J061847.02+091113.1	-158.97	-2.98	06:18:47.02	+09:11:13.1	5.75	0.21	0.01	0.53
JCMTLYS J062924.64+142845.3	-162.44	1.79	06:29:24.64	+14:28:45.3	7.25	0.09	0.01	0.60
JCMTLYS J061242.98+112030	-161.58	-3.27	06:12:42.98	+11:20:30.0	5.71	0.47	0.03	0.53
JCMTLYS J061252.84+235526.7	-172.61	2.79	06:12:52.84	+23:55:26.7	7.41	0.36	0.02	0.61
JCMTLYS J062355.26+09476.3	-158.91	-1.58	06:23:55.26	+09:47:06.3	7.29	0.10	0.01	0.60
JCMTLYS J061425.16+174518.2	-167.02	0.16	06:14:25.16	+17:45:18.2	6.21	0.10	0.01	0.55
JCMTLYS J063006.23+113852.9	-159.85	0.63	06:30:06.23	+11:38:52.9	6.57	0.11	0.01	0.57
JCMTLYS J063708.01+11237.7	-158.52	1.88	06:37:08.01	+11:02:37.7	5.56	0.10	0.01	0.52
JCMTLYS J061332.80+113132.6	-161.65	-3.00	06:13:32.80	+11:31:32.6	7.93	0.17	0.01	0.63
JCMTLYS J06028.69+24046.3	-174.07	0.36	06:00:28.69	+24:00:46.3	6.87	0.11	0.01	0.58
JCMTLYS J062105.09+14252.4	-163.32	-0.02	06:21:05.09	+14:25:02.4	6.97	0.10	0.01	0.59
JCMTLYS J062316.08+185122.1	-167.00	2.53	06:23:16.08	+18:51:22.1	6.42	0.08	0.00	0.56

Table A.1 continued from previous page

SASSy Name	*l*	*b*	*RA* (2000)	*Dec* (2000)	$Rad_{\rm eff}$ pc	$F_{\rm int}$ Jy	*error* Jy	*Aperture* Correction
JCMTLYS J063032.74+14160.8	-162.12	1.94	06:30:32.74	+14:16:00.8	5.97	0.07	0.00	0.54
JCMTLYS J06255.04+241752.5	-174.04	0.98	06:02:55.04	+24:17:52.5	6.87	0.11	0.01	0.58
JCMTLYS J054229.47+322452.6	176.68	1.25	05:42:29.47	+32:24:52.6	6.98	0.19	0.01	0.59
JCMTLYS J055814.05+294118.3	-179.25	2.75	05:58:14.05	+29:41:18.3	6.09	0.12	0.01	0.55
JCMTLYS J061425.82+174423.1	-167.01	0.15	06:14:25.82	+17:44:23.1	9.36	0.16	0.01	0.68
JCMTLYS J061959.09+132355.2	-162.55	-0.73	06:19:59.09	+13:23:55.2	6.37	0.09	0.01	0.56
JCMTLYS J061549.88+112944.9	-161.35	-2.53	06:15:49.88	+11:29:44.9	6.09	0.10	0.01	0.55
JCMTLYS J06111.41+172156.6	-168.21	-2.79	06:01:11.41	+17:21:56.6	10.19	0.19	0.01	0.71
JCMTLYS J064001.53+121528.8	-159.27	3.07	06:40:01.53	+12:15:28.8	5.40	0.20	0.01	0.51
JCMTLYS J062910.54+12823.6	-160.39	0.66	06:29:10.54	+12:08:23.6	6.60	0.11	0.01	0.57
JCMTLYS J062530.52+133054.8	-162.02	0.51	06:25:30.52	+13:30:54.8	6.35	0.08	0.00	0.56
JCMTLYS J062440.52+15295.4	-163.86	1.25	06:24:40.52	+15:29:05.4	6.46	0.07	0.00	0.57
JCMTLYS J062614.79+174735.7	-165.73	2.66	06:26:14.79	+17:47:35.7	8.56	0.20	0.01	0.65
JCMTLYS J063257.36+114821	-159.67	1.32	06:32:57.36	+11:48:21.0	6.01	0.09	0.01	0.54
JCMTLYS J06804.71+165151.8	-166.97	-1.60	06:08:04.71	+16:51:51.8	7.51	0.10	0.01	0.61
JCMTLYS J062537.54+11358.1	-159.84	-0.61	06:25:37.54	+11:03:58.1	6.56	0.10	0.01	0.57
JCMTLYS J06103.03+211722.1	-171.64	-0.88	06:01:03.03	+21:17:22.1	5.94	0.08	0.00	0.54

Table A.1 continued from previous page

SASSy Name	*l*	*b*	*RA* (2000)	*Dec* (2000)	$Rad_{\rm eff}$ pc	$F_{\rm int}$ Jy	*error* Jy	*Aperture* Correction
JCMTLYS J06438.78+161045.8	-166.77	-2.65	06:04:38.78	+16:10:45.8	7.98	0.30	0.02	0.63
JCMTLYS J061706.27+173010.8	-166.49	0.60	06:17:06.27	+17:30:10.8	6.40	0.09	0.01	0.56
JCMTLYS J062203.45+105023.5	-160.05	-1.49	06:22:03.45	+10:50:23.5	7.68	0.11	0.01	0.62
JCMTLYS J062322.68+1267.2	-161.02	-0.61	06:23:22.68	+12:06:07.2	7.62	0.10	0.01	0.62
JCMTLYS J061750.26+11640.9	-160.78	-2.28	06:17:50.26	+11:06:40.9	5.67	0.08	0.00	0.53
JCMTLYS J055604.13+305532.9	179.45	2.96	05:56:04.13	+30:55:32.9	6.10	0.18	0.01	0.55
JCMTLYS J062209.03+192723.3	-167.65	2.58	06:22:09.03	+19:27:23.3	7.03	0.10	0.01	0.59
JCMTLYS J064109.84+092939.9	-156.69	2.06	06:41:09.84	+09:29:39.9	56.02	28.56	1.71	1.07
JCMTLYS J064112.41+09296.4	-156.67	2.06	06:41:12.41	+09:29:06.4	38.60	16.98	1.02	1.02
JCMTLYS J063437.27+041242.6	-152.74	-1.81	06:34:37.27	+04:12:42.6	41.93	7.42	0.45	1.03
JCMTLYS J064058.36+103654	-157.70	2.53	06:40:58.36	+10:36:54.0	22.05	2.52	0.15	0.95
JCMTLYS J064115.51+092914.6	-156.67	2.07	06:41:15.51	+09:29:14.6	36.16	8.19	0.49	1.01
JCMTLYS J065245.71+014024.7	-148.41	1.06	06:52:45.71	+01:40:24.7	25.76	2.55	0.15	0.98
JCMTLYS J064713.48+00268.5	-147.94	-0.74	06:47:13.48	+00:26:08.5	19.33	1.84	0.11	0.92
JCMTLYS J065915.91-035930.5	-142.62	-0.08	06:59:15.91	-03:59:30.5	28.74	3.25	0.20	0.99
JCMTLYS J064106.34+093354.8	-156.76	2.08	06:41:06.34	+09:33:54.8	33.75	4.69	0.28	1.01
JCMTLYS J064106.20+093558.3	-156.79	2.09	06:41:06.20	+09:35:58.3	34.63	4.75	0.29	1.01

Table A.1 continued from previous page

SASSy Name	*l*	*b*	*RA* (2000)	*Dec* (2000)	$Rad_{\rm eff}$ pc	$F_{\rm int}$ Jy	*error* Jy	*Aperture* Correction
JCMTLYS J064118.11+09291.6	-156.66	2.08	06:41:18.11	+09:29:01.6	20.62	1.62	0.10	0.93
JCMTLYS J064516.20+002231.5	-148.11	-1.20	06:45:16.20	+00:22:31.5	24.66	1.23	0.07	0.97
JCMTLYS J065935.52-04463.4	-141.90	-0.36	06:59:35.52	-04:46:03.4	23.83	1.63	0.10	0.96
JCMTLYS J064059.15+10367.1	-157.69	2.52	06:40:59.15	+10:36:07.1	15.87	1.04	0.06	0.86
JCMTLYS J07023.09-043632.3	-141.95	-0.12	07:00:23.09	-04:36:32.3	21.02	1.03	0.06	0.94
JCMTLYS J063717.16+055729	-153.98	-0.42	06:37:17.16	+05:57:29.0	22.47	1.55	0.09	0.95
JCMTLYS J065937.44-074540	-139.23	-1.72	06:59:37.44	-07:45:40.0	18.92	0.90	0.05	0.91
JCMTLYS J064616.06+00630.1	-147.75	-1.10	06:46:16.06	+00:06:30.1	16.94	0.67	0.04	0.88
JCMTLYS J062357.87+062537.7	-155.93	-3.14	06:23:57.87	+06:25:37.7	15.92	2.06	0.12	0.86
JCMTLYS J064104.16+09359.2	-156.78	2.08	06:41:04.16	+09:35:09.2	32.06	3.82	0.23	1.00
JCMTLYS J063316.29+023025	-151.37	-2.89	06:33:16.29	+02:30:25.0	17.00	1.02	0.06	0.88
JCMTLYS J063102.90+09223	-157.72	-0.22	06:31:02.90	+09:22:03.0	8.10	0.53	0.03	0.64
JCMTLYS J064100.90+093527.8	-156.79	2.07	06:41:00.90	+09:35:27.8	26.93	2.19	0.13	0.98
JCMTLYS J064115.01+092714.4	-156.64	2.06	06:41:15.01	+09:27:14.4	17.31	0.91	0.05	0.89
JCMTLYS J064104.04+101511.5	-157.37	2.38	06:41:04.04	+10:15:11.5	24.50	1.91	0.11	0.97
JCMTLYS J064348.33-01817.9	-146.92	-2.22	06:43:48.33	-01:08:17.9	23.30	1.67	0.10	0.96
JCMTLYS J064105.57+101456.8	-157.37	2.38	06:41:05.57	+10:14:56.8	23.91	1.48	0.09	0.97

Table A.1 continued from previous page

SASSy Name	*l*	*b*	*RA* (2000)	*Dec* (2000)	$Rad_{\rm eff}$ pc	$F_{\rm int}$ Jy	*error* Jy	*Aperture* Correction
JCMTLYS J063619.32+041037.9	-152.51	-1.45	06:36:19.32	+04:10:37.9	10.95	0.53	0.03	0.74
JCMTLYS J07837.82-04192.2	-141.26	1.84	07:08:37.82	-04:19:02.2	19.08	0.84	0.05	0.91
JCMTLYS J065435.49-043214.8	-142.67	-1.37	06:54:35.49	-04:32:14.8	20.33	0.96	0.06	0.93
JCMTLYS J063230.83+101844.3	-158.39	0.54	06:32:30.83	+10:18:44.3	12.99	0.59	0.04	0.80
JCMTLYS J065611.13-03234.8	-143.51	-0.49	06:56:11.13	-03:23:04.8	13.15	0.43	0.03	0.80
JCMTLYS J07839.22-041922.2	-141.26	1.85	07:08:39.22	-04:19:22.2	17.18	0.58	0.03	0.88
JCMTLYS J064111.86+093532.1	-156.77	2.11	06:41:11.86	+09:35:32.1	16.38	0.63	0.04	0.87
JCMTLYS J063556.09+11022	-158.62	1.60	06:35:56.09	+11:00:22.0	16.92	0.57	0.03	0.88
JCMTLYS J07358.99-04161.5	-141.84	0.84	07:03:58.99	-04:16:01.5	7.39	0.20	0.01	0.61
JCMTLYS J064049.11+093437.4	-156.80	2.02	06:40:49.11	+09:34:37.4	20.35	1.19	0.07	0.93
JCMTLYS J064058.10+093618.1	-156.81	2.06	06:40:58.10	+09:36:18.1	29.17	1.53	0.09	1.00
JCMTLYS J063315.88+043455.2	-153.22	-1.94	06:33:15.88	+04:34:55.2	17.22	0.55	0.03	0.89
JCMTLYS J063136.25+02463.2	-151.80	-3.14	06:31:36.25	+02:46:03.2	11.51	0.87	0.05	0.75
JCMTLYS J07028.68-085127.5	-138.16	-2.04	07:00:28.68	-08:51:27.5	15.18	0.41	0.02	0.85
JCMTLYS J063213.01+031840.6	-152.21	-2.76	06:32:13.01	+03:18:40.6	8.16	1.03	0.06	0.64
JCMTLYS J07437.19-053953.5	-140.53	0.34	07:04:37.19	-05:39:53.5	8.09	0.34	0.02	0.63
JCMTLYS J065913.26-062118.4	-140.53	-1.17	06:59:13.26	-06:21:18.4	6.22	0.28	0.02	0.55

Table A.1 continued from previous page

SASSy Name	*l*	*b*	*RA* (2000)	*Dec* (2000)	$Rad_{\rm eff}$ pc	$F_{\rm int}$ Jy	*error* Jy	*Aperture* Correction
JCMTLYS J063524.71+035623.6	-152.40	-1.76	06:35:24.71	+03:56:23.6	16.09	0.45	0.03	0.86
JCMTLYS J064103.99+093540.3	-156.79	2.08	06:41:03.99	+09:35:40.3	10.55	0.36	0.02	0.72
JCMTLYS J065037.61-052059.5	-142.40	-2.62	06:50:37.61	-05:20:59.5	12.00	0.29	0.02	0.77
JCMTLYS J062334.68+095630	-159.08	-1.58	06:23:34.68	+09:56:30.0	13.92	0.46	0.03	0.82
JCMTLYS J064108.11+103114.7	-157.60	2.52	06:41:08.11	+10:31:14.7	12.43	0.28	0.02	0.78
JCMTLYS J064101.85+103526.8	-157.68	2.53	06:41:01.85	+10:35:26.8	13.53	0.44	0.03	0.81
JCMTLYS J062455.83+07059.4	-156.34	-2.65	06:24:55.83	+07:00:59.4	7.89	0.33	0.02	0.63
JCMTLYS J063151.57+041917.6	-153.15	-2.37	06:31:51.57	+04:19:17.6	17.52	0.49	0.03	0.89
JCMTLYS J063547.10+111337.6	-158.83	1.67	06:35:47.10	+11:13:37.6	12.20	50.47	3.03	0.77
JCMTLYS J064326.62+085740	-155.95	2.31	06:43:26.62	+08:57:40.0	8.77	0.19	0.01	0.66
JCMTLYS J064206.81+091019.4	-156.29	2.12	06:42:06.81	+09:10:19.4	10.13	0.18	0.01	0.71
JCMTLYS J07653.94-005738.9	-144.45	3.00	07:06:53.94	-00:57:38.9	9.91	0.52	0.03	0.70
JCMTLYS J062357.05+062513.4	-155.93	-3.14	06:23:57.05	+06:25:13.4	12.22	0.82	0.05	0.77
JCMTLYS J063432.63+041748.6	-152.82	-1.79	06:34:32.63	+04:17:48.6	16.20	0.32	0.02	0.87
JCMTLYS J062017.62+082127.5	-158.06	-3.04	06:20:17.62	+08:21:27.5	6.52	1.14	0.07	0.57
JCMTLYS J063309.72+04386.2	-153.28	-1.94	06:33:09.72	+04:38:06.2	13.49	0.29	0.02	0.81
JCMTLYS J063243.29+032247.7	-152.21	-2.61	06:32:43.29	+03:22:47.7	10.92	0.36	0.02	0.74

Table A.1 continued from previous page

SASSy Name	*l*	*b*	*RA* (2000)	*Dec* (2000)	$Rad_{\rm eff}$ pc	$F_{\rm int}$ Jy	*error* Jy	*Aperture* Correction
JCMTLYS J063328.62+04115.4	-152.70	-2.15	06:33:28.62	+04:01:15.4	14.36	0.34	0.02	0.83
JCMTLYS J061632.91+101234.5	-160.14	-2.98	06:16:32.91	+10:12:34.5	6.52	0.36	0.02	0.57
JCMTLYS J062359.94+062540.9	-155.93	-3.13	06:23:59.94	+06:25:40.9	8.05	0.55	0.03	0.63
JCMTLYS J065717.44-01948	-145.37	0.77	06:57:17.44	-01:09:48.0	12.31	0.19	0.01	0.78
JCMTLYS J064111.04+095557	-157.07	2.26	06:41:11.04	+09:55:57.0	10.69	0.27	0.02	0.73
JCMTLYS J063544.04+005816.5	-149.73	-3.05	06:35:44.04	+00:58:16.5	9.03	0.36	0.02	0.67
JCMTLYS J071012.83-022249.1	-142.80	3.09	07:10:12.83	-02:22:49.1	7.45	0.16	0.01	0.61
JCMTLYS J07953.70-032720.5	-141.88	2.52	07:09:53.70	-03:27:20.5	7.05	0.10	0.01	0.59
JCMTLYS J063927.18+091745.4	-156.70	1.59	06:39:27.18	+09:17:45.4	7.17	0.11	0.01	0.60
JCMTLYS J063409.52+042121.5	-152.92	-1.85	06:34:09.52	+04:21:21.5	14.08	0.29	0.02	0.82
JCMTLYS J07512.35-085956.2	-137.50	-1.06	07:05:12.35	-08:59:56.2	9.31	11.38	0.68	0.68
JCMTLYS J064449.38+002024.1	-148.13	-1.32	06:44:49.38	+00:20:24.1	14.20	0.28	0.02	0.82
JCMTLYS J063207.82+021127.8	-151.22	-3.29	06:32:07.82	+02:11:27.8	8.77	2.00	0.12	0.66
JCMTLYS J071100.22-033040.9	-141.71	2.74	07:11:00.22	-03:30:40.9	9.18	1.19	0.07	0.68
JCMTLYS J063829.53+004445.8	-149.21	-2.54	06:38:29.53	+00:44:45.8	8.39	0.14	0.01	0.65
JCMTLYS J07028.32-085110	-138.16	-2.04	07:00:28.32	-08:51:10.0	11.66	0.24	0.01	0.76
JCMTLYS J064945.72-012326.8	-146.02	-1.01	06:49:45.72	-01:23:26.8	5.85	0.08	0.00	0.54

Table A.1 continued from previous page

SASSy Name	*l*	*b*	*RA* (2000)	*Dec* (2000)	$Rad_{\rm eff}$ pc	$F_{\rm int}$ Jy	*error* Jy	*Aperture* Correction
JCMTLYS J065230.60+005311	-147.73	0.64	06:52:30.60	+00:53:11.0	6.56	0.07	0.00	0.57
JCMTLYS J064110.34+093542.4	-156.77	2.10	06:41:10.34	+09:35:42.4	14.34	0.40	0.02	0.83
JCMTLYS J062027.15+112420.7	-160.74	-1.57	06:20:27.15	+11:24:20.7	6.08	0.36	0.02	0.55
JCMTLYS J07245.32+011341.2	-146.87	3.08	07:02:45.32	+01:13:41.2	22.85	1.45	0.09	0.96
JCMTLYS J07714.89-032742.9	-142.18	1.93	07:07:14.89	-03:27:42.9	8.66	0.10	0.01	0.66
JCMTLYS J07242.07+011333.6	-146.88	3.06	07:02:42.07	+01:13:33.6	15.91	0.76	0.05	0.86
JCMTLYS J07304.19-065824.9	-139.54	-0.60	07:03:04.19	-06:58:24.9	11.64	0.28	0.02	0.76
JCMTLYS J062355.28+062511.6	-155.93	-3.15	06:23:55.28	+06:25:11.6	9.04	0.73	0.04	0.67
JCMTLYS J064058.50+093531.7	-156.79	2.06	06:40:58.50	+09:35:31.7	12.07	0.33	0.02	0.77
JCMTLYS J071425.69-051811.8	-139.72	2.67	07:14:25.69	-05:18:11.8	5.79	0.13	0.01	0.53
JCMTLYS J065917.67-035416.6	-142.70	-0.04	06:59:17.67	-03:54:16.6	9.24	0.14	0.01	0.68
JCMTLYS J064657.76-04641	-143.92	-2.87	06:46:57.76	-04:06:41.0	7.97	1.15	0.07	0.63
JCMTLYS J064213.81+09537.4	-156.21	2.11	06:42:13.81	+09:05:37.4	9.99	0.17	0.01	0.71
JCMTLYS J071404.92-041650.4	-140.67	3.07	07:14:04.92	-04:16:50.4	8.82	0.26	0.02	0.66
JCMTLYS J063156.76+031633.8	-152.21	-2.83	06:31:56.76	+03:16:33.8	6.66	0.16	0.01	0.57
JCMTLYS J064335.29+021024.5	-149.90	-0.75	06:43:35.29	+02:10:24.5	10.47	0.24	0.01	0.72
JCMTLYS J062421.28+063518.2	-156.03	-2.98	06:24:21.28	+06:35:18.2	6.72	0.53	0.03	0.58

Table A.1 continued from previous page

SASSy Name	*l*	*b*	*RA* (2000)	*Dec* (2000)	$Rad_{\rm eff}$ pc	$F_{\rm int}$ Jy	*error* Jy	*Aperture* Correction
JCMTLYS J062941.20+045555.5	-153.94	-2.57	06:29:41.20	+04:55:55.5	11.23	0.25	0.02	0.75
JCMTLYS J063107.17+10260.3	-158.66	0.29	06:31:07.17	+10:26:00.3	14.55	0.38	0.02	0.83
JCMTLYS J071034.98-075133.4	-137.90	0.64	07:10:34.98	-07:51:33.4	7.89	5.79	0.35	0.63
JCMTLYS J062409.08+065243.8	-156.31	-2.89	06:24:09.08	+06:52:43.8	7.52	0.22	0.01	0.61
JCMTLYS J07303.03-065829.4	-139.54	-0.61	07:03:03.03	-06:58:29.4	8.72	0.13	0.01	0.66
JCMTLYS J071339.40-05735.1	-139.97	2.58	07:13:39.40	-05:07:35.1	6.20	0.10	0.01	0.55
JCMTLYS J071119.92-031923.9	-141.84	2.90	07:11:19.92	-03:19:23.9	8.63	0.37	0.02	0.66
JCMTLYS J061648.61+09482.4	-159.74	-3.12	06:16:48.61	+09:48:02.4	6.07	0.38	0.02	0.55
JCMTLYS J064824.79+075822.1	-154.51	2.96	06:48:24.79	+07:58:22.1	7.34	2.33	0.14	0.60
JCMTLYS J071803.56-07531.6	-137.72	2.64	07:18:03.56	-07:05:31.6	6.06	0.27	0.02	0.55
JCMTLYS J065003.96+002955.7	-147.67	-0.08	06:50:03.96	+00:29:55.7	6.55	0.15	0.01	0.57
JCMTLYS J062354.23+062420.4	-155.92	-3.16	06:23:54.23	+06:24:20.4	9.64	0.64	0.04	0.69
JCMTLYS J065303.19-072152.8	-140.32	-2.99	06:53:03.19	-07:21:52.8	7.26	0.23	0.01	0.60
JCMTLYS J065556.45+03482.6	-149.94	2.73	06:55:56.45	+03:48:02.6	6.84	0.25	0.01	0.58
JCMTLYS J062400.19+062522.5	-155.92	-3.13	06:24:00.19	+06:25:22.5	8.39	0.48	0.03	0.65
JCMTLYS J064054.57+103328.8	-157.66	2.49	06:40:54.57	+10:33:28.8	9.42	0.17	0.01	0.69
JCMTLYS J065343.71-072056.8	-140.26	-2.84	06:53:43.71	-07:20:56.8	6.19	0.11	0.01	0.55

Table A.1 continued from previous page

SASSy Name	*l*	*b*	*RA* (2000)	*Dec* (2000)	$Rad_{\rm eff}$ pc	$F_{\rm int}$ Jy	*error* Jy	*Aperture* Correction
JCMTLYS J07243.81+011323.2	-146.87	3.07	07:02:43.81	+01:13:23.2	20.12	1.14	0.07	0.93
JCMTLYS J064306.50+105044.6	-157.67	3.10	06:43:06.50	+10:50:44.6	9.41	13.67	0.82	0.69
JCMTLYS J07307.98-051310.8	-141.09	0.21	07:03:07.98	-05:13:10.8	6.45	0.09	0.01	0.56
JCMTLYS J065151.89+031458.6	-149.91	1.58	06:51:51.89	+03:14:58.6	6.63	0.11	0.01	0.57
JCMTLYS J065144.04+021823.6	-149.09	1.12	06:51:44.04	+02:18:23.6	9.91	0.21	0.01	0.70
JCMTLYS J063506.91+012951	-150.27	-2.95	06:35:06.91	+01:29:51.0	7.75	0.53	0.03	0.62
JCMTLYS J062455.62+111835.8	-160.14	-0.65	06:24:55.62	+11:18:35.8	6.55	0.33	0.02	0.57
JCMTLYS J064152.57-003120	-147.69	-2.37	06:41:52.57	-00:31:20.0	8.17	0.28	0.02	0.64
JCMTLYS J065646.22+012637.9	-147.75	1.84	06:56:46.22	+01:26:37.9	16.49	0.29	0.02	0.87
JCMTLYS J063234.86+02243	-151.04	-3.26	06:32:34.86	+02:02:43.0	7.59	0.65	0.04	0.61
JCMTLYS J07028.55-091254.4	-137.84	-2.20	07:00:28.55	-09:12:54.4	8.42	0.12	0.01	0.65
JCMTLYS J065716.33-091835.1	-138.11	-2.95	06:57:16.33	-09:18:35.1	5.67	0.12	0.01	0.53
JCMTLYS J07602.99-055435.7	-140.14	0.54	07:06:02.99	-05:54:35.7	5.81	0.07	0.00	0.53
JCMTLYS J065025.99-055211.7	-141.95	-2.90	06:50:25.99	-05:52:11.7	6.28	0.13	0.01	0.56
JCMTLYS J063159.87+031715.7	-152.22	-2.82	06:31:59.87	+03:17:15.7	6.00	0.17	0.01	0.54
JCMTLYS J065947.34+015749.6	-147.87	2.75	06:59:47.34	+01:57:49.6	6.57	0.33	0.02	0.57
JCMTLYS J062147.80+103928.2	-159.92	-1.63	06:21:47.80	+10:39:28.2	10.27	0.24	0.01	0.71

Table A.1 continued from previous page

SASSy Name	*l*	*b*	*RA* (2000)	*Dec* (2000)	$Rad_{\rm eff}$ pc	$F_{\rm int}$ Jy	*error* Jy	*Aperture* Correction
JCMTLYS J065537.99+03433.7	-149.90	2.63	06:55:37.99	+03:43:03.7	8.29	0.56	0.03	0.64
JCMTLYS J063658.90+06427.8	-154.12	-0.43	06:36:58.90	+06:04:27.8	8.06	0.14	0.01	0.63
JCMTLYS J065325.29-035511.3	-143.35	-1.35	06:53:25.29	-03:55:11.3	6.36	0.07	0.00	0.56
JCMTLYS J063622.23+105449.1	-158.49	1.66	06:36:22.23	+10:54:49.1	7.57	0.12	0.01	0.61
JCMTLYS J07653.65-00579.6	-144.46	3.00	07:06:53.65	-00:57:09.6	11.59	0.52	0.03	0.76
JCMTLYS J07133.44-064133.9	-139.96	-0.81	07:01:33.44	-06:41:33.9	7.26	0.08	0.00	0.60
JCMTLYS J063330.04+04018	-152.68	-2.15	06:33:30.04	+04:00:18.0	15.39	0.32	0.02	0.85
JCMTLYS J071828.07-07327.4	-137.70	2.75	07:18:28.07	-07:03:27.4	5.47	0.23	0.01	0.52
JCMTLYS J061847.02+091114.3	-158.97	-2.98	06:18:47.02	+09:11:14.3	6.07	0.22	0.01	0.55
JCMTLYS J07313.86-091322	-137.52	-1.60	07:03:13.86	-09:13:22.0	6.58	0.24	0.01	0.57
JCMTLYS J065914.48-035446.9	-142.70	-0.05	06:59:14.48	-03:54:46.9	16.32	0.26	0.02	0.87
JCMTLYS J064827.47-023112.9	-145.16	-1.81	06:48:27.47	-02:31:12.9	6.24	0.08	0.00	0.55
JCMTLYS J064109.24+093255.1	-156.73	2.08	06:41:09.24	+09:32:55.1	14.34	0.32	0.02	0.83
JCMTLYS J063408.91+04227	-152.93	-1.84	06:34:08.91	+04:22:07.0	9.31	0.13	0.01	0.68
JCMTLYS J065712.97-011325.3	-145.32	0.73	06:57:12.97	-01:13:25.3	11.43	0.19	0.01	0.75
JCMTLYS J07619.72-061138.8	-139.86	0.47	07:06:19.72	-06:11:38.8	5.79	0.10	0.01	0.53
JCMTLYS J062330.40+07433.1	-156.56	-2.94	06:23:30.40	+07:04:33.1	6.51	0.45	0.03	0.57

Table A.1 continued from previous page

SASSy Name	*l*	*b*	*RA* (2000)	*Dec* (2000)	$Rad_{\rm eff}$ pc	$F_{\rm int}$ Jy	*error* Jy	*Aperture* Correction
JCMTLYS J071228.56-06030.4	-139.32	1.91	07:12:28.56	-06:00:30.4	9.50	0.09	0.01	0.69
JCMTLYS J065915.94-035813	-142.64	-0.07	06:59:15.94	-03:58:13.0	12.48	0.22	0.01	0.78
JCMTLYS J065101.85+013950	-148.60	0.67	06:51:01.85	+01:39:50.0	6.79	0.10	0.01	0.58
JCMTLYS J063413.99+042130.6	-152.91	-1.83	06:34:13.99	+04:21:30.6	8.19	0.13	0.01	0.64
JCMTLYS J065207.67+013313.2	-148.37	0.86	06:52:07.67	+01:33:13.2	6.58	0.07	0.00	0.57
JCMTLYS J064155.40+011843.8	-149.32	-1.52	06:41:55.40	+01:18:43.8	10.03	0.12	0.01	0.71
JCMTLYS J07427.98-065621.1	-139.41	-0.28	07:04:27.98	-06:56:21.1	6.16	0.09	0.01	0.55
JCMTLYS J065844.39-03415.9	-142.96	-0.06	06:58:44.39	-03:41:05.9	12.31	0.23	0.01	0.78
JCMTLYS J065603.24-075013.6	-139.56	-2.55	06:56:03.24	-07:50:13.6	6.88	0.10	0.01	0.58
JCMTLYS J062819.88+045853.8	-154.14	-2.85	06:28:19.88	+04:58:53.8	6.69	0.31	0.02	0.58
JCMTLYS J065646.85+012658.5	-147.75	1.85	06:56:46.85	+01:26:58.5	17.28	0.33	0.02	0.89
JCMTLYS J07553.67+00033.3	-145.43	3.22	07:05:53.67	+00:00:33.3	6.86	0.38	0.02	0.58
JCMTLYS J071314.52-033731	-141.35	3.18	07:13:14.52	-03:37:31.0	6.08	0.22	0.01	0.55
JCMTLYS J062421.53+071029.4	-156.55	-2.70	06:24:21.53	+07:10:29.4	6.93	0.23	0.01	0.59
JCMTLYS J065218.41+013423.5	-148.37	0.91	06:52:18.41	+01:34:23.5	10.01	0.44	0.03	0.71
JCMTLYS J062301.17+081243.5	-157.62	-2.51	06:23:01.17	+08:12:43.5	7.34	0.13	0.01	0.60
JCMTLYS J07653.43-05623.4	-140.76	1.10	07:06:53.43	-05:06:23.4	6.80	0.08	0.00	0.58

Table A.1 continued from previous page

SASSy Name	*l*	*b*	*RA* (2000)	*Dec* (2000)	$Rad_{\rm eff}$ pc	$F_{\rm int}$ Jy	*error* Jy	*Aperture* Correction
JCMTLYS J065417.04-081449	-139.40	-3.12	06:54:17.04	-08:14:49.0	6.86	0.32	0.02	0.58
JCMTLYS J07512.86-05481	-140.34	0.41	07:05:12.86	-05:48:01.0	13.01	0.18	0.01	0.80
JCMTLYS J071231.94-04136.2	-140.90	2.75	07:12:31.94	-04:13:06.2	6.25	0.08	0.00	0.56
JCMTLYS J065254.35+053136.6	-151.82	2.84	06:52:54.35	+05:31:36.6	7.47	0.20	0.01	0.61
JCMTLYS J064810.94+073545	-154.20	2.74	06:48:10.94	+07:35:45.0	9.95	0.29	0.02	0.70
JCMTLYS J064737.74+001415.4	-147.71	-0.74	06:47:37.74	+00:14:15.4	9.41	0.21	0.01	0.68
JCMTLYS J065645.64+012717.1	-147.76	1.85	06:56:45.64	+01:27:17.1	11.25	0.16	0.01	0.75
JCMTLYS J062550.76+075259	-157.00	-2.05	06:25:50.76	+07:52:59.0	6.30	0.11	0.01	0.56
JCMTLYS J061644.84+10372.6	-160.47	-2.74	06:16:44.84	+10:37:02.6	6.52	0.34	0.02	0.57
JCMTLYS J07908.49-054053.5	-139.99	1.33	07:09:08.49	-05:40:53.5	7.10	0.09	0.01	0.59
JCMTLYS J064006.24+064542.1	-154.37	0.57	06:40:06.24	+06:45:42.1	8.07	0.12	0.01	0.63
JCMTLYS J063658.81+023956.7	-151.09	-2.00	06:36:58.81	+02:39:56.7	6.21	0.08	0.00	0.55
JCMTLYS J063452.42+07285.3	-155.60	-0.26	06:34:52.42	+07:28:05.3	6.31	0.06	0.00	0.56
JCMTLYS J07650.29-064026.5	-139.38	0.36	07:06:50.29	-06:40:26.5	6.16	0.09	0.01	0.55
JCMTLYS J063614.51+01314.3	-150.15	-2.69	06:36:14.51	+01:31:04.3	9.20	0.41	0.02	0.68
JCMTLYS J063553.19+0103.2	-149.73	-3.00	06:35:53.19	+01:00:03.2	9.89	0.32	0.02	0.70
JCMTLYS J07051.89-085652.5	-138.03	-1.99	07:00:51.89	-08:56:52.5	10.93	0.18	0.01	0.74

Table A.1 continued from previous page

SASSy Name	*l*	*b*	*RA* (2000)	*Dec* (2000)	$Rad_{\rm eff}$ pc	$F_{\rm int}$ Jy	*error* Jy	*Aperture* Correction
JCMTLYS J07905.30-044831.8	-140.77	1.72	07:09:05.30	-04:48:31.8	7.32	0.10	0.01	0.60
JCMTLYS J07656.50-005933.8	-144.41	3.00	07:06:56.50	-00:59:33.8	7.70	0.31	0.02	0.62
JCMTLYS J065307.01+043349.2	-150.94	2.45	06:53:07.01	+04:33:49.2	6.00	0.09	0.01	0.54
JCMTLYS J065937.24-044028.5	-141.98	-0.31	06:59:37.24	-04:40:28.5	11.79	0.22	0.01	0.76
JCMTLYS J07301.39-064043.5	-139.81	-0.48	07:03:01.39	-06:40:43.5	8.03	0.12	0.01	0.63
JCMTLYS J065009.24-052921.6	-142.32	-2.78	06:50:09.24	-05:29:21.6	6.30	0.11	0.01	0.56
JCMTLYS J062833.74+081042.3	-156.95	-1.31	06:28:33.74	+08:10:42.3	6.75	0.10	0.01	0.58
JCMTLYS J065213.38+02915.2	-148.90	1.16	06:52:13.38	+02:09:15.2	8.41	0.39	0.02	0.65
JCMTLYS J064032.52+061329.7	-153.85	0.42	06:40:32.52	+06:13:29.7	6.06	0.07	0.00	0.55
JCMTLYS J062814.24+07540.9	-156.03	-1.89	06:28:14.24	+07:05:40.9	7.34	0.10	0.01	0.60
JCMTLYS J065230.88-042712.1	-142.98	-1.79	06:52:30.88	-04:27:12.1	6.14	0.09	0.01	0.55
JCMTLYS J07254.10-091610.4	-137.52	-1.69	07:02:54.10	-09:16:10.4	6.91	0.16	0.01	0.59
JCMTLYS J065738.34+011713.9	-147.51	1.97	06:57:38.34	+01:17:13.9	5.91	0.07	0.00	0.54
JCMTLYS J065520.77-053822.9	-141.60	-1.70	06:55:20.77	-05:38:22.9	8.00	0.10	0.01	0.63
JCMTLYS J065454.81-024122.2	-144.28	-0.45	06:54:54.81	-02:41:22.2	6.21	0.06	0.00	0.55
JCMTLYS J071123.29-04926.8	-141.09	2.53	07:11:23.29	-04:09:26.8	6.26	0.06	0.00	0.56
JCMTLYS J07243.84+011251.9	-146.86	3.07	07:02:43.84	+01:12:51.9	11.19	0.43	0.03	0.74

Table A.1 continued from previous page

SASSy Name	*l*	*b*	*RA* (2000)	*Dec* (2000)	$Rad_{\rm eff}$ pc	$F_{\rm int}$ Jy	*error* Jy	*Aperture* Correction
JCMTLYS J07210.93-052549.4	-141.01	-0.09	07:02:10.93	-05:25:49.4	5.85	0.07	0.00	0.54
JCMTLYS J064747.23-035758.3	-143.95	-2.62	06:47:47.23	-03:57:58.3	7.31	1.64	0.10	0.60
JCMTLYS J065200.31+03837.6	-149.80	1.56	06:52:00.31	+03:08:37.6	5.97	0.09	0.01	0.54
JCMTLYS J063139.36+024613.9	-151.79	-3.13	06:31:39.36	+02:46:13.9	9.10	0.40	0.02	0.67
JCMTLYS J064435.86+094529	-156.53	2.93	06:44:35.86	+09:45:29.0	7.55	0.34	0.02	0.61
JCMTLYS J071323.57-06430.7	-139.16	2.09	07:13:23.57	-06:04:30.7	5.55	0.08	0.00	0.52
JCMTLYS J07816.02-064955.2	-139.07	0.61	07:08:16.02	-06:49:55.2	6.87	0.09	0.01	0.58
JCMTLYS J07537.98-041725.1	-141.63	1.19	07:05:37.98	-04:17:25.1	6.86	0.06	0.00	0.58
JCMTLYS J071103.51-03726.1	-142.05	2.93	07:11:03.51	-03:07:26.1	6.51	1.09	0.07	0.57
JCMTLYS J065059.90+06208.6	-152.76	2.79	06:50:59.90	+06:20:08.6	6.70	0.14	0.01	0.58
JCMTLYS J07513.41-054740.6	-140.34	0.41	07:05:13.41	-05:47:40.6	11.84	0.19	0.01	0.76
JCMTLYS J065050.54+00148.3	-147.35	-0.03	06:50:50.54	+00:14:08.3	8.50	0.08	0.00	0.65
JCMTLYS J064709.62-033052.6	-144.43	-2.55	06:47:09.62	-03:30:52.6	6.40	0.09	0.01	0.56
JCMTLYS J071617.44-052622.7	-139.39	3.02	07:16:17.44	-05:26:22.7	8.30	1.28	0.08	0.64
JCMTLYS J07652.93-005647.2	-144.46	3.00	07:06:52.93	-00:56:47.2	7.87	0.30	0.02	0.63
JCMTLYS J061758.29+094054	-159.50	-2.92	06:17:58.29	+09:40:54.0	6.94	0.14	0.01	0.59
JCMTLYS J063603.21+034113.5	-152.10	-1.73	06:36:03.21	+03:41:13.5	6.67	0.06	0.00	0.57

Table A.1 continued from previous page

SASSy Name	*l*	*b*	*RA* (2000)	*Dec* (2000)	$Rad_{\rm eff}$ pc	$F_{\rm int}$ Jy	*error* Jy	*Aperture* Correction
JCMTLYS J064032.17+064159.9	-154.27	0.64	06:40:32.17	+06:41:59.9	7.33	0.10	0.01	0.60
JCMTLYS J061750.75+104952.8	-160.53	-2.41	06:17:50.75	+10:49:52.8	7.72	0.24	0.01	0.62
JCMTLYS J07459.75+00411.3	-145.58	3.05	07:04:59.75	+00:04:11.3	6.06	0.62	0.04	0.55
JCMTLYS J065942.64+004219.6	-146.75	2.16	06:59:42.64	+00:42:19.6	7.11	0.12	0.01	0.59
JCMTLYS J065955.71+02628.8	-147.98	2.85	06:59:55.71	+02:06:28.8	6.57	0.24	0.01	0.57
JCMTLYS J065323.95+05123	-151.32	2.72	06:53:23.95	+05:01:23.0	6.01	0.11	0.01	0.54
JCMTLYS J065559.28-002723.1	-146.14	0.80	06:55:59.28	-00:27:23.1	6.89	0.09	0.01	0.58
JCMTLYS J065852.56+012144.4	-147.43	2.28	06:58:52.56	+01:21:44.4	6.55	0.09	0.01	0.57
JCMTLYS J071149.81-07550.5	-137.70	0.89	07:11:49.81	-07:55:00.5	7.11	0.26	0.02	0.59
JCMTLYS J065702.20-044634.7	-142.18	-0.93	06:57:02.20	-04:46:34.7	5.90	0.06	0.00	0.54
JCMTLYS J065904.94-032846.3	-143.10	0.11	06:59:04.94	-03:28:46.3	7.29	0.10	0.01	0.60
JCMTLYS J062738.81+05317.2	-154.70	-2.75	06:27:38.81	+05:31:07.2	6.70	0.14	0.01	0.58
JCMTLYS J061815.41+105622.3	-160.58	-2.27	06:18:15.41	+10:56:22.3	6.95	0.19	0.01	0.59
JCMTLYS J065156.12-00941.2	-146.87	0.04	06:51:56.12	-00:09:41.2	6.10	0.07	0.00	0.55
JCMTLYS J065419.00-04389.4	-142.61	-1.47	06:54:19.00	-04:38:09.4	6.52	0.09	0.01	0.57
JCMTLYS J071101.63-053545.3	-139.85	1.79	07:11:01.63	-05:35:45.3	6.19	0.05	0.00	0.55
JCMTLYS J07309.71-063037.7	-139.94	-0.37	07:03:09.71	-06:30:37.7	6.38	0.08	0.00	0.56

Table A.1 continued from previous page

SASSy Name	*l*	*b*	*RA* (2000)	*Dec* (2000)	$Rad_{\rm eff}$ pc	$F_{\rm int}$ Jy	*error* Jy	*Aperture* Correction
JCMTLYS J065615.35+011816.2	-147.68	1.67	06:56:15.35	+01:18:16.2	20.09	0.40	0.02	0.93
JCMTLYS J065141.07+0312.2	-149.73	1.43	06:51:41.07	+03:01:02.2	5.97	0.10	0.01	0.54
JCMTLYS J063603.26+013854.8	-150.29	-2.67	06:36:03.26	+01:38:54.8	6.82	0.28	0.02	0.58
JCMTLYS J063637.33+064412.5	-154.75	-0.21	06:36:37.33	+06:44:12.5	6.73	0.11	0.01	0.58
JCMTLYS J07708.82-04026.3	-141.71	1.66	07:07:08.82	-04:00:26.3	6.86	0.08	0.00	0.58
JCMTLYS J071524.30-051442.7	-139.66	2.91	07:15:24.30	-05:14:42.7	7.25	3.13	0.19	0.60
JCMTLYS J071335.85-074757.7	-137.60	1.33	07:13:35.85	-07:47:57.7	6.06	0.15	0.01	0.55
JCMTLYS J065501.95-042740.7	-142.69	-1.23	06:55:01.95	-04:27:40.7	6.33	0.08	0.00	0.56
JCMTLYS J062140.34+074218.1	-157.33	-3.04	06:21:40.34	+07:42:18.1	6.29	0.24	0.01	0.56
JCMTLYS J063846.55-001119.2	-148.34	-2.90	06:38:46.55	-00:11:19.2	6.34	0.22	0.01	0.56
JCMTLYS J063742.68+1311.1	-160.21	2.91	06:37:42.68	+13:01:01.1	7.57	0.26	0.02	0.61
JCMTLYS J065415.70-06539.9	-140.61	-2.51	06:54:15.70	-06:53:09.9	7.92	0.11	0.01	0.63
JCMTLYS J065919.68-035855.4	-142.63	-0.06	06:59:19.68	-03:58:55.4	11.43	0.16	0.01	0.75
JCMTLYS J062925.42+084140	-157.31	-0.89	06:29:25.42	+08:41:40.0	7.74	0.11	0.01	0.62
JCMTLYS J063532.53+035852.4	-152.42	-1.71	06:35:32.53	+03:58:52.4	8.18	0.12	0.01	0.64
JCMTLYS J071324.33-035122.2	-141.12	3.11	07:13:24.33	-03:51:22.2	7.51	0.20	0.01	0.61
JCMTLYS J062504.73+055621.5	-155.37	-3.12	06:25:04.73	+05:56:21.5	8.71	0.31	0.02	0.66

Table A.1 continued from previous page

SASSy Name	*l*	*b*	*RA* (2000)	*Dec* (2000)	$Rad_{\rm eff}$ pc	$F_{\rm int}$ Jy	*error* Jy	*Aperture* Correction
JCMTLYS J064137.88+064959.3	-154.26	0.94	06:41:37.88	+06:49:59.3	6.94	0.07	0.00	0.59
JCMTLYS J071003.25-064150.3	-138.99	1.06	07:10:03.25	-06:41:50.3	7.04	0.08	0.00	0.59
JCMTLYS J065308.71+013026.9	-148.22	1.07	06:53:08.71	+01:30:26.9	6.78	0.07	0.00	0.58
JCMTLYS J063009.04+04349.7	-153.57	-2.63	06:30:09.04	+04:34:09.7	6.89	0.09	0.01	0.58
JCMTLYS J07604.57-02443.6	-142.96	2.01	07:06:04.57	-02:44:03.6	7.29	0.10	0.01	0.60
JCMTLYS J065647.62-06036.9	-141.11	-1.55	06:56:47.62	-06:00:36.9	6.25	0.08	0.00	0.56
JCMTLYS J065907.90-092541.8	-137.80	-2.59	06:59:07.90	-09:25:41.8	5.45	0.12	0.01	0.52
JCMTLYS J063156.58+04197.5	-153.14	-2.35	06:31:56.58	+04:19:07.5	6.68	0.09	0.01	0.58
JCMTLYS J065138.34+023556	-149.36	1.23	06:51:38.34	+02:35:56.0	6.82	0.10	0.01	0.58
JCMTLYS J064946.25+01518.6	-148.91	0.47	06:49:46.25	+01:51:08.6	9.33	0.11	0.01	0.68
JCMTLYS J07337.68-05213.8	-141.20	0.41	07:03:37.68	-05:02:13.8	6.27	0.06	0.00	0.56
JCMTLYS J07709.07-00262.9	-144.89	3.30	07:07:09.07	-00:26:02.9	7.56	3.18	0.19	0.61
JCMTLYS J065157.32-031453.7	-144.12	-1.37	06:51:57.32	-03:14:53.7	5.77	0.07	0.00	0.53
JCMTLYS J063245.87+024624.6	-151.67	-2.88	06:32:45.87	+02:46:24.6	6.22	0.13	0.01	0.55
JCMTLYS J07702.61-04847.2	-141.60	1.57	07:07:02.61	-04:08:47.2	7.21	0.06	0.00	0.60
JCMTLYS J065040.98-052822.5	-142.28	-2.66	06:50:40.98	-05:28:22.5	5.68	0.07	0.00	0.53
JCMTLYS J062740.07+10356.8	-159.18	-0.39	06:27:40.07	+10:35:06.8	8.95	0.12	0.01	0.67

Table A.1 continued from previous page

SASSy Name	*l*	*b*	*RA* (2000)	*Dec* (2000)	$Rad_{\rm eff}$ pc	$F_{\rm int}$ Jy	*error* Jy	*Aperture* Correction
JCMTLYS J065416.83-065455.2	-140.59	-2.52	06:54:16.83	-06:54:55.2	6.77	0.07	0.00	0.58
JCMTLYS J065952.91-004932.7	-145.37	1.50	06:59:52.91	-00:49:32.7	6.05	0.08	0.00	0.55
JCMTLYS J065214.87+004031.2	-147.58	0.49	06:52:14.87	+00:40:31.2	7.68	0.05	0.00	0.62
JCMTLYS J065954.37+005348.3	-146.90	2.29	06:59:54.37	+00:53:48.3	7.12	0.12	0.01	0.59
JCMTLYS J061630.70+101316.6	-160.15	-2.98	06:16:30.70	+10:13:16.6	6.52	3.69	0.22	0.57
JCMTLYS J065438.77-053713.5	-141.70	-1.85	06:54:38.77	-05:37:13.5	6.84	0.08	0.00	0.58
JCMTLYS J065906.66-071839.3	-139.69	-1.63	06:59:06.66	-07:18:39.3	7.07	0.06	0.00	0.59
JCMTLYS J064113.87+034454.1	-151.57	-0.56	06:41:13.87	+03:44:54.1	6.67	0.09	0.01	0.57
JCMTLYS J07459.69-054243.2	-140.44	0.40	07:04:59.69	-05:42:43.2	6.22	0.09	0.01	0.55
JCMTLYS J071049.41-021315.9	-142.88	3.29	07:10:49.41	-02:13:15.9	5.94	0.19	0.01	0.54
JCMTLYS J07436.96-065215.4	-139.45	-0.22	07:04:36.96	-06:52:15.4	6.35	0.09	0.01	0.56
JCMTLYS J065859.21+01396.9	-147.68	2.43	06:58:59.21	+01:39:06.9	7.15	0.10	0.01	0.60
JCMTLYS J07332.63+001949.1	-145.98	2.84	07:03:32.63	+00:19:49.1	5.85	0.17	0.01	0.54
JCMTLYS J071319.16-073524.5	-137.82	1.37	07:13:19.16	-07:35:24.5	6.96	0.10	0.01	0.59
JCMTLYS J065531.18-00739.2	-146.49	0.85	06:55:31.18	-00:07:39.2	6.51	0.07	0.00	0.57
JCMTLYS J063215.51+032347.2	-152.28	-2.71	06:32:15.51	+03:23:47.2	7.81	0.32	0.02	0.62
JCMTLYS J062811.80+09319.6	-157.77	-0.99	06:28:11.80	+09:03:19.6	6.75	0.09	0.01	0.58

Table A.1 continued from previous page

SASSy Name	*l*	*b*	*RA* (2000)	*Dec* (2000)	$Rad_{\rm eff}$ pc	$F_{\rm int}$ Jy	*error* Jy	*Aperture* Correction
JCMTLYS J064230.65-00657.4	-147.98	-2.04	06:42:30.65	-00:06:57.4	6.55	0.08	0.00	0.57
JCMTLYS J063357.49+015016.6	-150.70	-3.05	06:33:57.49	+01:50:16.6	6.19	0.21	0.01	0.55
JCMTLYS J063931.22-00159.7	-148.20	-2.77	06:39:31.22	-00:15:09.7	6.12	0.21	0.01	0.55
JCMTLYS J071425.15-045944.6	-140.00	2.81	07:14:25.15	-04:59:44.6	7.10	0.12	0.01	0.59
JCMTLYS J07033.67-093737.7	-137.46	-2.37	07:00:33.67	-09:37:37.7	6.02	0.18	0.01	0.55
JCMTLYS J065648.13+012721.6	-147.75	1.86	06:56:48.13	+01:27:21.6	12.81	0.19	0.01	0.79
JCMTLYS J065944.47+00564.8	-146.95	2.27	06:59:44.47	+00:56:04.8	7.12	0.10	0.01	0.59
JCMTLYS J064750.49+073230.4	-154.19	2.64	06:47:50.49	+07:32:30.4	6.73	0.19	0.01	0.58
JCMTLYS J063205.62+082413.3	-156.75	-0.43	06:32:05.62	+08:24:13.3	6.09	0.06	0.00	0.55
JCMTLYS J063343.16+122742.8	-160.16	1.79	06:33:43.16	+12:27:42.8	7.38	0.13	0.01	0.61
JCMTLYS J064936.65+04204.7	-151.13	1.57	06:49:36.65	+04:20:04.7	6.23	0.10	0.01	0.55
JCMTLYS J063310.94+074634.9	-156.06	-0.49	06:33:10.94	+07:46:34.9	6.75	0.09	0.01	0.58
JCMTLYS J063245.50+023641.2	-151.53	-2.96	06:32:45.50	+02:36:41.2	6.64	0.14	0.01	0.57
JCMTLYS J063715.03+00014.9	-148.69	-3.15	06:37:15.03	+00:00:14.9	7.51	0.23	0.01	0.61
JCMTLYS J07708.73-02915.3	-143.36	2.51	07:07:08.73	-02:09:15.3	5.75	0.07	0.00	0.53
JCMTLYS J07020.53-093335.7	-137.55	-2.39	07:00:20.53	-09:33:35.7	5.44	0.12	0.01	0.52
JCMTLYS J07512.15-05922.7	-140.91	0.70	07:05:12.15	-05:09:22.7	6.25	0.04	0.00	0.56

Table A.1 continued from previous page

SASSy Name	*l*	*b*	*RA* (2000)	*Dec* (2000)	$Rad_{\rm eff}$ pc	$F_{\rm int}$ Jy	*error* Jy	*Aperture* Correction
JCMTLYS J07151.17+011223.2	-146.96	2.87	07:01:51.17	+01:12:23.2	6.53	0.07	0.00	0.57
JCMTLYS J071126.13-08043.5	-137.66	0.76	07:11:26.13	-08:00:43.5	9.82	0.93	0.06	0.70
JCMTLYS J062445.89+112413.8	-160.24	-0.64	06:24:45.89	+11:24:13.8	6.09	0.50	0.03	0.55
JCMTLYS J065504.34+013913.8	-148.13	1.56	06:55:04.34	+01:39:13.8	9.59	0.11	0.01	0.69
JCMTLYS J07125.63-062733	-140.18	-0.73	07:01:25.63	-06:27:33.0	6.94	0.08	0.00	0.59
JCMTLYS J07055.37-09519.3	-137.90	-2.04	07:00:55.37	-09:05:19.3	6.77	0.07	0.00	0.58
JCMTLYS J065442.23-08558.9	-139.48	-2.96	06:54:42.23	-08:05:58.9	5.95	0.39	0.02	0.54
JCMTLYS J065025.57+054849.6	-152.36	2.42	06:50:25.57	+05:48:49.6	6.26	0.08	0.00	0.56
JCMTLYS J071444.04-052735.8	-139.55	2.67	07:14:44.04	-05:27:35.8	6.73	0.18	0.01	0.58
JCMTLYS J063054.82+075646.9	-156.48	-0.90	06:30:54.82	+07:56:46.9	6.53	0.08	0.00	0.57
JCMTLYS J062810.74+07554.2	-156.04	-1.90	06:28:10.74	+07:05:54.2	7.53	0.09	0.01	0.61
JCMTLYS J063955.71+013955.6	-149.86	-1.80	06:39:55.71	+01:39:55.6	7.39	0.08	0.00	0.61
JCMTLYS J07621.08-035450.7	-141.88	1.52	07:06:21.08	-03:54:50.7	7.22	0.06	0.00	0.60
JCMTLYS J065327.60-07154.2	-140.58	-2.75	06:53:27.60	-07:01:54.2	8.06	0.10	0.01	0.63
JCMTLYS J064055.87+005535.3	-149.09	-1.91	06:40:55.87	+00:55:35.3	5.94	0.09	0.01	0.54
JCMTLYS J064117.32+054748.6	-153.38	0.39	06:41:17.32	+05:47:48.6	6.05	0.07	0.00	0.55
JCMTLYS J063047.39+073310.8	-156.14	-1.11	06:30:47.39	+07:33:10.8	6.08	0.06	0.00	0.55

Table A.1 continued from previous page

SASSy Name	*l*	*b*	*RA* (2000)	*Dec* (2000)	$Rad_{\rm eff}$ pc	$F_{\rm int}$ Jy	*error* Jy	*Aperture* Correction
JCMTLYS J065713.90-031614.2	-143.50	-0.20	06:57:13.90	-03:16:14.2	6.38	0.09	0.01	0.56
JCMTLYS J065833.45-01308.9	-144.92	0.90	06:58:33.45	-01:30:08.9	7.21	0.09	0.01	0.60
JCMTLYS J063813.42+101115.8	-157.63	1.73	06:38:13.42	+10:11:15.8	9.72	0.16	0.01	0.70
JCMTLYS J065713.03-01479	-144.82	0.47	06:57:13.03	-01:47:09.0	7.89	0.09	0.01	0.63
JCMTLYS J064001.56+122043.2	-159.35	3.11	06:40:01.56	+12:20:43.2	6.55	0.23	0.01	0.57
JCMTLYS J07151.37+015510.8	-147.59	3.19	07:01:51.37	+01:55:10.8	10.99	0.85	0.05	0.74
JCMTLYS J07512.51-11436.8	-135.65	-2.01	07:05:12.51	-11:04:36.8	36.84	5.89	0.35	1.01
JCMTLYS J074451.93-24740.6	-119.68	0.07	07:44:51.93	-24:07:40.6	29.70	5.74	0.34	1.00
JCMTLYS J073209.87-16588.9	-127.38	1.00	07:32:09.87	-16:58:08.9	34.42	5.01	0.30	1.01
JCMTLYS J074428.10-20832.7	-123.18	1.98	07:44:28.10	-20:08:32.7	21.77	1.44	0.09	0.95
JCMTLYS J07343.05-11337.1	-135.39	-2.56	07:03:43.05	-11:33:07.1	26.95	2.41	0.14	0.99
JCMTLYS J07510.74-121858.9	-134.55	-2.59	07:05:10.74	-12:18:58.9	25.23	1.73	0.10	0.97
JCMTLYS J071417.30-121616.8	-133.56	-0.59	07:14:17.30	-12:16:16.8	24.98	1.79	0.11	0.97
JCMTLYS J071329.52-121648.9	-133.65	-0.77	07:13:29.52	-12:16:48.9	18.02	0.85	0.05	0.90
JCMTLYS J073016.87-183554.9	-126.17	-0.18	07:30:16.87	-18:35:54.9	31.03	2.56	0.15	1.00
JCMTLYS J07444.72-11720.1	-135.66	-2.14	07:04:44.72	-11:07:20.1	29.54	1.76	0.11	1.00
JCMTLYS J072301.78-144130.1	-130.43	0.15	07:23:01.78	-14:41:30.1	21.13	1.11	0.07	0.94

Table A.1 continued from previous page

SASSy Name	*l*	*b*	*RA* (2000)	*Dec* (2000)	$Rad_{\rm eff}$ pc	$F_{\rm int}$ Jy	*error* Jy	*Aperture* Correction
JCMTLYS J071006.08-103151.4	-135.58	-0.70	07:10:06.08	-10:31:51.4	24.26	1.65	0.10	0.97
JCMTLYS J07511.22-11515.8	-135.64	-2.02	07:05:11.22	-11:05:15.8	23.57	1.46	0.09	0.96
JCMTLYS J074524.53-253750.4	-118.32	-0.57	07:45:24.53	-25:37:50.4	14.39	0.68	0.04	0.83
JCMTLYS J071005.53-10317.3	-135.59	-0.69	07:10:05.53	-10:31:07.3	18.01	1.10	0.07	0.90
JCMTLYS J071638.69-092543.7	-135.81	1.24	07:16:38.69	-09:25:43.7	16.46	0.59	0.04	0.87
JCMTLYS J074930.75-234546.2	-119.47	1.17	07:49:30.75	-23:45:46.2	10.64	1.49	0.09	0.73
JCMTLYS J07823.42-102915.6	-135.81	-1.05	07:08:23.42	-10:29:15.6	17.03	0.66	0.04	0.88
JCMTLYS J07703.37-112018.1	-135.21	-1.73	07:07:03.37	-11:20:18.1	17.81	0.72	0.04	0.90
JCMTLYS J071859.92-18239.7	-127.92	-2.28	07:18:59.92	-18:02:39.7	15.40	0.83	0.05	0.85
JCMTLYS J07830.16-103222.9	-135.75	-1.05	07:08:30.16	-10:32:22.9	16.17	0.63	0.04	0.87
JCMTLYS J065937.46-074539.8	-139.23	-1.72	06:59:37.46	-07:45:39.8	19.32	0.91	0.05	0.92
JCMTLYS J07503.62-121635.6	-134.60	-2.60	07:05:03.62	-12:16:35.6	17.76	0.76	0.05	0.89
JCMTLYS J07920.07-105026.7	-135.39	-1.01	07:09:20.07	-10:50:26.7	19.36	0.82	0.05	0.92
JCMTLYS J071931.89-175024.9	-128.05	-2.07	07:19:31.89	-17:50:24.9	16.27	0.75	0.05	0.87
JCMTLYS J071418.52-121527.2	-133.57	-0.58	07:14:18.52	-12:15:27.2	17.13	0.68	0.04	0.88
JCMTLYS J072935.27-175649.6	-126.82	-0.01	07:29:35.27	-17:56:49.6	8.66	0.59	0.04	0.66
JCMTLYS J07827.43-103131.6	-135.77	-1.05	07:08:27.43	-10:31:31.6	15.08	0.36	0.02	0.84

Table A.1 continued from previous page

SASSy Name	*l*	*b*	*RA* (2000)	*Dec* (2000)	$Rad_{\rm eff}$ pc	$F_{\rm int}$ Jy	*error* Jy	*Aperture* Correction
JCMTLYS J072956.44-182749.6	-126.32	-0.19	07:29:56.44	-18:27:49.6	17.35	0.62	0.04	0.89
JCMTLYS J07922.14-105036.4	-135.39	-1.00	07:09:22.14	-10:50:36.4	17.19	0.51	0.03	0.88
JCMTLYS J07527.67-111323.4	-135.49	-2.03	07:05:27.67	-11:13:23.4	11.41	0.28	0.02	0.75
JCMTLYS J073553.03-19168.2	-124.94	0.66	07:35:53.03	-19:16:08.2	16.75	0.66	0.04	0.88
JCMTLYS J07856.41-102914.6	-135.75	-0.93	07:08:56.41	-10:29:14.6	13.70	0.37	0.02	0.81
JCMTLYS J071903.63-07051.3	-137.67	2.90	07:19:03.63	-07:00:51.3	7.75	2.69	0.16	0.62
JCMTLYS J065940.52-09753.8	-138.00	-2.34	06:59:40.52	-09:07:53.8	9.97	0.30	0.02	0.70
JCMTLYS J073829.15-162011.6	-127.20	2.63	07:38:29.15	-16:20:11.6	11.01	0.87	0.05	0.74
JCMTLYS J073934.36-161913.7	-127.08	2.86	07:39:34.36	-16:19:13.7	7.69	0.86	0.05	0.62
JCMTLYS J07028.60-085120.4	-138.16	-2.04	07:00:28.60	-08:51:20.4	20.31	0.58	0.03	0.93
JCMTLYS J073319.73-18400	-125.76	0.42	07:33:19.73	-18:40:00.0	8.46	0.44	0.03	0.65
JCMTLYS J07859.80-111238.2	-135.10	-1.25	07:08:59.80	-11:12:38.2	13.47	0.29	0.02	0.81
JCMTLYS J073117.65-203433.8	-124.32	-0.92	07:31:17.65	-20:34:33.8	7.38	0.11	0.01	0.61
JCMTLYS J073538.85-184848.7	-125.37	0.83	07:35:38.85	-18:48:48.7	18.66	0.54	0.03	0.91
JCMTLYS J073158.90-191751.6	-125.36	-0.16	07:31:58.90	-19:17:51.6	12.14	0.36	0.02	0.77
JCMTLYS J07511.20-11552.7	-135.63	-2.03	07:05:11.20	-11:05:52.7	22.39	0.54	0.03	0.95
JCMTLYS J07451.93-12934.6	-134.72	-2.59	07:04:51.93	-12:09:34.6	12.11	0.25	0.01	0.77

Table A.1 continued from previous page

SASSy Name	*l*	*b*	*RA* (2000)	*Dec* (2000)	$Rad_{\rm eff}$ pc	$F_{\rm int}$ Jy	*error* Jy	*Aperture* Correction
JCMTLYS J072144.59-21106.8	-124.86	-3.17	07:21:44.59	-21:10:06.8	11.38	4.41	0.26	0.75
JCMTLYS J071911.59-114926.8	-133.40	0.68	07:19:11.59	-11:49:26.8	7.33	0.10	0.01	0.60
JCMTLYS J07513.58-103929.8	-136.02	-1.82	07:05:13.58	-10:39:29.8	13.89	0.25	0.01	0.82
JCMTLYS J073423.69-204939	-123.75	-0.41	07:34:23.69	-20:49:39.0	8.19	0.19	0.01	0.64
JCMTLYS J07417.77-103223.3	-136.23	-1.97	07:04:17.77	-10:32:23.3	6.07	0.08	0.00	0.55
JCMTLYS J07517.39-111019.5	-135.56	-2.04	07:05:17.39	-11:10:19.5	11.41	0.17	0.01	0.75
JCMTLYS J071053.39-121528.6	-133.96	-1.32	07:10:53.39	-12:15:28.6	6.72	0.09	0.01	0.58
JCMTLYS J071012.81-103442.6	-135.53	-0.69	07:10:12.81	-10:34:42.6	7.54	0.13	0.01	0.61
JCMTLYS J073319.94-22111.1	-122.68	-1.28	07:33:19.94	-22:11:01.1	13.78	0.32	0.02	0.81
JCMTLYS J071514.30-10649.8	-135.37	0.62	07:15:14.30	-10:06:49.8	6.75	0.16	0.01	0.58
JCMTLYS J071127.49-125851.6	-133.25	-1.53	07:11:27.49	-12:58:51.6	7.11	0.09	0.01	0.59
JCMTLYS J07357.90-045937.2	-141.20	0.50	07:03:57.90	-04:59:37.2	9.85	8.35	0.50	0.70
JCMTLYS J073108.75-191524.9	-125.49	-0.32	07:31:08.75	-19:15:24.9	10.40	0.24	0.01	0.72
JCMTLYS J074438.78-20741.8	-123.18	2.03	07:44:38.78	-20:07:41.8	11.87	0.23	0.01	0.76
JCMTLYS J071000.84-103054.6	-135.61	-0.71	07:10:00.84	-10:30:54.6	10.26	0.20	0.01	0.71
JCMTLYS J07514.09-103953.5	-136.01	-1.82	07:05:14.09	-10:39:53.5	9.82	0.15	0.01	0.70
JCMTLYS J07816.45-144418.1	-132.05	-3.03	07:08:16.45	-14:44:18.1	6.45	0.19	0.01	0.56

Table A.1 continued from previous page

SASSy Name	*l*	*b*	*RA* (2000)	*Dec* (2000)	$Rad_{\rm eff}$ pc	$F_{\rm int}$ Jy	*error* Jy	*Aperture* Correction
JCMTLYS J073532.63-184528.7	-125.43	0.83	07:35:32.63	-18:45:28.7	10.78	0.25	0.01	0.73
JCMTLYS J07515.47-1153.4	-135.64	-2.01	07:05:15.47	-11:05:03.4	12.48	0.17	0.01	0.78
JCMTLYS J074401.23-262041.4	-117.86	-1.20	07:44:01.23	-26:20:41.4	6.10	0.10	0.01	0.55
JCMTLYS J07945.55-102841.6	-135.67	-0.75	07:09:45.55	-10:28:41.6	10.26	0.19	0.01	0.71
JCMTLYS J073455.19-14145.9	-129.46	2.90	07:34:55.19	-14:14:05.9	6.84	2.99	0.18	0.58
JCMTLYS J07427.17-102831.7	-136.27	-1.90	07:04:27.17	-10:28:31.7	8.92	0.13	0.01	0.67
JCMTLYS J07303.80-065825.5	-139.54	-0.61	07:03:03.80	-06:58:25.5	16.03	0.37	0.02	0.86
JCMTLYS J071425.13-12655.8	-133.69	-0.49	07:14:25.13	-12:06:55.8	12.35	0.23	0.01	0.78
JCMTLYS J065704.49-07523	-140.12	-1.98	06:57:04.49	-07:05:23.0	8.43	0.18	0.01	0.65
JCMTLYS J07253.66-113055.5	-135.52	-2.72	07:02:53.66	-11:30:55.5	6.72	0.20	0.01	0.58
JCMTLYS J07146.44-064932.7	-139.82	-0.82	07:01:46.44	-06:49:32.7	8.28	0.14	0.01	0.64
JCMTLYS J071935.76-173917.8	-128.20	-1.97	07:19:35.76	-17:39:17.8	8.70	0.16	0.01	0.66
JCMTLYS J07846.18-103647.2	-135.66	-1.03	07:08:46.18	-10:36:47.2	12.62	0.19	0.01	0.79
JCMTLYS J073102.09-251019.8	-120.31	-3.18	07:31:02.09	-25:10:19.8	10.55	11.22	0.67	0.72
JCMTLYS J071900.51-065921.9	-137.70	2.90	07:19:00.51	-06:59:21.9	10.15	0.67	0.04	0.71
JCMTLYS J07617.53-142024.5	-132.62	-3.27	07:06:17.53	-14:20:24.5	7.27	0.35	0.02	0.60
JCMTLYS J073012.71-244120.2	-120.83	-3.11	07:30:12.71	-24:41:20.2	6.81	0.58	0.03	0.58

Table A.1 continued from previous page

SASSy Name	*l*	*b*	*RA* (2000)	*Dec* (2000)	$Rad_{\rm eff}$ pc	$F_{\rm int}$ Jy	*error* Jy	*Aperture* Correction
JCMTLYS J074219.24-194728.4	-123.74	1.72	07:42:19.24	-19:47:28.4	7.19	0.11	0.01	0.60
JCMTLYS J07052.59-094447.1	-137.32	-2.35	07:00:52.59	-09:44:47.1	6.95	0.07	0.00	0.59
JCMTLYS J072156.46-084754.4	-135.76	2.69	07:21:56.46	-08:47:54.4	8.94	0.35	0.02	0.67
JCMTLYS J07519.47-122018.2	-134.51	-2.57	07:05:19.47	-12:20:18.2	17.84	0.39	0.02	0.90
JCMTLYS J075614.00-231721.5	-119.08	2.74	07:56:14.00	-23:17:21.5	5.79	0.15	0.01	0.53
JCMTLYS J073046.21-151726.2	-129.01	1.51	07:30:46.21	-15:17:26.2	13.15	0.22	0.01	0.80
JCMTLYS J075747.07-245439.6	-117.51	2.20	07:57:47.07	-24:54:39.6	6.28	0.09	0.01	0.56
JCMTLYS J071746.62-183344.5	-127.60	-2.77	07:17:46.62	-18:33:44.5	8.51	0.36	0.02	0.65
JCMTLYS J073654.70-14476.8	-128.74	3.05	07:36:54.70	-14:47:06.8	7.58	0.17	0.01	0.61
JCMTLYS J07519.73-111113.3	-135.54	-2.04	07:05:19.73	-11:11:13.3	11.04	0.14	0.01	0.74
JCMTLYS J073725.90-273811.7	-117.46	-3.12	07:37:25.90	-27:38:11.7	7.57	0.36	0.02	0.61
JCMTLYS J07326.31-091956.1	-137.40	-1.60	07:03:26.31	-09:19:56.1	12.74	0.22	0.01	0.79
JCMTLYS J071701.34-141142.2	-131.55	-0.90	07:17:01.34	-14:11:42.2	7.47	0.08	0.00	0.61
JCMTLYS J074847.17-243644.3	-118.82	0.60	07:48:47.17	-24:36:44.3	8.73	0.71	0.04	0.66
JCMTLYS J065531.21-072831	-139.95	-2.50	06:55:31.21	-07:28:31.0	9.07	0.56	0.03	0.67
JCMTLYS J072218.16-203913	-125.25	-2.81	07:22:18.16	-20:39:13.0	7.04	0.19	0.01	0.59
JCMTLYS J071240.32-14176.3	-131.96	-1.87	07:12:40.32	-14:17:06.3	6.88	0.10	0.01	0.58

Table A.1 continued from previous page

SASSy Name	*l*	*b*	*RA* (2000)	*Dec* (2000)	$Rad_{\rm eff}$ pc	$F_{\rm int}$ Jy	*error* Jy	*Aperture* Correction
JCMTLYS J072106.81-155956.2	-129.49	-0.87	07:21:06.81	-15:59:56.2	9.80	6.76	0.41	0.70
JCMTLYS J071558.17-182038.9	-127.99	-3.05	07:15:58.17	-18:20:38.9	6.35	0.29	0.02	0.56
JCMTLYS J074051.25-17585.2	-125.50	2.32	07:40:51.25	-17:58:05.2	6.70	0.08	0.01	0.58
JCMTLYS J071755.04-19854.6	-127.07	-3.02	07:17:55.04	-19:08:54.6	8.32	0.46	0.03	0.64
JCMTLYS J073532.86-184513.2	-125.43	0.84	07:35:32.86	-18:45:13.2	8.44	0.16	0.01	0.65
JCMTLYS J07053.03-085645.4	-138.03	-1.99	07:00:53.03	-08:56:45.4	13.07	0.20	0.01	0.80
JCMTLYS J07444.04-11643.6	-135.67	-2.13	07:04:44.04	-11:06:43.6	6.73	0.07	0.00	0.58
JCMTLYS J073341.55-131520.2	-130.46	3.11	07:33:41.55	-13:15:20.2	7.99	0.32	0.02	0.63
JCMTLYS J065603.33-075014.1	-139.56	-2.55	06:56:03.33	-07:50:14.1	8.76	0.14	0.01	0.66
JCMTLYS J07908.05-053914.3	-140.02	1.34	07:09:08.05	-05:39:14.3	7.75	0.38	0.02	0.62
JCMTLYS J071026.00-145326.1	-131.67	-2.63	07:10:26.00	-14:53:26.1	7.26	3.00	0.18	0.60
JCMTLYS J073947.06-19946.4	-124.58	1.51	07:39:47.06	-19:09:46.4	6.86	0.10	0.01	0.58
JCMTLYS J07546.66-103728.6	-135.99	-1.68	07:05:46.66	-10:37:28.6	13.58	0.20	0.01	0.81
JCMTLYS J075555.66-255113	-116.92	1.35	07:55:55.66	-25:51:13.0	6.77	0.28	0.02	0.58
JCMTLYS J072152.69-075426.3	-136.55	3.10	07:21:52.69	-07:54:26.3	8.62	0.29	0.02	0.66
JCMTLYS J071931.66-153843.3	-129.99	-1.04	07:19:31.66	-15:38:43.3	6.84	0.08	0.00	0.58
JCMTLYS J07248.82-1035.8	-136.83	-2.07	07:02:48.82	-10:03:05.8	7.91	0.10	0.01	0.63

Table A.1 continued from previous page

SASSy Name	*l*	*b*	*RA* (2000)	*Dec* (2000)	$Rad_{\rm eff}$ pc	$F_{\rm int}$ Jy	*error* Jy	*Aperture* Correction
JCMTLYS J075418.08-23128.9	-119.39	2.40	07:54:18.08	-23:12:08.9	6.21	0.08	0.01	0.55
JCMTLYS J073611.73-253011.4	-119.46	-2.32	07:36:11.73	-25:30:11.4	7.42	0.11	0.01	0.61
JCMTLYS J07214.30-1066.7	-136.85	-2.22	07:02:14.30	-10:06:06.7	6.30	0.08	0.01	0.56
JCMTLYS J07605.73-101144.5	-136.33	-1.42	07:06:05.73	-10:11:44.5	6.75	0.09	0.01	0.58
JCMTLYS J074715.04-26387.6	-117.25	-0.72	07:47:15.04	-26:38:07.6	6.61	0.34	0.02	0.57
JCMTLYS J074032.81-16193.4	-126.97	3.07	07:40:32.81	-16:19:03.4	9.56	0.90	0.05	0.69
JCMTLYS J072137.44-21828.4	-124.89	-3.18	07:21:37.44	-21:08:28.4	8.67	6.58	0.39	0.66
JCMTLYS J073154.17-143853.6	-129.45	2.06	07:31:54.17	-14:38:53.6	10.23	0.15	0.01	0.71
JCMTLYS J071845.72-165245.7	-128.98	-1.78	07:18:45.72	-16:52:45.7	9.77	0.15	0.01	0.70
JCMTLYS J071236.30-07412.3	-137.82	1.17	07:12:36.30	-07:41:02.3	6.10	0.07	0.00	0.55
JCMTLYS J072014.18-071730.8	-137.29	3.02	07:20:14.18	-07:17:30.8	7.56	1.09	0.07	0.61
JCMTLYS J073224.35-154215.7	-128.46	1.66	07:32:24.35	-15:42:15.7	8.90	0.12	0.01	0.67
JCMTLYS J075855.55-232629	-118.63	3.19	07:58:55.55	-23:26:29.0	6.35	2.05	0.12	0.56
JCMTLYS J07614.76-10740.9	-136.38	-1.35	07:06:14.76	-10:07:40.9	6.31	0.09	0.01	0.56
JCMTLYS J073541.09-233123	-121.25	-1.46	07:35:41.09	-23:31:23.0	10.55	0.17	0.01	0.72
JCMTLYS J074549.71-27651.8	-116.99	-1.24	07:45:49.71	-27:06:51.8	6.23	0.28	0.02	0.55
JCMTLYS J074155.32-181230.5	-125.16	2.42	07:41:55.32	-18:12:30.5	9.32	0.16	0.01	0.68

Table A.1 continued from previous page

SASSy Name	*l*	*b*	*RA* (2000)	*Dec* (2000)	$Rad_{\rm eff}$ pc	$F_{\rm int}$ Jy	*error* Jy	*Aperture* Correction
JCMTLYS J073016.97-191024.8	-125.66	-0.46	07:30:16.97	-19:10:24.8	9.05	0.17	0.01	0.67
JCMTLYS J075044.43-231648.2	-119.74	1.66	07:50:44.43	-23:16:48.2	7.30	0.12	0.01	0.60
JCMTLYS J071824.30-062821.8	-138.23	3.00	07:18:24.30	-06:28:21.8	7.37	0.25	0.02	0.61
JCMTLYS J07952.49-052250.8	-140.18	1.63	07:09:52.49	-05:22:50.8	6.98	0.21	0.01	0.59
JCMTLYS J072523.41-22112.8	-123.70	-2.82	07:25:23.41	-22:01:12.8	5.76	0.13	0.01	0.53
JCMTLYS J074214.42-175659	-125.35	2.61	07:42:14.42	-17:56:59.0	6.50	0.63	0.04	0.57
JCMTLYS J07616.79-131319.1	-133.62	-2.76	07:06:16.79	-13:13:19.1	9.62	0.62	0.04	0.69
JCMTLYS J073206.57-253756.4	-119.79	-3.19	07:32:06.57	-25:37:56.4	10.03	5.64	0.34	0.71
JCMTLYS J073234.57-171737.3	-127.05	0.93	07:32:34.57	-17:17:37.3	9.42	0.11	0.01	0.69
JCMTLYS J072408.93-203843.1	-125.05	-2.42	07:24:08.93	-20:38:43.1	8.84	0.10	0.01	0.66
JCMTLYS J072937.12-134932.2	-130.43	1.97	07:29:37.12	-13:49:32.2	6.66	0.11	0.01	0.57
JCMTLYS J07547.19-104753.1	-135.83	-1.76	07:05:47.19	-10:47:53.1	7.34	0.08	0.00	0.60
JCMTLYS J07457.35-125848.6	-133.98	-2.94	07:04:57.35	-12:58:48.6	7.11	0.20	0.01	0.59
JCMTLYS J071844.55-16528.6	-128.99	-1.78	07:18:44.55	-16:52:08.6	7.20	0.08	0.01	0.60
JCMTLYS J075954.69-253338	-116.71	2.27	07:59:54.69	-25:33:38.0	6.59	1.47	0.09	0.57
JCMTLYS J072454.50-135630.5	-130.88	0.91	07:24:54.50	-13:56:30.5	7.83	0.09	0.01	0.62
JCMTLYS J07800.00-102620.4	-135.90	-1.11	07:08:00.00	-10:26:20.4	11.92	0.15	0.01	0.77

Table A.1 continued from previous page

SASSy Name	*l*	*b*	*RA* (2000)	*Dec* (2000)	$Rad_{\rm eff}$ pc	$F_{\rm int}$ Jy	*error* Jy	*Aperture* Correction
JCMTLYS J074210.23-254853.6	-118.53	-1.30	07:42:10.23	-25:48:53.6	6.14	0.08	0.00	0.55
JCMTLYS J07356.16-08221.6	-138.20	-1.05	07:03:56.16	-08:22:01.6	6.32	0.07	0.00	0.56
JCMTLYS J07955.74-103218	-135.59	-0.74	07:09:55.74	-10:32:18.0	7.15	0.08	0.00	0.60
JCMTLYS J07844.30-103716.2	-135.66	-1.04	07:08:44.30	-10:37:16.2	9.08	0.09	0.01	0.67
JCMTLYS J075335.59-223532.8	-119.99	2.58	07:53:35.59	-22:35:32.8	6.98	0.09	0.01	0.59
JCMTLYS J07829.20-10321.1	-135.76	-1.05	07:08:29.20	-10:32:01.1	8.92	0.10	0.01	0.67
JCMTLYS J072203.79-091147.3	-135.39	2.53	07:22:03.79	-09:11:47.3	6.54	0.15	0.01	0.57
JCMTLYS J073000.73-183154.8	-126.26	-0.20	07:30:00.73	-18:31:54.8	11.65	0.17	0.01	0.76
JCMTLYS J073043.58-124512.5	-131.25	2.72	07:30:43.58	-12:45:12.5	8.52	1.02	0.06	0.65
JCMTLYS J071517.69-081050.6	-137.07	1.53	07:15:17.69	-08:10:50.6	7.56	0.09	0.01	0.61
JCMTLYS J071224.18-111534.6	-134.67	-0.53	07:12:24.18	-11:15:34.6	11.67	0.18	0.01	0.76
JCMTLYS J071218.93-155418.6	-130.56	-2.70	07:12:18.93	-15:54:18.6	6.21	0.08	0.00	0.55
JCMTLYS J072033.83-071545.9	-137.27	3.11	07:20:33.83	-07:15:45.9	9.86	2.15	0.13	0.70
JCMTLYS J075954.66-234915.4	-118.19	3.18	07:59:54.66	-23:49:15.4	8.26	1.34	0.08	0.64
JCMTLYS J065535.05-071716.9	-140.11	-2.40	06:55:35.05	-07:17:16.9	7.90	0.32	0.02	0.63
JCMTLYS J073318.16-22649.6	-122.75	-1.25	07:33:18.16	-22:06:49.6	9.01	0.16	0.01	0.67
JCMTLYS J072742.44-201858.6	-124.95	-1.53	07:27:42.44	-20:18:58.6	6.86	0.12	0.01	0.58

Table A.1 continued from previous page

SASSy Name	*l*	*b*	*RA* (2000)	*Dec* (2000)	$Rad_{\rm eff}$ pc	$F_{\rm int}$ Jy	*error* Jy	*Aperture* Correction
JCMTLYS J07122.51-085637.9	-137.98	-1.88	07:01:22.51	-08:56:37.9	6.75	0.07	0.00	0.58
JCMTLYS J074742.25-19403.1	-123.21	2.88	07:47:42.25	-19:40:03.1	7.33	2.50	0.15	0.60
JCMTLYS J065923.01-09429.3	-137.53	-2.66	06:59:23.01	-09:42:09.3	8.08	0.18	0.01	0.63
JCMTLYS J074626.56-225725.5	-120.52	0.97	07:46:26.56	-22:57:25.5	5.86	0.09	0.01	0.54
JCMTLYS J07921.03-102810.5	-135.72	-0.83	07:09:21.03	-10:28:10.5	13.91	0.24	0.01	0.82
JCMTLYS J072257.19-18926.9	-127.38	-1.50	07:22:57.19	-18:09:26.9	6.56	0.07	0.00	0.57
JCMTLYS J074320.99-171730.5	-125.79	3.17	07:43:20.99	-17:17:30.5	7.28	0.39	0.02	0.60
JCMTLYS J071441.62-16051.8	-130.20	-2.24	07:14:41.62	-16:00:51.8	8.62	0.13	0.01	0.66
JCMTLYS J072916.31-193144.2	-125.47	-0.84	07:29:16.31	-19:31:44.2	6.88	0.12	0.01	0.58
JCMTLYS J072331.29-09311.7	-135.35	2.92	07:23:31.29	-09:03:11.7	8.27	1.02	0.06	0.64
JCMTLYS J073113.18-211029.8	-123.80	-1.22	07:31:13.18	-21:10:29.8	5.78	0.07	0.00	0.53
JCMTLYS J073715.64-20814.5	-124.02	0.51	07:37:15.64	-20:08:14.5	6.44	0.07	0.00	0.56
JCMTLYS J072718.55-104732	-133.37	2.92	07:27:18.55	-10:47:32.0	6.51	0.35	0.02	0.57
JCMTLYS J073124.76-153944.3	-128.61	1.47	07:31:24.76	-15:39:44.3	7.58	0.08	0.01	0.61
JCMTLYS J073051.07-212320.8	-123.66	-1.40	07:30:51.07	-21:23:20.8	6.98	0.09	0.01	0.59
JCMTLYS J072311.50-15933.6	-130.00	-0.03	07:23:11.50	-15:09:33.6	8.79	0.24	0.01	0.66
JCMTLYS J072226.64-202222.7	-125.48	-2.65	07:22:26.64	-20:22:22.7	6.47	0.21	0.01	0.57

Table A.1 continued from previous page

SASSy Name	*l*	*b*	*RA* (2000)	*Dec* (2000)	$Rad_{\rm eff}$ pc	$F_{\rm int}$ Jy	*error* Jy	*Aperture* Correction
JCMTLYS J072124.16-074346.5	-136.76	3.08	07:21:24.16	-07:43:46.5	7.93	0.23	0.01	0.63
JCMTLYS J07226.03-051014.4	-141.21	0.08	07:02:26.03	-05:10:14.4	6.76	0.48	0.03	0.58
JCMTLYS J072836.75-21579.7	-123.41	-2.13	07:28:36.75	-21:57:09.7	12.37	0.24	0.01	0.78
JCMTLYS J07237.60-121315.5	-134.92	-3.10	07:02:37.60	-12:13:15.5	9.78	3.29	0.20	0.70
JCMTLYS J071057.77-151548.5	-131.28	-2.69	07:10:57.77	-15:15:48.5	7.80	0.12	0.01	0.62
JCMTLYS J073531.19-245414.8	-120.06	-2.16	07:35:31.19	-24:54:14.8	6.22	0.09	0.01	0.55
JCMTLYS J074203.53-164356.7	-126.43	3.18	07:42:03.53	-16:43:56.7	6.54	0.62	0.04	0.57
JCMTLYS J075558.44-23951.2	-119.22	2.75	07:55:58.44	-23:09:51.2	7.74	0.22	0.01	0.62
JCMTLYS J071810.86-194435.8	-126.51	-3.24	07:18:10.86	-19:44:35.8	6.50	0.46	0.03	0.57
JCMTLYS J074215.77-164244.2	-126.42	3.23	07:42:15.77	-16:42:44.2	7.49	1.21	0.07	0.61
JCMTLYS J072805.06-105521.4	-133.17	3.02	07:28:05.06	-10:55:21.4	8.23	0.36	0.02	0.64
JCMTLYS J073506.59-222732.1	-122.24	-1.06	07:35:06.59	-22:27:32.1	5.94	0.07	0.00	0.54
JCMTLYS J071956.36-071612.5	-137.34	2.97	07:19:56.36	-07:16:12.5	7.56	0.63	0.04	0.61
JCMTLYS J071745.96-184950	-127.36	-2.90	07:17:45.96	-18:49:50.0	6.54	0.27	0.02	0.57
JCMTLYS J073123.21-144229.9	-129.45	1.92	07:31:23.21	-14:42:29.9	11.26	0.14	0.01	0.75
JCMTLYS J074023.09-25464.4	-118.77	-1.62	07:40:23.09	-25:46:04.4	6.15	0.10	0.01	0.55
JCMTLYS J073618.45-27830.1	-118.01	-3.09	07:36:18.45	-27:08:30.1	6.98	0.22	0.01	0.59

Table A.1 continued from previous page

SASSy Name	*l*	*b*	*RA* (2000)	*Dec* (2000)	$Rad_{\rm eff}$ pc	$F_{\rm int}$ Jy	*error* Jy	*Aperture* Correction
JCMTLYS J07619.66-061137.7	-139.86	0.47	07:06:19.66	-06:11:37.7	6.10	0.11	0.01	0.55
JCMTLYS J073434.69-223529.3	-122.18	-1.23	07:34:34.69	-22:35:29.3	6.73	0.10	0.01	0.58
JCMTLYS J075325.02-255442.4	-117.16	0.84	07:53:25.02	-25:54:42.4	8.17	0.28	0.02	0.64
JCMTLYS J073737.12-261943	-118.58	-2.44	07:37:37.12	-26:19:43.0	5.53	0.09	0.01	0.52
JCMTLYS J07733.91-143943.6	-132.20	-3.15	07:07:33.91	-14:39:43.6	7.82	0.46	0.03	0.62
JCMTLYS J07333.67-123549.5	-134.48	-3.07	07:03:33.67	-12:35:49.5	7.31	0.13	0.01	0.60
JCMTLYS J065417.11-081449.3	-139.40	-3.12	06:54:17.11	-08:14:49.3	6.73	0.29	0.02	0.58
JCMTLYS J073442.73-245713.1	-120.10	-2.35	07:34:42.73	-24:57:13.1	5.61	0.07	0.00	0.53
JCMTLYS J075515.20-26112	-116.86	1.13	07:55:15.20	-26:01:12.0	8.01	0.49	0.03	0.63
JCMTLYS J072616.57-093214	-134.60	3.29	07:26:16.57	-09:32:14.0	7.15	0.47	0.03	0.60
JCMTLYS J071441.84-051537	-139.73	2.75	07:14:41.84	-05:15:37.0	7.18	0.21	0.01	0.60
JCMTLYS J072610.47-105456	-133.40	2.61	07:26:10.47	-10:54:56.0	8.24	0.25	0.02	0.64
JCMTLYS J073348.85-131031	-130.51	3.17	07:33:48.85	-13:10:31.0	6.66	0.29	0.02	0.57
JCMTLYS J07024.12-085140.2	-138.16	-2.05	07:00:24.12	-08:51:40.2	6.95	0.09	0.01	0.59
JCMTLYS J072428.11-09185.8	-135.02	3.01	07:24:28.11	-09:18:05.8	6.95	0.22	0.01	0.59
JCMTLYS J072040.97-125828.4	-132.21	0.46	07:20:40.97	-12:58:28.4	6.91	0.07	0.00	0.59
JCMTLYS J072756.13-20407.2	-124.61	-1.66	07:27:56.13	-20:40:07.2	10.81	0.18	0.01	0.73

Table A.1 continued from previous page

SASSy Name	*l*	*b*	*RA* (2000)	*Dec* (2000)	$Rad_{\rm eff}$ pc	$F_{\rm int}$ Jy	*error* Jy	*Aperture* Correction
JCMTLYS J07915.01-102714.8	-135.75	-0.85	07:09:15.01	-10:27:14.8	7.35	0.11	0.01	0.60
JCMTLYS J074029.77-16204	-126.96	3.05	07:40:29.77	-16:20:04.0	6.56	0.22	0.01	0.57
JCMTLYS J072219.34-20585.9	-124.97	-2.95	07:22:19.34	-20:58:05.9	6.03	0.17	0.01	0.55
JCMTLYS J071719.94-14329.9	-131.21	-0.99	07:17:19.94	-14:32:09.9	6.67	0.05	0.00	0.57
JCMTLYS J071657.22-094011.1	-135.56	1.20	07:16:57.22	-09:40:11.1	6.75	0.08	0.01	0.58
JCMTLYS J071813.85-10655.5	-135.02	1.27	07:18:13.85	-10:06:55.5	6.08	0.06	0.00	0.55
JCMTLYS J074328.42-172242.7	-125.70	3.15	07:43:28.42	-17:22:42.7	7.09	0.74	0.04	0.59
JCMTLYS J07810.80-12283.2	-134.08	-2.01	07:08:10.80	-12:28:03.2	8.39	0.09	0.01	0.65
JCMTLYS J072711.14-121453.5	-132.10	2.20	07:27:11.14	-12:14:53.5	6.70	0.10	0.01	0.58
JCMTLYS J071022.68-092034.8	-136.60	-0.09	07:10:22.68	-09:20:34.8	6.76	0.06	0.00	0.58
JCMTLYS J07537.52-105052.2	-135.81	-1.82	07:05:37.52	-10:50:52.2	6.94	0.08	0.00	0.59
JCMTLYS J072759.62-214318.6	-123.68	-2.15	07:27:59.62	-21:43:18.6	6.98	0.10	0.01	0.59
JCMTLYS J072853.38-215151.2	-123.46	-2.03	07:28:53.38	-21:51:51.2	8.46	0.08	0.01	0.65
JCMTLYS J071844.95-1253.2	-133.22	0.46	07:18:44.95	-12:05:03.2	7.32	0.07	0.00	0.60
JCMTLYS J072108.72-10717.8	-134.68	1.90	07:21:08.72	-10:07:17.8	7.35	0.14	0.01	0.60
JCMTLYS J071711.58-18384.4	-127.60	-2.93	07:17:11.58	-18:38:04.4	6.75	0.39	0.02	0.58
JCMTLYS J073300.60-16469.2	-127.46	1.27	07:33:00.60	-16:46:09.2	6.57	0.06	0.00	0.57

Table A.1 continued from previous page

SASSy Name	*l*	*b*	*RA* (2000)	*Dec* (2000)	$Rad_{\rm eff}$ pc	$F_{\rm int}$ Jy	*error* Jy	*Aperture* Correction
JCMTLYS J074002.98-23829	-121.09	-0.40	07:40:02.98	-23:08:29.0	5.67	0.10	0.01	0.53
JCMTLYS J073847.63-251838.9	-119.34	-1.71	07:38:47.63	-25:18:38.9	7.09	0.09	0.01	0.59
JCMTLYS J073631.85-265756	-118.14	-2.96	07:36:31.85	-26:57:56.0	6.29	0.14	0.01	0.56
JCMTLYS J07642.41-112111.3	-135.23	-1.81	07:06:42.41	-11:21:11.3	7.89	0.10	0.01	0.63
JCMTLYS J075558.91-244331.9	-117.88	1.95	07:55:58.91	-24:43:31.9	5.72	0.07	0.00	0.53
JCMTLYS J073712.82-18915.8	-125.76	1.47	07:37:12.82	-18:09:15.8	6.71	0.08	0.00	0.58
JCMTLYS J07004.82-062324.5	-140.40	-1.00	07:00:04.82	-06:23:24.5	6.75	0.11	0.01	0.58
JCMTLYS J074924.40-234217.3	-119.53	1.18	07:49:24.40	-23:42:17.3	6.40	0.10	0.01	0.56
JCMTLYS J074550.92-27714.5	-116.98	-1.24	07:45:50.92	-27:07:14.5	7.71	0.33	0.02	0.62
JCMTLYS J072230.73-213055.7	-124.47	-3.17	07:22:30.73	-21:30:55.7	8.65	0.39	0.02	0.66
JCMTLYS J073455.91-203253.9	-123.93	-0.16	07:34:55.91	-20:32:53.9	6.43	0.10	0.01	0.56
JCMTLYS J071750.88-185229.4	-127.32	-2.91	07:17:50.88	-18:52:29.4	6.54	0.41	0.02	0.57
JCMTLYS J07637.69-132656.7	-133.38	-2.79	07:06:37.69	-13:26:56.7	8.03	0.30	0.02	0.63
JCMTLYS J071851.15-182224.2	-127.65	-2.46	07:18:51.15	-18:22:24.2	8.51	0.13	0.01	0.65
JCMTLYS J074211.67-165815	-126.21	3.09	07:42:11.67	-16:58:15.0	8.94	0.19	0.01	0.67
JCMTLYS J073443.76-193756.1	-124.76	0.24	07:34:43.76	-19:37:56.1	6.47	0.11	0.01	0.57
JCMTLYS J073551.00-235025.2	-120.95	-1.58	07:35:51.00	-23:50:25.2	6.27	0.10	0.01	0.56

Table A.1 continued from previous page

SASSy Name	*l*	*b*	*RA* (2000)	*Dec* (2000)	$Rad_{\rm eff}$ pc	$F_{\rm int}$ Jy	*error* Jy	*Aperture* Correction
JCMTLYS J072426.75-143546.3	-130.35	0.50	07:24:26.75	-14:35:46.3	6.00	0.10	0.01	0.54
JCMTLYS J08116.07-243534.7	-117.37	3.04	08:01:16.07	-24:35:34.7	6.97	0.31	0.02	0.59
JCMTLYS J08124.75-243247	-117.39	3.09	08:01:24.75	-24:32:47.0	6.08	0.29	0.02	0.55
JCMTLYS J065724.06-09518.1	-138.30	-2.82	06:57:24.06	-09:05:18.1	7.15	0.10	0.01	0.60
JCMTLYS J07429.38-101430.1	-136.47	-1.79	07:04:29.38	-10:14:30.1	10.39	0.17	0.01	0.72
JCMTLYS J07302.23-103548.4	-136.32	-2.27	07:03:02.23	-10:35:48.4	6.74	0.08	0.00	0.58
JCMTLYS J073228.68-133953.2	-130.24	2.65	07:32:28.68	-13:39:53.2	10.79	0.19	0.01	0.73
JCMTLYS J072216.05-081313.9	-136.23	3.03	07:22:16.05	-08:13:13.9	9.56	0.28	0.02	0.69
JCMTLYS J071047.43-13437.3	-133.24	-1.72	07:10:47.43	-13:04:37.3	7.31	0.06	0.00	0.60
JCMTLYS J071402.14-164954.9	-129.55	-2.76	07:14:02.14	-16:49:54.9	6.81	0.22	0.01	0.58
JCMTLYS J071443.95-151644.1	-130.85	-1.89	07:14:43.95	-15:16:44.1	6.00	0.07	0.00	0.54
JCMTLYS J073659.02-233149.6	-121.10	-1.20	07:36:59.02	-23:31:49.6	5.67	0.07	0.00	0.53
JCMTLYS J075349.04-223529.1	-119.97	2.62	07:53:49.04	-22:35:29.1	6.04	0.09	0.01	0.55
JCMTLYS J07403.87-112047.6	-135.54	-2.39	07:04:03.87	-11:20:47.6	11.03	0.14	0.01	0.74
JCMTLYS J07039.33-11752.3	-136.11	-3.03	07:00:39.33	-11:07:52.3	11.28	1.16	0.07	0.75

Appendix B

Clump Properties

Derived clump properties of the host molecular clumps. The first column gives Submillimetre Name (*AGAL* for ATLASGAL objects; *JCMTLSY* for SASSy) with superscripts denoting publication clump source was adopted from: [1]Urquhart et al. 2013b; [2]Urquhart et al. 2014d; [3]Thompson et. al. in prep. The remaining columns include: Complex that clump belongs to (if any); H II Region Density; Radial Velocity; Heliocentric Distance; Galactocentric Radius; Flag denoting source of adopted distance information ([1]Urquhart et al. 2018; [2]Urquhart et al. 2013b; [3]Urquhart et al. 2014d; [4]Adopted from RMS database); Effective Radius of clump; Peak and Integrated submillimetre fluxes; Gas-to-dust Ratio Value with Giannetti et al. 2015 correction; Column Density; Corrected Column Density; Clump Mass; Corrected Clump Mass. All log values are base 10. This table will also be available in electronic machine readable form at CDS.

Submm Name	*Complex*	*HII*	v_{lsr} [km s^{-1}]	*D* [kpc]	R_{GC} [kpc]	*Flag*	*Radius* [pc]	*Peak Flux* [Jy beam^{-1}]	*Int Flux* [Jy]	*R*	*Log* N_{H_2} [cm^{-2}]	*Log* N_{H_2} (corr) [cm^{-2}]	*Log M* [M$_\odot$]	*Log M (corr)* [M$_\odot$]
[1]AGAL010.299−00.147	W31-North	1	12.8	3.5	4.9	1	2.77	7.67	54.18	73.5	19.13	19	3.38	3.25
[1]AGAL010.321−00.257	W31-South	1	32.2	3	5.4	1	2.48	2.39	14.93	81.25	18.62	18.53	2.69	2.6
[1]AGAL010.472+00.027	–	2	66.7	8.5	1.6	1	5.54	35.01	88.12	37.95	19.79	19.37	4.36	3.94
[1]AGAL010.624−00.384	W31-North	4	-2.5	5	3.6	1	3.84	33.1	116.87	56.65	19.76	19.52	4.03	3.78
[1]AGAL010.957+00.022	–	1	21.4	2.9	5.5	1	1.42	3.03	13.55	82.89	18.73	18.64	2.62	2.54
[1]AGAL010.964+00.011	–	1	19.2	2.9	5.5	1	0.51	1.33	5.4	82.89	18.37	18.29	2.22	2.14
[1]AGAL011.031+00.026	–	1	18.1	2.9	5.5	1	0.34	0.47	1.39	82.89	17.92	17.84	1.63	1.55
[1]AGAL011.034+00.061	–	1	15.4	2.9	5.5	1	0.81	1.77	6.05	82.89	18.49	18.41	2.27	2.19
[1]AGAL011.109−00.397	W31-North	1	-1.1	5	3.6	1	4.3	3.53	42.04	56.65	18.79	18.55	3.58	3.33
[1]AGAL011.902−00.141	–	2	38.4	3.1	5.4	1	1.8	3.17	20.03	81.25	18.75	18.66	2.84	2.75
[1]AGAL011.936−00.616	–	1	37	3.4	5.1	1	2.1	7.22	45.64	76.51	19.1	18.99	3.28	3.17
[1]AGAL011.946−00.036	–	1	39.1	3.1	5.4	1	1.15	1.75	7.62	81.25	18.49	18.4	2.42	2.33
[1]AGAL012.198−00.034	–	1	50.7	11.9	4.1	1	3.18	2.92	7.42	62.62	18.71	18.51	3.58	3.38
[1]AGAL012.208−00.102	–	1	24.5	13.4	5.5	1	6.55	11.58	37.39	82.89	19.31	19.23	4.39	4.31
[2]AGAL012.418+00.506	–	1	18	1.8	6.6	1	1.03	7.26	32.69	103.32	19.11	19.12	2.59	2.6
[1]AGAL012.431−00.049	–	1	21.1	2.6	5.9	1	0.64	0.72	5.71	89.8	18.1	18.06	2.15	2.1
[1]AGAL012.431−01.114	–	1	39.8	3	5.4	1	1.08	4.28	14.73	81.25	18.88	18.79	2.68	2.59
[1]AGAL012.804−00.199	W33	2	35.4	2.6	5.9	1	3.09	36.48	339.23	89.8	19.81	19.76	3.92	3.87
[1]AGAL012.998−00.357	–	1	14.4	1.3	7.1	1	0.48	2.29	9.86	114.21	18.6	18.66	1.78	1.84
[1]AGAL013.209−00.144	–	1	51.1	2.6	5.9	1	1.63	3.09	30.64	89.8	18.73	18.69	2.88	2.83
[1]AGAL013.384+00.064	–	1	15.6	1.9	6.5	1	0.62	1.11	5.45	101.27	18.29	18.3	1.85	1.86
[1]AGAL013.872+00.281	–	1	48.5	3.9	4.6	1	2.36	5.52	29.72	69.21	18.99	18.83	3.22	3.06
[1]AGAL014.246−00.071	–	1	60.2	10.6	3.2	1	4.56	2.98	11.43	52.29	18.72	18.44	3.67	3.39
[1]AGAL014.607+00.012	–	1	25.1	2.5	6	1	1.25	2.74	16.62	91.62	18.68	18.64	2.58	2.54
[1]AGAL014.777−00.334	–	1	33.2	3.1	5.4	1	0.65	0.95	4.02	81.25	18.22	18.13	2.15	2.06
[1]AGAL016.144+00.009	–	1	44.8	12.3	4.9	1	2.58	0.99	2.51	73.5	18.24	18.11	3.14	3.01

Table B.1 continued from previous page

Submm Name	*Complex*	*HII*	$v_{\rm lsr}$ [km s^{-1}]	*D* [kpc]	$R_{\rm GC}$ [kpc]	*Flag*	*Radius* [pc]	*Peak Flux* [Jy beam^{-1}]	*Int Flux* [Jy]	*R*	*Log* N_{H_2} [cm^{-2}]	*Log* N_{H_2} (corr) [cm^{-2}]	*Log M* [M$_\odot$]	*Log M (corr)* [M$_\odot$]
[1]AGAL016.942−00.072	–	1	-3.3	15.9	8.3	1	4.62	1.43	6.94	145.24	18.4	18.56	3.8	3.97
[1]AGAL017.029−00.071	–	1	93.2	10.1	3.2	1	2.12	1.27	3.42	52.29	18.35	18.07	3.1	2.82
[1]AGAL017.112−00.114	–	1	93.1	10.1	3.2	1	1.18	0.62	1.82	52.29	18.04	17.76	2.83	2.55
[1]AGAL017.554+00.167	–	1	20.6	1.9	6.6	1	0.4	0.52	2.38	103.32	17.96	17.98	1.49	1.51
[1]AGAL017.986+00.126	–	1	19.2	1.8	6.6	1	0.21	0.42	1.27	103.32	17.87	17.88	1.17	1.19
[1]AGAL018.148−00.284	–	1	56.8	3.4	5.2	1	1.31	3.38	18.71	78.05	18.77	18.67	2.9	2.79
[1]AGAL018.301−00.389	–	1	32.3	3.2	5.4	1	1.94	4.19	28.31	81.25	18.87	18.78	3.02	2.93
[1]AGAL018.444−00.004	–	1	53.5	11.8	4.7	1	4.81	1.45	9.18	70.62	18.41	18.26	3.67	3.52
[1]AGAL018.461−00.002	–	1	52.4	11.8	4.7	1	6.86	3.68	20.38	70.62	18.81	18.66	4.01	3.86
[1]AGAL018.666+00.026	–	1	77.7	10.1	3.5	1	1.18	1.57	4.29	55.53	18.44	18.19	3.2	2.95
[1]AGAL018.711+00.001	–	1	28.3	2.4	6.1	1	0.81	1.08	6.34	93.48	18.28	18.25	2.12	2.09
[1]AGAL018.761+00.261	–	1	20.8	14.1	6.8	1	6.4	1.27	10.44	107.55	18.35	18.38	3.88	3.91
[2]AGAL018.823−00.486	–	1	65.2	5	4	1	4.83	2.26	52.57	61.38	18.6	18.39	3.68	3.47
[1]AGAL018.824−00.467	–	1	63	5	4	1	0.58	1.58	2.65	61.38	18.44	18.23	2.38	2.17
[1]AGAL018.833−00.301	–	1	39.5	12.7	5.5	1	4.88	1.31	7.99	82.89	18.36	18.28	3.67	3.59
[1]AGAL019.003+00.129	–	1	68	5	4	1	1.28	1.29	4.15	61.38	18.36	18.14	2.58	2.36
[1]AGAL019.076−00.287	–	2	66	5	4	1	4.3	5.03	41.64	61.38	18.95	18.73	3.58	3.37
[1]AGAL019.472+00.171	–	1	20	14.1	6.8	1	10.34	6.47	29.96	107.55	19.06	19.09	4.34	4.37
[2]AGAL019.508−00.447	–	1	63.2	5	4	1	1.98	0.48	4.06	61.38	17.93	17.71	2.57	2.35
[1]AGAL019.609−00.234	–	2	40.8	12.6	5.5	1	6.6	19.2	44.85	82.89	19.53	19.45	4.41	4.33
[1]AGAL019.726−00.114	–	1	60.2	5.1	3.9	1	1.36	1.09	7.61	60.16	18.28	18.06	2.86	2.64
[1]AGAL019.754−00.129	–	1	120.6	7.8	2.8	1	2.72	1.87	11.23	48.26	18.52	18.2	3.39	3.08
[1]AGAL020.081−00.136	–	3	41.1	12.6	5.5	1	5.28	7.68	18.43	82.89	19.13	19.05	4.03	3.94
[1]AGAL020.362−00.012	–	1	52.2	3.4	5.3	1	0.87	1.95	4.84	79.63	18.53	18.44	2.31	2.21
[1]AGAL020.761−00.062	–	1	57	11.7	4.9	1	2.86	1.42	4.19	73.5	18.4	18.26	3.32	3.18
[1]AGAL020.962−00.074	–	1	30.9	12.8	5.8	1	1.49	0.42	1.4	88.02	17.87	17.81	2.92	2.87

Table B.1 continued from previous page

Submm Name	*Complex*	*HII*	v_{lsr} [km s^{-1}]	*D* [kpc]	R_{GC} [kpc]	*Flag*	*Radius* [pc]	*Peak Flux* [Jy beam^{-1}]	*Int Flux* [Jy]	*R*	*Log* N_{H_2} [cm^{-2}]	*Log* N_{H_2} (corr) [cm^{-2}]	*Log M* [M$_\odot$]	*Log M (corr)* [M$_\odot$]
[1]AGAL021.356−00.176	–	1	91.2	10	3.8	1	1.86	0.87	3.57	58.97	18.18	17.95	3.11	2.88
[1]AGAL021.386−00.254	–	1	91	10	3.8	1	3.72	2.6	9.28	58.97	18.66	18.43	3.53	3.3
[1]AGAL021.598−00.161	–	1	-2.1	15.7	8.5	1	1.83	0.38	1.8	151.18	17.82	18	3.21	3.39
[1]AGAL021.873+00.007	–	1	22.4	13.9	6.9	1	6.31	1.61	8.92	109.72	18.45	18.49	3.8	3.84
[2]AGAL022.756−00.482	–	1	77	4.6	4.5	1	0.54	0.43	1.93	67.84	17.88	17.71	2.17	2
[1]AGAL023.199+00.001	–	1	76.2	5.9	3.8	1	2.61	2.71	17.8	58.97	18.68	18.45	3.35	3.12
[1]AGAL023.264+00.077	–	1	77.6	5.9	3.8	1	1.85	2.98	8.8	58.97	18.72	18.49	3.05	2.82
[1]AGAL023.454−00.201	–	1	101	5.9	3.8	1	0.55	1.25	3.38	58.97	18.34	18.11	2.63	2.4
[1]AGAL023.482+00.097	–	1	85.4	5.9	3.8	1	2.81	2.02	12.4	58.97	18.55	18.32	3.2	2.97
[1]AGAL023.711+00.171	–	1	113	6.1	3.7	1	5.11	3.13	33.46	57.8	18.74	18.5	3.66	3.42
[1]AGAL023.866−00.122	–	1	75.6	6.2	3.7	1	4.26	1.9	26.29	57.8	18.52	18.29	3.56	3.33
[1]AGAL023.897+00.064	–	1	39.2	12.4	5.8	1	3.75	1.84	9.1	88.02	18.51	18.45	3.71	3.65
[1]AGAL023.954+00.151	–	1	80.7	4.8	4.4	1	4.64	2.8	36.11	66.5	18.69	18.51	3.48	3.3
[1]AGAL024.183+00.121	–	1	113.5	7.8	3.4	1	2.72	1.51	5.69	54.43	18.42	18.16	3.1	2.84
[1]AGAL024.491−00.039	–	1	109.7	6	3.8	1	3.77	6.39	30.26	58.97	19.05	18.82	3.6	3.37
[1]AGAL024.506−00.221	–	1	99	5.8	3.9	1	3.98	1.93	17.55	60.16	18.53	18.31	3.33	3.11
[1]AGAL024.789+00.082	–	2	110.2	6	3.8	1	2.93	15.52	56.56	58.97	19.44	19.21	3.87	3.64
[2]AGAL025.303+00.531	–	1	12.4	1.7	6.8	1	0.2	0.49	1.4	107.55	17.94	17.97	1.17	1.2
[1]AGAL025.382−00.182	W42	2	64.3	2.7	6	1	1.7	3.35	30.35	91.62	18.77	18.73	2.9	2.87
[1]AGAL025.392+00.034	–	1	-13	15.6	8.8	1	6.53	1.88	11.95	160.55	18.52	18.72	4.02	4.23
[1]AGAL025.396+00.562	–	2	15.9	13.9	7.3	1	5.34	2.48	10.93	118.88	18.64	18.71	3.88	3.96
[1]AGAL025.398−00.141	–	2	94.9	10.2	4.5	1	6.17	4.45	36.66	67.84	18.89	18.72	4.14	3.97
[1]AGAL025.709+00.044	–	1	99.2	10.2	4.5	1	3.32	1.98	8.85	67.84	18.54	18.37	3.52	3.36
[1]AGAL025.801−00.156	–	1	94.2	10.2	4.5	1	3.2	1.81	6.62	67.84	18.5	18.33	3.4	3.23
[1]AGAL026.089−00.056	–	1	28	13.5	7	1	3.46	1.23	5.64	111.94	18.33	18.38	3.57	3.62
[1]AGAL026.107−00.094	–	1	25.2	13.5	7	1	1.57	0.74	1.11	111.94	18.11	18.16	2.87	2.92

Table B.1 continued from previous page

Submm Name	*Complex*	*HII*	v_{lsr} [km s^{-1}]	*D* [kpc]	R_{GC} [kpc]	*Flag*	*Radius* [pc]	*Peak Flux* [Jy beam^{-1}]	*Int Flux* [Jy]	*R*	*Log* N_{H_2} [cm^{-2}]	*Log* N_{H_2} (corr) [cm^{-2}]	*Log M* [M$_\odot$]	*Log M (corr)* [M$_\odot$]
[1]AGAL026.546+00.416	–	1	86.1	9.9	4.4	1	4.26	1.38	8.91	66.5	18.38	18.21	3.5	3.32
[2]AGAL026.546+00.416	–	1	86.1	9.9	4.4	1	4.26	1.38	8.91	66.5	18.38	18.21	3.5	3.32
[1]AGAL026.596−00.022	–	1	22.9	1.8	6.8	1	0.4	1.43	5.24	107.55	18.4	18.43	1.79	1.82
[1]AGAL026.607−00.212	–	1	108.2	7.6	3.7	1	0.88	0.86	1.69	57.8	18.18	17.94	2.55	2.31
[1]AGAL027.184−00.081	–	1	25.6	13.4	7.1	1	4.68	3.07	9.69	114.21	18.73	18.79	3.8	3.86
[1]AGAL027.279+00.147	–	1	28.1	13.4	7.1	1	2.18	1.91	5.7	114.21	18.53	18.58	3.57	3.63
[1]AGAL027.366−00.166	–	1	91.2	8	3.9	1	3.72	10.93	30.69	60.16	19.28	19.06	3.85	3.63
[1]AGAL027.564+00.086	–	1	84.2	9.7	4.5	1	5.19	2.19	14.5	67.84	18.59	18.42	3.7	3.53
[1]AGAL027.936+00.206	–	1	41.7	2.7	6.1	1	0.82	1.53	7.48	93.48	18.43	18.4	2.3	2.27
[1]AGAL027.978+00.077	–	1	74.9	4.5	4.9	1	1.99	1.46	9.49	73.5	18.41	18.28	2.84	2.71
[1]AGAL028.199−00.049	–	2	95.9	6.1	4.2	1	3.26	9.49	35.49	63.89	19.22	19.03	3.68	3.49
[1]AGAL028.288−00.362	–	1	48.8	11.6	5.8	1	7.69	2.74	25.73	88.02	18.68	18.63	4.1	4.04
[1]AGAL028.451+00.002	–	1	-12.9	15.4	9	1	5.2	0.93	6.02	167.11	18.21	18.44	3.71	3.94
[1]AGAL028.581+00.146	–	1	-13.9	15.4	9	1	1.79	0.63	1.86	167.11	18.04	18.27	3.2	3.43
[1]AGAL028.608+00.019	–	1	101.2	7.4	4	1	4.48	2.93	20.21	61.38	18.71	18.5	3.6	3.39
[1]AGAL028.649+00.027	–	1	103.6	7.4	4	1	2.84	3.1	13.53	61.38	18.74	18.52	3.43	3.22
[1]AGAL028.687+00.177	–	1	83.9	9.7	4.7	1	0.9	0.71	1.85	70.62	18.1	17.95	2.8	2.65
[1]AGAL029.954−00.016	–	1	97.2	5.2	4.7	1	3.57	12.01	57.01	70.62	19.32	19.17	3.75	3.6
[1]AGAL030.008−00.272	–	1	101.8	5.2	4.7	1	2.36	2.46	17.12	70.62	18.64	18.48	3.23	3.07
[1]AGAL030.251+00.054	–	1	70.9	5.2	4.7	1	2.9	1.07	7.66	70.62	18.27	18.12	2.88	2.73
[1]AGAL030.534+00.021	–	2	48	2.7	6.2	1	1.29	2.24	9.78	95.37	18.6	18.57	2.41	2.39
[1]AGAL030.588−00.042	–	1	41.7	2.7	6.2	1	1.73	4.46	25.61	95.37	18.89	18.87	2.83	2.81
[1]AGAL030.718−00.082	W43	1	93.9	5.2	4.7	1	2.78	8.33	50.64	70.62	19.17	19.01	3.7	3.55
[1]AGAL030.753−00.051	W43	1	97.7	5.2	4.7	1	2.06	4.96	33.49	70.62	18.94	18.79	3.52	3.37
[1]AGAL030.866+00.114	–	1	39.8	2.7	6.2	1	1.13	3.23	13.16	95.37	18.75	18.73	2.54	2.52
[1]AGAL030.959+00.086	–	1	39.7	2.7	6.2	1	1.19	1.67	8.77	95.37	18.47	18.45	2.37	2.35

Table B.1 continued from previous page

Submm Name	*Complex*	*HII*	v_{lsr} [km s^{-1}]	*D* [kpc]	R_{GC} [kpc]	*Flag*	*Radius* [pc]	*Peak Flux* [Jy beam^{-1}]	*Int Flux* [Jy]	*R*	*Log* N_{H_2} [cm^{-2}]	*Log* N_{H_2} (corr) [cm^{-2}]	*Log M* [M$_\odot$]	*Log M (corr)* [M$_\odot$]
[1]AGAL031.054+00.469	–	1	33.8	2	6.7	1	0.95	1.04	7.43	105.41	18.26	18.28	2.03	2.06
[1]AGAL031.059+00.094	–	1	16.8	13.2	7.4	1	1.08	0.69	1.13	121.28	18.08	18.17	2.85	2.94
[2]AGAL031.071+00.049	–	1	38.9	2.7	6.2	1	0.66	0.74	2.76	95.37	18.11	18.09	1.86	1.84
[1]AGAL031.158+00.047	–	2	39.2	2.7	6.2	1	1.07	1.7	8.87	95.37	18.48	18.45	2.37	2.35
[1]AGAL031.243−00.111	–	2	20.9	12.9	7.2	1	3.3	3.5	8	116.52	18.79	18.86	3.68	3.75
[1]AGAL031.281+00.062	g31.4+0.3	1	109	5.2	4.7	1	3.75	6.86	40.97	70.62	19.08	18.93	3.6	3.45
[1]AGAL031.396−00.257	g31.4+0.3	2	87	5.2	4.7	1	1.63	5.61	12.95	70.62	18.99	18.84	3.1	2.95
[1]AGAL031.412+00.307	g31.4+0.3	1	97.6	5.2	4.7	1	3.45	22.74	61.68	70.62	19.6	19.45	3.78	3.63
[1]AGAL031.581+00.077	g31.4+0.3	1	96.1	5.2	4.7	1	1.57	4.76	12.6	70.62	18.92	18.77	3.09	2.94
[1]AGAL032.149+00.134	g31.4+0.3	1	93.9	5.2	4.8	1	2.96	3.93	25.01	72.04	18.84	18.7	3.39	3.25
[1]AGAL032.272−00.226	–	1	20.2	12.8	7.2	1	2.38	1.04	3.35	116.52	18.26	18.33	3.3	3.37
[1]AGAL032.471+00.204	–	1	49.6	3	6	1	1.29	1.5	9.87	91.62	18.42	18.38	2.51	2.47
[1]AGAL032.739+00.192	–	1	19.1	13	7.5	1	5.9	1.05	8.28	123.74	18.27	18.36	3.71	3.8
[1]AGAL032.744−00.076	–	2	37.2	11.7	6.5	1	4.36	5.37	14.26	101.27	18.97	18.98	3.85	3.86
[1]AGAL032.797+00.191	–	2	14.6	13	7.5	1	5.9	12.25	31.65	123.74	19.33	19.43	4.29	4.38
[1]AGAL032.926+00.606	–	1	-34.1	15.1	9.3	1	1.76	0.85	2.79	177.46	18.17	18.42	3.36	3.61
[1]AGAL033.133−00.092	–	1	76.7	9.4	5.2	1	3.5	4.41	15.27	78.05	18.89	18.78	3.69	3.58
[1]AGAL033.416−00.002	–	1	75.1	5.4	4.9	1	3.27	1.45	15.89	73.5	18.41	18.27	3.23	3.09
[1]AGAL033.811−00.187	–	1	46	10.8	6	1	2.76	1.8	6.46	91.62	18.5	18.46	3.44	3.4
[1]AGAL033.914+00.109	–	1	107.5	6.5	4.7	1	3.78	6.92	31.26	70.62	19.08	18.93	3.68	3.53
[1]AGAL034.089+00.436	–	1	33.3	11.7	6.7	1	2.31	0.52	3.94	105.41	17.96	17.98	3.29	3.31
[1]AGAL034.133+00.471	–	2	35	11.6	6.6	1	4.05	1.54	5.61	103.32	18.43	18.45	3.44	3.45
[1]AGAL034.196−00.592	–	1	58.2	3.6	5.8	1	0.96	1.68	4.98	88.02	18.47	18.41	2.37	2.31
[1]AGAL034.258+00.154	G34.3+0.1	3	57.2	1.6	7.1	1	1.08	55.65	217	114.21	19.99	20.05	3.3	3.36
[1]AGAL034.401+00.226	G34.3+0.1	1	57.4	1.6	7.1	1	0.74	7.34	40.67	114.21	19.11	19.17	2.58	2.64
[1]AGAL034.591+00.242	–	1	-24.1	15	9.4	1	1.75	0.64	1.66	181.05	18.05	18.31	3.13	3.39

Table B.1 continued from previous page

Submm Name	*Complex*	*HII*	v_{lsr} [km s^{-1}]	*D* [kpc]	R_{GC} [kpc]	*Flag*	*Radius* [pc]	*Peak Flux* [Jy beam^{-1}]	*Int Flux* [Jy]	*R*	*Log* N_{H_2} [cm^{-2}]	*Log* N_{H_2} (corr) [cm^{-2}]	*Log M* [M$_\odot$]	*Log M (corr)* [M$_\odot$]
[1]AGAL035.026+00.349	–	1	53.2	2.3	6.6	1	0.91	5.38	17.42	103.32	18.98	18.99	2.52	2.54
[2]AGAL035.197−00.742	–	2	33.9	2.2	6.7	1	3.94	12.35	132.07	105.41	19.34	19.36	3.37	3.39
[1]AGAL035.466+00.141	–	1	74.1	4.7	5.3	1	2.57	4.16	23.2	79.63	18.86	18.77	3.27	3.17
[1]AGAL035.579−00.031	–	1	52.7	10.4	6.1	1	4.84	5.14	18.05	93.48	18.96	18.93	3.85	3.82
[1]AGAL036.406+00.021	–	2	57.8	3.5	5.9	1	0.77	2.38	5.41	89.8	18.62	18.57	2.38	2.33
[2]AGAL036.878−00.474	–	1	61.1	9.9	6	1	2.19	1.13	4.7	91.62	18.3	18.26	3.22	3.19
[2]AGAL036.919+00.482	–	2	-30.3	14.8	9.5	1	1.72	0.74	1.49	184.71	18.11	18.38	3.07	3.34
[1]AGAL037.546−00.112	–	1	51.8	9.7	6	1	3.5	2.5	9.43	91.62	18.64	18.6	3.51	3.47
[1]AGAL037.734−00.112	–	1	46.5	9.7	6	1	3.05	2.95	9.32	91.62	18.71	18.68	3.5	3.47
[2]AGAL037.757+00.561	–	1	13.2	0.9	7.7	1	0.1	0.76	2.34	128.8	18.13	18.24	0.84	0.95
[1]AGAL037.819+00.412	–	2	18	12.3	7.7	1	3.58	2.94	7.57	128.8	18.71	18.82	3.62	3.73
[1]AGAL037.867−00.601	–	1	50.7	10	6.2	2	1	1.67	5.05	95.37	18.47	18.45	3.26	3.24
[1]AGAL037.874−00.399	–	1	60.8	9.7	6	1	4.4	5.37	18.45	91.62	18.97	18.94	3.8	3.76
[1]AGAL038.646−00.226	–	1	69.2	4.7	5.7	2	0.53	0.84	2.86	86.28	18.17	18.11	2.36	2.3
[1]AGAL038.652+00.087	–	1	-36.5	14.6	9.6	1	2.38	0.77	3.62	188.45	18.13	18.41	3.45	3.72
[1]AGAL038.694−00.452	–	2	50.9	9.8	6.2	1	1.94	1.8	4.51	95.37	18.5	18.48	3.2	3.18
[1]AGAL038.876+00.309	–	1	-16.2	14.2	9.4	1	4.46	0.99	3.82	181.05	18.24	18.5	3.45	3.7
[1]AGAL039.196+00.226	–	1	-26.5	14.5	9.6	1	1.69	0.59	1.52	188.45	18.02	18.29	3.06	3.34
[1]AGAL039.884−00.346	–	1	58.5	9.3	6.1	1	2.81	1.79	7.05	93.48	18.5	18.47	3.35	3.32
[1]AGAL040.424+00.699	–	1	12.7	11.9	7.7	1	4.29	1.51	7.81	128.8	18.42	18.53	3.6	3.71
[1]AGAL041.741+00.097	–	1	13.2	11.7	7.8	1	2.04	1.12	3.25	131.4	18.29	18.41	3.21	3.33
[1]AGAL042.108−00.447	–	1	55.1	3.4	6.3	1	1.15	1.16	6	97.3	18.31	18.3	2.4	2.39
[1]AGAL042.434−00.261	–	1	65.3	4.4	5.9	1	1.02	1.55	8.97	89.8	18.44	18.39	2.8	2.75
[1]AGAL043.148+00.014	W49	5	10.2	11.1	7.6	1	5.55	5.76	48.87	126.24	19.01	19.11	4.34	4.44
[1]AGAL043.164−00.029	W49	2	14.3	11.1	7.6	1	7.49	13.51	86.15	126.24	19.38	19.48	4.59	4.69
[1]AGAL043.166+00.011	W49	13	2.9	11.1	7.6	1	10.2	62.19	319.98	126.24	20.04	20.14	5.16	5.26

Table B.1 continued from previous page

Submm Name	*Complex*	*HII*	v_{lsr} [km s^{-1}]	*D* [kpc]	R_{GC} [kpc]	*Flag*	*Radius* [pc]	*Peak Flux* [Jy beam^{-1}]	*Int Flux* [Jy]	*R*	*Log* N_{H_2} [cm^{-2}]	*Log* N_{H_2} (corr) [cm^{-2}]	*Log M* [M$_\odot$]	*Log M (corr)* [M$_\odot$]
[1]AGAL043.179−00.519	–	1	58	8.5	6.2	1	4.85	4.15	21.36	95.37	18.86	18.84	3.75	3.73
[1]AGAL043.236−00.047	–	1	8.2	11.1	7.6	1	5.29	4.46	18.83	126.24	18.89	19	3.93	4.03
[1]AGAL043.306−00.212	–	2	59.6	4.2	6	1	1.08	3.57	7.95	91.62	18.8	18.76	2.71	2.67
[1]AGAL043.794−00.127	–	2	43.7	6	5.8	1	1.54	6.36	13.83	88.02	19.05	18.99	3.26	3.2
[1]AGAL043.889−00.786	G43.89-0.81	1	54	4.4	6	1	2.82	3.73	26.45	91.62	18.82	18.78	3.27	3.23
[1]AGAL043.967+00.994	–	1	-19.7	13.6	9.5	1	1.58	0.65	1.29	184.71	18.06	18.32	2.94	3.2
[1]AGAL044.309+00.041	–	1	56.3	8.1	6.2	1	3.58	2.51	12.23	95.37	18.64	18.62	3.46	3.44
[1]AGAL044.422+00.537	–	1	-51.5	13.8	9.8	1	1.61	0.61	2.09	196.16	18.03	18.32	3.16	3.45
[1]AGAL045.071+00.132	G45.14+0.14	2	59.2	8	6.3	1	3.26	7	20.13	97.3	19.09	19.08	3.67	3.66
[1]AGAL045.121+00.131	G45.14+0.14	2	58.7	8	6.3	1	5.49	7.58	42.78	97.3	19.12	19.11	4	3.99
[1]AGAL045.454+00.061	–	5	59	8.4	6.5	1	6.06	3.9	35.12	101.27	18.84	18.84	3.95	3.96
[1]AGAL045.466+00.046	–	1	62.1	8.4	6.5	1	4.98	5.49	30.79	101.27	18.98	18.99	3.9	3.9
[1]AGAL048.606+00.022	G48.61+0.02	4	17.5	10.8	8.2	1	6.28	4.36	26.25	142.36	18.88	19.04	4.05	4.2
[2]AGAL048.634+00.231	–	1	7.3	10.8	8.2	1	3.14	1.04	6.57	142.36	18.26	18.42	3.44	3.6
[2]AGAL048.919−00.277	–	5	68.6	5.3	6.3	1	4.93	2.84	55.61	97.3	18.7	18.69	3.75	3.74
[1]AGAL048.931−00.281	W51	3	68.9	5.3	6.3	1	1.17	2.17	8.36	97.3	18.58	18.57	2.93	2.92
[2]AGAL048.953−00.286	–	1	71	5.3	6.3	1	2.84	2.11	17.69	97.3	18.57	18.56	3.26	3.24
[1]AGAL048.991−00.299	W51	1	67.4	5.3	6.3	1	5.67	6.61	76.7	97.3	19.07	19.05	3.89	3.88
[1]AGAL049.268−00.337	W51	1	67.8	5.3	6.3	1	3.27	4.83	32.27	97.3	18.93	18.92	3.52	3.51
[1]AGAL049.369−00.301	W51	2	50.6	5.3	6.3	1	4.93	8.62	82.82	97.3	19.18	19.17	3.93	3.91
[2]AGAL049.472−00.367	–	1	67.5	5.3	6.3	1	5.12	18.59	253.2	97.3	19.51	19.5	4.41	4.4
[1]AGAL049.489−00.369	W51	1	60.1	5.3	6.3	1	2.84	41.67	184.76	97.3	19.86	19.85	4.28	4.26
[2]AGAL049.489−00.389	–	2	57.9	5.3	6.3	1	3.39	79.14	313.69	97.3	20.14	20.13	4.51	4.49
[2]AGAL050.046+00.767	–	1	-29.6	12.8	9.8	1	1.49	0.57	1.15	196.16	18	18.29	2.84	3.13
[1]AGAL050.284−00.391	–	2	16.1	9.6	7.7	1	2.35	2.28	6.07	128.8	18.6	18.71	3.31	3.42
[1]AGAL050.314+00.676	–	1	25.9	1.8	7.3	1	0.44	1.94	6.12	118.88	18.53	18.61	1.86	1.93

Table B.1 continued from previous page

Submm Name	*Complex*	*HII*	v_{lsr} [km s^{-1}]	*D* [kpc]	R_{GC} [kpc]	*Flag*	*Radius* [pc]	*Peak Flux* [Jy beam^{-1}]	*Int Flux* [Jy]	*R*	*Log* N_{H_2} [cm^{-2}]	*Log* N_{H_2} (corr) [cm^{-2}]	*Log M* [M$_\odot$]	*Log M (corr)* [M$_\odot$]
[1]AGAL051.678+00.719	–	1	2.6	10.9	8.7	1	2.66	3.06	7.29	157.36	18.73	18.93	3.5	3.69
[2]AGAL052.201+00.721	–	1	0.5	10.9	8.7	1	2.28	1.24	4.23	157.36	18.34	18.54	3.26	3.46
[1]AGAL052.752+00.334	–	2	15	9.6	8	1	1.68	1.11	3.54	136.77	18.29	18.43	3.07	3.21
[2]AGAL053.037+00.112	–	1	4.4	9.8	8.2	1	2.28	1.84	4.95	142.36	18.51	18.66	3.24	3.39
[2]AGAL053.164−00.246	–	1	61	5.4	6.7	1	1.07	1.63	4.23	105.41	18.46	18.48	2.65	2.67
[2]AGAL053.184+00.209	–	1	1.6	9.8	8.2	1	1.14	0.93	2.77	142.36	18.21	18.37	2.99	3.14
[1]AGAL053.959+00.031	–	1	41.1	4	6.8	1	0.74	1.31	3.47	107.55	18.36	18.39	2.3	2.34
[2]AGAL055.158−00.299	–	2	40.7	3.9	6.9	1	0.91	1.59	7.68	109.72	18.45	18.49	2.63	2.67
[2]AGAL057.548−00.269	–	1	4.3	8.9	8.3	1	1.04	0.89	2.42	145.24	18.19	18.36	2.84	3
[1]AGAL058.774+00.644	–	2	32.1	2.2	7.5	1	0.61	2.03	6.13	123.74	18.55	18.64	2.03	2.12
[1]AGAL059.602+00.912	–	1	36.4	3.5	7.2	1	0.98	2.6	8.19	116.52	18.66	18.73	2.56	2.63
[2]AGAL280.621−01.187	–	1	28.6	7.07	10	3	0.58	0.86	3.76	204.17	18.18	18.49	2.83	3.14
[2]AGAL281.586−00.972	–	1	-2.1	6.97	9.85	3	1.35	4.09	19.55	198.13	18.86	19.15	3.54	3.83
[2]AGAL281.846−01.609	–	1	-7.2	6.97	9.82	3	0.47	2.04	6.3	196.94	18.55	18.85	3.05	3.34
[2]AGAL283.227−00.936	–	1	-8.3	6.97	9.68	3	–	0.89	1.69	191.5	18.19	18.48	2.47	2.76
[2]AGAL284.016−00.857	–	1	8.8	5.71	9.02	3	2.05	7.39	60.36	167.78	19.11	19.34	3.85	4.08
[2]AGAL285.264−00.049	–	1	3.4	–	–	–	–	10.73	33.61	–	19.28	–	–	–
[2]AGAL285.596−00.851	–	1	9.8	6.19	9.07	3	0.45	1.66	5.79	169.47	18.46	18.69	2.91	3.14
[2]AGAL286.394−01.351	–	1	39.3	9.33	10.7	3	1.36	2.75	15.78	234.91	18.68	19.06	3.7	4.07
[2]AGAL289.083−00.411	–	2	–	–	–	–	–	1.53	9.1	–	18.43	–	–	–
[2]AGAL289.881−00.797	–	1	19.1	8.12	9.55	3	0.51	2.73	7.75	186.57	18.68	18.95	3.27	3.54
[2]AGAL290.878−01.217	–	1	15.7	8.01	9.38	3	–	1	2.42	180.33	18.24	18.5	2.75	3.01
[2]AGAL291.066−00.796	–	1	19.7	8.44	9.59	3	1.06	1.41	8.09	188.07	18.39	18.67	3.32	3.6
[2]AGAL293.828−00.746	–	1	32.9	10.33	10.4	3	0.9	3.6	8.91	221.21	18.8	19.15	3.54	3.88
[2]AGAL293.963−00.977	–	1	33	10.37	10.4	3	–	0.76	2.54	221.21	18.13	18.47	3	3.34
[2]AGAL295.153−00.587	–	1	35	10.84	10.56	3	0.79	1.1	14.68	228.41	18.29	18.64	3.8	4.16

Table B.1 continued from previous page

Submm Name	*Complex*	*HII*	v_{lsr} [km s^{-1}]	*D* [kpc]	R_{GC} [kpc]	*Flag*	*Radius* [pc]	*Peak Flux* [Jy beam^{-1}]	*Int Flux* [Jy]	*R*	*Log* N_{H_2} [cm^{-2}]	*Log* N_{H_2} (corr) [cm^{-2}]	*Log M* [M$_\odot$]	*Log M (corr)* [M$_\odot$]
[2]AGAL295.556−01.377	–	1	37.3	11.16	10.72	3	–	0.79	1.86	235.85	18.14	18.52	2.92	3.3
[2]AGAL297.254−00.752	–	1	–	–	–	–	–	0.85	4.29	–	18.17	–	–	–
[2]AGAL297.456−00.762	–	1	28.6	10.76	10.18	3	0.63	1.68	4.15	211.67	18.47	18.8	3.24	3.57
[2]AGAL298.182−00.786	–	1	22.7	10.37	9.83	3	1.46	3.99	14.37	197.34	18.85	19.14	3.75	4.04
[2]AGAL298.224−00.339	–	1	32.8	4.73	7.52	3	1.61	5.8	57.38	124.23	19.01	19.1	3.67	3.76
[2]AGAL298.833+00.126	–	1	21.4	10.41	9.76	3	0.55	1.67	5.7	194.59	18.47	18.76	3.35	3.64
[2]AGAL298.859−00.437	–	1	28.5	11.08	10.2	3	3.54	3.9	36.75	212.52	18.84	19.16	4.21	4.54
[2]AGAL300.969+01.146	–	1	-42.5	3.4	7.2	1	2.37	7.39	47.92	116.52	19.11	19.18	3.3	3.37
[2]AGAL301.136−00.226	–	2	-39.6	4.6	7.2	1	1.98	22.62	58.64	116.52	19.6	19.67	3.65	3.72
[2]AGAL301.731+01.104	–	1	-39.1	3.3	7.2	1	1.54	2.79	22.9	116.52	18.69	18.76	2.96	3.02
[2]AGAL301.814+00.781	–	1	-37.1	3.5	7.2	1	0.9	1.63	8.14	116.52	18.46	18.52	2.56	2.63
[2]AGAL302.021+00.251	–	1	-44.9	4.3	7.1	1	1.2	2.24	7.83	114.21	18.6	18.65	2.72	2.78
[2]AGAL302.149−00.949	–	1	31.4	11.1	9.7	1	1.81	0.94	2.89	192.26	18.22	18.5	3.11	3.4
[2]AGAL302.486−00.031	–	1	-37.1	3.2	7.2	1	0.93	2.07	8.92	116.52	18.56	18.63	2.52	2.59
[2]AGAL303.118−00.972	–	1	26	1.6	7.6	1	0.09	1.45	2.75	126.24	18.41	18.51	1.41	1.51
[2]AGAL303.536−00.597	–	1	18.9	10.5	9.1	1	0.98	0.79	4.07	170.49	18.14	18.37	3.21	3.44
[2]AGAL303.999+00.279	–	1	30.7	11.6	9.8	1	1.35	0.59	1.53	196.16	18.02	18.31	2.87	3.17
[2]AGAL305.196+00.034	–	1	-35.6	3.8	6.9	1	2.48	5.28	41.11	109.72	18.97	19.01	3.33	3.37
[2]AGAL307.736−00.596	–	1	36.7	12.9	10.2	1	1.5	0.74	2.3	212.52	18.11	18.44	3.14	3.47
[2]AGAL308.029−01.052	–	1	41.8	13.4	10.6	1	1.87	1.03	3.08	230.25	18.26	18.62	3.3	3.67
[2]AGAL308.057−00.397	–	1	-12.9	0.9	7.8	1	0.39	3.32	15.61	131.4	18.77	18.88	1.66	1.78
[2]AGAL308.917+00.122	–	1	-49.9	3.9	6.6	1	1.82	2.93	17.32	103.32	18.71	18.73	2.98	2.99
[2]AGAL309.179−00.031	–	2	-16.4	9.4	7.7	1	2.3	1.13	5.23	128.8	18.3	18.41	3.22	3.33
[2]AGAL309.891+00.397	–	1	-57.6	5.5	6.4	1	2.11	1.79	11.17	99.27	18.5	18.49	3.09	3.09
[2]AGAL309.921+00.477	–	1	-56.7	5.5	6.4	1	2.43	7.35	30.45	99.27	19.11	19.11	3.52	3.52
[2]AGAL311.139−00.236	–	1	33.2	13.4	10.1	1	1.56	0.65	3.22	208.31	18.06	18.38	3.32	3.64

Table B.1 continued from previous page

Submm Name	*Complex*	*HII*	v_{lsr} [km s^{-1}]	*D* [kpc]	R_{GC} [kpc]	*Flag*	*Radius* [pc]	*Peak Flux* [Jy beam^{-1}]	*Int Flux* [Jy]	*R*	*Log* N_{H_2} [cm^{-2}]	*Log* N_{H_2} (corr) [cm^{-2}]	*Log M* [M$_\odot$]	*Log M (corr)* [M$_\odot$]
[2]AGAL311.177−00.072	–	1	-38.9	2.7	6.9	1	0.57	1.36	5.27	109.72	18.38	18.42	2.14	2.18
[2]AGAL311.424+00.597	–	1	-48.6	7.4	6.5	1	0.86	0.78	1.2	101.27	18.14	18.14	2.38	2.38
[2]AGAL311.626+00.289	–	1	-48.1	4.1	6.4	1	1.91	7.66	29.09	99.27	19.13	19.13	3.25	3.25
[2]AGAL311.642−00.381	–	1	35.1	13.7	10.3	1	1.59	2.17	6.84	216.82	18.58	18.92	3.67	4
[2]AGAL312.108+00.309	–	1	-47.1	3.4	6.6	1	1.58	3.26	17.95	103.32	18.76	18.77	2.88	2.89
[2]AGAL312.306+00.661	–	1	-10.2	1	7.7	1	0.08	1.1	2.72	128.8	18.29	18.4	0.99	1.1
[2]AGAL312.383−00.416	–	1	-25	9.5	7.3	1	1.11	1.06	4.23	118.88	18.27	18.35	3.14	3.22
[2]AGAL312.546−00.281	–	1	-25.4	9.73	7.42	3	0.9	1.17	5.57	121.77	18.31	18.4	3.28	3.37
[2]AGAL314.219+00.271	–	2	-60.3	4.2	6.2	1	2.35	7.21	38.21	95.37	19.1	19.08	3.39	3.37
[2]AGAL316.139−00.506	–	1	-60.7	7.7	6	1	4.03	3.45	21.68	91.62	18.78	18.74	3.67	3.63
[2]AGAL317.429−00.561	–	1	27.4	14.4	10	1	4.36	2.41	7.83	204.17	18.63	18.94	3.77	4.08
[2]AGAL317.889−00.059	–	1	18.6	13.6	9.3	1	4.11	1.41	6.11	177.46	18.39	18.64	3.61	3.86
[2]AGAL318.724−00.224	–	1	-22.4	11.1	7.3	1	1.29	1.37	2.63	118.88	18.38	18.46	3.07	3.15
[2]AGAL318.914−00.164	–	1	-22.3	11.2	7.3	1	3.52	4.24	14	118.88	18.87	18.95	3.8	3.88
[2]AGAL319.161−00.422	–	1	-16	11.6	7.6	1	6.88	3.81	30.78	126.24	18.83	18.93	4.18	4.28
[2]AGAL319.399−00.012	–	2	-19.2	11.6	7.5	1	3.64	3.51	14.63	123.74	18.79	18.88	3.85	3.95
[2]AGAL319.451−00.022	–	1	-16.7	11.6	7.5	1	1.35	0.95	1.36	123.74	18.22	18.32	2.82	2.92
[2]AGAL320.232−00.284	–	1	-66.3	8.6	5.8	1	3.9	6.8	22.85	88.02	19.08	19.02	3.79	3.73
[2]AGAL320.414+00.116	–	1	-6.3	12.5	8.1	1	6.25	0.97	14.95	139.54	18.23	18.38	3.93	4.07
[2]AGAL320.427+00.102	–	1	-5.9	12.5	8.1	1	4.36	1.99	10.34	139.54	18.54	18.69	3.77	3.91
[2]AGAL320.676+00.244	–	1	-59.5	3.7	6	1	2.02	1.77	15.59	91.62	18.49	18.45	2.89	2.85
[2]AGAL320.779+00.244	–	1	-7.2	12.6	8.1	1	5.57	1.52	11.32	139.54	18.43	18.57	3.81	3.96
[2]AGAL321.126−00.266	–	1	14.4	14	9.2	1	2.28	1.11	2.63	173.94	18.29	18.53	3.27	3.51
[2]AGAL321.379−00.301	–	1	-57.6	9.5	6	1	6.19	2	16.05	91.62	18.55	18.51	3.72	3.68
[2]AGAL321.719+01.176	–	1	-40.2	2.4	6.6	1	1.59	5.08	45.77	103.32	18.95	18.96	2.98	3
[2]AGAL323.917+00.034	–	1	-56	10	5.9	1	6.98	0.8	11.72	89.8	18.15	18.1	3.63	3.58

Table B.1 continued from previous page

Submm Name	*Complex*	*HII*	v_{lsr} [km s^{-1}]	*D* [kpc]	R_{GC} [kpc]	*Flag*	*Radius* [pc]	*Peak Flux* [Jy beam^{-1}]	*Int Flux* [Jy]	*R*	*Log* N_{H_2} [cm^{-2}]	*Log* N_{H_2} (corr) [cm^{-2}]	*Log M* [M$_\odot$]	*Log M (corr)* [M$_\odot$]
[2]AGAL324.201+00.121	–	2	-87.5	6.8	4.9	1	4.35	10.48	47.04	73.5	19.27	19.13	3.9	3.76
[2]AGAL326.449−00.749	–	1	-66.3	3.8	5.6	1	1.02	3.1	7.55	84.57	18.74	18.66	2.6	2.52
[2]AGAL326.472−00.377	–	1	-54.6	3.3	5.9	1	1.65	5.38	22.65	89.8	18.98	18.93	2.95	2.91
[2]AGAL326.724+00.614	–	1	-41.5	1.8	6.9	1	1.34	8.56	47.48	109.72	19.18	19.22	2.75	2.79
[2]AGAL326.881−00.269	–	1	-46.1	3.5	5.8	1	2	0.86	9.27	88.02	18.18	18.12	2.62	2.56
[2]AGAL327.129+00.526	–	1	-84.1	5	5	1	0.58	0.57	5.46	74.99	18	17.88	2.7	2.57
[2]AGAL327.403+00.444	–	1	-80	5	5	1	2.62	11.16	37.66	74.99	19.29	19.17	3.53	3.41
[2]AGAL327.629−00.359	–	2	-74.1	4.2	5.3	1	1.56	0.98	5.68	79.63	18.24	18.14	2.56	2.46
[2]AGAL327.638−00.147	–	1	-40.8	2.6	6.3	1	0.45	0.94	4.34	97.3	18.22	18.21	2.03	2.02
[2]AGAL327.764−00.347	–	1	-74.5	4.2	5.3	1	2.54	3.14	24.32	79.63	18.74	18.64	3.19	3.09
[2]AGAL327.848+00.016	–	1	-51.8	3.1	6	1	0.36	0.57	1	91.62	18	17.96	1.54	1.5
[2]AGAL327.894+00.149	–	1	-91.4	8.47	4.69	3	1.89	2.64	18.65	70.47	18.67	18.51	3.69	3.53
[2]AGAL328.166+00.587	–	1	-93.5	7.1	4.4	1	2.48	2.04	7.87	66.5	18.55	18.38	3.16	2.98
[2]AGAL328.236−00.547	–	1	-40.2	2.7	6.2	1	2.8	10.09	135.6	95.37	19.25	19.23	3.56	3.53
[2]AGAL328.424−00.087	–	1	33.3	17.5	11.3	1	2.04	0.56	1.67	264.91	17.99	18.42	3.27	3.69
[2]AGAL328.566−00.534	–	2	-46.6	2.7	6.2	1	1.85	12.53	72.41	95.37	19.34	19.32	3.28	3.26
[2]AGAL328.961+00.566	–	2	-93.5	8.6	4.6	1	3.6	3.22	16.53	69.21	18.75	18.59	3.65	3.49
[2]AGAL329.337+00.147	–	1	-107.1	6	4.4	1	3.14	8.88	36.32	66.5	19.19	19.02	3.68	3.5
[2]AGAL329.424−00.162	–	1	-76.8	4.4	5.1	1	2.05	2.8	16.21	76.51	18.69	18.58	3.06	2.94
[2]AGAL329.472+00.216	–	1	-101.5	6	4.4	1	3.98	1.99	19.46	66.5	18.54	18.37	3.41	3.23
[2]AGAL329.476+00.841	–	1	-82.6	4.9	4.8	1	1.14	1.62	5	72.04	18.45	18.31	2.64	2.5
[2]AGAL329.599+00.054	–	1	-100.8	6	4.4	1	3	0.78	7.08	66.5	18.14	17.96	2.97	2.79
[2]AGAL329.816+00.141	–	1	-85	5	4.8	1	2.39	2.59	12.24	72.04	18.66	18.52	3.05	2.9
[2]AGAL330.284+00.492	–	1	-93.5	5.4	4.5	1	1.88	2	7.5	67.84	18.55	18.38	2.9	2.73
[2]AGAL330.294−00.394	–	3	-80	9.8	4.9	1	5.13	6.21	21.59	73.5	19.04	18.9	3.88	3.74
[2]AGAL330.879−00.367	–	1	-63.3	4	5.2	1	3.4	18.65	99.85	78.05	19.52	19.41	3.76	3.66

Table B.1 continued from previous page

Submm Name	*Complex*	*HII*	v_{lsr} [km s^{-1}]	*D* [kpc]	R_{GC} [kpc]	*Flag*	*Radius* [pc]	*Peak Flux* [Jy beam^{-1}]	*Int Flux* [Jy]	*R*	*Log* N_{H_2} [cm^{-2}]	*Log* N_{H_2} (corr) [cm^{-2}]	*Log M* [M$_\odot$]	*Log M (corr)* [M$_\odot$]
[2]AGAL330.954−00.182	–	2	-91.6	5.3	4.5	1	2.96	47.21	108.68	67.84	19.92	19.75	4.04	3.88
[2]AGAL331.134−00.484	–	1	-67.7	4	5.2	1	4.79	4.21	89.14	78.05	18.87	18.76	3.71	3.61
[2]AGAL331.146+00.136	–	1	-75.3	10.1	4.9	1	6.23	0.97	13.02	73.5	18.23	18.1	3.68	3.55
[2]AGAL331.361+01.066	–	1	-78.3	4.5	4.9	1	1.94	2.37	17.48	73.5	18.62	18.49	3.11	2.98
[2]AGAL331.418−00.356	–	1	-63.9	4	5.2	1	3.49	3.48	39.81	78.05	18.79	18.68	3.36	3.26
[2]AGAL331.491−00.116	–	1	-88	5.3	4.5	1	4.99	5.06	76.54	67.84	18.95	18.78	3.89	3.72
[2]AGAL331.546−00.067	–	1	-88.1	5.3	4.5	1	4.56	4.69	65.08	67.84	18.92	18.75	3.82	3.65
[2]AGAL332.156−00.449	–	1	-55.6	3.6	5.4	1	2.43	5.23	43.13	81.25	18.96	18.87	3.31	3.22
[2]AGAL332.296−00.094	–	2	-48.2	3.1	5.8	1	2.24	7.04	34.52	88.02	19.09	19.04	3.08	3.03
[2]AGAL332.544−00.124	–	1	-47.5	3.1	5.8	1	2.49	2.03	26.3	88.02	18.55	18.5	2.96	2.91
[2]AGAL332.766−00.007	–	1	-95.6	5.6	4.2	1	2.02	1.14	12.75	63.89	18.3	18.11	3.16	2.97
[2]AGAL332.826−00.549	–	1	-57.3	3.6	5.4	1	3.31	32.86	139.92	81.25	19.76	19.67	3.82	3.73
[2]AGAL333.018+00.766	–	1	-47.8	3	5.8	1	2.79	8.75	91.46	88.02	19.19	19.13	3.48	3.42
[2]AGAL333.134−00.431	–	2	-51.9	3.6	5.4	1	3.64	25.64	246.03	81.25	19.65	19.56	4.06	3.97
[2]AGAL333.284−00.387	–	1	-51.6	3.6	5.4	1	2.93	14.43	129.29	81.25	19.4	19.31	3.78	3.69
[2]AGAL333.339−00.127	–	1	-59.7	3.8	5.3	1	1.24	1.01	3.43	79.63	18.25	18.15	2.25	2.16
[2]AGAL333.604−00.212	–	–	-47.7	3.6	5.4	1	4.06	36.15	273.32	81.25	19.8	19.71	4.11	4.02
[2]AGAL333.679−00.431	–	1	-5.6	14.7	8.1	1	5.82	0.57	7.19	139.54	18	18.15	3.75	3.9
[2]AGAL333.724+00.364	–	1	-33	2.3	6.3	1	2.3	2.15	43.39	97.3	18.58	18.57	2.92	2.91
[2]AGAL334.328−00.286	–	1	-38.1	3.1	5.7	1	0.83	1.2	4.13	86.28	18.32	18.26	2.16	2.09
[2]AGAL334.722−00.654	–	1	-44.6	3	5.8	1	1.08	0.83	4.6	88.02	18.16	18.11	2.18	2.12
[2]AGAL335.197−00.389	–	1	-37.1	2.9	5.8	1	0.98	0.55	4.96	88.02	17.99	17.93	2.18	2.12
[2]AGAL335.391−00.291	–	1	-19.8	13.7	7	1	1.59	0.68	1.43	111.94	18.08	18.13	2.99	3.04
[2]AGAL335.944+00.029	–	1	-54.8	3.5	5.3	1	0.86	0.48	2.39	79.63	17.93	17.83	2.03	1.93
[2]AGAL335.980+00.196	–	1	-56.2	3.88	5.2	3	0.32	0.33	4.02	78.05	17.76	17.66	2.34	2.23
[2]AGAL336.359−00.137	–	1	-79.6	5	4.2	1	4.77	3.49	28.7	63.89	18.79	18.59	3.42	3.22

Table B.1 continued from previous page

Submm Name	*Complex*	*HII*	v_{lsr} [km s^{-1}]	*D* [kpc]	R_{GC} [kpc]	*Flag*	*Radius* [pc]	*Peak Flux* [Jy beam^{-1}]	*Int Flux* [Jy]	*R*	*Log* N_{H_2} [cm^{-2}]	*Log* N_{H_2} (corr) [cm^{-2}]	*Log M* [M$_\odot$]	*Log M (corr)* [M$_\odot$]
[2]AGAL336.369−00.004	–	1	-128	6.7	3.5	1	4.05	5.9	27.59	55.53	19.02	18.76	3.65	3.4
[2]AGAL336.411−00.256	–	1	-86.2	5	4.2	1	3.84	3.9	33.52	63.89	18.84	18.64	3.48	3.29
[2]AGAL336.824+00.027	–	1	-75	4.7	4.4	1	3.94	5.94	57.08	66.5	19.02	18.84	3.66	3.48
[2]AGAL336.984−00.184	–	1	-75.1	4.6	4.5	1	1.28	1.47	3.72	67.84	18.41	18.24	2.46	2.29
[2]AGAL336.994−00.027	–	1	-119.8	7.7	3.3	1	3.49	11.01	27.6	53.35	19.29	19.01	3.77	3.5
[2]AGAL337.004+00.322	–	1	-62.8	11.3	4.9	1	3.29	2.28	6.67	73.5	18.6	18.47	3.49	3.36
[2]AGAL337.406−00.402	–	1	-41.4	3	5.7	1	1.64	18.35	58.81	86.28	19.51	19.44	3.28	3.22
[2]AGAL337.632−00.079	–	1	-56.5	3.6	5.2	1	1.38	2.2	12.97	78.05	18.59	18.48	2.79	2.68
[2]AGAL337.666−00.177	–	1	-53.1	3.6	5.2	1	1.38	3.05	10.88	78.05	18.73	18.62	2.71	2.6
[2]AGAL337.704−00.054	–	1	-46.5	12.1	5.4	1	5.77	13.58	41.31	81.25	19.38	19.29	4.34	4.25
[2]AGAL337.712+00.087	–	3	-75.7	10.8	4.4	1	8.29	9.73	48.94	66.5	19.23	19.06	4.32	4.14
[2]AGAL337.844−00.376	–	1	-40.4	3	5.7	1	1.08	3.32	9.9	86.28	18.77	18.7	2.51	2.45
[2]AGAL337.999−00.149	–	1	-65.7	4.1	4.8	1	0.62	1.04	2.7	72.04	18.26	18.12	2.22	2.07
[2]AGAL338.074+00.011	–	1	-39.7	3	5.7	1	1.88	7.28	48.89	86.28	19.11	19.04	3.2	3.14
[2]AGAL338.289−00.377	–	1	-12.4	1.1	7.3	1	0.13	0.47	1.88	118.88	17.92	17.99	0.92	0.99
[2]AGAL338.332+00.131	–	1	-35.1	2.7	5.9	1	1.16	4.73	18.94	89.8	18.92	18.87	2.7	2.65
[2]AGAL338.436+00.057	–	1	-30.3	2.7	5.9	1	1.92	4.88	44.91	89.8	18.93	18.89	3.08	3.03
[2]AGAL338.569−00.144	–	2	-117	7.1	3.1	1	3.22	3.71	11.46	51.25	18.81	18.52	3.32	3.03
[2]AGAL338.682−00.084	–	1	-18.2	1.5	7	1	0.23	1.19	2.39	111.94	18.32	18.37	1.29	1.34
[2]AGAL338.926+00.634	–	1	-61.6	4.2	4.7	1	2.69	6.04	31.85	70.62	19.03	18.87	3.31	3.16
[2]AGAL339.106+00.147	–	1	-78.2	4.8	4.2	1	1.9	1.98	8.64	63.89	18.54	18.35	2.86	2.66
[2]AGAL339.584−00.127	–	1	-33.5	2.6	6	1	0.97	3.78	16.13	91.62	18.82	18.78	2.6	2.56
[2]AGAL339.746+00.094	–	1	-54.8	11.8	4.9	1	1.92	0.98	2.87	73.5	18.24	18.1	3.16	3.03
[2]AGAL339.943−00.092	–	1	-51.2	3.6	5.1	1	1.51	1.76	9.77	76.51	18.49	18.37	2.66	2.55
[2]AGAL340.054−00.244	–	1	-53	3.6	5.1	1	2.97	12.06	54.3	76.51	19.33	19.21	3.41	3.29
[2]AGAL340.073+00.927	–	1	-74.3	4.7	4.2	1	2.19	2.69	15.1	63.89	18.67	18.48	3.08	2.89

Table B.1 continued from previous page

Submm Name	*Complex*	*HII*	v_{lsr} [km s^{-1}]	*D* [kpc]	R_{GC} [kpc]	*Flag*	*Radius* [pc]	*Peak Flux* [Jy beam^{-1}]	*Int Flux* [Jy]	*R*	*Log* N_{H_2} [cm^{-2}]	*Log* N_{H_2} (corr) [cm^{-2}]	*Log M* [M$_\odot$]	*Log M (corr)* [M$_\odot$]
[2]AGAL340.248−00.374	–	1	-50.4	3.6	5.1	1	3.43	5.14	61.32	76.51	18.96	18.84	3.46	3.34
[2]AGAL341.702+00.051	–	1	-16.7	14	6.6	1	4.56	1.17	5.53	103.32	18.31	18.33	3.6	3.61
[2]AGAL342.058+00.421	–	1	-70.1	10.9	3.9	1	8.75	3.87	37.67	60.16	18.83	18.61	4.21	3.99
[2]AGAL342.386+00.122	–	1	-6	1.2	7.2	1	0.59	0.95	7.68	116.52	18.22	18.29	1.6	1.67
[2]AGAL343.502−00.014	–	1	-27.5	2.6	5.9	1	2.15	6.21	45.12	89.8	19.04	18.99	3.04	3
[2]AGAL343.929+00.124	–	1	8.6	17.1	9.4	1	1.99	1.06	3.02	181.05	18.27	18.53	3.51	3.76
[2]AGAL344.424+00.046	–	1	-65.9	4.9	3.8	1	4.39	4.83	51.89	58.97	18.93	18.7	3.66	3.43
[2]AGAL345.003−00.224	–	1	-27.1	1.4	7	1	1.84	18.51	137.14	111.94	19.51	19.56	2.99	3.04
[2]AGAL345.408−00.952	–	1	-19.6	1.4	7	1	1.42	11.66	138.63	111.94	19.31	19.36	2.99	3.04
[2]AGAL345.488+00.314	–	1	-17.3	2.4	6.1	1	2.15	17.27	143.5	93.48	19.48	19.45	3.48	3.45
[2]AGAL345.493+01.469	–	2	-12.6	2.4	6.1	1	1.73	18.03	142.67	93.48	19.5	19.47	3.47	3.45
[2]AGAL345.526−00.052	–	1	-3.7	1.4	7	1	0.81	1.1	16.4	111.94	18.29	18.34	2.07	2.12
[2]AGAL345.548−00.081	–	1	-6	1.4	7	1	0.16	0.68	3.74	111.94	18.08	18.13	1.43	1.47
[2]AGAL345.649+00.009	–	1	-10.8	1.4	7	1	0.6	7.35	22.87	111.94	19.11	19.16	2.21	2.26
[2]AGAL346.076−00.056	–	1	-83.9	10.2	2.9	1	5.1	2.38	11.57	49.24	18.62	18.31	3.64	3.33
[2]AGAL346.232−00.321	–	1	-11.5	14.98	7.02	3	1.31	0.78	2.65	112.39	18.14	18.19	3.33	3.39
[2]AGAL347.304+00.014	–	1	-8.9	1.4	7	1	0.16	0.69	1.68	111.94	18.08	18.13	1.08	1.13
[2]AGAL347.602+00.244	–	1	-94.8	9.8	2.4	1	5.82	1.66	33.03	44.55	18.46	18.11	4.06	3.71
[2]AGAL347.627+00.149	–	1	-93.3	9.8	2.4	1	9.01	5.71	45.37	44.55	19	18.65	4.2	3.85
[2]AGAL347.871+00.014	–	1	-30.9	12.9	5	1	6.75	3.16	17.56	74.99	18.74	18.62	4.03	3.9
[2]AGAL348.144+00.257	–	1	-70.4	10.6	3	1	5.55	0.98	10.79	50.23	18.24	17.94	3.64	3.34
[2]AGAL348.531−00.972	–	1	-15.4	3.4	5.1	1	2.02	4.94	52.54	76.51	18.94	18.82	3.34	3.23
[2]AGAL348.549−00.337	–	1	10.4	17.8	9.8	1	2.07	0.45	1.05	196.16	17.9	18.19	3.08	3.37
[2]AGAL348.698−01.027	–	1	-12.7	3.4	5.1	1	1.5	11.98	47.36	76.51	19.32	19.21	3.3	3.18
[2]AGAL348.893−00.179	–	1	7.7	11.2	3.29	3	1.47	3.02	7.8	53.24	18.72	18.45	3.55	3.28
[2]AGAL349.091+00.106	–	1	-77.6	10.5	2.8	1	12.09	5.75	34.28	48.26	19	18.69	4.14	3.82

Table B.1 continued from previous page

Submm Name	*Complex*	*HII*	v_{lsr} [km s^{-1}]	*D* [kpc]	R_{GC} [kpc]	*Flag*	*Radius* [pc]	*Peak Flux* [Jy beam^{-1}]	*Int Flux* [Jy]	*R*	*Log* N_{H_2} [cm^{-2}]	*Log* N_{H_2} (corr) [cm^{-2}]	*Log M* [M$_\odot$]	*Log M (corr)* [M$_\odot$]
[2]AGAL349.721+00.122	–	1	17.6	22.1	13.9	1	4.37	1.6	3.26	445.96	18.5	19.15	3.76	4.41
[3]JCMTLSY J004956.23+654345.2	–	1	-63.5	5	11.9	4	0.81	0.33	6.88	298.74	17.79	18.27	2.77	3.25
[3]JCMTLSY J010750.96+652121.7	–	1	-86.3	7.9	14.4	4	2.1	0.75	34.1	492.95	18.15	18.84	3.87	4.56
[3]JCMTLSY J011636.99+645041.2	–	1	-53.7	4.1	11.3	4	0.95	0.45	15.47	264.91	17.92	18.35	2.95	3.38
[3]JCMTLSY J011648.61+644542.6	–	1	-54.9	4.2	11.4	4	0.81	0.44	9.69	270.27	17.92	18.35	2.77	3.2
[3]JCMTLSY J020806.83+604606.8	–	1	-55.6	4.5	11.9	4	1.76	1.17	87.36	298.74	18.34	18.82	3.79	4.26
[3]JCMTLSY J022520.88+620454.9	–	1	-40.3	2	9.9	4	0.31	0.23	4.79	200.12	17.63	17.93	1.82	2.12
[3]JCMTLSY J022531.18+620619.5	–	2	–	2	9.9	4	1.46	7.37	1025.4	200.12	19.14	19.44	4.15	4.45
[3]JCMTLSY J022540.29+620548.5	–	1	–	2	9.9	4	2.16	10.4	2678.68	200.12	19.29	19.59	4.57	4.87
[3]JCMTLSY J022703.84+615221.1	–	1	-48.1	2	9.9	4	1.96	17.69	2038.62	200.12	19.52	19.82	4.45	4.75
[3]JCMTLSY J030723.84+583046.1	–	1	-39.8	3.2	11	4	1.96	1.19	220.96	249.46	18.35	18.74	3.89	4.29
[3]JCMTLSY J031016.80+565031.5	–	1	-40	3.2	11.1	4	0.64	0.21	6.83	254.51	17.59	18	2.38	2.79
[3]JCMTLSY J032731.06+581922.0	–	1	-46.7	4.2	11.9	4	1.12	0.57	24.59	298.74	18.03	18.5	3.18	3.65
[3]JCMTLSY J041107.55+510846.0	–	1	-25.1	2.3	10.5	4	0.34	0.22	4.49	225.68	17.61	17.97	1.91	2.27
[3]JCMTLSY J043620.47+511257.8	–	1	-36.2	4.4	12.5	4	1.95	1.26	140.08	336.9	18.37	18.9	3.97	4.5
[3]JCMTLSY J044027.12+502827.3	–	1	-35.6	4.5	12.6	4	0.84	0.26	7.36	343.72	17.69	18.22	2.71	3.25
[3]JCMTLSY J053020.69+310125.7	–	1	-18.9	2	10.4	4	0.37	0.4	11.89	221.21	17.87	18.22	2.22	2.56
[3]JCMTLSY J060906.84+215039.2	–	1	-1.2	2	10.4	4	1.03	1.87	177.9	221.21	18.54	18.89	3.39	3.74
[3]JCMTLSY J061012.12+124852.3	–	1	25.1	4.6	12.9	4	0.81	0.39	14.33	365.01	17.86	18.43	3.02	3.58
[3]JCMTLSY J061253.65+180027.1	–	1	8.8	2	10.4	4	1.32	3.84	575.36	221.21	18.86	19.2	3.9	4.25
[3]JCMTLSY J061320.97+152411.4	–	1	16.3	2	10.4	4	0.45	0.35	15.2	221.21	17.82	18.16	2.32	2.67
[3]JCMTLSY J062147.49+103924.6	–	1	34.2	5.8	14	4	0.9	0.22	5.81	454.99	17.61	18.27	2.83	3.49
[3]JCMTLSY J062334.68+095629.4	–	1	34.6	5.5	13.7	4	1.11	0.41	11.84	428.45	17.88	18.52	3.09	3.72
[3]JCMTLSY J063315.98+043454.5	–	1	14	1.2	9.5	4	0.3	0.36	15.43	184.71	17.83	18.09	1.89	2.15
[3]JCMTLSY J064615.97+000630.8	–	1	42.4	4.3	12.2	4	1.06	0.59	18.59	317.25	18.04	18.54	3.07	3.58
[3]JCMTLSY J065915.57−035932.8	–	1	25.1	1.3	9.5	4	0.54	1.16	101.52	184.71	18.34	18.6	2.77	3.04

Table B.1 continued from previous page

Submm Name	*Complex*	*HII*	v_{lsr} [km s^{-1}]	*D* [kpc]	R_{GC} [kpc]	*Flag*	*Radius* [pc]	*Peak Flux* [Jy beam^{-1}]	*Int Flux* [Jy]	*R*	*Log* N_{H_2} [cm^{-2}]	*Log* N_{H_2} (corr) [cm^{-2}]	*Log M* [M$_\odot$]	*Log M (corr)* [M$_\odot$]
[3]JCMTLSY J073538.53−184855.1	–	1	46.8	3.5	10.8	4	0.95	0.27	15.38	239.66	17.7	18.08	2.81	3.19
[3]JCMTLSY J074451.83−240744.3	–	1	66.8	5.4	12	4	2.33	2.52	179.97	304.79	18.67	19.16	4.26	4.74
[3]JCMTLSY J194815.31+280727.4	–	1	-55.3	11.7	11	4	2.19	0.54	0.53	249.46	18	18.4	2.4	2.8
[3]JCMTLSY J194914.48+265010.9	–	1	–	–	–	–	–	0.68	2.39	–	18.1	–	–	–
[3]JCMTLSY J195803.01+314407.3	–	1	-65.5	11.7	11.6	4	2.08	0.33	0.32	281.32	17.79	18.24	2.18	2.63
[3]JCMTLSY J200137.46+333527.5	–	1	-22.9	7.4	9.1	4	3.75	0.54	2.28	170.49	18	18.24	2.64	2.87
[3]JCMTLSY J200145.71+333244.3	–	1	-25.2	7.6	9.2	4	7.8	12.68	47.43	173.94	19.37	19.62	3.98	4.22
[3]JCMTLSY J200154.35+333412.3	–	1	-22.8	7.4	9.1	4	6.34	4.82	29.31	170.49	18.95	19.19	3.74	3.98
[3]JCMTLSY J200850.00+333734.3	–	1	-17.9	6.8	8.9	4	2.34	0.87	1.87	163.79	18.21	18.43	2.48	2.69
[3]JCMTLSY J201146.54+364928.5	–	1	-36.2	7.7	9.7	4	3.23	0.45	1.96	192.26	17.92	18.21	2.6	2.89
[3]JCMTLSY J201215.26+364254.5	–	1	-36.2	7.7	9.7	4	2.02	0.28	0.55	192.26	17.72	18	2.05	2.34
[3]JCMTLSY J201217.25+342809.9	–	1	-71	11.3	11.9	4	2.02	0.24	0.24	298.74	17.65	18.13	2.03	2.5
[3]JCMTLSY J201334.05+361456.3	–	1	-53.1	9.3	10.6	4	3.15	0.54	1.36	230.25	18	18.37	2.61	2.97
[3]JCMTLSY J201627.62+365458.5	–	1	-55.2	9.3	10.8	4	2.56	0.41	0.73	239.66	17.88	18.26	2.34	2.72
[3]JCMTLSY J201938.82+405638.3	–	1	0.9	1.4	8.2	4	0.78	1.65	7.43	142.36	18.49	18.64	1.7	1.86
[3]JCMTLSY J202038.86+393751.2	–	1	2.1	1.4	8.2	4	1.28	5.16	37	142.36	18.98	19.14	2.4	2.55
[3]JCMTLSY J202144.08+372637.5	–	1	1.4	1.4	8.2	4	1.23	6.57	35.23	142.36	19.09	19.24	2.38	2.53
[3]JCMTLSY J202355.04+373812.5	–	1	-2.7	1.4	8.2	4	0.94	1.23	9.05	142.36	18.36	18.52	1.79	1.94
[3]JCMTLSY J202611.17+390348.6	–	1	-73.6	10.4	11.9	4	2.58	0.54	0.83	298.74	18	18.48	2.49	2.97
[3]JCMTLSY J202712.76+392639.5	–	1	-4.5	1.4	8.2	4	0.39	0.96	1.66	142.36	18.25	18.41	1.05	1.2
[3]JCMTLSY J202758.70+393210.1	–	1	-54.5	8.5	10.7	4	1.02	0.31	0.16	234.91	17.76	18.13	1.6	1.97
[3]JCMTLSY J202810.18+405336.8	–	1	-43	7.3	10	4	3.08	0.85	3.07	204.17	18.2	18.51	2.75	3.06
[3]JCMTLSY J202816.75+405301.8	–	2	-43.1	7.3	10	4	3.34	0.48	2.48	204.17	17.95	18.26	2.66	2.97
[3]JCMTLSY J202931.93+390113.2	–	1	-3.6	1.4	8.2	4	0.5	0.6	1.55	142.36	18.05	18.2	1.02	1.17
[3]JCMTLSY J202936.77+390109.3	–	1	-2.9	1.4	8.2	4	0.5	0.45	1.23	142.36	17.92	18.08	0.92	1.07
[3]JCMTLSY J202952.19+404844.7	–	1	-2.5	1.4	8.3	4	0.4	0.69	1.08	145.24	18.11	18.27	0.86	1.03

Table B.1 continued from previous page

Submm Name	*Complex*	*HII*	v_{lsr} [km s^{-1}]	*D* [kpc]	R_{GC} [kpc]	*Flag*	*Radius* [pc]	*Peak Flux* [Jy beam^{-1}]	*Int Flux* [Jy]	*R*	*Log* N_{H_2} [cm^{-2}]	*Log* N_{H_2} (corr) [cm^{-2}]	*Log M* [M$_\odot$]	*Log M (corr)* [M$_\odot$]
[3]JCMTLSY J203028.83+411555.3	–	1	-4.3	1.4	8.3	4	1.14	3.23	17.06	145.24	18.78	18.94	2.06	2.23
[3]JCMTLSY J203153.40+391937.6	–	1	-60.6	9	11	4	2.46	0.3	0.57	249.46	17.75	18.15	2.2	2.6
[3]JCMTLSY J203222.01+434050.3	–	1	0.3	1.4	8.3	4	0.54	0.89	2.26	145.24	18.22	18.38	1.19	1.35
[3]JCMTLSY J203608.17+413955.9	–	1	11.5	1.4	8.3	4	1.11	1.54	12.71	145.24	18.46	18.62	1.94	2.1
[3]JCMTLSY J203652.09+413622.0	–	1	-3.1	1.4	8.3	4	1.21	3.37	16.94	145.24	18.8	18.96	2.06	2.22
[3]JCMTLSY J203836.71+423735.4	–	1	8.1	1.4	8.3	4	1.73	21.9	100.78	145.24	19.61	19.77	2.83	3
[3]JCMTLSY J203900.93+422248.0	–	1	-2.8	1.4	8.3	4	0.89	21.82	73.28	145.24	19.61	19.77	2.7	2.86
[3]JCMTLSY J203900.97+421931.5	–	2	-2.4	1.2	8.3	4	1.52	18.33	143.38	145.24	19.53	19.7	2.85	3.02
[3]JCMTLSY J203901.27+422203.6	–	1	-3.8	1.4	8.3	4	1.09	10.32	50.6	145.24	19.29	19.45	2.54	2.7
[3]JCMTLSY J203925.53+411959.2	–	1	-2	1.4	8.3	4	0.81	1.08	7.28	145.24	18.31	18.47	1.69	1.86
[3]JCMTLSY J204233.19+425645.6	–	1	-4.1	1.4	8.3	4	0.57	1.05	3.33	145.24	18.29	18.46	1.35	1.52
[3]JCMTLSY J205413.82+445408.8	–	1	-35.8	5.5	9.6	4	2.82	1.88	6.02	188.45	18.55	18.82	2.8	3.07
[3]JCMTLSY J210135.07+485456.5	–	1	-70.3	8.1	11.6	4	1.81	0.3	0.44	281.32	17.75	18.2	2	2.45
[3]JCMTLSY J210912.93+500101.0	–	1	–	–	–	–	–	1.74	4.86	–	18.51	–	–	–
[3]JCMTLSY J211339.11+521406.6	–	1	–	–	–	–	–	0.23	0.46	–	17.63	–	–	–
[3]JCMTLSY J212044.92+515326.6	–	1	-66.2	7.1	11.3	4	2.04	1.3	1.85	264.91	18.39	18.81	2.51	2.93
[3]JCMTLSY J212152.98+521057.3	–	1	-59.1	6.4	10.9	4	1.21	0.32	0.47	244.51	17.78	18.17	1.82	2.21
[3]JCMTLSY J213520.84+534711.5	–	1	-68.9	7	11.5	4	2.33	0.6	1.26	275.74	18.05	18.49	2.33	2.77
[3]JCMTLSY J214301.23+545616.9	–	1	-63.9	6.3	11.2	4	3.49	3.16	7.75	259.66	18.77	19.19	3.03	3.44
[3]JCMTLSY J215201.89+564743.7	–	1	-61.4	5.8	11.1	4	1.25	0.36	0.53	254.51	17.83	18.23	1.79	2.2
[3]JCMTLSY J215338.71+562750.3	–	1	-62.9	6	11.1	4	1.47	0.92	1.12	254.51	18.24	18.64	2.14	2.55
[3]JCMTLSY J223245.00+582811.2	–	1	-52.1	4.5	10.6	4	2.16	1.57	6.11	230.25	18.47	18.83	2.63	2.99
[3]JCMTLSY J224928.87+595453.1	–	1	-49.2	4.1	10.4	4	2.21	1.24	7.88	221.21	18.37	18.71	2.66	3.01
[3]JCMTLSY J225450.92+595254.9	–	1	-53	4.4	10.7	4	1.96	0.34	1.48	234.91	17.8	18.17	2	2.37
[3]JCMTLSY J225905.07+592821.3	–	1	-46.7	3.8	10.3	4	2.49	1.5	6.28	216.82	18.45	18.78	2.5	2.83
[3]JCMTLSY J231545.69+595239.3	–	1	-52.9	4.3	10.7	4	0.96	0.35	0.57	234.91	17.82	18.19	1.56	1.93

Table B.1 continued from previous page

Submm Name	*Complex*	*HII*	$v_{\rm lsr}$ [km s^{-1}]	*D* [kpc]	$R_{\rm GC}$ [kpc]	*Flag*	*Radius* [pc]	*Peak Flux* [Jy beam^{-1}]	*Int Flux* [Jy]	*R*	*Log* N_{H_2} [cm^{-2}]	*Log* N_{H_2} (corr) [cm^{-2}]	*Log M* [M$_\odot$]	*Log M (corr)* [M$_\odot$]
[3]JCMTLSY J231603.89+600153.8	–	2	-44.1	3.5	10.2	4	2.99	2.51	22.89	212.52	18.67	19	2.99	3.31
[3]JCMTLSY J231609.69+595922.1	–	1	-42.1	3.3	10.1	4	1.75	1.64	6.16	208.31	18.49	18.81	2.37	2.68
[3]JCMTLSY J235307.69+624705.9	–	1	-46.7	3.5	10.5	4	1.07	0.76	1.58	225.68	18.15	18.51	1.83	2.18

Appendix C

H II Region Properties

Derived H II region properties for the full sample. Columns are as follows - Radio Name (in galactic coordinates); Submillimetre Name (as previously defined); Offset between radio and submillimetre centres; Radio Peak and Integrated fluxes; Angular Diameter; Physical Diameter; Frequency of observations; Lyman continuum flux; Bolometric Luminosity; Associated Ratio. All log values are base 10.

Radio Name	*Submm Name*	*Offset*	*Peak Flux*	*Int Flux*	*d*	*d*	*Freq*	*Log* $N_{\rm Ly}$	*Log* $L_{\rm bol}$	*Log*	*Log*	*Log*	*Log*
		["]	[Jy/beam]	[Jy]	["]	[pc]	[GHz]	[photons s^{-1}]	[$L_\odot$]	$L_{\rm bol}/M$	$L_{\rm bol}/M_{\rm corr}$	$N_{\rm Ly}/M$	$N_{\rm Ly}/M_{\rm corr}$
[1]G010.3009−00.1477	AGAL010.299−00.147	5.2	56.37	631.39	5.2	0.09	5	47.84	5.17	1.79	1.92	44.46	44.59
[1]G010.3204−00.2586	AGAL010.321−00.257	4.1	14.61	18.2	–	–	5	46.17	–	–	–	43.48	43.57
[1]G010.4736+00.0274	AGAL010.472+00.027	3.9	12.3	19.3	1.4	0.06	5	47.1	5.65	1.29	1.71	42.73	43.16
[1]G010.4724+00.0275	AGAL010.472+00.027	0.8	22.34	38.43	1.7	0.07	5	47.4	5.65	1.29	1.71	43.03	43.45
[1]G010.6240−00.3813	AGAL010.624−00.384	10.6	38.23	71.65	1.4	0.03	5	47.21	5.72	1.69	1.94	43.18	43.43
[1]G010.6218−00.3848	AGAL010.624−00.384	8.5	16.81	37.06	1.7	0.04	5	46.92	5.72	1.69	1.94	42.9	43.14
[1]G010.6234−00.3837	AGAL010.624−00.384	2.5	305.58	1952.22	4.4	0.11	5	48.64	5.72	1.69	1.94	44.62	44.86
[1]G010.6223−00.3788	AGAL010.624−00.384	19	97.9	483.33	5.6	0.14	5	48.04	5.72	1.69	1.94	44.01	44.26
[1]G010.9584+00.0221	AGAL010.957+00.022	3.8	109.11	195.97	1.6	0.02	5	47.17	4.02	1.4	1.48	44.55	44.64
[1]G010.9656+00.0089	AGAL010.964+00.011	6.8	7.86	51.75	4.6	0.06	5	46.59	3.46	1.24	1.33	44.38	44.46
[1]G011.0328+00.0274	AGAL011.031+00.026	9.2	3.58	5.69	1.2	0.02	5	45.63	2.71	1.09	1.17	44.01	44.09
[1]G011.0339+00.0616	AGAL011.034+00.061	6.1	21.01	103.36	6.93	0.1	5	46.89	3.81	1.54	1.63	44.63	44.71
[1]G011.1104−00.3985	AGAL011.109−00.397	7.8	51.55	305.37	8.2	0.2	5	47.84	4.69	1.11	1.36	44.26	44.5
[1]G011.9039−00.1411	AGAL011.902−00.141	6.3	11.11	16.81	1.1	0.02	5	46.16	3.59	0.74	0.83	43.32	43.41
[1]G011.9032−00.1407	AGAL011.902−00.141	3.6	5.59	25.57	2.8	0.04	5	46.34	3.59	0.74	0.83	43.5	43.59
[1]G011.9368−00.6158	AGAL011.936−00.616	6	163.93	1155.9	5.7	0.09	5	48.08	4.75	1.47	1.58	44.8	44.91
[1]G011.9446−00.0369	AGAL011.946−00.036	2.8	61.58	943.58	14.6	0.22	5	47.91	4.29	1.87	1.96	45.49	45.58
[1]G012.1988−00.0345	AGAL012.198−00.034	4	19.68	62.71	2.2	0.13	5	47.9	4.98	1.39	1.6	44.32	44.52
[1]G012.2081−00.1019	AGAL012.208−00.102	2.2	72.18	207.87	2.4	0.16	5	48.53	5.52	1.13	1.21	44.14	44.22
[2]G012.4180+00.5038	AGAL012.418+00.506	–	3.52	6.23	1.3	0.01	5	45.26	3.9	1.31	1.3	42.67	42.66
[1]G012.4294−00.0479	AGAL012.431−00.049	7.2	13.78	45.17	2.3	0.03	5	46.44	3.15	1.01	1.05	44.29	44.34
[1]G012.4317−01.1112	AGAL012.431−01.114	10.2	9.67	69.01	4.1	0.06	5	46.75	4.87	2.19	2.28	44.06	44.16
[1]G012.8131−00.1976	AGAL012.804−00.199	31.1	131.04	1500.39	5.2	0.07	5	47.96	–	–	–	44.04	44.09
[1]G012.8050−00.2007	AGAL012.804−00.199	8	287.9	12616.4	16.2	0.2	5	48.89	–	–	–	44.96	45.01
[1]G012.9995−00.3583	AGAL012.998−00.357	7.8	4.76	20.14	2.7	0.02	5	45.49	2.9	1.11	1.06	43.7	43.65
[1]G013.2099−00.1428	AGAL013.209−00.144	5.1	40.72	946.76	8.2	0.1	5	47.76	4.2	1.33	1.37	44.88	44.93

Table C.1 continued from previous page

Radio Name	*Submm Name*	*Offset*	*Peak Flux*	*Int Flux*	*d*	*d*	*Freq*	*Log* $N_{\rm Ly}$	*Log* $L_{\rm bol}$	*Log*	*Log*	*Log*	*Log*
		["]	[Jy/beam]	[Jy]	["]	[pc]	[GHz]	[photons s^{-1}]	[$L_\odot$]	$L_{\rm bol}/M$	$L_{\rm bol}/M_{\rm corr}$	$N_{\rm Ly}/M$	$N_{\rm Ly}/M_{\rm corr}$
[1]G013.3850+00.0684	AGAL013.384+00.064	7.6	10.49	603.94	19.1	0.18	5	47.29	3.52	1.67	1.66	45.44	45.43
[1]G013.8726+00.2818	AGAL013.872+00.281	3.7	24.71	1447.55	15.4	0.29	5	48.3	5.11	1.89	2.05	45.08	45.24
[1]G014.2460−00.0728	AGAL014.246−00.071	8	11.4	51.26	3.6	0.19	5	47.71	4.32	0.65	0.94	44.05	44.33
[1]G014.5988+00.0198	AGAL014.607+00.012	40.6	2.89	4.39	1.1	0.01	5	45.39	3.74	1.17	1.21	42.82	42.85
[1]G014.7785−00.3328	AGAL014.777−00.334	6	11.02	18.25	1.8	0.03	5	46.2	3	0.85	0.94	44.05	44.14
[1]G016.1448+00.0088	AGAL016.144+00.009	2.8	13.02	14.76	–	–	5	47.3	4.24	1.1	1.23	44.16	44.3
[1]G016.9445−00.0738	AGAL016.942−00.072	8.4	97.73	519.34	3.1	0.24	5	49.07	5.23	1.42	1.26	45.27	45.11
[1]G017.0299−00.0696	AGAL017.029−00.071	5.3	2.12	5.38	1.9	0.09	5	46.69	4.06	0.95	1.24	43.59	43.87
[1]G017.1141−00.1124	AGAL017.112−00.114	8.6	4.82	17.21	2.4	0.12	5	47.2	4.52	1.69	1.97	44.37	44.65
[1]G017.5549+00.1654	AGAL017.554+00.167	8.3	3.29	7.13	1.6	0.01	5	45.36	2.33	0.84	0.82	43.87	43.86
[1]G017.9850+00.1266	AGAL017.986+00.126	3.4	1.85	10.42	3.2	0.03	5	45.48	2.33	1.16	1.14	44.31	44.29
[1]G018.1460−00.2839	AGAL018.148−00.284	10.3	10.54	856.18	23.4	0.39	5	47.95	4.61	1.72	1.82	45.05	45.16
[1]G018.3024−00.3910	AGAL018.301−00.389	8.4	48.02	1277.88	14.6	0.23	5	48.07	4.74	1.72	1.81	45.05	45.14
[1]G018.4433−00.0056	AGAL018.444−00.004	6.3	31.48	81.31	1.9	0.11	5	48.01	4.68	1.01	1.16	44.34	44.49
[1]G018.4614−00.0038	AGAL018.461−00.002	4.6	121.64	342.12	2.3	0.13	5	48.63	5.38	1.37	1.52	44.62	44.77
[1]G018.6654+00.0294	AGAL018.666+00.026	12.8	4.19	5.65	–	–	5	46.71	4.53	1.33	1.58	43.51	43.77
[1]G018.7106+00.0002	AGAL018.711+00.001	2.3	71.64	107.46	1.4	0.02	5	46.75	3.07	0.95	0.98	44.62	44.65
[1]G018.7612+00.2630	AGAL018.761+00.261	7.9	36.07	51.38	–	–	5	47.96	5.1	1.22	1.19	44.09	44.05
[2]G018.8373−00.4727	AGAL018.823−00.486	46.73	1.14	2.55	1.59	0.04	5	45.76	4.39	0.71	0.92	42.08	42.29
[1]G018.8250−00.4675	AGAL018.824−00.467	2.9	4.02	11.41	2	0.05	5	46.41	3.62	1.23	1.45	44.03	44.24
[1]G018.8338−00.3002	AGAL018.833−00.301	1.9	29.02	131.38	6.5	0.4	5	48.28	4.91	1.24	1.32	44.61	44.69
[1]G019.0035+00.1280	AGAL019.003+00.129	5.4	1.91	6.41	2.3	0.06	5	46.16	3.37	0.79	1	43.58	43.79
[1]G019.0767−00.2882	AGAL019.076−00.287	4.2	62.94	129.48	2	0.05	5	47.46	5.12	1.54	1.76	43.89	44.1
[1]G019.0754−00.2874	AGAL019.076−00.287	3.8	23.43	380.69	8.4	0.2	5	47.93	5.12	1.54	1.76	44.36	44.57
[1]G019.4752+00.1728	AGAL019.472+00.171	11.5	7.03	37.22	3.4	0.23	5	47.82	5.36	1.02	0.99	43.49	43.46
[2]G019.5093−00.4374	AGAL019.508−00.447	–	3.31	6.55	0.61	0.01	5	46.17	3.66	1.09	1.3	43.6	43.81

Table C.1 continued from previous page

Radio Name	*Submm Name*	*Offset* ["]	*Peak Flux* [Jy/beam]	*Int Flux* [Jy]	*d* ["]	*d* [pc]	*Freq* [GHz]	*Log* N_{Ly} [photons s^{-1}]	*Log* L_{bol} [$L_\odot$]	*Log* L_{bol}/M	*Log* L_{bol}/M_{corr}	*Log* N_{Ly}/M	*Log* N_{Ly}/M_{corr}
[1]G019.6090−00.2313	AGAL019.609−00.234	9.8	89.71	259.95	3.5	0.21	5	48.57	6.01	1.6	1.68	44.16	44.24
[1]G019.6087−00.2351	AGAL019.609−00.234	4.1	153.16	2900.88	13	0.79	5	49.62	6.01	1.6	1.68	45.2	45.29
[1]G019.7281−00.1135	AGAL019.726−00.114	7.7	6.16	26.23	3	0.07	5	46.79	3.61	0.75	0.97	43.93	44.15
[1]G019.7549−00.1282	AGAL019.754−00.129	4.5	30.71	36.52	–	–	5	47.3	4.54	1.15	1.46	43.91	44.22
[1]G020.0797−00.1337	AGAL020.081−00.136	8.7	6.74	14.09	1.6	0.1	5	47.3	5.68	1.66	1.74	43.28	43.36
[1]G020.0809−00.1362	AGAL020.081−00.136	0.3	137	498.19	2.6	0.16	5	48.85	5.68	1.66	1.74	44.83	44.91
[1]G020.0720−00.1421	AGAL020.081−00.136	38.4	39.74	210.13	5.2	0.32	5	48.48	5.68	1.66	1.74	44.45	44.53
[1]G020.3633−00.0136	AGAL020.362−00.012	4.3	16.35	55.11	2.5	0.04	5	46.76	3.32	1.01	1.11	44.45	44.55
[1]G020.7619−00.0646	AGAL020.761−00.062	9	3.72	10.03	2	0.11	5	47.09	4.78	1.47	1.6	43.77	43.91
[1]G020.9636−00.0744	AGAL020.962−00.074	5.2	4.11	11.28	2	0.12	5	47.22	4.38	1.46	1.52	44.3	44.36
[1]G021.3571−00.1766	AGAL021.356−00.176	4.9	15.35	24.93	1.2	0.06	5	47.35	4.56	1.45	1.68	44.24	44.47
[1]G021.3855−00.2541	AGAL021.386−00.254	1.8	62.56	113.91	1.6	0.08	5	48.01	4.91	1.38	1.61	44.48	44.71
[1]G021.6034−00.1685	AGAL021.598−00.161	34.8	4.17	19.84	3.4	0.26	5	47.64	4.06	0.86	0.68	44.44	44.26
[1]G021.8751+00.0075	AGAL021.873+00.007	4.8	19.52	566.73	11.4	0.77	5	48.99	5.31	1.52	1.48	45.2	45.16
[2]G022.7576−00.4801	AGAL022.756−00.482	–	1.25	2.64	1.41	0.03	5	45.7	3.67	1.5	1.67	43.53	43.7
[1]G023.1974−00.0006	AGAL023.199+00.001	8	4.34	10.01	1.7	0.05	5	46.5	4.06	0.7	0.93	43.14	43.37
[1]G023.2654+00.0765	AGAL023.264+00.077	5.3	19.24	88.57	4.3	0.12	5	47.44	4.29	1.25	1.48	44.4	44.63
[1]G023.4553−00.2010	AGAL023.454−00.201	4.3	11.02	14.39	1.71	0.05	5	46.65	3.83	1.2	1.43	44.02	44.25
[1]G023.4835+00.0964	AGAL023.482+00.097	5.5	4.01	8.23	1.5	0.04	5	46.41	4.11	0.91	1.14	43.22	43.45
[1]G023.7110+00.1705	AGAL023.711+00.171	0.9	30.76	208.5	4.4	0.13	5	47.84	5.03	1.37	1.61	44.19	44.43
[1]G023.8618−00.1250	AGAL023.866−00.122	17.4	6.43	39.16	3.8	0.11	5	47.13	4.82	1.25	1.49	43.57	43.81
[1]G023.8985+00.0647	AGAL023.897+00.064	5	5.8	43.42	3.8	0.23	5	47.78	4.86	1.16	1.21	44.07	44.13
[1]G023.9564+00.1493	AGAL023.954+00.151	6.5	42.72	1161.18	13.1	0.3	5	48.38	5.15	1.67	1.85	44.9	45.08
[1]G024.1839+00.1199	AGAL024.183+00.121	5.4	3	3.79	–	–	5	46.32	4.16	1.06	1.33	43.22	43.48
[1]G024.4921−00.0386	AGAL024.491−00.039	5.7	19.3	140.12	4.2	0.12	5	47.66	4.9	1.31	1.54	44.06	44.29
[1]G024.5065−00.2224	AGAL024.506−00.221	6.9	15	205.57	6	0.17	5	47.79	4.73	1.39	1.62	44.46	44.68

Table C.1 continued from previous page

Radio Name	*Submm Name*	*Offset*	*Peak Flux*	*Int Flux*	*d*	*d*	*Freq*	*Log* $N_{\rm Ly}$	*Log* $L_{\rm bol}$	*Log*	*Log*	*Log*	*Log*
		["]	[Jy/beam]	[Jy]	["]	[pc]	[GHz]	[photons s^{-1}]	[$L_\odot$]	$L_{\rm bol}/M$	$L_{\rm bol}/M_{\rm corr}$	$N_{\rm Ly}/M$	$N_{\rm Ly}/M_{\rm corr}$
[1]G024.7898+00.0833	AGAL024.789+00.082	3.6	12.54	12.54	–	–	5	46.61	5.17	1.3	1.53	42.74	42.97
[1]G024.7889+00.0824	AGAL024.789+00.082	1.2	20.49	36.49	1.5	0.04	5	47.07	5.17	1.3	1.53	43.2	43.43
[2]G025.3053+00.5303	AGAL025.303+00.531	10.24	3.34	29.94	3	0.02	5	45.89	2.66	1.49	1.46	44.72	44.69
[1]G025.3824−00.1812	AGAL025.382−00.182	4	36.62	200.13	3.1	0.04	5	47.12	5.12	2.22	2.26	44.21	44.25
[1]G025.3809−00.1815	AGAL025.382−00.182	9.5	28.64	460.83	8.3	0.11	5	47.48	5.12	2.22	2.26	44.58	44.61
[1]G025.3948+00.0332	AGAL025.392+00.034	9.4	29.26	296.86	4.4	0.33	5	48.81	5.31	1.28	1.08	44.79	44.58
[1]G025.3970+00.5614	AGAL025.396+00.562	5.6	78.34	121.17	1.4	0.09	5	48.32	5.07	1.18	1.11	44.44	44.36
[1]G025.3983+00.5617	AGAL025.396+00.562	9.4	18.55	51.93	2	0.13	5	47.96	5.07	1.18	1.11	44.07	44
[1]G025.3991−00.1366	AGAL025.398−00.141	16.2	7.91	29.38	3	0.15	5	47.44	5.99	1.85	2.02	43.3	43.47
[1]G025.3981−00.1411	AGAL025.398−00.141	1.2	125.02	2132.24	8.5	0.42	5	49.3	5.99	1.85	2.02	45.16	45.33
[1]G025.7157+00.0487	AGAL025.709+00.044	28.8	10.66	20.79	1.8	0.09	5	47.29	5.06	1.53	1.7	43.77	43.93
[1]G025.8011−00.1568	AGAL025.801−00.156	3.8	22.54	31.95	1.79	0.09	5	47.48	4.95	1.55	1.72	44.08	44.25
[1]G026.0916−00.0565	AGAL026.089−00.056	9.2	3.99	11.59	2.1	0.14	5	47.28	4.75	1.17	1.13	43.71	43.66
[1]G026.1094−00.0937	AGAL026.107−00.094	7	4.26	4.72	–	–	5	46.89	4.69	1.83	1.78	44.02	43.97
[2]G026.5443+00.4160	AGAL026.546+00.416	6.97	12.52	556.31	7.4	0.36	5	48.69	5.23	1.73	1.91	45.19	45.37
[1]G026.5444+00.4169	AGAL026.546+00.416	6.4	12.23	413.36	12.5	0.6	5	48.56	5.23	1.73	1.91	45.06	45.24
[1]G026.5976−00.0236	AGAL026.596−00.022	7.5	31.06	69.92	2.2	0.02	5	46.31	3.09	1.3	1.27	44.52	44.49
[1]G026.6089−00.2121	AGAL026.607−00.212	5.3	25.51	201.41	6.4	0.24	5	48.02	3.95	1.4	1.64	45.47	45.71
[1]G027.1859−00.0816	AGAL027.184−00.081	6.3	10.8	19.78	1.4	0.09	5	47.5	5.27	1.47	1.41	43.7	43.65
[1]G027.2800+00.1447	AGAL027.279+00.147	10.8	41.16	428.04	5.5	0.36	5	48.84	4.92	1.35	1.29	45.27	45.21
[1]G027.3644−00.1657	AGAL027.366−00.166	5.6	31.44	60.14	1.7	0.07	5	47.54	4.85	0.99	1.21	43.69	43.91
[1]G027.5637+00.0845	AGAL027.564+00.086	10.4	5.96	162.53	12.2	0.57	5	48.14	4.6	0.9	1.07	44.44	44.61
[1]G027.9352+00.2056	AGAL027.936+00.206	2.5	3.89	4.44	–	–	5	45.46	3.42	1.12	1.15	43.17	43.2
[1]G027.9782+00.0789	AGAL027.978+00.077	2.4	4.97	124	9.3	0.2	5	47.35	4.23	1.39	1.52	44.51	44.64
[1]G028.2003−00.0494	AGAL028.199−00.049	4.4	99.1	161.66	1.6	0.05	5	47.73	5.11	1.43	1.63	44.05	44.25
[1]G028.1985−00.0503	AGAL028.199−00.049	5.1	33.62	136.26	2.7	0.08	5	47.66	5.11	1.43	1.63	43.98	44.17

Table C.1 continued from previous page

Radio Name	*Submm Name*	*Offset* ["]	*Peak Flux* [Jy/beam]	*Int Flux* [Jy]	*d* ["]	*d* [pc]	*Freq* [GHz]	*Log* $N_{\rm Ly}$ [photons s^{-1}]	*Log* $L_{\rm bol}$ [$L_\odot$]	*Log* $L_{\rm bol}/M$	*Log* $L_{\rm bol}/M_{\rm corr}$	*Log* $N_{\rm Ly}/M$	*Log* $N_{\rm Ly}/M_{\rm corr}$
[1]G028.2879−00.3641	AGAL028.288−00.362	6.3	98	552.77	4.4	0.25	5	48.83	5.9	1.8	1.85	44.73	44.78
[1]G028.4518+00.0027	AGAL028.451+00.002	3.5	14.14	33.75	1.8	0.13	5	47.86	4.57	0.85	0.63	44.14	43.92
[1]G028.5816+00.1447	AGAL028.581+00.146	4.2	3.95	40.03	5.1	0.38	5	47.93	4.18	0.97	0.75	44.73	44.5
[1]G028.6082+00.0185	AGAL028.608+00.019	4.4	41.36	210.15	3.3	0.12	5	48.02	4.95	1.35	1.56	44.41	44.62
[1]G028.6523+00.0273	AGAL028.649+00.027	10.4	16.62	228.85	5.5	0.2	5	48.05	4.52	1.09	1.31	44.62	44.83
[1]G028.6869+00.1770	AGAL028.687+00.177	2	12.67	102.98	5.1	0.24	5	47.94	4.42	1.62	1.77	45.14	45.29
[1]G029.9559−00.0168	AGAL029.954−00.016	11.3	196.18	3116.2	9.5	0.24	5	48.88	5.7	1.95	2.1	45.13	45.28
[1]G030.0096−00.2734	AGAL030.008−00.272	4.8	3.91	4.54	–	–	5	46.04	3.76	0.54	0.69	42.82	42.97
[1]G030.2527+00.0540	AGAL030.251+00.054	6	7.35	96.79	5.6	0.14	5	47.37	3.99	1.11	1.26	44.5	44.65
[1]G030.5313+00.0205	AGAL030.534+00.021	9.3	8.76	85.54	5.3	0.07	5	46.75	3.95	1.53	1.56	44.34	44.36
[1]G030.5353+00.0204	AGAL030.534+00.021	2.7	80.02	710.36	6.1	0.08	5	47.67	3.95	1.53	1.56	45.26	45.28
[1]G030.5887−00.0428	AGAL030.588−00.042	4.4	65.1	92.37	–	–	5	46.78	4.05	1.21	1.24	43.95	43.97
[1]G030.7197−00.0829	AGAL030.718−00.082	8.9	101.36	969.33	4.3	0.11	5	48.37	4.74	1.04	1.19	44.68	44.83
[1]G030.7532−00.0511	AGAL030.753−00.051	2.4	62.72	301.66	2.9	0.07	5	47.87	5.55	2.03	2.18	44.35	44.5
[1]G030.8662+00.1143	AGAL030.866+00.114	0.8	134.58	325.47	2.7	0.04	5	47.33	4.12	1.57	1.6	44.79	44.81
[1]G030.9581+00.0869	AGAL030.959+00.086	5.9	6.56	25.79	2.8	0.04	5	46.23	3.59	1.23	1.25	43.86	43.88
[1]G031.0495+00.4697	AGAL031.054+00.469	17	9.63	13.64	1.08	0.01	5	45.69	3.5	1.46	1.44	43.66	43.64
[1]G031.0595+00.0922	AGAL031.059+00.094	7.2	6.5	11.7	1.3	0.08	5	47.26	4.55	1.7	1.61	44.41	44.33
[2]G031.0709+00.0508	AGAL031.071+00.049	4.52	8.3	248.6	–	–	5	47.21	3.76	1.9	1.92	45.35	45.37
[1]G031.1596+00.0448	AGAL031.158+00.047	12.4	18.7	23.83	–	–	5	46.19	3.27	0.9	0.92	43.82	43.84
[1]G031.1590+00.0465	AGAL031.158+00.047	6.4	3.89	7.04	1.4	0.02	5	45.66	3.27	0.9	0.92	43.29	43.31
[1]G031.2435−00.1103	AGAL031.243−00.111	4.1	133.77	353.06	2.2	0.14	5	48.72	5.28	1.6	1.53	45.04	44.97
[1]G031.2448−00.1132	AGAL031.243−00.111	11.3	8.6	37.39	2.8	0.18	5	47.75	5.28	1.6	1.53	44.06	44
[1]G031.2801+00.0632	AGAL031.281+00.062	6.7	13.05	268.86	9.2	0.23	5	47.82	4.84	1.24	1.39	44.21	44.36
[2]G031.3940−00.2590	AGAL031.396−00.257	2.26	21.6	120.1	–	–	5	47.47	4.85	1.74	1.89	44.36	44.51
[1]G031.3959−00.2570	AGAL031.396−00.257	5.3	6.57	80.96	9.9	0.25	5	47.29	4.85	1.74	1.89	44.19	44.34

Table C.1 continued from previous page

Radio Name	*Submm Name*	*Offset* ["]	*Peak Flux* [Jy/beam]	*Int Flux* [Jy]	*d* ["]	*d* [pc]	*Freq* [GHz]	*Log* $N_{\rm Ly}$ [photons s^{-1}]	*Log* $L_{\rm bol}$ [$L_\odot$]	*Log* $L_{\rm bol}/M$	*Log* $L_{\rm bol}/M_{\rm corr}$	*Log* $N_{\rm Ly}/M$	*Log* $N_{\rm Ly}/M_{\rm corr}$
[1]G031.4130+00.3065	AGAL031.412+00.307	1.5	47.87	954.8	9.3	0.23	5	48.37	4.85	1.06	1.21	44.58	44.74
[1]G031.5815+00.0744	AGAL031.581+00.077	11.3	5.61	14.48	1.9	0.05	5	46.55	4.44	1.35	1.5	43.45	43.61
[1]G032.1502+00.1329	AGAL032.149+00.134	9.3	23.24	533.63	12.3	0.31	5	48.11	4.57	1.18	1.32	44.72	44.87
[1]G032.2730−00.2258	AGAL032.272−00.226	1.1	18.09	309.28	9.7	0.6	5	48.66	4.61	1.31	1.24	45.36	45.29
[1]G032.4727+00.2036	AGAL032.471+00.204	7.5	49.71	97.38	1.7	0.02	5	46.9	3.48	0.97	1.01	44.39	44.43
[1]G032.7398+00.1940	AGAL032.739+00.192	6.1	3.04	3.39	–	–	5	46.71	4.13	0.42	0.33	43.01	42.91
[1]G032.7441−00.0755	AGAL032.744−00.076	1.1	5.61	7.93	–	–	5	46.99	5	1.15	1.15	43.14	43.13
[1]G032.7492−00.0643	AGAL032.744−00.076	45.6	6.43	13.12	1.5	0.09	5	47.21	5	1.15	1.15	43.36	43.35
[1]G032.7982+00.1937	AGAL032.797+00.191	11	9.81	17.22	1.3	0.08	5	47.42	6.1	1.81	1.71	43.13	43.04
[1]G032.7966+00.1909	AGAL032.797+00.191	2.9	279.13	3123.37	9.9	0.62	5	49.68	6.1	1.81	1.71	45.39	45.3
[1]G032.9273+00.6060	AGAL032.926+00.606	8.7	44.3	285.57	6.6	0.48	5	48.77	4.73	1.37	1.12	45.4	45.16
[1]G033.1328−00.0923	AGAL033.133−00.092	1.1	101.04	378.59	3.7	0.17	5	48.48	5.03	1.34	1.44	44.79	44.9
[1]G033.4163−00.0036	AGAL033.416−00.002	8.2	7.14	75.16	8.6	0.23	5	47.3	4.15	0.92	1.05	44.07	44.2
[1]G033.8100−00.1864	AGAL033.811−00.187	4.9	57.46	107.63	1.6	0.08	5	48.05	5.23	1.79	1.83	44.62	44.65
[1]G033.9145+00.1105	AGAL033.914+00.109	2.4	95.47	842.22	10	0.32	5	48.51	5.17	1.49	1.64	44.82	44.98
[1]G034.0901+00.4365	AGAL034.089+00.436	3.9	3.95	9.62	1.9	0.11	5	47.07	4.43	1.14	1.11	43.78	43.76
[2]G034.1335+00.4707	AGAL034.133+00.471	3.65	11.74	454.19	8.41	0.47	5	48.74	4.96	1.53	1.51	45.3	45.29
[1]G034.1324+00.4700	AGAL034.133+00.471	1.3	11.16	425.01	10	0.56	5	48.71	4.96	1.53	1.51	45.27	45.26
[1]G034.1978−00.5912	AGAL034.196−00.592	8.6	2.24	10.54	2.9	0.05	5	46.09	3.6	1.23	1.28	43.72	43.78
[1]G034.2573+00.1523	AGAL034.258+00.154	6.6	50.41	50.41	–	–	5	46.06	4.79	1.48	1.43	42.76	42.7
[1]G034.2581+00.1533	AGAL034.258+00.154	3.8	35.87	35.87	–	–	5	45.92	4.79	1.48	1.43	42.61	42.55
[1]G034.2572+00.1535	AGAL034.258+00.154	1.3	328.48	1762.63	5.6	0.04	5	47.61	4.79	1.48	1.43	44.3	44.25
[1]G034.4032+00.2277	AGAL034.401+00.226	10.9	6.61	8.92	–	–	5	45.31	3.5	0.92	0.87	42.74	42.68
[1]G034.5920+00.2434	AGAL034.591+00.242	5.3	6.13	20.23	2.3	0.17	5	47.61	4.12	0.98	0.72	44.48	44.22
[1]G035.0242+00.3502	AGAL035.026+00.349	7	10.7	11.44	–	–	5	45.74	4.11	1.58	1.57	43.21	43.2
[2]G035.1989−00.7422	AGAL035.197−00.742	7.27	2.1	3.5	0.83	0.01	5	45.18	–	–	–	41.82	41.79

Table C.1 continued from previous page

Radio Name	*Submm Name*	*Offset* ["]	*Peak Flux* [Jy/beam]	*Int Flux* [Jy]	*d* ["]	*d* [pc]	*Freq* [GHz]	*Log* N_{Ly} [photons s^{-1}]	*Log* L_{bol} [$L_\odot$]	*Log* L_{bol}/M	*Log* L_{bol}/M_{corr}	*Log* N_{Ly}/M	*Log* N_{Ly}/M_{corr}
[2]G035.1958−00.7436	AGAL035.197−00.742	7.27	2.43	6	1.4	0.01	5	45.42	–	–	–	42.05	42.03
[1]G035.4669+00.1394	AGAL035.466+00.141	8.3	33.35	317.6	4.9	0.11	5	47.8	4.67	1.4	1.5	44.53	44.63
[1]G035.5781−00.0305	AGAL035.579−00.031	3.1	75.96	187.75	2	0.1	5	48.26	5.31	1.46	1.49	44.41	44.44
[1]G036.4062+00.0221	AGAL036.406+00.021	4.5	7.94	9.31	–	–	5	46.01	3.87	1.49	1.53	43.63	43.68
[1]G036.4057+00.0226	AGAL036.406+00.021	6.3	14.53	22.34	1.1	0.02	5	46.39	3.87	1.49	1.53	44.01	44.06
[2]G036.8777−00.4731	AGAL036.878−00.474	4.52	3.48	5.65	1.05	0.05	5	46.7	4.05	0.83	0.87	43.47	43.51
[2]G036.9210+00.4820	AGAL036.919+00.482	3.43	1.37	2.83	1.34	0.1	5	46.75	4.2	1.12	0.86	43.67	43.41
[2]G036.9204+00.4825	AGAL036.919+00.482	3.43	1.75	4.23	1.56	0.11	5	46.92	4.2	1.12	0.86	43.85	43.58
[1]G037.5457−00.1120	AGAL037.546−00.112	3.1	34.46	406.46	8	0.38	5	48.54	5.1	1.59	1.63	45.03	45.07
[1]G037.7347−00.1128	AGAL037.734−00.112	2.2	11.69	16.02	–	–	5	47.13	4.6	1.1	1.14	43.63	43.67
[2]G037.7567+00.5603	AGAL037.757+00.561	–	1.38	45.83	7.54	0.03	5	45.52	1.82	0.98	0.87	44.69	44.58
[1]G037.8209+00.4125	AGAL037.819+00.412	6.3	10.74	20.24	1.6	0.1	5	47.44	4.77	1.15	1.04	43.82	43.71
[1]G037.8197+00.4140	AGAL037.819+00.412	6.2	3.34	25.99	4	0.24	5	47.55	4.77	1.15	1.04	43.93	43.82
[1]G037.8683−00.6008	AGAL037.867−00.601	2.8	38.53	210.28	5	0.24	5	48.28	–	–	–	45.01	45.03
[1]G037.8731−00.3996	AGAL037.874−00.399	1.5	255.65	2561.21	8.8	0.41	5	49.34	5.72	1.92	1.96	45.54	45.57
[1]G038.6465−00.2260	AGAL038.646−00.226	3	4.12	11.52	2	0.05	5	46.36	–	–	–	44	44.06
[1]G038.6529+00.0875	AGAL038.652+00.087	1.9	6.94	7.84	–	–	5	47.18	4.02	0.57	0.29	43.73	43.45
[2]G038.6932−00.4525	AGAL038.694−00.452	2.3	11.52	26.54	1.46	0.07	5	47.36	4.24	1.05	1.07	44.16	44.18
[1]G038.6934−00.4524	AGAL038.694−00.452	2.3	6.2	19.88	2.2	0.1	5	47.24	4.24	1.05	1.07	44.04	44.06
[1]G038.8756+00.3080	AGAL038.876+00.309	3.5	77.93	311.31	3.2	0.22	5	48.75	4.74	1.29	1.04	45.31	45.05
[1]G039.1956+00.2255	AGAL039.196+00.226	2.2	43.81	62.27	1.2	0.08	5	48.07	4.39	1.32	1.05	45.01	44.73
[1]G039.8824−00.3460	AGAL039.884−00.346	5.6	48.46	276.87	3.5	0.16	5	48.33	4.65	1.3	1.33	44.99	45.02
[1]G040.4251+00.7002	AGAL040.424+00.699	4.5	4.8	11.1	2.5	0.14	5	47.15	4.82	1.22	1.11	43.55	43.44
[1]G041.7419+00.0973	AGAL041.741+00.097	4.1	41.62	227.4	5.4	0.31	5	48.45	4.62	1.41	1.29	45.24	45.12
[1]G042.1090−00.4469	AGAL042.108−00.447	4.7	9.88	14.8	1.1	0.02	5	46.19	3.69	1.29	1.3	43.79	43.8
[1]G042.4345−00.2605	AGAL042.434−00.261	1.2	21.95	83.65	3.3	0.07	5	47.16	4	1.2	1.25	44.36	44.41

Table C.1 continued from previous page

Radio Name	*Submm Name*	*Offset* ["]	*Peak Flux* [Jy/beam]	*Int Flux* [Jy]	*d* ["]	*d* [pc]	*Freq* [GHz]	*Log* $N_{\rm Ly}$ [photons s^{-1}]	*Log* $L_{\rm bol}$ [$L_\odot$]	*Log* $L_{\rm bol}/M$	*Log* $L_{\rm bol}/M_{\rm corr}$	*Log* $N_{\rm Ly}/M$	*Log* $N_{\rm Ly}/M_{\rm corr}$
[1]G043.1489+00.0130	AGAL043.148+00.014	6.5	36.47	44.13	–	–	5	47.69	5.93	1.59	1.48	43.35	43.25
[1]G043.1520+00.0115	AGAL043.148+00.014	18.9	111.08	306.63	2.1	0.11	5	48.53	5.93	1.59	1.48	44.19	44.09
[2]G043.1470+00.0136	AGAL043.148+00.014	4.34	70.16	393.2	2.61	0.14	5	48.64	5.93	1.59	1.48	44.3	44.2
[2]G043.1459+00.0139	AGAL043.148+00.014	4.34	74.35	448.1	2.8	0.15	5	48.7	5.93	1.59	1.48	44.36	44.26
[1]G043.1460+00.0139	AGAL043.148+00.014	3.7	76.36	694.6	6	0.32	5	48.89	5.93	1.59	1.48	44.55	44.45
[2]G043.1616−00.0242	AGAL043.164−00.029	4.4	19.72	58.51	1.92	0.1	5	47.81	6.21	1.62	1.52	43.23	43.12
[1]G043.1651−00.0283	AGAL043.164−00.029	5.1	242.92	2714.29	9.5	0.51	5	49.48	6.21	1.62	1.52	44.89	44.79
[1]G043.1674+00.0128	AGAL043.166+00.011	8.9	61.62	74.54	–	–	5	47.92	6.91	1.75	1.65	42.76	42.66
[1]G043.1684+00.0124	AGAL043.166+00.011	11	63.6	63.6	–	–	5	47.85	6.91	1.75	1.65	42.69	42.59
[1]G043.1706−00.0003	AGAL043.166+00.011	43.8	115.85	170.72	1	0.05	5	48.28	6.91	1.75	1.65	43.12	43.02
[1]G043.1657+00.0116	AGAL043.166+00.011	2.9	65.21	98.25	1.1	0.06	5	48.04	6.91	1.75	1.65	42.88	42.78
[1]G043.1652+00.0129	AGAL043.166+00.011	7.8	98.11	160.07	1.4	0.08	5	48.25	6.91	1.75	1.65	43.09	42.99
[1]G043.1699+00.0115	AGAL043.166+00.011	14.9	21.68	43.79	1.5	0.08	5	47.69	6.91	1.75	1.65	42.53	42.43
[1]G043.1684+00.0087	AGAL043.166+00.011	11.7	78.74	185.25	1.8	0.1	5	48.31	6.91	1.75	1.65	43.16	43.06
[1]G043.1720+00.0080	AGAL043.166+00.011	24.6	38.57	98.59	2.1	0.11	5	48.04	6.91	1.75	1.65	42.88	42.78
[1]G043.1716+00.0001	AGAL043.166+00.011	44	16.42	51.74	2.2	0.12	5	47.76	6.91	1.75	1.65	42.6	42.5
[1]G043.1665+00.0106	AGAL043.166+00.011	2.9	218.73	1365.68	3.4	0.18	5	49.18	6.91	1.75	1.65	44.02	43.92
[1]G043.1677+00.0196	AGAL043.166+00.011	33.2	20.71	115.47	3.9	0.21	5	48.11	6.91	1.75	1.65	42.95	42.85
[1]G043.1763+00.0248	AGAL043.166+00.011	62.7	24.92	159.42	4.3	0.23	5	48.25	6.91	1.75	1.65	43.09	42.99
[1]G043.1701+00.0078	AGAL043.166+00.011	21.2	90.46	1108.08	7.4	0.4	5	49.09	6.91	1.75	1.65	43.93	43.83
[1]G043.1778−00.5181	AGAL043.179−00.519	6.8	12.49	181.65	7	0.29	5	48.07	4.97	1.22	1.24	44.32	44.34
[1]G043.2371−00.0453	AGAL043.236−00.047	9.1	29.18	178.78	3.5	0.19	5	48.3	5.14	1.21	1.11	44.37	44.27
[2]G043.3060−00.2110	AGAL043.306−00.212	5.51	6.91	8.59	0.52	0.01	5	46.13	4.08	1.37	1.41	43.43	43.47
[1]G043.3064−00.2114	AGAL043.306−00.212	4.7	7.85	20.08	2	0.04	5	46.5	4.08	1.37	1.41	43.8	43.83
[1]G043.7954−00.1274	AGAL043.794−00.127	4.4	19.29	24.58	1	0.03	5	46.9	5.09	1.83	1.88	43.64	43.7
[1]G043.7960−00.1286	AGAL043.794−00.127	7.8	3.71	9.78	1.8	0.05	5	46.5	5.09	1.83	1.88	43.24	43.3

Table C.1 continued from previous page

Radio Name	*Submm Name*	*Offset*	*Peak Flux*	*Int Flux*	*d*	*d*	*Freq*	*Log* $N_{\rm Ly}$	*Log* $L_{\rm bol}$	*Log*	*Log*	*Log*	*Log*
		["]	[Jy/beam]	[Jy]	["]	[pc]	[GHz]	[photons s^{-1}]	[$L_\odot$]	$L_{\rm bol}/M$	$L_{\rm bol}/M_{\rm corr}$	$N_{\rm Ly}/M$	$N_{\rm Ly}/M_{\rm corr}$
[1]G043.8894−00.7840	AGAL043.889−00.786	8.1	96.5	528.18	5.2	0.11	5	47.96	4.4	1.13	1.17	44.69	44.73
[1]G043.9675+00.9939	AGAL043.967+00.994	0.7	31.88	41.33	–	–	5	47.84	4.19	1.25	0.99	44.9	44.63
[1]G044.3103+00.0410	AGAL044.309+00.041	4.1	4.37	5.47	–	–	5	46.51	4.52	1.06	1.08	43.04	43.07
[1]G044.4228+00.5377	AGAL044.422+00.537	1.7	3.74	4.27	–	–	5	46.86	4.31	1.15	0.86	43.7	43.41
[1]G045.0712+00.1321	AGAL045.071+00.132	1.7	105.64	146.67	1.2	0.05	5	47.93	5.68	2.01	2.02	44.26	44.27
[1]G045.0694+00.1323	AGAL045.071+00.132	6.3	26.99	46.17	1.3	0.05	5	47.42	5.68	2.01	2.02	43.75	43.77
[1]G045.1242+00.1356	AGAL045.121+00.131	20	8.43	62.55	4.6	0.18	5	47.56	6.03	2.03	2.04	43.56	43.57
[1]G045.1223+00.1321	AGAL045.121+00.131	5.8	299.72	2984.27	7.3	0.28	5	49.24	6.03	2.03	2.04	45.24	45.25
[2]G045.4602+00.0617	AGAL045.454+00.061	5.77	6.63	14.76	1.83	0.07	5	46.97	5.84	1.89	1.88	43.02	43.01
[1]G045.4559+00.0613	AGAL045.454+00.061	6.2	10.18	51.59	3	0.12	5	47.52	5.84	1.89	1.88	43.56	43.56
[2]G045.4447+00.0511	AGAL045.454+00.061	5.77	9.06	78.29	5.25	0.21	5	47.7	5.84	1.89	1.88	43.74	43.74
[2]G045.4541+00.0594	AGAL045.454+00.061	5.77	78.96	1263.36	6.59	0.27	5	48.9	5.84	1.89	1.88	44.95	44.94
[1]G045.4545+00.0591	AGAL045.454+00.061	5.8	61.84	1029.45	7.5	0.31	5	48.82	5.84	1.89	1.88	44.86	44.86
[1]G045.4656+00.0452	AGAL045.466+00.046	2.8	48.33	62.26	–	–	5	47.6	5.63	1.74	1.73	43.7	43.69
[1]G048.6057+00.0228	AGAL048.606+00.022	1.3	26.75	36.16	–	–	5	47.58	5.65	1.6	1.45	43.53	43.38
[2]G048.6061+00.0240	AGAL048.606+00.022	17.18	3.33	3.8	0.38	0.02	5	46.6	5.65	1.6	1.45	42.55	42.4
[2]G048.6106+00.0283	AGAL048.606+00.022	17.18	2.26	4.55	1.29	0.07	5	46.68	5.65	1.6	1.45	42.63	42.48
[2]G048.6100+00.0269	AGAL048.606+00.022	17.18	6.86	61.24	3.76	0.2	5	47.81	5.65	1.6	1.45	43.76	43.61
[2]G048.6441+00.2249	AGAL048.634+00.231	2.23	4.51	8.97	1.19	0.06	5	46.97	4.19	0.75	0.6	43.53	43.38
[2]G048.9123−00.2925	AGAL048.919−00.277	–	4.3	31.13	3.02	0.08	5	46.9	5.3	1.55	1.56	43.14	43.15
[2]G048.9222−00.2757	AGAL048.919−00.277	–	2.5	23.61	3.51	0.09	5	46.78	5.3	1.55	1.56	43.02	43.03
[2]G048.9184−00.2619	AGAL048.919−00.277	–	2.59	25.87	3.58	0.09	5	46.82	5.3	1.55	1.56	43.06	43.07
[2]G048.9170−00.2962	AGAL048.919−00.277	–	3.37	37.99	3.86	0.1	5	46.98	5.3	1.55	1.56	43.23	43.24
[2]G048.9096−00.2881	AGAL048.919−00.277	–	2.7	41.52	4.57	0.12	5	47.02	5.3	1.55	1.56	43.27	43.28
[2]G048.9297−00.2796	AGAL048.931−00.281	–	5.13	51.55	3.6	0.09	5	47.12	4.32	1.39	1.4	44.18	44.2
[2]G048.9259−00.2797	AGAL048.931−00.281	–	2.61	41	4.63	0.12	5	47.02	4.32	1.39	1.4	44.08	44.1

Table C.1 continued from previous page

Radio Name	*Submm Name*	*Offset* ["]	*Peak Flux* [Jy/beam]	*Int Flux* [Jy]	*d* ["]	*d* [pc]	*Freq* [GHz]	*Log* $N_{\rm Ly}$ [photons s^{-1}]	*Log* $L_{\rm bol}$ [$L_\odot$]	*Log* $L_{\rm bol}/M$	*Log* $L_{\rm bol}/M_{\rm corr}$	*Log* $N_{\rm Ly}/M$	*Log* $N_{\rm Ly}/M_{\rm corr}$
[1]G048.9296−00.2793	AGAL048.931−00.281	4.5	12.15	185.39	6	0.15	5	47.67	4.32	1.39	1.4	44.74	44.75
[2]G048.9412−00.2851	AGAL048.953−00.286	–	1.85	11.8	2.94	0.08	5	46.47	4.22	0.96	0.98	43.22	43.23
[1]G048.9901−00.2988	AGAL048.991−00.299	3	5.44	7.53	0.55	0.01	5	46.28	–	–	–	42.39	42.4
[1]G049.2679−00.3374	AGAL049.268−00.337	1.5	5.97	102.61	6	0.15	5	47.41	4.49	0.98	0.99	43.9	43.91
[1]G049.3666−00.3010	AGAL049.369−00.301	9.2	29.71	180.93	3.4	0.09	5	47.66	–	–	–	43.73	43.75
[1]G049.3704−00.3012	AGAL049.369−00.301	4.4	42.62	414.43	4.4	0.11	5	48.02	–	–	–	44.09	44.11
[2]G049.4628−00.3817	AGAL049.472−00.367	70.38	31.41	229.7	3.04	0.08	5	47.76	6.38	1.97	1.98	43.35	43.36
[1]G049.4905−00.3688	AGAL049.489−00.369	5.7	335.65	3821.72	5.6	0.14	5	48.99	6.17	1.9	1.91	44.71	44.72
[2]G049.4917−00.3801	AGAL049.489−00.389	32.56	95.76	1350	4.35	0.11	5	48.53	6.29	1.79	1.8	44.03	44.04
[2]G049.4862−00.3805	AGAL049.489−00.389	32.56	98.21	1995	5.27	0.14	5	48.7	6.29	1.79	1.8	44.2	44.21
[2]G050.0457+00.7683	AGAL050.046+00.767	–	8.11	16.8	1.39	0.09	5	47.39	4.05	1.21	0.92	44.56	44.27
[2]G050.2833−00.3903	AGAL050.284−00.391	3.2	6.4	8.18	0.6	0.03	5	46.83	5.24	1.93	1.82	43.52	43.41
[1]G050.2834−00.3904	AGAL050.284−00.391	6.1	6.53	156.78	16.7	0.78	5	48.11	5.24	1.93	1.82	44.81	44.7
[1]G050.3152+00.6762	AGAL050.314+00.676	4.5	46.28	81.31	1.5	0.01	5	46.37	3.31	1.45	1.38	44.52	44.44
[1]G051.6785+00.7193	AGAL051.678+00.719	3.7	15.87	22.55	–	–	5	47.38	5.04	1.54	1.34	43.88	43.69
[2]G052.2025+00.7216	AGAL052.201+00.721	11.32	0.91	7.81	3.76	0.2	5	46.92	4.53	1.27	1.07	43.66	43.46
[1]G052.7533+00.3340	AGAL052.752+00.334	1.7	16.62	386.03	8.5	0.4	5	48.51	4.35	1.27	1.14	45.43	45.3
[2]G052.7530+00.3343	AGAL052.752+00.334	1.84	8.99	388.6	10	0.47	5	48.51	4.35	1.27	1.14	45.43	45.3
[2]G053.0370+00.1122	AGAL053.037+00.112	6.09	1.1	1.31	0.71	0.03	5	46.05	4.26	1.02	0.87	42.82	42.66
[2]G053.1652−00.2471	AGAL053.164−00.246	5.95	1.34	1.51	0.73	0.02	5	45.6	3.65	1	0.98	42.95	42.92
[2]G053.1864+00.2088	AGAL053.184+00.209	10.62	2.75	95.89	8.33	0.4	5	47.92	4.07	1.09	0.94	44.93	44.78
[1]G053.9589+00.0320	AGAL053.959+00.031	4.4	21.48	46	1.8	0.03	5	46.82	3.64	1.34	1.3	44.52	44.48
[2]G055.1611−00.2978	AGAL055.158−00.299	0.45	0.79	1.49	1.14	0.02	5	45.31	3.69	1.06	1.02	42.68	42.64
[2]G055.1586−00.2985	AGAL055.158−00.299	0.45	0.77	10.42	5.37	0.1	5	46.15	3.69	1.06	1.02	43.53	43.49
[2]G057.5473−00.2718	AGAL057.548−00.269	9.77	5.99	85.66	6.31	0.27	5	47.79	4.54	1.7	1.53	44.94	44.78
[1]G058.7739+00.6457	AGAL058.774+00.644	5.7	1.44	4.76	2.3	0.02	5	45.32	3.43	1.4	1.3	43.28	43.19

Table C.1 continued from previous page

Radio Name	*Submm Name*	*Offset* ["]	*Peak Flux* [Jy/beam]	*Int Flux* [Jy]	*d* ["]	*d* [pc]	*Freq* [GHz]	*Log* N_{Ly} [photons s^{-1}]	*Log* L_{bol} [$L_\odot$]	*Log* L_{bol}/M	*Log* L_{bol}/M_{corr}	*Log* N_{Ly}/M	*Log* N_{Ly}/M_{corr}
[2]G058.7737+00.6456	AGAL058.774+00.644	–	0.96	17.66	4.97	0.05	5	45.89	3.43	1.4	1.3	43.85	43.76
[1]G059.6027+00.9118	AGAL059.602+00.912	1.9	53.77	68.76	–	–	5	46.88	3.98	1.42	1.35	44.32	44.25
[2]G280.6213−01.1870	AGAL280.621−01.187	2.57	11.56	64.29	5.8	0.2	4.8	47.46	4.1	1.27	0.96	44.63	44.32
[2]G281.5860−00.9710	AGAL281.586−00.972	5.24	52.41	764.6	9.22	0.31	4.8	48.52	4.83	1.29	1	44.98	44.69
[2]G281.8450−01.6090	AGAL281.846−01.609	3.6	18.9	47.78	2.8	0.09	4.8	47.32	4.4	1.35	1.06	44.27	43.98
[2]G283.2268−00.9355	AGAL283.227−00.936	2.84	11.46	11.27	0.7	0.02	4.8	46.69	4.58	2.11	1.82	44.22	43.93
[2]G284.0154−00.8575	AGAL284.016−00.857	0.23	253	371.5	1.85	0.05	4.8	48.04	5.17	1.32	1.09	44.18	43.96
[2]G285.2625−00.0522	AGAL285.264−00.049	–	87.15	292	3.64	–	4.8	–	–	–	–	–	–
[2]G285.5974−00.8514	AGAL285.596−00.851	5.9	1.82	2.24	1.16	0.03	4.8	45.89	4.24	1.33	1.1	42.98	42.75
[2]G286.3941−01.3516	AGAL286.394−01.351	3.3	107.9	174.9	1.61	0.07	4.8	48.14	5.02	1.32	0.95	44.44	44.07
[2]G289.0807−00.4082	AGAL289.083−00.411	10.2	26.74	34.78	1.31	–	4.8	–	–	–	–	–	–
[2]G289.0843−00.4131	AGAL289.083−00.411	10.2	11.53	15.29	1.41	–	4.8	–	–	–	–	–	–
[2]G289.8799−00.7974	AGAL289.881−00.797	3.18	82.21	427	4.35	0.17	4.8	48.4	4.85	1.58	1.31	45.13	44.86
[2]G290.8776−01.2180	AGAL290.878−01.217	2.39	2.35	3.76	1.75	0.07	4.8	46.33	3.97	1.22	0.96	43.58	43.33
[2]G291.0671−00.7947	AGAL291.066−00.796	5.75	2.6	14.09	4.26	0.17	4.8	46.95	4.37	1.05	0.77	43.63	43.36
[2]G293.8284−00.7443	AGAL293.828−00.746	6.1	20.13	98	4.49	0.22	4.8	47.97	4.9	1.36	1.02	44.43	44.09
[2]G293.9626−00.9781	AGAL293.963−00.977	6.55	8.09	24.77	2.79	0.14	4.8	47.38	4.57	1.57	1.23	44.38	44.04
[2]G295.1520−00.5881	AGAL295.153−00.587	3.16	11.37	12	1.2	0.06	4.8	47.1	4.27	0.47	0.11	43.3	42.95
[2]G295.5568−01.3787	AGAL295.556−01.377	9.14	5.68	40.63	5.87	0.32	4.8	47.66	3.41	0.49	0.11	44.73	44.36
[2]G297.2529−00.7540	AGAL297.254−00.752	6.2	1.77	2.36	1.05	–	4.8	–	–	–	–	–	–
[2]G297.4568−00.7629	AGAL297.456−00.762	2.49	3.12	3.36	0.4	0.02	4.8	46.54	3.66	0.42	0.09	43.3	42.97
[2]G298.1828−00.7859	AGAL298.182−00.786	3.71	152.8	1711	8.38	0.42	4.8	49.22	5.24	1.49	1.2	45.47	45.17
[2]G298.2243−00.3391	AGAL298.224−00.339	0.35	369.9	1348	3.39	0.08	4.8	48.43	5.78	2.11	2.02	44.76	44.67
[2]G298.8325+00.1272	AGAL298.833+00.126	5.02	33.63	57.6	1.96	0.1	4.8	47.75	4.42	1.07	0.78	44.4	44.11
[2]G298.8604−00.4347	AGAL298.859−00.437	10.89	79.46	158.6	2.15	0.12	4.8	48.24	5.39	1.18	0.85	44.03	43.7
[2]G300.9687+01.1475	AGAL300.969+01.146	6.99	88.57	101.5	0.77	0.01	4.8	47.02	5.61	2.31	2.24	43.72	43.65

Table C.1 continued from previous page

Radio Name	*Submm Name*	*Offset* ["]	*Peak Flux* [Jy/beam]	*Int Flux* [Jy]	*d* ["]	*d* [pc]	*Freq* [GHz]	*Log* N_{Ly} [photons s^{-1}]	*Log* L_{bol} [$L_\odot$]	*Log* L_{bol}/M	*Log* L_{bol}/M_{corr}	*Log* N_{Ly}/M	*Log* N_{Ly}/M_{corr}
[2]G301.1364−00.2256	AGAL301.136−00.226	2.21	79.16	83.83	0.42	0.01	4.8	47.2	5.39	1.74	1.67	43.55	43.48
[2]G301.1364−00.2235	AGAL301.136−00.226	2.21	115.2	126.3	0.73	0.02	4.8	47.38	5.39	1.74	1.67	43.73	43.66
[2]G301.7314+01.1034	AGAL301.731+01.104	4.18	56.23	113.6	2.37	0.04	4.8	47.04	3.84	0.89	0.82	44.09	44.02
[2]G301.8144+00.7818	AGAL301.814+00.781	3.28	3.08	42.14	8.12	0.14	4.8	46.67	4.12	1.56	1.5	44.11	44.04
[2]G302.0218+00.2539	AGAL302.021+00.251	11.9	47.89	59.48	0.81	0.02	4.8	46.99	3.92	1.2	1.14	44.27	44.22
[2]G302.1525−00.9485	AGAL302.149−00.949	11.73	5.66	39.17	6.52	0.35	4.8	47.64	4.52	1.41	1.13	44.52	44.24
[2]G302.4868−00.0315	AGAL302.486−00.031	4.42	10.18	23.41	2.67	0.04	4.8	46.33	3.73	1.21	1.15	43.81	43.74
[2]G303.1173−00.9714	AGAL303.118−00.972	3.19	192.9	411.8	2.45	0.02	4.8	46.98	3.03	1.62	1.52	45.57	45.47
[2]G303.5351−00.5971	AGAL303.536−00.597	3.08	5.04	8.68	2.05	0.1	4.8	46.93	4.03	0.82	0.59	43.72	43.49
[2]G303.9976+00.2801	AGAL303.999+00.279	6.85	6.56	33.04	4.97	0.28	4.8	47.6	4.23	1.35	1.06	44.73	44.43
[2]G305.1961+00.0331	AGAL305.196+00.034	1.47	155.7	1361	6.68	0.12	4.8	48.25	5.13	1.79	1.75	44.91	44.87
[2]G307.7358−00.5944	AGAL307.736−00.596	5.01	2.27	2.89	1.18	0.07	4.8	46.63	4.05	0.91	0.58	43.49	43.16
[2]G308.0299−01.0525	AGAL308.029−01.052	3	17.06	29.06	1.55	0.1	4.8	47.67	4.72	1.41	1.05	44.37	44
[2]G308.0561−00.3961	AGAL308.057−00.397	–	43.71	54.09	0.95	0	4.8	45.59	2.63	0.97	0.85	43.93	43.81
[2]G308.9176+00.1218	AGAL308.917+00.122	3.09	51.05	247.4	4	0.08	4.8	47.53	5.03	2.05	2.03	44.55	44.53
[2]G309.1760−00.0277	AGAL309.179−00.031	8.69	2.72	5.1	1.78	0.08	4.8	46.61	4.5	1.28	1.17	43.38	43.27
[2]G309.1785−00.0287	AGAL309.179−00.031	8.69	2.53	7.57	2.62	0.12	4.8	46.78	4.5	1.28	1.17	43.55	43.44
[2]G309.8888+00.3975	AGAL309.891+00.397	7.21	3.45	1.25	3.42	0.09	4.8	45.53	4.86	1.77	1.77	42.44	42.44
[2]G309.9207+00.4787	AGAL309.921+00.477	4.47	138.6	220.2	1.42	0.04	4.8	47.78	5.32	1.8	1.8	44.25	44.25
[2]G311.1361−00.2373	AGAL311.139−00.236	12.01	3.1	3	0.99	0.06	4.8	46.68	4.29	0.97	0.65	43.36	43.04
[2]G311.1790−00.0725	AGAL311.177−00.072	5.42	1.99	4.84	2.6	0.03	4.8	45.5	3.22	1.07	1.03	43.36	43.32
[2]G311.4262+00.5966	AGAL311.424+00.597	7.79	3.24	24.88	5.13	0.18	4.8	47.09	4.44	2.06	2.05	44.71	44.7
[2]G311.6275+00.2902	AGAL311.626+00.289	7.55	137.8	460.9	2.85	0.06	4.8	47.84	4.95	1.7	1.71	44.59	44.6
[2]G311.6427−00.3801	AGAL311.642−00.381	2.65	87.21	101.3	0.8	0.05	4.8	48.23	5.15	1.48	1.15	44.56	44.23
[2]G312.1083+00.3085	AGAL312.108+00.309	–	27.42	287.47	7.16	0.12	4.8	47.47	4.68	1.8	1.79	44.6	44.58
[2]G312.3073+00.6607	AGAL312.306+00.661	4.47	11.43	20.47	1.2	0.01	4.8	45.26	2.56	1.57	1.46	44.27	44.16

Table C.1 continued from previous page

Radio Name	*Submm Name*	*Offset* ["]	*Peak Flux* [Jy/beam]	*Int Flux* [Jy]	*d* ["]	*d* [pc]	*Freq* [GHz]	*Log* N_{Ly} [photons s^{-1}]	*Log* L_{bol} [$L_\odot$]	*Log* L_{bol}/M	*Log* L_{bol}/M_{corr}	*Log* N_{Ly}/M	*Log* N_{Ly}/M_{corr}
^{2}G312.3834−00.4154	AGAL312.383−00.416	2.34	2.75	3	0.99	0.05	4.8	46.39	4.47	1.33	1.25	43.24	43.17
^{2}G312.5476−00.2810	AGAL312.546−00.281	6.19	7.49	9.54	1.02	0.05	4.8	46.91	–	–	–	43.63	43.54
^{2}G314.2200+00.2730	AGAL314.219+00.271	8.13	8.91	12.84	3.5	0.07	4.8	46.31	4.75	1.36	1.38	42.92	42.94
^{2}G314.2208+00.2725	AGAL314.219+00.271	8.13	4.96	5.92	3.5	0.07	4.8	45.97	4.75	1.36	1.38	42.58	42.6
^{2}G316.1387−00.5026	AGAL316.139−00.506	11.73	13.85	1864	24.77	0.92	4.8	49	5.2	1.53	1.57	45.33	45.36
^{2}G317.4288−00.5607	AGAL317.429−00.561	1.01	5.9	6.64	0.72	0.05	4.8	47.09	5.37	1.6	1.29	43.32	43.01
^{2}G317.8893−00.0579	AGAL317.889−00.059	3.88	4.64	6.36	1.19	0.08	4.8	47.02	4.8	1.19	0.94	43.41	43.16
^{2}G318.7249−00.2226	AGAL318.724−00.224	6.09	12.93	28.03	2.34	0.13	4.8	47.49	4.56	1.49	1.41	44.42	44.34
^{2}G318.9144−00.1639	AGAL318.914−00.164	0.74	122.2	1308	6.2	0.34	4.8	49.17	5.58	1.78	1.7	45.36	45.29
^{2}G319.1628−00.4205	AGAL319.161−00.422	9.9	56.19	332.4	4.61	0.26	4.8	48.6	5.41	1.23	1.13	44.43	44.32
^{2}G319.3985−00.0123	AGAL319.399−00.012	163.35	47.49	60.55	0.96	0.05	4.8	47.86	5.74	1.89	1.8	44.01	43.92
^{2}G319.3997−00.0126	AGAL319.399−00.012	163.35	80.76	141.9	1.52	0.09	4.8	48.23	5.74	1.89	1.8	44.38	44.29
^{2}G319.4519−00.0217	AGAL319.451−00.022	4.88	38.49	79.77	1.85	0.1	4.8	47.98	4.7	1.88	1.78	45.16	45.07
^{2}G320.2336−00.2836	AGAL320.232−00.284	–	160.6	267.7	1.63	0.07	4.8	48.25	5.16	1.37	1.43	44.46	44.52
^{2}G320.4155+00.1170	AGAL320.414+00.116	6.74	4.29	15.3	3.04	0.18	4.8	47.33	5.16	1.24	1.09	43.4	43.26
^{2}G320.4272+00.1029	AGAL320.427+00.102	1.79	6.67	6.46	1.02	0.06	4.8	46.96	4.96	1.19	1.05	43.19	43.04
^{2}G320.6742+00.2456	AGAL320.676+00.244	6.65	9.83	13.56	1.29	0.02	4.8	46.22	3.78	0.89	0.93	43.33	43.37
^{2}G320.7778+00.2423	AGAL320.779+00.244	7.67	7.97	18.54	2.33	0.14	4.8	47.42	4.82	1.01	0.86	43.61	43.46
^{2}G321.1253−00.2654	AGAL321.126−00.266	3.35	13.4	24.4	1.78	0.12	4.8	47.63	4.49	1.22	0.98	44.36	44.12
^{2}G321.3803−00.3017	AGAL321.379−00.301	12.68	1.56	1.91	0.88	0.04	4.8	46.19	4.77	1.04	1.08	42.47	42.51
^{2}G321.7207+01.1734	AGAL321.719+01.176	9.38	58.88	2124	13.81	0.16	4.8	48.04	4.77	1.79	1.77	45.06	45.04
^{2}G323.9158+00.0336	AGAL323.917+00.034	5.43	22.16	156	9.57	0.46	4.8	48.15	4.77	1.14	1.19	44.52	44.56
^{2}G324.2018+00.1211	AGAL324.201+00.121	5.05	256.5	477.6	2.35	0.08	4.8	48.3	5.68	1.78	1.92	44.4	44.53
^{2}G324.2003+00.1196	AGAL324.201+00.121	5.05	286.6	1592	5.44	0.18	4.8	48.82	5.68	1.78	1.92	44.92	45.06
^{2}G326.4483−00.7485	AGAL326.449−00.749	3.84	4.54	4.7	1	0.02	4.8	45.78	3.99	1.39	1.46	43.19	43.26
^{2}G326.4725−00.3779	AGAL326.472−00.377	1.99	151.7	342.5	2.61	0.04	4.8	47.52	4.36	1.41	1.45	44.57	44.62

Table C.1 continued from previous page

Radio Name	*Submm Name*	*Offset* ["]	*Peak Flux* [Jy/beam]	*Int Flux* [Jy]	*d* ["]	*d* [pc]	*Freq* [GHz]	*Log* N_{Ly} [photons s^{-1}]	*Log* L_{bol} [$L_\odot$]	*Log* L_{bol}/M	*Log* L_{bol}/M_{corr}	*Log* N_{Ly}/M	*Log* N_{Ly}/M_{corr}
^{2}G326.7239+00.6147	AGAL326.724+00.614	4.23	70.97	258.7	1.99	0.02	4.8	46.88	4.55	1.8	1.76	44.13	44.09
^{2}G326.8863−00.2764	AGAL326.881−00.269	–	9.22	268.8	14.25	0.24	4.8	47.47	3.97	1.35	1.41	44.85	44.91
^{2}G327.1307+00.5257	AGAL327.129+00.526	–	15.31	17.55	0.83	0.02	4.8	46.59	3.02	0.33	0.45	43.9	44.02
^{2}G327.4019+00.4446	AGAL327.403+00.444	3.33	75.32	87.24	1	0.02	4.8	47.29	4.76	1.23	1.35	43.76	43.88
^{2}G327.6309−00.3577	AGAL327.629−00.359	–	8.85	240.26	17.86	0.36	4.8	47.58	4.27	1.71	1.81	45.02	45.12
^{2}G327.6288−00.3540	AGAL327.629−00.359	–	1.16	1.42	26.19	0.53	4.8	45.35	4.27	1.71	1.81	42.79	42.89
^{2}G327.6371−00.1460	AGAL327.638−00.147	–	2.67	2.67	1.1	0.01	4.8	45.21	2.66	0.63	0.64	43.18	43.19
^{2}G327.7599−00.3517	AGAL327.764−00.347	–	5.08	3.42	5.27	0.11	4.8	45.73	4.83	1.64	1.74	42.54	42.64
^{2}G327.8481+00.0179	AGAL327.848+00.016	7.86	11.79	18.33	1.93	0.03	4.8	46.2	2.96	1.42	1.46	44.66	44.69
^{2}G327.9009+00.1538	AGAL327.894+00.149	29.81	2.56	2.81	1.1	0.05	4.8	46.26	–	–	–	42.57	42.72
^{2}G328.1642+00.5867	AGAL328.166+00.587	6.68	4.63	5.23	0.77	0.03	4.8	46.37	4.32	1.16	1.33	43.21	43.39
^{2}G328.2364−00.5474	AGAL328.236−00.547	–	6.82	8.25	1.11	0.01	4.8	45.73	–	–	–	42.18	42.2
^{2}G328.4238−00.0893	AGAL328.424−00.087	–	10.07	21.36	2.02	0.17	4.8	47.77	4.18	0.91	0.49	44.5	44.08
^{2}G328.5739−00.5303	AGAL328.566−00.534	3.37	184.7	326.57	5.32	0.07	4.8	47.33	5.28	1.99	2.01	44.05	44.07
^{2}G328.5758−00.5290	AGAL328.566−00.534	3.37	71.26	259.87	5.32	0.07	4.8	47.23	5.28	1.99	2.01	43.95	43.97
^{2}G328.9589+00.5680	AGAL328.961+00.566	9.51	2.93	3.98	1.3	0.05	4.8	46.42	4.98	1.33	1.49	42.77	42.93
^{2}G328.9581+00.5659	AGAL328.961+00.566	9.51	6.99	14.09	2.2	0.09	4.8	46.97	4.98	1.33	1.49	43.32	43.48
^{2}G329.3376+00.1466	AGAL329.337+00.147	3.15	274.6	1292	4.73	0.14	4.8	48.62	5.69	2.01	2.19	44.94	45.12
^{2}G329.4213−00.1619	AGAL329.424−00.162	10.2	7.41	417.9	17.6	0.38	4.8	47.86	4.24	1.19	1.3	44.8	44.92
^{2}G329.4719+00.2147	AGAL329.472+00.216	4.23	36.1	594.1	10.46	0.3	4.8	48.28	4.83	1.42	1.6	44.88	45.05
^{2}G329.4772+00.8424	AGAL329.476+00.841	8.07	2.84	83.87	12.51	0.3	4.8	47.26	4.13	1.49	1.63	44.62	44.76
^{2}G329.5979+00.0563	AGAL329.599+00.054	–	13.18	78.52	5.57	0.16	4.8	47.4	4.4	1.43	1.61	44.44	44.61
^{2}G329.8152+00.1409	AGAL329.816+00.141	2.43	4.33	4.77	1.11	0.03	4.8	46.03	4.04	0.99	1.14	42.98	43.13
^{2}G330.2838+00.4933	AGAL330.284+00.492	3.66	33.99	44.93	1.46	0.04	4.8	47.07	4.11	1.21	1.37	44.17	44.34
^{2}G330.2959−00.3951	AGAL330.294−00.394	6.28	72.72	78.36	0.98	0.05	4.8	47.83	5.62	1.74	1.88	43.95	44.09
^{2}G330.2955−00.3927	AGAL330.294−00.394	6.28	164.3	194.4	1.04	0.05	4.8	48.22	5.62	1.74	1.88	44.35	44.48

Table C.1 continued from previous page

Radio Name	*Submm Name*	*Offset*	*Peak Flux*	*Int Flux*	*d*	*d*	*Freq*	*Log* $N_{\rm Ly}$	*Log* $L_{\rm bol}$	*Log*	*Log*	*Log*	*Log*
		["]	[Jy/beam]	[Jy]	["]	[pc]	[GHz]	[photons s^{-1}]	[$L_\odot$]	$L_{\rm bol}/M$	$L_{\rm bol}/M_{\rm corr}$	$N_{\rm Ly}/M$	$N_{\rm Ly}/M_{\rm corr}$
^{2}G330.2929−00.3932	AGAL330.294−00.394	6.28	173.7	279.3	2	0.1	4.8	48.38	5.62	1.74	1.88	44.5	44.64
^{2}G330.8793−00.3669	AGAL330.879−00.367	34.96	92.5	771.2	7.12	0.14	4.8	48.04	5.4	1.63	1.74	44.28	44.39
^{2}G330.9567−00.1806	AGAL330.954−00.182	2.78	35.38	54.93	2.14	0.05	4.8	47.14	5.78	1.73	1.9	43.1	43.26
^{2}G330.9536−00.1820	AGAL330.954−00.182	2.78	444.4	1017	3.03	0.08	4.8	48.41	5.78	1.73	1.9	44.36	44.53
^{2}G331.1190−00.4958	AGAL331.134−00.484	21.92	12.21	13.53	0.63	0.01	4.8	46.29	–	–	–	42.57	42.68
^{2}G331.1456+00.1347	AGAL331.146+00.136	4.09	10.2	108.8	8.32	0.41	4.8	48	4.35	0.67	0.8	44.31	44.45
^{2}G331.3525+01.0657	AGAL331.361+01.066	29.82	29.32	43.19	1.39	0.03	4.8	46.89	4.86	1.75	1.88	43.79	43.92
^{2}G331.4182−00.3544	AGAL331.418−00.356	6.07	20.73	80.66	3.72	0.07	4.8	47.06	4.37	1	1.11	43.7	43.81
^{2}G331.4912−00.1153	AGAL331.491−00.116	2.34	125.1	147.5	0.87	0.02	4.8	47.57	5.41	1.52	1.68	43.68	43.85
^{2}G331.5424−00.0664	AGAL331.546−00.067	13.15	71.36	74.97	0.38	0.01	4.8	47.28	5.72	1.89	2.06	43.45	43.62
^{2}G332.1535−00.4489	AGAL332.156−00.449	8.35	101.2	1697	8.7	0.15	4.8	48.29	5.08	1.77	1.86	44.99	45.08
^{2}G332.2911−00.0916	AGAL332.296−00.094	9.05	7.22	30.1	4.6	0.07	4.8	46.41	4.3	1.22	1.28	43.33	43.39
^{2}G332.2944−00.0963	AGAL332.296−00.094	9.05	19.11	175.6	7.55	0.11	4.8	47.18	4.3	1.22	1.28	44.1	44.15
^{2}G332.5432−00.1281	AGAL332.544−00.124	14.46	4.65	42.16	6.3	0.09	4.8	46.56	4.59	1.63	1.68	43.6	43.65
^{2}G332.7656−00.0080	AGAL332.766−00.007	1.79	4.34	24.57	4.72	0.13	4.8	46.84	4.46	1.3	1.5	43.68	43.87
^{2}G332.8260−00.5493	AGAL332.826−00.549	1.66	461.6	1259	2.81	0.05	4.8	48.17	5.54	1.72	1.81	44.35	44.44
^{2}G333.0170+00.7623	AGAL333.018+00.766	42.26	8.53	46.94	4.99	0.07	4.8	46.58	4.46	0.98	1.04	43.1	43.16
^{2}G333.1349−00.4320	AGAL333.134−00.431	21.33	355.6	497.6	1.74	0.03	4.8	47.76	5.82	1.76	1.85	43.7	43.79
^{2}G333.1304−00.4263	AGAL333.134−00.431	21.33	424.07	2581.99	7.72	0.13	4.8	48.48	5.82	1.76	1.85	44.41	44.5
^{2}G333.2853−00.3890	AGAL333.284−00.387	7.62	421.4	4984	8.82	0.15	4.8	48.76	5.44	1.65	1.74	44.98	45.07
^{2}G333.3398−00.1276	AGAL333.339−00.127	3.97	2.21	3.3	1.34	0.02	4.8	45.63	3.7	1.45	1.54	43.38	43.47
^{2}G333.6043−00.2126	AGAL333.604−00.212	142.32	393.6	7108	9.23	0.16	4.8	48.92	–	–	–	44.81	44.9
^{2}G333.6787−00.4350	AGAL333.679−00.431	15.15	28	33.3	0.87	0.06	4.8	47.81	4.76	1.01	0.86	44.06	43.91
^{2}G333.7258+00.3653	AGAL333.724+00.364	–	9.82	443.4	16.3	0.18	4.8	47.32	–	–	–	44.4	44.41
^{2}G334.3278−00.2865	AGAL334.328−00.286	–	4.83	9.3	1.97	0.03	4.8	45.9	3.18	1.02	1.08	43.74	43.81
^{2}G334.7226−00.6534	AGAL334.722−00.654	1.7	33.27	703.6	12.88	0.19	4.8	47.75	3.54	1.36	1.42	45.58	45.63

Table C.1 continued from previous page

Radio Name	*Submm Name*	*Offset*	*Peak Flux*	*Int Flux*	*d*	*d*	*Freq*	*Log* $N_{\rm Ly}$	*Log* $L_{\rm bol}$	*Log*	*Log*	*Log*	*Log*
		["]	[Jy/beam]	[Jy]	["]	[pc]	[GHz]	[photons s^{-1}]	[$L_\odot$]	$L_{\rm bol}/M$	$L_{\rm bol}/M_{\rm corr}$	$N_{\rm Ly}/M$	$N_{\rm Ly}/M_{\rm corr}$
[2]G335.1974−00.3876	AGAL335.197−00.389	5.54	4.31	57.52	9.44	0.13	4.8	46.64	3.07	0.89	0.94	44.46	44.51
[2]G335.3905−00.2903	AGAL335.391−00.291	1.67	11.69	12.72	0.78	0.05	4.8	47.33	3.97	0.98	0.93	44.34	44.29
[2]G335.9465+00.0292	AGAL335.944+00.029	9.46	1.42	3.94	2.74	0.05	4.8	45.64	3.18	1.15	1.25	43.61	43.71
[2]G335.9790+00.1957	AGAL335.980+00.196	5.6	5.36	164.3	15.38	0.29	4.8	47.35	–	–	–	45	45.11
[2]G336.3600−00.1371	AGAL336.359−00.137	–	43.94	553.2	8.89	0.22	4.8	48.09	4.92	1.5	1.7	44.68	44.87
[2]G336.3678−00.0042	AGAL336.369−00.004	5.43	257	523.6	2.72	0.09	4.8	48.32	4.79	1.14	1.4	44.67	44.93
[2]G336.4103−00.2575	AGAL336.411−00.256	–	5.99	6.49	1.15	0.03	4.8	46.16	4.58	1.1	1.3	42.68	42.87
[2]G336.8230+00.0278	AGAL336.824+00.027	29.59	41.14	53.05	1.03	0.02	4.8	47.02	4.56	0.9	1.08	43.36	43.54
[2]G336.9833−00.1832	AGAL336.984−00.184	4.84	17.25	17.96	0.37	0.01	4.8	46.53	4.24	1.78	1.95	44.08	44.24
[2]G336.9901−00.0245	AGAL336.994−00.027	18.32	28.95	129.1	5.04	0.19	4.8	47.84	5.24	1.46	1.74	44.06	44.34
[2]G337.0042+00.3240	AGAL337.004+00.322	5.24	81.46	249.3	3.9	0.21	4.8	48.46	4.87	1.38	1.51	44.96	45.1
[2]G337.4038−00.4023	AGAL337.406−00.402	7.55	83.91	90.34	0.63	0.01	4.8	46.86	4.89	1.6	1.67	43.58	43.64
[2]G337.6324−00.0781	AGAL337.632−00.079	4.13	28.1	30.95	0.65	0.01	4.8	46.56	3.61	0.82	0.93	43.77	43.88
[2]G337.6654−00.1757	AGAL337.666−00.177	6.67	69.75	670.8	8.31	0.15	4.8	47.89	3.9	1.19	1.3	45.18	45.29
[2]G337.7053−00.0530	AGAL337.704−00.054	12.83	74.86	76.34	0.27	0.02	4.8	48	5.41	1.07	1.16	43.66	43.75
[2]G337.7127+00.0881	AGAL337.712+00.087	28.58	7.53	6.4	1.38	0.07	4.8	46.83	5.34	1.02	1.2	42.51	42.69
[2]G337.7111+00.0856	AGAL337.712+00.087	28.58	42.69	102.6	3.03	0.16	4.8	48.03	5.34	1.02	1.2	43.71	43.89
[2]G337.7082+00.0942	AGAL337.712+00.087	28.58	40.34	144.9	4.37	0.23	4.8	48.18	5.34	1.02	1.2	43.86	44.04
[2]G337.8439−00.3746	AGAL337.844−00.376	4.6	10.55	11.12	1.35	0.02	4.8	45.95	4.41	1.9	1.97	43.44	43.51
[2]G338.0004−00.1473	AGAL337.999−00.149	4.63	4.4	6.09	1.44	0.03	4.8	45.96	3.94	1.72	1.87	43.75	43.89
[2]G338.0754+00.0122	AGAL338.074+00.011	11.59	164.7	542.3	3.44	0.05	4.8	47.64	4.46	1.26	1.32	44.44	44.5
[2]G338.2888−00.3712	AGAL338.289−00.377	–	9.6	87.3	7.94	0.04	4.8	45.98	2.09	1.17	1.1	45.06	44.98
[2]G338.3316+00.1322	AGAL338.332+00.131	5.8	201.5	235.7	1.07	0.01	4.8	47.19	4.25	1.55	1.6	44.49	44.53
[2]G338.4356+00.0592	AGAL338.436+00.057	6.03	92.52	685.5	6.56	0.09	4.8	47.65	4.51	1.43	1.48	44.58	44.62
[2]G338.5712−00.1443	AGAL338.569−00.144	3.87	20.86	36.1	2.22	0.08	4.8	47.21	5.12	1.8	2.09	43.89	44.18
[2]G338.5680−00.1443	AGAL338.569−00.144	3.87	125.5	230.4	2.42	0.08	4.8	48.02	5.12	1.8	2.09	44.7	44.99

Table C.1 continued from previous page

Radio Name	*Submm Name*	*Offset*	*Peak Flux*	*Int Flux*	*d*	*d*	*Freq*	*Log* $N_{\rm Ly}$	*Log* $L_{\rm bol}$	*Log*	*Log*	*Log*	*Log*
		["]	[Jy/beam]	[Jy]	["]	[pc]	[GHz]	[photons s^{-1}]	[$L_\odot$]	$L_{\rm bol}/M$	$L_{\rm bol}/M_{\rm corr}$	$N_{\rm Ly}/M$	$N_{\rm Ly}/M_{\rm corr}$
[2]G338.6810−00.0843	AGAL338.682−00.084	4.19	42.64	69.1	1.57	0.01	4.8	46.14	2.86	1.56	1.52	44.85	44.8
[2]G338.9223+00.6244	AGAL338.926+00.634	36.24	104.6	144	1.32	0.03	4.8	47.36	4.73	1.42	1.57	44.05	44.2
[2]G339.1037+00.1484	AGAL339.106+00.147	9.31	31.03	42.89	1.44	0.03	4.8	46.95	4.29	1.43	1.62	44.09	44.28
[2]G339.5834−00.1288	AGAL339.584−00.127	9.39	1.46	2.8	2.19	0.03	4.8	45.23	3.44	0.84	0.88	42.63	42.67
[2]G339.7465+00.0952	AGAL339.746+00.094	4.48	8.6	14.93	1.82	0.1	4.8	47.27	4.45	1.29	1.43	44.11	44.24
[2]G339.9426−00.0934	AGAL339.943−00.092	–	1.43	8.36	5.24	0.09	4.8	45.99	3.56	0.89	1.01	43.32	43.44
[2]G340.0560−00.2435	AGAL340.054−00.244	4.37	157.3	376.7	3.08	0.05	4.8	47.64	5.11	1.71	1.82	44.23	44.35
[2]G340.0705+00.9277	AGAL340.073+00.927	6.57	9.89	48.79	4.68	0.11	4.8	46.98	4.56	1.47	1.67	43.9	44.1
[2]G340.2486−00.3715	AGAL340.248−00.374	49.08	105.9	129.5	1.18	0.02	4.8	47.18	4.48	1.01	1.13	43.72	43.83
[2]G341.7017+00.0523	AGAL341.702+00.051	–	54.1	158	3.51	0.24	4.8	48.44	4.96	1.37	1.35	44.85	44.83
[2]G342.0594+00.4204	AGAL342.058+00.421	5.86	14.78	56.48	4.11	0.22	4.8	47.78	–	–	–	43.57	43.79
[2]G342.3840+00.1228	AGAL342.386+00.122	6.91	5.52	9.57	1.96	0.01	4.8	45.09	2.57	0.96	0.9	43.49	43.42
[2]G343.5024−00.0138	AGAL343.502−00.014	0.24	33.85	176.9	5.59	0.07	4.8	47.03	4.47	1.42	1.47	43.99	44.03
[2]G343.9293+00.1251	AGAL343.929+00.124	–	6.98	6.82	1.3	0.11	4.8	47.25	4.9	1.39	1.13	43.75	43.49
[2]G344.4256+00.0462	AGAL344.424+00.046	5.66	205.4	2139	8.79	0.21	4.8	48.66	5.39	1.73	1.96	45.01	45.24
[2]G345.0035−00.2243	AGAL345.003−00.224	6.06	78.48	140	1.69	0.01	4.8	46.39	–	–	–	43.4	43.35
[2]G345.4072−00.9514	AGAL345.408−00.952	–	125.3	163.2	1.28	0.01	4.8	46.46	5.12	2.13	2.08	43.46	43.41
[2]G345.4877+00.3150	AGAL345.488+00.314	3.03	500.7	1980	4.86	0.06	4.8	48.01	4.89	1.42	1.44	44.53	44.56
[2]G345.4937+01.4687	AGAL345.493+01.469	3.92	4.64	4.82	1.37	0.02	4.8	45.4	5.71	2.23	2.26	41.92	41.95
[2]G345.4906+01.4734	AGAL345.493+01.469	3.92	2.97	3.03	1.37	0.02	4.8	45.19	5.71	2.23	2.26	41.72	41.75
[2]G345.5275−00.0515	AGAL345.526−00.052	6.34	2.79	5.98	2.28	0.02	4.8	45.02	3.07	1	0.95	42.95	42.91
[2]G345.5472−00.0802	AGAL345.548−00.081	2.65	38.13	50.27	0.83	0.01	4.8	45.95	2.53	1.1	1.05	44.52	44.47
[2]G345.6490+00.0098	AGAL345.649+00.009	2.52	627.4	2205	4.61	0.03	4.8	47.59	4.01	1.8	1.75	45.38	45.33
[2]G346.0772−00.0554	AGAL346.076−00.056	5.05	8.31	46.15	5.52	0.27	4.8	47.63	4.88	1.24	1.54	43.99	44.3
[2]G346.2333−00.3197	AGAL346.232−00.321	5.05	4.09	4.74	1.01	0.07	4.8	46.98	–	–	–	43.64	43.59
[2]G347.3050+00.0149	AGAL347.304+00.014	4.36	5.6	7.85	1.54	0.01	4.8	45.14	2.24	1.17	1.12	44.06	44.01

Table C.1 continued from previous page

Radio Name	*Submm Name*	*Offset*	*Peak Flux*	*Int Flux*	*d*	*d*	*Freq*	*Log* $N_{\rm Ly}$	*Log* $L_{\rm bol}$	*Log*	*Log*	*Log*	*Log*
		["]	[Jy/beam]	[Jy]	["]	[pc]	[GHz]	[photons s^{-1}]	[$L_\odot$]	$L_{\rm bol}/M$	$L_{\rm bol}/M_{\rm corr}$	$N_{\rm Ly}/M$	$N_{\rm Ly}/M_{\rm corr}$
[2]G347.6006+00.2438	AGAL347.602+00.244	6.56	23.81	51.22	2.42	0.11	4.8	47.64	4.48	0.42	0.77	43.58	43.93
[2]G347.6283+00.1483	AGAL347.627+00.149	45.15	71.86	83.18	0.69	0.03	4.8	47.85	6.05	1.85	2.2	43.66	44.01
[2]G347.8707+00.0139	AGAL347.871+00.014	1.16	127.8	206.1	2.09	0.13	4.8	48.49	5.23	1.21	1.33	44.46	44.59
[2]G348.1485+00.2568	AGAL348.144+00.257	–	1.52	6.1	4.24	0.22	4.8	46.79	4.7	1.06	1.36	43.14	43.44
[2]G348.5309−00.9718	AGAL348.531−00.972	1.66	13.65	364	14.86	0.24	4.8	47.58	4.33	0.99	1.1	44.23	44.35
[2]G348.5503−00.3387	AGAL348.549−00.337	5.72	20.63	24.12	0.96	0.08	4.8	47.84	4.25	1.17	0.88	44.75	44.46
[2]G348.6979−01.0275	AGAL348.698−01.027	1.24	437.7	1151	2.37	0.04	4.8	48.08	5.24	1.95	2.06	44.78	44.89
[2]G348.8920−00.1793	AGAL348.893−00.179	2.01	65.23	185.7	3.14	0.17	4.8	48.32	–	–	–	44.77	45.04
[2]G349.1049+00.1139	AGAL349.091+00.106	58.4	19.09	26.45	1.51	0.08	4.8	47.42	5.72	1.58	1.89	43.28	43.6
[2]G349.7215+00.1214	AGAL349.721+00.122	6.12	29.24	35.69	1	0.11	4.8	48.19	5.6	1.84	1.19	44.43	43.78
[3]G122.7761+02.8562	JCMTLSY J004956.23+654345.2	8.2	–	1.1	–	–	5	45.39	4.19	1.42	0.94	42.62	42.14
[3]G124.6424+02.5395	JCMTLSY J010750.96+652121.7	4.93	57.4	306.5	–	–	5	48.24	4.35	0.48	-0.21	44.37	43.68
[3]G125.6045+02.1038A	JCMTLSY J011636.99+645041.2	3.56	2.5	2.6	–	–	5	45.59	3.81	0.86	0.43	42.64	42.22
[3]G125.6322+02.0219	JCMTLSY J011648.61+644542.6	7.65	–	–	–	–	–	–	3.46	0.69	0.26	–	–
[3]G132.1570−00.7241	JCMTLSY J020806.83+604606.8	12.43	6.6	342.8	–	–	5	47.8	4.3	0.51	0.04	44.01	43.53
[3]G133.6948+01.1937	JCMTLSY J022520.88+620454.9	45.16	–	24.8	–	–	5	45.95	3.08	1.26	0.96	44.13	43.83
[3]G133.6923+01.2270	JCMTLSY J022531.18+620619.5	41.58	63.6	422	–	–	5	47.18	4.3	0.15	-0.15	43.03	42.73
[3]G133.6945+01.2166B	JCMTLSY J022531.18+620619.5	2.72	63.6	422	–	–	5	47.18	4.3	0.15	-0.15	43.03	42.73
[3]G133.7184+01.2237	JCMTLSY J022540.29+620548.5	36.51	–	–	–	–	–	–	5.44	0.87	0.57	–	–
[3]G133.9476+01.0648	JCMTLSY J022703.84+615221.1	5.48	386.1	1209.2	–	–	9	47.66	4.92	0.47	0.17	43.21	42.91
[3]G139.9091+00.1969B	JCMTLSY J030723.84+583046.1	3.56	2.3	20	–	–	9	46.29	4	0.11	-0.29	42.4	42
[3]G141.0822−01.0560	JCMTLSY J031016.80+565031.5	2.96	–	–	–	–	–	–	3.42	1.04	0.63	–	–
[3]G142.2446+01.4299	JCMTLSY J032731.06+581922.0	2.54	6.5	7.4	–	–	5	46.07	4.12	0.94	0.47	42.89	42.42
[3]G151.6209−00.2680	JCMTLSY J041107.55+510846.0	64.34	–	1.1	–	–	5	44.72	3.33	1.42	1.06	42.8	42.45
[3]G154.3472+02.6099	JCMTLSY J043620.47+511257.8	4.89	4.1	113	–	–	5	47.29	4.44	0.47	-0.06	43.32	42.79
[3]G155.3319+02.5989	JCMTLSY J044027.12+502827.3	2.21	2.2	10.8	–	–	5	46.29	4.39	1.68	1.14	43.58	43.05

Table C.1 continued from previous page

Radio Name	*Submm Name*	*Offset* ["]	*Peak Flux* [Jy/beam]	*Int Flux* [Jy]	*d* ["]	*d* [pc]	*Freq* [GHz]	*Log* N_{Ly} [photons s^{-1}]	*Log* L_{bol} [$L_\odot$]	*Log* L_{bol}/M	*Log* L_{bol}/M_{corr}	*Log* N_{Ly}/M	*Log* N_{Ly}/M_{corr}
[3]G176.4661−01.6758	JCMTLSY J053020.69+310125.7	2.35	–	0.6	–	–	5	44.33	3.09	0.87	0.53	42.12	41.77
[3]G188.7954+01.0302	JCMTLSY J060906.84+215039.2	3.82	2	3.7	–	–	5	45.12	3.75	0.36	0.01	41.73	41.39
[3]G196.8298−03.1052	JCMTLSY J061012.12+124852.3	5.37	1.4	8.4	–	–	5	46.2	4.7	1.68	1.12	43.18	42.62
[3]G192.5843−00.0417	JCMTLSY J061253.65+180027.1	3.3	4.5	10.2	–	–	5	45.56	4.72	0.82	0.47	41.66	41.32
[3]G194.9259−01.1946	JCMTLSY J061320.97+152411.4	14.51	–	1	–	–	5	44.56	3.2	0.88	0.53	42.23	41.89
[3]G200.0789−01.6323	JCMTLSY J062147.49+103924.6	7.02	1.5	1.9	–	–	5	45.76	3.81	0.98	0.32	42.93	42.27
[3]G200.9166−01.5827	JCMTLSY J062334.68+095629.4	9.96	–	1	–	–	5	45.43	4.21	1.12	0.49	42.34	41.71
[3]G206.7804−01.9395B	JCMTLSY J063315.98+043454.5	1.86	–	0.6	–	–	5	43.89	2.82	0.93	0.67	42.01	41.74
[3]G212.2468−01.1034	JCMTLSY J064615.97+000630.8	9.38	–	0.9	–	–	5	45.18	3.44	0.37	-0.14	42.1	41.6
[3]G217.3771−00.0828	JCMTLSY J065915.57−035932.8	3.88	4.9	35	–	–	5	45.73	3.91	1.14	0.87	42.95	42.69
[3]G234.6358+00.8281	JCMTLSY J073538.53−184855.1	6.99	–	0.8	–	–	5	44.95	4.05	1.24	0.86	42.13	41.75
[3]G240.3156+00.0715	JCMTLSY J074451.83−240744.3	3.53	–	12.4	–	–	8.6	46.54	4.32	0.06	-0.42	42.28	41.79
[3]G064.1528+01.2817	JCMTLSY J194815.31+280727.4	5.03	12.6	25.7	–	–	5	47.5	4.3	1.9	1.5	45.1	44.7
[3]G063.1538+00.4375B	JCMTLSY J194914.48+265010.9	9.49	–	–	–	–	–	–	–	–	–	–	–
[3]G068.3418+01.3138	JCMTLSY J195803.01+314407.3	0.64	1.4	7.8	–	–	5	46.98	4.52	2.34	1.89	44.8	44.35
[3]G070.3164+01.6493	JCMTLSY J200137.46+333527.5	2.62	–	4.5	–	–	5	46.35	4.08	1.44	1.21	43.71	43.48
[3]G070.2928+01.6002	JCMTLSY J200145.71+333244.3	1	283.7	2691	–	–	5	49.15	5.71	1.73	1.49	45.17	44.93
[3]G070.3329+01.5864	JCMTLSY J200154.35+333412.3	12.6	59.4	467.7	–	–	5	48.36	4.76	1.02	0.78	44.62	44.39
[3]G071.1499+00.3996	JCMTLSY J200850.00+333734.3	2.49	14.1	319.8	–	–	5	48.12	4.49	2.01	1.8	45.65	45.43
[3]G074.1606+01.6431	JCMTLSY J201146.54+364928.5	7.09	–	–	–	–	–	–	3.89	1.29	1	–	–
[3]G074.1201+01.5035	JCMTLSY J201215.26+364254.5	5.78	–	0.9	–	–	5	45.68	3.88	1.83	1.54	43.63	43.35
[3]G072.2479+00.2617A	JCMTLSY J201217.25+342809.9	1.11	–	0.9	–	–	5	46.01	3.71	1.68	1.21	43.99	43.51
[3]G073.8775+01.0245	JCMTLSY J201334.05+361456.3	4.18	4.3	128.6	–	–	5	48	4.35	1.74	1.38	45.39	45.03
[3]G074.7541+00.9132	JCMTLSY J201627.62+365458.5	2.64	5.7	64.5	–	–	5	47.7	4.48	2.14	1.76	45.36	44.98
[3]G078.4373+02.6584A	JCMTLSY J201938.82+405638.3	7.33	3.7	82.2	–	–	9	46.19	3.71	2.01	1.85	44.48	44.33
[3]G077.4622+01.7600B	JCMTLSY J202038.86+393751.2	4.19	12.8	24.9	–	–	5	45.64	3.64	1.24	1.09	43.24	43.09

Table C.1 continued from previous page

Radio Name	*Submm Name*	*Offset*	*Peak Flux*	*Int Flux*	*d*	*d*	*Freq*	*Log* $N_{\rm Ly}$	*Log* $L_{\rm bol}$	*Log*	*Log*	*Log*	*Log*
		["]	[Jy/beam]	[Jy]	["]	[pc]	[GHz]	[photons s^{-1}]	[$L_\odot$]	$L_{\rm bol}/M$	$L_{\rm bol}/M_{\rm corr}$	$N_{\rm Ly}/M$	$N_{\rm Ly}/M_{\rm corr}$
[3]G075.7822+00.3421	JCMTLSY J202144.08+372637.5	1.6	20.4	32.5	–	–	5	45.76	4.18	1.8	1.65	43.38	43.23
[3]G076.1877+00.0974	JCMTLSY J202355.04+373812.5	2.88	10	396.7	–	–	5	46.84	3.45	1.66	1.51	45.06	44.9
[3]G077.6092+00.5569	JCMTLSY J202611.17+390348.6	4.69	–	–	–	–	–	–	3.84	1.35	0.87	–	–
[3]G078.0342+00.6155	JCMTLSY J202712.76+392639.5	7.54	–	–	–	–	–	–	2.64	1.59	1.44	–	–
[3]G078.1952+00.5497	JCMTLSY J202758.70+393210.1	4.73	–	1.1	–	–	5	45.85	4.19	2.59	2.22	44.25	43.88
[3]G079.3202+01.3131	JCMTLSY J202810.18+405336.8	0.81	4.6	6.1	–	–	5	46.47	4.12	1.37	1.06	43.71	43.4
[3]G079.3248+01.2901	JCMTLSY J202816.75+405301.8	2.46	1.7	6.4	–	–	9	46.51	4.26	1.6	1.29	43.85	43.54
[3]G079.3305+01.2823	JCMTLSY J202816.75+405301.8	37.04	–	1.8	–	–	5	45.94	4.26	1.6	1.29	43.28	42.97
[3]G077.9550+00.0058	JCMTLSY J202931.93+390113.2	5.37	–	–	–	–	–	–	3.06	2.04	1.89	–	–
[3]G077.9637−00.0075	JCMTLSY J202936.77+390109.3	6.57	1.8	12.2	–	–	9	45.36	4.03	3.11	2.96	44.44	44.28
[3]G079.4436+01.0033	JCMTLSY J202952.19+404844.7	6.58	1.2	2.2	–	–	5	44.59	2.52	1.66	1.49	43.72	43.56
[3]G079.8749+01.1821	JCMTLSY J203028.83+411555.3	16.04	–	0.8	–	–	5	44.15	3.02	0.96	0.79	42.09	41.92
[3]G078.4705−00.1830	JCMTLSY J203153.40+391937.6	2.12	–	1.2	–	–	5	45.94	4.23	2.03	1.63	43.74	43.34
[3]G082.0333+02.3249	JCMTLSY J203222.01+434050.3	6.01	–	1.3	–	–	5	44.36	2.18	0.99	0.83	43.18	43.01
[3]G080.8282+00.5670B	JCMTLSY J203608.17+413955.9	8.09	–	1.8	–	–	8.6	44.53	2.58	0.64	0.48	42.59	42.43
[3]G080.8645+00.4197	JCMTLSY J203652.09+413622.0	2.17	33.6	50.8	–	–	5	45.95	3.96	1.9	1.74	43.89	43.73
[3]G081.8789+00.7822	JCMTLSY J203836.71+423735.4	26.24	3.8	145.3	–	–	5	46.41	4.04	1.21	1.04	43.57	43.41
[3]G081.7220+00.5699	JCMTLSY J203900.93+422248.0	4.93	–	14.3	–	–	5	45.4	4.07	1.37	1.21	42.71	42.54
[3]G081.6802+00.5405A	JCMTLSY J203900.97+421931.5	12.08	187.1	6310.2	–	–	5	47.91	3.36	0.51	0.34	45.06	44.9
[3]G081.6802+00.5405B	JCMTLSY J203900.97+421931.5	12.08	146.2	792.7	–	–	5	47.01	3.36	0.51	0.34	44.16	44
[3]G081.7133+00.5589	JCMTLSY J203901.27+422203.6	14.71	–	18.8	–	–	5	45.52	3.28	0.74	0.58	42.99	42.82
[3]G080.9383−00.1268	JCMTLSY J203925.53+411959.2	3.82	9.1	213	–	–	5	46.57	4.5	2.81	2.64	44.88	44.72
[3]G082.5682+00.4040B	JCMTLSY J204233.19+425645.6	4.31	3.6	9	–	–	5	45.2	3.68	2.33	2.16	43.85	43.69
[3]G085.4102+00.0032B	JCMTLSY J205413.82+445408.8	2.23	28.4	31.2	–	–	5	46.93	4.3	1.5	1.23	44.13	43.85
[3]G089.2727+01.6703	JCMTLSY J210135.07+485456.5	4.62	2	12.6	–	–	5	46.87	3.97	1.97	1.52	44.87	44.42
[3]G090.9207+01.4872	JCMTLSY J210912.93+500101.0	3.64	–	–	–	–	–	–	–	–	–	–	–

Table C.1 continued from previous page

Radio Name	*Submm Name*	*Offset* ["]	*Peak Flux* [Jy/beam]	*Int Flux* [Jy]	*d* ["]	*d* [pc]	*Freq* [GHz]	*Log* $N_{\rm Ly}$ [photons s^{-1}]	*Log* $L_{\rm bol}$ [$L_\odot$]	*Log* $L_{\rm bol}/M$	*Log* $L_{\rm bol}/M_{\rm corr}$	*Log* $N_{\rm Ly}/M$	*Log* $N_{\rm Ly}/M_{\rm corr}$
[3]G093.0166+02.4953	JCMTLSY J211339.11+521406.6	1.68	–	–	–	–	–	–	–	–	–	–	–
[3]G093.5304+01.4745	JCMTLSY J212044.92+515326.6	2.68	–	–	–	–	–	–	5.41	2.9	2.48	–	–
[3]G093.8588+01.5551	JCMTLSY J212152.98+521057.3	10.3	2	34.1	–	–	5	47.1	4.06	2.24	1.85	45.28	44.89
[3]G096.4353+01.3233B	JCMTLSY J213520.84+534711.5	1.7	1.8	42.7	–	–	5	47.27	3.95	1.62	1.18	44.95	44.51
[3]G098.0361+01.4462	JCMTLSY J214301.23+545616.9	2.78	91.9	137.5	–	–	5	47.69	5	1.97	1.56	44.66	44.25
[3]G100.1974+02.0643	JCMTLSY J215201.89+564743.7	3.66	1.4	38.6	–	–	5	47.07	3.65	1.86	1.45	45.28	44.87
[3]G100.1620+01.6647B	JCMTLSY J215338.71+562750.3	5.09	–	1	–	–	5	45.51	3.8	1.66	1.25	43.37	42.96
[3]G105.6270+00.3388	JCMTLSY J223245.00+582811.2	9.77	13.2	197.5	–	–	5	47.56	4.28	1.65	1.29	44.93	44.56
[3]G108.1973+00.5781	JCMTLSY J224928.87+595453.1	3.57	2.5	9.2	–	–	5	46.14	4.44	1.78	1.43	43.48	43.14
[3]G108.7825+00.2510	JCMTLSY J225450.92+595254.9	9.49	–	–	–	–	–	–	3.07	1.07	0.7	–	–
[3]G109.0974−00.3458	JCMTLSY J225905.07+592821.3	8.67	–	29	–	–	8.6	46.6	4.37	1.87	1.54	44.1	43.77
[3]G111.1919−00.7965	JCMTLSY J231545.69+595239.3	7.05	–	1.1	–	–	5	45.26	3.76	2.2	1.83	43.7	43.33
[3]G111.2824−00.6639B	JCMTLSY J231603.89+600153.8	4.47	6.5	90.8	–	–	5	47	4.37	1.38	1.06	44.01	43.69
[3]G111.2925−00.6569	JCMTLSY J231603.89+600153.8	29.19	–	–	–	–	–	–	4.37	1.38	1.06	–	–
[3]G111.2786−00.7076	JCMTLSY J231609.69+595922.1	6.25	1.6	3.5	–	–	5	45.54	4.05	1.68	1.37	43.17	42.85
[3]G116.3282+00.6627	JCMTLSY J235307.69+624705.9	22.82	–	–	–	–	–	–	3.43	1.6	1.25	–	–

Appendix D

VLA Non-Detections for SASSy Clumps

Target	*RA* (2000)	*Dec* (2000)	*RMS* [mJy]	*Upper Limit* [mJy]	*Image Quality Notes*
"G177.503+3.180 "	" 05:52:20.890000 "	" +32.42.44.00000 "	0.01	0.04	" noise
" "G179.179+1.162 "	" 05:48:14.140001 "	" +30.14.25.30000 "	0.04	0.13	" sidelobes
" "G179.219+2.222 "	" 05:52:33.260000 "	" +30.44.57.00000 "	0.02	0.05	" sidelobes
" "G179.409+1.834 "	" 05:51:27.310000 "	" +30.23.15.50000 "	0.01	0.04	" neighbouring source
" "G180.115+3.236 "	" 05:58:43.129999 "	" +30.29.04.20000 "	0.02	0.05	" neighbouring source
" "G182.445+3.132 "	" 06:03:34.529999 "	" +28.24.34.79999 "	0.02	0.05	" noise
" "G183.125+2.574 "	" 06:02:52.990000 "	" +27.32.35.89999 "	0.01	0.03	" noise
" "G179.982-0.712 "	" 05:42:48.420000 "	" +28.34.41.90000 "	0.04	0.11	" sidelobes
" "G180.304-0.517 "	" 05:44:20.030000 "	" +28.24.24.59999 "	0.01	0.04	" noise
" "G180.255+0.673 "	" 05:48:51.680000 "	" +29.03.59.20000 "	0.03	0.09	" neighbouring source
" "G182.092-3.235 "	" 05:38:12.840000 "	" +25.27.11.69999 "	0.01	0.04	" noise
" "G183.886-3.239 "	" 05:42:22.060000 "	" +23.55.51.40001 "	0.01	0.04	" noise
" "G183.747-0.42 "	" 05:52:40.710000 "	" +25.30.25.20000 "	0.01	0.04	" noise
" "G186.217+3.288 "	" 06:12:20.870000 "	" +25.11.16.39999 "	0.03	0.10	" neighbouring source
" "G189.929-0.681 "	" 06:05:04.800000 "	" +20.01.08.00000 "	0.01	0.04	" noise
" "G192.344-3.298 "	" 06:00:29.000000 "	" +16.37.51.79999 "	0.03	0.09	" sidelobes
" "G191.639-3.068 "	" 05:59:51.720000 "	" +17.21.19.79999 "	0.01	0.04	" sidelobes

Table D.1 continued from previous page

Target	*RA* (2000)	*Dec* (2000)	*RMS* [mJy]	*Upper Limit* [mJy]	*Image Quality Notes*
" "G191.285-2.9 "	" 05:59:44.400000 "	" +17.44.47.69999 "	0.02	0.05	" sidelobes
" "G190.675-3.187 "	" 05:57:25.140000 "	" +18.07.56.60001 "	0.01	0.04	" neighbouring source
" "G190.041-3.188 "	" 05:56:04.990000 "	" +18.40.49.30001 "	0.01	0.04	" noise
" "G188.431-3.135 "	" 05:52:50.630001 "	" +20.05.43.79999 "	0.01	0.04	" noise
" "G187.416-2.93 "	" 05:51:24.000000 "	" +21.04.20.39999 "	0.01	0.04	" noise
" "G195.387+2.827 "	" 06:29:02.150000 "	" +16.53.03.50001 "	0.03	0.08	" sidelobes
" "G195.389+2.929 "	" 06:29:25.150000 "	" +16.55.48.30000 "	0.02	0.05	" sidelobes
" "G195.395+2.930 "	" 06:29:25.920001 "	" +16.55.32.60001 "	0.02	0.05	" neighbouring source
" "G195.667+2.926 "	" 06:29:56.620001 "	" +16.40.56.70000 "	0.04	0.12	" sidelobes
" "G198.296-3.155 "	" 06:12:53.520000 "	" +11.30.13.00001 "	0.04	0.11	" sidelobes
" "G198.307-3.176 "	" 06:12:50.320000 "	" +11.29.03.60001 "	0.06	0.19	" sidelobes
" "G199.850-2.983 "	" 06:16:30.700000 "	" +10.13.13.20000 "	0.01	0.03	" noise
" "G201.936-3.038 "	" 06:20:17.709999 "	" +08.21.25.80001 "	0.10	0.30	" sidelobes
" "G201.167+1.673 "	" 06:35:47.050000 "	" +11.13.35.79999 "	0.01	0.04	" noise
" "G202.329+3.097 "	" 06:43:06.470001 "	" +10.50.42.80000 "	0.01	0.04	" noise
" "G205.487+2.958 "	" 06:48:24.700000 "	" +07.58.20.49999 "	0.03	0.10	" sidelobes
" "G207.491-1.449 "	" 06:36:19.390000 "	" +04.10.32.10001 "	0.05	0.14	" sidelobes

Table D.1 continued from previous page

Target	*RA* (2000)	*Dec* (2000)	*RMS* [mJy]	*Upper Limit* [mJy]	*Image Quality Notes*
" "G208.775-3.291 "	" 06:32:07.800001 "	" +02.11.24.30001 "	0.02	0.07	" neighbouring source
" "G207.789-2.756 "	" 06:32:12.960001 "	" +03.18.38.50000 "	0.01	0.04	" noise
" "G204.067-3.138 "	" 06:23:57.070000 "	" +06.25.44.80001 "	0.01	0.03	" noise
" "G202.281-0.218 "	" 06:31:02.840001 "	" +09.22.00.00001 "	0.01	0.04	" noise
" "G211.104+1.155 "	" 06:52:13.340000 "	" +02.09.10.90000 "	0.02	0.06	" sidelobes
" "G212.410+3.194 "	" 07:01:51.890000 "	" +01.55.11.29999 "	0.02	0.06	" noise
" "G216.084-2.867 "	" 06:46:57.660000 "	" -04.06.42.49999 "	0.05	0.14	" neighbouring source
" "G216.049-2.618 "	" 06:47:47.200000 "	" -03.58.00.20000 "	0.02	0.05	" noise
" "G214.416+3.048 "	" 07:04:59.720000 "	" +00.04.12.20000 "	0.03	0.08	" sidelobes
" "G215.112+3.296 "	" 07:07:09.040001 "	" -00.26.04.80000 "	0.14	0.43	" sidelobes
" "G218.803+0.501 "	" 07:03:58.010000 "	" -04.59.39.50000 "	1.17	3.51	" sidelobes
" "G217.954+2.930 "	" 07:11:03.290000 "	" -03.07.28.20000 "	0.02	0.05	" noise
" "G218.292+2.740 "	" 07:11:00.180000 "	" -03.30.41.79999 "	0.03	0.09	" neighbouring source
" "G220.339+2.913 "	" 07:15:24.250000 "	" -05.14.44.20001 "	0.02	0.05	" neighbouring source
" "G220.613+3.017 "	" 07:16:17.170000 "	" -05.26.23.20000 "	0.02	0.06	" sidelobes
" "G222.503-1.063 "	" 07:05:12.290000 "	" -08.59.57.70001 "	0.02	0.06	" sidelobes
" "G222.104+0.641 "	" 07:10:34.930000 "	" -07.51.35.10000 "	0.03	0.10	" sidelobes

Table D.1 continued from previous page

Target	*RA* (2000)	*Dec* (2000)	*RMS* [mJy]	*Upper Limit* [mJy]	*Image Quality Notes*
" "G222.337+0.757 "	" 07:11:25.940001 "	" -08.00.47.00000 "	0.03	0.09	" sidelobes
" "G223.889-3.034 "	" 07:00:39.080000 "	" -11.07.55.19999 "	0.02	0.06	" neighbouring source
" "G225.081-3.1 "	" 07:02:37.490000 "	" -12.13.17.70001 "	0.06	0.19	" neighbouring source
" "G226.380-2.765 "	" 07:06:16.620000 "	" -13.13.22.80000 "	0.03	0.09	" neighbouring source
" "G228.326-2.635 "	" 07:10:25.930000 "	" -14.53.28.20000 "	0.01	0.04	" neighbouring source
" "G230.505-0.871 "	" 07:21:06.820000 "	" -15.59.57.80000 "	0.02	0.07	" noise
" "G228.754+2.717 "	" 07:30:43.600000 "	" -12.45.16.89999 "	0.02	0.05	" neighbouring source
" "G222.331+2.895 "	" 07:19:03.640000 "	" -07.00.52.80001 "	0.02	0.06	" noise
" "G222.660+2.968 "	" 07:19:56.369999 "	" -07.16.17.89999 "	0.01	0.04	" noise
" "G222.713+3.023 "	" 07:20:14.040000 "	" -07.17.32.70001 "	0.02	0.07	" sidelobes
" "G222.725+3.109 "	" 07:20:33.800001 "	" -07.15.48.50000 "	0.05	0.15	" sidelobes
" "G224.653+2.915 "	" 07:23:31.069999 "	" -09.03.16.60000 "	0.04	0.11	" noise
" "G225.401+3.288 "	" 07:26:16.770000 "	" -09.32.15.70000 "	0.02	0.05	" noise
" "G230.545+2.897 "	" 07:34:55.150000 "	" -14.14.06.89999 "	0.02	0.06	" noise
" "G232.684-2.905 "	" 07:17:50.780000 "	" -18.52.30.80000 "	0.02	0.05	" noise
" "G233.181-0.012 "	" 07:29:35.210000 "	" -17.56.49.50000 "	0.02	0.05	" neighbouring source
" "G232.802+2.627 "	" 07:38:29.280000 "	" -16.20.14.19999 "	0.02	0.05	" noise

Table D.1 continued from previous page

Target	*RA* (2000)	*Dec* (2000)	*RMS* [mJy]	*Upper Limit* [mJy]	*Image Quality Notes*
" "G232.915+2.862 "	" 07:39:34.260000 "	" -16.19.13.80001 "	0.02	0.05	" sidelobes
" "G233.028+3.068 "	" 07:40:32.940000 "	" -16.19.02.10001 "	0.10	0.31	" sidelobes
" "G233.569+3.178 "	" 07:42:03.570000 "	" -16.43.59.40000 "	0.14	0.43	" noise
" "G233.575+3.231 "	" 07:42:15.810000 "	" -16.42.44.10000 "	0.18	0.55	" sidelobes
" "G235.106-3.178 "	" 07:21:37.350000 "	" -21.08.30.10000 "	0.02	0.05	" noise
" "G235.143-3.167 "	" 07:21:44.460001 "	" -21.10.07.59999 "	0.01	0.04	" noise
" "G234.299+3.152 "	" 07:43:28.360000 "	" -17.22.45.80000 "	0.07	0.22	" sidelobes
" "G234.650+2.614 "	" 07:42:14.419999 "	" -17.57.01.60001 "	0.02	0.05	" neighbouring source
" "G236.786+2.878 "	" 07:47:42.200000 "	" -19.40.05.30001 "	0.02	0.05	" noise
" "G239.688-3.18 "	" 07:31:02.060001 "	" -25.10.23.90001 "	0.02	0.06	" neighbouring source
" "G240.209-3.188 "	" 07:32:06.500000 "	" -25.37.59.20000 "	0.02	0.07	" noise
" "G240.536+1.171 "	" 07:49:30.840001 "	" -23.45.51.30001 "	0.15	0.45	" sidelobes
" "G241.183+0.598 "	" 07:48:47.079999 "	" -24.36.45.59999 "	0.02	0.05	" noise
" "G241.370+3.186 "	" 07:58:55.540000 "	" -23.26.30.99999 "	0.01	0.04	" noise
" "G241.813+3.179 "	" 07:59:54.650000 "	" -23.49.21.80001 "	0.02	0.06	" noise
" "G243.295+2.268 "	" 07:59:54.580000 "	" -25.33.40.10001 "	0.05	0.15	" sidelobes
" "G147.864+2.833 "	" 04:06:31.000000 "	" +55.57.19.90000 "	0.02	0.05	" noise

Table D.1 continued from previous page

Target	*RA* (2000)	*Dec* (2000)	*RMS* [mJy]	*Upper Limit* [mJy]	*Image Quality Notes*
" "G151.392+3.128 "	" 04:25:33.569999 "	" +53.43.17.30000 "	0.02	0.05	" sidelobes
" "G154.052-2.839 "	" 04:11:13.420000 "	" +47.35.35.50000 "	0.02	0.05	" noise
" "G153.448-3.16 "	" 04:07:17.640000 "	" +47.45.57.50000 "	0.02	0.07	" sidelobes
" "G152.344-1.17 "	" 04:10:31.860000 "	" +49.58.41.60001 "	0.04	0.13	" sidelobes
" "G151.348-1.97 "	" 04:02:35.550000 "	" +50.03.02.70000 "	0.03	0.09	" sidelobes
" "G151.137-2.751 "	" 03:58:26.330000 "	" +49.35.52.29999 "	0.01	0.04	" neighbouring source
" "G150.761-3.044 "	" 03:55:29.970001 "	" +49.37.00.10000 "	0.04	0.13	" sidelobes
" "G150.351-1.346 "	" 04:00:26.490001 "	" +51.10.31.59999 "	0.30	0.90	" sidelobes
" "G153.787+3.022 "	" 04:35:53.499999 "	" +51.54.22.00000 "	0.01	0.04	" neighbouring source
" "G153.774+3.081 "	" 04:36:07.360000 "	" +51.57.20.40000 "	0.01	0.04	" sidelobes
" "G156.015+2.948 "	" 04:44:55.079999 "	" +50.11.23.60000 "	0.08	0.24	" sidelobes
" "G156.778+3.203 "	" 04:49:11.350001 "	" +49.46.20.00000 "	0.02	0.05	" noise
" "G157.922+1.110 "	" 04:44:01.060000 "	" +47.32.45.00001 "	0.06	0.17	" neighbouring source
" "G157.999+0.561 "	" 04:41:52.439999 "	" +47.07.40.39999 "	0.01	0.03	" noise
" "G157.806-1.352 "	" 04:32:51.620000 "	" +45.59.15.00001 "	0.01	0.03	" neighbouring source
" "G156.120-2.857 "	" 04:19:52.070000 "	" +46.09.00.29999 "	0.06	0.19	" sidelobes
" "G157.894+2.088 "	" 04:48:20.680000 "	" +48.12.07.89999 "	0.01	0.03	" neighbouring source

Table D.1 continued from previous page

Target	*RA* (2000)	*Dec* (2000)	*RMS* [mJy]	*Upper Limit* [mJy]	*Image Quality Notes*
" "G157.771+3.182 "	" 04:52:58.090000 "	" +48.59.42.89999 "	0.01	0.04	" noise
" "G157.942+3.015 "	" 04:52:50.240001 "	" +48.45.23.60000 "	0.02	0.06	" sidelobes
" "G157.863+3.154 "	" 04:53:11.390001 "	" +48.54.19.60000 "	0.14	0.43	" sidelobes
" "G158.022+2.933 "	" 04:52:45.490000 "	" +48.38.36.70000 "	0.02	0.05	" neighbouring source
" "G158.709+3.183 "	" 04:56:32.100001 "	" +48.15.59.00001 "	0.02	0.05	" noise
" "G161.494-3.145 "	" 04:39:16.470000 "	" +42.03.15.19999 "	0.02	0.05	" noise
" "G160.511-2.448 "	" 04:38:32.880000 "	" +43.15.03.40001 "	0.01	0.04	" noise
" "G160.002+3.000 "	" 05:00:25.899999 "	" +47.08.22.70000 "	0.01	0.04	" noise
" "G160.654+1.974 "	" 04:58:04.750000 "	" +45.59.36.50000 "	0.02	0.07	" sidelobes
" "G162.069+3.022 "	" 05:07:46.820000 "	" +45.30.40.69999 "	0.02	0.05	" sidelobes
" "G162.381+2.860 "	" 05:08:05.940000 "	" +45.09.52.99999 "	0.10	0.29	" sidelobes
" "G162.411+2.894 "	" 05:08:21.320000 "	" +45.09.39.60000 "	0.02	0.06	" noise
" "G163.661+3.160 "	" 05:13:42.790000 "	" +44.18.38.09999 "	0.01	0.03	" noise
" "G165.689+3.182 "	" 05:20:15.530000 "	" +42.40.10.00001 "	0.01	0.03	" sidelobes
" "G165.771-0.258 "	" 05:05:36.720000 "	" +40.34.52.00000 "	0.01	0.04	" noise
" "G166.451-2.665 "	" 04:57:54.070000 "	" +38.34.11.10001 "	0.01	0.04	" noise
" "G172.685+2.900 "	" 05:39:01.850001 "	" +36.40.46.30000 "	0.02	0.07	" neighbouring source

Table D.1 continued from previous page

Target	*RA* (2000)	*Dec* (2000)	*RMS* [mJy]	*Upper Limit* [mJy]	*Image Quality Notes*
" "G167.221+3.162 "	" 05:24:49.350000 "	" +41.23.43.00000 "	0.05	0.15	" neighbouring source
" "G167.732+3.208 "	" 05:26:32.289999 "	" +40.59.54.10000 "	0.02	0.05	" sidelobes
" "G167.736+3.246 "	" 05:26:43.050000 "	" +41.00.57.19999 "	0.01	0.04	" neighbouring source
" "G168.241+3.115 "	" 05:27:37.170000 "	" +40.31.25.90000 "	0.01	0.04	" noise
" "G169.019+3.171 "	" 05:30:06.680000 "	" +39.54.23.50001 "	0.06	0.18	" sidelobes
" "G170.339+2.984 "	" 05:33:01.350001 "	" +38.42.03.50000 "	0.02	0.05	" sidelobes
" "G234.208+3.17 "	" 07:43:20.830000 "	" -17.17.30.70000 "	0.11	0.33	" sidelobes
" "G234.24+0.419 "	" 07:33:19.619999 "	" -18.39.58.69999 "	0.01	0.04	" noise
" "G239.174-3.114 "	" 07:30:12.580000 "	" -24.41.22.90001 "	0.02	0.07	" sidelobes
" "G233.492-3.24 "	" 07:18:10.840000 "	" -19.44.39.10000 "	0.01	0.04	" neighbouring source
" "G227.806-3.146 "	" 07:07:33.970000 "	" -14.39.48.39999 "	0.02	0.05	" neighbouring source
" "G220.053-2.5 "	" 06:55:31.160000 "	" -07.28.35.00001 "	0.09	0.28	" sidelobes
" "G219.474-1.172 "	" 06:59:13.190000 "	" -06.21.19.40001 "	0.85	2.56	" sidelobes
" "G218.784+0.081 "	" 07:02:25.890000 "	" -05.10.10.59999 "	0.01	0.04	" noise
" "G219.475+0.338 "	" 07:04:37.140000 "	" -05.39.55.90000 "	0.01	0.04	" noise
" "G219.982+1.341 "	" 07:09:08.360000 "	" -05.39.18.10000 "	0.06	0.19	" sidelobes
" "G222.304+2.896 "	" 07:19:00.540000 "	" -06.59.25.20000 "	0.02	0.06	" noise

Table D.1 continued from previous page

Target	*RA* (2000)	*Dec* (2000)	*RMS* [mJy]	*Upper Limit* [mJy]	*Image Quality Notes*
" "G201.71+1.507 "	" 06:36:11.920000 "	" +10.40.09.10000 "	0.02	0.07	" neighbouring source
" "G203.242+2.075 "	" 06:41:05.850000 "	" +09.34.05.00001 "	0.05	0.16	" sidelobes
" "G203.326+2.062 "	" 06:41:12.350000 "	" +09.29.11.30000 "	0.05	0.16	" neighbouring source
" "G203.332+2.073 "	" 06:41:15.520000 "	" +09.29.11.69999 "	0.05	0.14	" sidelobes
" "G210.1+2.626 "	" 06:55:37.980000 "	" +03.42.59.60000 "	0.03	0.09	" sidelobes
" "G211.631+0.909 "	" 06:52:18.210000 "	" +01.34.20.59999 "	0.02	0.05	" noise
" "G208.957-3.258 "	" 06:32:34.850000 "	" +02.02.41.90000 "	0.04	0.11	" sidelobes
" "G208.204-3.143 "	" 06:31:36.309999 "	" +02.45.55.10001 "	0.01	0.04	" neighbouring source
" "G204.071-3.15 "	" 06:23:55.070000 "	" +06.25.12.30000 "	0.02	0.06	" sidelobes
" "G204.079-3.131 "	" 06:23:59.970001 "	" +06.25.20.39999 "	0.02	0.05	" noise
" "G204.075-3.129 "	" 06:24:00.030000 "	" +06.25.37.70000 "	0.02	0.05	" noise
" "G203.972-2.976 "	" 06:24:21.290000 "	" +06.35.20.59999 "	0.02	0.05	" noise
" "G203.443-2.936 "	" 06:23:30.310000 "	" +07.04.29.90001 "	0.02	0.06	" noise
" "G200.256-3.118 "	" 06:16:48.600000 "	" +09.47.59.40000 "	0.01	0.04	" noise
" "G199.864-2.981 "	" 06:16:32.860000 "	" +10.12.32.70000 "	0.01	0.04	" noise
" "G199.864-2.981 "	" 06:16:32.870000 "	" +10.12.32.00000 "	0.00	0.00	" noise
" "G199.76-0.639 "	" 06:24:45.830000 "	" +11.24.09.70001 "	0.02	0.05	" sidelobes

Table D.1 continued from previous page

Target	*RA* (2000)	*Dec* (2000)	*RMS* [mJy]	*Upper Limit* [mJy]	*Image Quality Notes*
" "G199.261-1.572 "	" 06:20:26.990000 "	" +11.24.20.40000 "	0.02	0.06	" noise
" "G198.419-3.271 "	" 06:12:43.060000 "	" +11.20.27.50001 "	0.03	0.08	" sidelobes
" "G198.413-3.265 "	" 06:12:43.700000 "	" +11.20.56.10001 "	0.05	0.14	" sidelobes
" "G194.663-0.223 "	" 06:16:22.770000 "	" +16.05.39.50001 "	0.02	0.05	" noise
" "G186.703+0.379 "	" 06:02:13.500001 "	" +23.20.57.90001 "	0.11	0.34	" sidelobes
" "G187.465+2.163 "	" 06:10:38.220000 "	" +23.33.16.30001 "	0.02	0.05	" noise
" "G190.355-3.244 "	" 05:56:32.430000 "	" +18.22.52.00001 "	0.09	0.26	" sidelobes
" "G186.17-3.275 "	" 05:47:23.200000 "	" +21.57.56.39999 "	0.02	0.05	" neighbouring source
" "G133.695+1.21 "	" 02:25:30.130000 "	" +62.06.00.50001 "	27.80	83.40	" neighbouring source
" "G133.748+1.198 "	" 02:25:53.440000 "	" +62.04.10.30000 "	12.50	37.50	" sidelobes
" "G132.378-3.291 "	" 02:03:59.429999 "	" +58.14.36.40001 "	0.10	0.31	" sidelobes
" "G133.567-2.937 "	" 02:13:24.339999 "	" +58.13.54.70001 "	0.01	0.04	" noise
" "G137.897+1.464 "	" 02:58:19.210001 "	" +60.35.44.40001 "	0.01	0.04	" sidelobes
" "G140.743-3.209 "	" 03:00:35.810000 "	" +55.07.56.79999 "	0.01	0.03	" noise
" "G141.307-3.048 "	" 03:04:35.450000 "	" +55.00.06.70000 "	0.01	0.04	" sidelobes
" "G141.057-0.536 "	" 03:12:04.300000 "	" +57.18.06.50000 "	0.01	0.04	" noise
" "G142.612-3.264 "	" 03:11:37.640000 "	" +54.09.45.00000 "	0.01	0.04	" sidelobes

Table D.1 continued from previous page

Target	*RA* (2000)	*Dec* (2000)	*RMS* [mJy]	*Upper Limit* [mJy]	*Image Quality Notes*
" "G142.903-3.139 "	" 03:13:46.180001 "	" +54.07.10.60000 "	0.01	0.04	" noise
" "G143.146+3.13 "	" 03:40:47.220000 "	" +59.11.04.00000 "	0.00	0.00	" sidelobes
" "G147.483-3.056 "	" 03:39:14.350000 "	" +51.38.04.99999 "	0.02	0.06	" noise
" "G147.935-2.835 "	" 03:42:25.080000 "	" +51.32.22.29999 "	0.02	0.05	" sidelobes
" "G147.95-2.767 "	" 03:42:45.290000 "	" +51.35.06.20001 "	0.03	0.09	" noise
" "G147.936-2.651 "	" 03:43:08.420000 "	" +51.41.06.90000 "	0.30	0.89	" neighbouring source
" "G146.213+2.386 "	" 03:55:24.610001 "	" +56.41.56.40000 "	0.01	0.04	" neighbouring source
" "G153.708-3.016 "	" 04:09:00.860000 "	" +47.41.50.09999 "	0.05	0.15	" sidelobes
" "G157.943+3.015 "	" 04:52:50.240001 "	" +48.45.23.60000 "	0.02	0.05	" sidelobes
" "G159.192+3.204 "	" 04:58:24.999999 "	" +47.54.07.20000 "	0.02	0.06	" sidelobes
" "G159.791+3.179 "	" 05:00:29.620000 "	" +47.24.53.99999 "	0.01	0.04	" noise
" "G161.737-3.05 "	" 04:40:31.440000 "	" +41.56.10.90000 "	0.01	0.03	" noise
" "G162.268-2.705 "	" 04:43:47.570000 "	" +41.45.51.70000 "	0.01	0.03	" noise
" "G163.998-3.15 "	" 04:47:56.430000 "	" +40.09.40.90001 "	0.01	0.04	" neighbouring source
" "G167.196+3.171 "	" 05:24:46.910000 "	" +41.25.17.90000 "	0.02	0.06	" sidelobes
" "G167.25+3.155 "	" 05:24:52.440000 "	" +41.22.02.39999 "	0.02	0.07	" sidelobes
" "G169.042+3.175 "	" 05:30:11.450000 "	" +39.53.25.40000 "	0.04	0.13	" sidelobes

Table D.1 continued from previous page

Target	*RA* (2000)	*Dec* (2000)	*RMS* [mJy]	*Upper Limit* [mJy]	*Image Quality Notes*
" "G170.785+2.531 "	" 05:32:19.010000 "	" +38.04.50.20001 "	0.01	0.04	" noise
" "G176.333+1.751 "	" 05:43:38.660000 "	" +32.58.37.40001 "	0.01	0.04	" neighbouring source
" "G180.316-0.084 "	" 05:46:02.640000 "	" +28.37.23.79999 "	0.01	0.04	" sidelobes
" "G179.228+2.211 "	" 05:52:31.930000 "	" +30.44.07.40000 "	0.02	0.05	" sidelobes
"					

Bibliography

Anderson, L.D., Bania, T.M., Balser, D.S., et al., 2014. the Wise Catalog of Galactic H Ii Regions. *The Astrophysical Journal Supplement Series*, 212(1):1.

Armentrout, W.P., Anderson, L.D., Balser, D.S., et al., 2017. High-Mass Star Formation in the Outer Scutum-Centaurus Arm. *The Astrophysical Journal*, 841(121).

Ascenso, J., Alves, J., and Lago, M.T.V.T., 2009. No Evidence for Mass Segregation in Massive Young Clusters. *Astronomy & Astrophysics*, 495(1):147.

Bally, J. and Zinnecker, H., 2005. The Birth of High Mass Stars: Accretion and/or Mergers? *The Astronomical Journal*, 129(5):2281.

Bania, T.M., Anderson, L.D., Balser, D.S., et al., 2010. the Green Bank Telescope Galactic H Ii Region Discovery Survey. *The Astrophysical Journal*, 718(2):L106.

Barnes, A.T., Longmore, S.N., Avison, A., et al., 2019. Young massive star cluster formation in the Galactic Centre is driven by global gravitational collapse of high-mass molecular clouds. *Monthly Notices of the Royal Astronomical Society*, 486(1):283.

Barnes, P.J., Muller, E., Indermuehle, B., et al., 2015. THE THREE-MM ULTIMATE MOPRA MILKY WAY SURVEY. I. SURVEY OVERVIEW, INITIAL DATA RELEASES, and FIRST RESULTS. *Astrophysical Journal*, 812(1):6.

Battisti, A.J. and Heyer, M.H., 2013. THE DENSE GAS MASS FRACTION OF MOLECULAR CLOUDS IN THE MILKY WAY. *The Astrophysical Journal*, 780(2).

Becker, R.H., White, R.L., Helfand, D.J., et al., 1994. A 5 GHz VLA survey of the galactic plane. *The Astrophysical Journal Supplement Series*, 91:347.

Becker, R.H., White, R.L., McLean, B.J., et al., 1990. A 20 centimeter survey of compact sources in the northern Galactic plane. *The Astrophysical Journal*, 358:485.

Benincasa, S.M., Wadsley, J.W., Couchman, H.M.P., et al., 2019. A Tale of Two Clump Masses: A new way to study clump formation in simulations. *Monthly Notices of the Royal Astronomical Society*.

Benjamin, R.A., Churchwell, E., Babler, B.L., et al., 2003. GLIMPSE. I. An SIRTF Legacy Project to Map the Inner Galaxy. *Publications of the Astronomical Society of the Pacific*, 115(810):953.

Berry, D., 2014. FellWalker - a clump identification algorithm. *Astronomy and Computing*, 1411:6267.

Berry, D.S., 2007. CUPID – A 3D Clump Identification and Analysis Package. *Starlink User Note*, 255:425.

Bertin, E. and Arnouts, S., 1996. SExtractor: Software for source extraction.

Bigiel, F., Leroy, A., and Walter, F., 2011. Scaling relations between gas and star formation in nearby galaxies. In *Proceedings of the International Astronomical Union*, volume 6, pages 327–334.

Bigiel, F., Leroy, A., Walter, F., et al., 2008. The star formation law in nearby galaxies on SUB-KPC scales. *Astronomical Journal*, 136(6):2846.

Billington, S.J., Urquhart, J.S., Konig, C., et al., 2019. ATLASGAL – physical parameters of dust clumps associated with 6.7 GHz methanol masers.

Boggess, N.W., Mather, J.C., Weiss, R., et al., 1992. The COBE mission - Its design and performance two years after launch. *The Astrophysical Journal*, 397:420.

Bolatto, A.D., Leroy, A.K., Jameson, K., et al., 2011. The state of the gas and the relation between gas and star formation at low metallicity: The small magellanic cloud. *Astrophysical Journal*, 741(1):12.

Bolatto, A.D., Leroy, A.K., Rosolowsky, E., et al., 2008. The Resolved Properties of Extragalactic Giant Molecular Clouds. *The Astrophysical Journal*, 686:948.

Boley, P.A., Linz, H., van Boekel, R., et al., 2012. On the massive young stellar object AFGL 4176. *Astronomy & Astrophysics*, 557:C1.

Bonnell, I.A., Bate, M.R., Clarke, C.J., et al., 1997. Accretion and the Stellar Mass Spectrum in Small Clusters. *Monthly Notices of the Royal Astronomical Society*, 285(1):201.

Bonnell, I.A., Bate, M.R., and Zinnecker, H., 1998. On the Formation of Massive Stars. *Monthly Notices of the Royal Astronomical Society*, 298(1):93.

Bonnell, I.A., Vine, S.G., and Bate, M.R., 2004. Massive Star Formation: Nurture, not Nature. *Monthly Notices of the Royal Astronomical Society*, 349(2):735.

Boulanger, F., Bernard, J.P., Lagache, G., et al., 2001. Galactic Far-Infrared Diffuse Emission. *Symposium - International Astronomical Union*, 204:47.

Braine, J., Duc, P.A., Lisenfeld, U., et al., 2001. On-going galaxy formation. *Astrophysics and Space Science*, 281(1-2):407.

Brand, J. and Blitz, L., 1993. The Velocity Field of the Outer Galaxy. *Astronomy and Astrophysics*, 275:67.

Bronfman, L., Nyman, L.A., and May, J., 1996. A CS(2-1) survey of IRAS point sources with color characteristics of ultra-compact H II regions. *Astronomy and Astrophysics Supplement Series*, 115(1):81.

Burton, M.G., Braiding, C., Glueck, C., et al., 2013. The mopra Southern galactic plane CO survey.

Carey, S.J., Noriega-Crespo, A., Mizuno, D.R., et al., 2009. MIPSGAL: A Survey of the Inner Galactic Plane at 24 and 70 μm. *Publications of the Astronomical Society of the Pacific*, 121(875):76.

Carpenter, J.M., Snell, R.L., and Schloerb, F.P., 1990. Molecular Clouds Associated with Luminous Far-Infrared Sources in the Outer Galaxy. *The Astrophysical Journal Journal*, 362:147.

Caswell, J.L., Fuller, G.A., Green, J.A., et al., 2010. The 6-GHz methanol multibeam maser catalogue - I. Galactic Centre region, longitudes 345° to 6°. *Monthly Notices of the Royal Astronomical Society*, 404(2):1029.

Cavichia, O., Mollá, M., Costa, R.D.D., et al., 2013. The star formation rate in the inner Milky Way Galaxy. *Proceedings of the International Astronomical Union*, 8(S292):98.

Cesaroni, R., Pestalozzi, M., Beltrán, M.T., et al., 2015. Infrared emission of young HII regions: a Herschel /Hi-GAL study. *Astronomy & Astrophysics*, 579:A71.

Chabrier, G., 2003. Galactic Stellar and Substellar Initial Mass Function. *Publications of the Astronomical Society of the Pacific*, 115(809):763.

Chapin, E.L., Berry, D.S., Gibb, A.G., et al., 2013. SCUBA-2: Iterative map-making with the sub-millimetre user reduction facility. *Monthly Notices of the Royal Astronomical Society*, 430(4):2545.

Chiang, Y.K. and Ménard, B., 2018. Extragalactic Imprints in Galactic Dust Maps. *The Astrophysical Journal*, 870(2):120.

Cohen, R.S. and Thaddeus, P., 1977. An out-of-plane galactic carbon monoxide survey. *The Astrophysical Journal*, 217:L155.

Contreras, Y., Schuller, F., Urquhart, J.S., et al., 2013. ATLASGAL - Compact source catalogue: 330 < l < 21. *Astronomy & Astrophysics*, 45:1.

Crowther, P.A., Schnurr, O., Hirschi, R., et al., 2010. The R136 Star Cluster Hosts Several Stars whose Individual Masses Greatly Exceed the Accepted 150 M. Stellar Mass Limit. *Monthly Notices of the Royal Astronomical Society*, 408(2):731.

Csengeri, T., Bontemps, S., Wyrowski, F., et al., 2017. The ATLASGAL survey: The sample of young massive cluster progenitors. *A&A*, 601.

Csengeri, T., Urquhart, J.S., Schuller, F., et al., 2014. The ATLASGAL survey: a catalog of dust condensations in the Galactic plane. *A&A*, 565.

Currie, M.J., Berry, D.S., and Jenness et al., T., 2014. Starlink Software in 2013. *Astronomical Data Analysis Software and Systems XXIII*, 485:391.

Dame, T.M., Hartmann, D., and Thaddeus, P., 2001. The Milky Way in Molecular Clouds: A New Complete CO Survey. *The Astrophysical Journal*, 547(2):792.

Davies, B., Hoare, M.G., Lumsden, S.L., et al., 2011. The Red MSX Source Survey: Critical Tests of Accretion Models for the Formation of Massive Stars. *Monthly Notices of the Royal Astronomical Society*, 416(2):972.

Dempsey, J.T., Friberg, P., Jenness, T., et al., 2013a. SCUBA-2: On-sky calibration using sub-millimetre standard sources. *Monthly Notices of the Royal Astronomical Society*, 430(4):2534.

Dempsey, J.T., Thomas, H.S., and Currie, M.J., 2013b. CO (3-2) high-resolution survey of the galactic plane: R1. *Astrophysical Journal, Supplement Series*, 209(1):8.

Draine, B.T., Dale, D.A., Bendo, G., et al., 2007. Dust Masses, PAH Abundances, and Starlight Intensities in the SINGS Galaxy Sample. *The Astrophysical Journal*, 663(2):866.

Dunham, M.K., Rosolowsky, E., Evans, N.J., et al., 2011. The Bolocam Galactic Plane Survey. VII. Characterizing the properties of massive star-forming regions. *Astrophysical Journal*, 741(2):110.

Dwek, E., 1998. The Evolution of the Elemental Abundances in the Gas and Dust Phases of the Galaxy. *The Astrophysical Journal*, 501(2):643.

Eden, D.J., Moore, T.J.T., Morgan, L.K., et al., 2012. Star formation in galactic spiral arms and the interarm regions. *Mon. Not. R. Astron. Soc*, 000(13):1.

Eden, D.J., Moore, T.J.T., Plume, R., et al., 2017. The JCMT Plane Survey: First complete data release - emission maps and compact source catalogue. *MNRAS*, 000:1.

Eden, D.J., Moore, .J.T., Urquhart, J.S., et al., 2015. Star formation scales and efficiency in Galactic spiral arms. *MNRAS*, 452(1):289.

Elia, D., Molinari, S., Fukui, Y., et al., 2013. The first hi-gal observations of the outer galaxy: A look at star formation in the third galactic quadrant in the longitude range 216.°5 225.°5. *Astrophysical Journal*, 772(1):45.

Elia, D., Molinari, S., Schisano, E., et al., 2017. The Hi-GAL compact source catalogue - I. The physical properties of the clumps in the inner Galaxy ($-71.0 < l < 67.0$). *MNRAS*, 471:100.

Ellingsen, S.P., Shabala, S.S., and Kurtz, S.E., 2005. Extended emission associated with young H II regions. *Monthly Notices of the Royal Astronomical Society*, 357(3):1003.

Englmaier, P. and Gerhard, O., 1999. Gas dynamics and large-scale morphology of the Milky Way galaxy. *Monthly Notices of the Royal Astronomical Society*, 304(3):512.

Ferrière, K.M., 2001. The interstellar environment of our galaxy. *Reviews of Modern Physics*, 73(4):1031.

Fontani, F., Cesaroni, R., and Furuya, R.S., 2010. Class I and Class II methanol masers in high-mass star forming regions.

Fontani, F., Pascucci, I., Caselli, P., et al., 2007. Comparative Study of Complex N- and O-bearing Molecules in Hot Molecular Cores. *Astronomy & Astrophysics*, 470:639.

Fujita, S., Torii, K., Kuno, N., et al., 2019. Massive star formation in W51 A triggered by cloud–cloud collisions. *Publications of the Astronomical Society of Japan*.

Gao, Y. and Solomon, P.M., 2004. The Star Formation Rate and Dense Molecular Gas in Galaxies. *The Astrophysical Journal*, 606(1):271.

Garay, G., Faundez, S., Mardones, D., et al., 2004. Discovery of Four New Massive and Dense Cold Cores. *The Astrophysical Journal*, 610(1):313.

Gennaro, M., Bik, A., Brandner, W., et al., 2012. Multiple episodes of star formation in the CN15/16/17 molecular complex. *Astronomy & Astrophysics*, 542:A74.

Genzel, R., Eisenhauer, F., and Gillessen, S., 2010. The Galactic center massive black hole and nuclear star cluster. *Reviews of Modern Physics*, 82(4):3121.

Giannetti, A., Leurini, S., König, C., et al., 2017. Galactocentric variation of the gas-to-dust ratio and its relation with metallicity. *A&A*, 606(L12).

Giannetti, A., Wyrowski, F., Leurini, S., et al., 2015. Infrared dark clouds on the far side of the Galaxy. *Astronomy & Astrophysics*, 580(L7).

Giveon, U., Becker, R.H., Helfand, D.J., et al., 2005. A New Catalog of Radio Compact H ii Regions in the Milky Way. *The Astronomical Journal*, 129(1):348.

Gnedin, O.Y., Brown, W.R., Geller, M.J., et al., 2010. The mass profile of the galaxy to 80 kpc. *Astrophysical Journal Letters*, 720(1 PART 2):L108.

Green, J.A., Cohen, R.J., Caswell, J.L., et al., 2007. The methanol multibeam survey. In *Proceedings of the International Astronomical Union*, volume 3, pages 218–222.

Griffin, M., Swinyard, B., Vigroux, L., et al., 2008. Herschel-SPIRE: design, ground test results, and predicted performance. In J.M. Oschmann Jr., M.W.M. de Graauw, and H.A. MacEwen, editors, *Space Telescopes and Instrumentation 2008: Optical, Infrared, and Millimeter. Edited by Oschmann, Jacobus M., Jr.; de Graauw, Mattheus W. M.; MacEwen, Howard A. Proceedings of the SPIE, Volume 7010, article id. 701006, 12 pp. (2008).*, volume 7010, page 701006.

Heyer, M.H. and Brunt, C.M., 2004. The Universality of Turbulence in Galactic Molecular Clouds. *The Astrophysical Journal*, 615(1):L45.

Hildebrand, R.H., 1983. The Determination of Cloud Masses and Dust Characteristics from Submillimetre Thermal Emission. *Quarterly Journal for Royal Astronomical Society*, 24(3):267.

Hindson, L., Thompson, M.A., Urquhart, J.S., et al., 2012. The G305 star-forming complex: A wide-area radio survey of ultracompact Hii regions. *Monthly Notices of the Royal Astronomical Society*, 421(4):3418.

Hirashita, H. and Harada, N., 2017. Effects of dust evolution on the abundances of CO and H2. *MNRAS*, 467(1):699.

Hoare, M.G., Lumsden, S.L., Oudmaijer, R.D., et al., 2005. The RMS survey : Massive young stars throughout the galaxy. (227):370.

Hoare, M.G., Purcell, C.R., Churchwell, E.B., et al., 2012. The Coordinated Radio and Infrared Survey for High-Mass Star Formation (The CORNISH Survey). I. Survey Design. *Publications of the Astronomical Society of the Pacific*, 124(919):939.

Immer, K., Menten, K.M., Schuller, F., et al., 2012. A multi-wavelength view of the Galactic center dust ridge reveals little star formation. *Astronomy & Astrophysics*, 548:A120.

Izumi, N., Kobayashi, N., Yasui, C., et al., 2017. Star formation activity beyond the outer Arm I: WISE-selected candidate star-forming regions. *The Astronomical Journal*, 154(4):27.

Jackson, J.M., Rathborne, J.M., Foster, J.B., et al., 2013. MALT90: The Millimetre Astronomy Legacy Team 90 GHz Survey. *Publications of the Astronomical Society of Australia*, 30:e057.

Junichi, B., Takayuki, R.S., Keiichi, W., et al., 2010. On the Interpretation of the l-v Features in the Milky Way Galaxy. *Publ Astron Soc Japan*, 62(6):1413.

Kainulainen, J., Alves, J., Beuther, H., et al., 2011. Mass reservoirs surrounding massive infrared dark clouds. *Astronomy & Astrophysics*, 536:A48.

Kalberla, P.M. and Kerp, J., 2009. The H i Distribution of the Milky Way. *Annual Review of Astronomy and Astrophysics*, 47(1):27.

Kalberla, P.M.W., Burton, W.B., Hartmann, D., et al., 2005. The Leiden/Argentine/Bonn (LAB) Survey of Galactic HI. *Astronomy & Astrophysics*, 440(2):775.

Kalcheva, I.E., Hoare, M.G., Urquhart, J.S., et al., 2018. The coordinated radio and infrared survey for high-mass star formation. *Astronomy & Astrophysics*, 615:A103.

Kauffmann, J., Bertoldi, F., Bourke, T.L., et al., 2008. MAMBO mapping of Spitzer c2d small clouds and cores. *Astronomy and Astrophysics*, 487(3):993.

Kennicutt, R.C., 2005. The Role of Massive Stars in Astrophysics. *Proceedings of the International Astronomical Union*, 1(S227):3.

Kennicutt, R.C., Calzetti, D., Walter, F., et al., 2007. Star Formation in NGC 5194 (M51a). II. The Spatially-Resolved Star Formation Law.

Kennicutt, R.C., Edgar, B.K., and Hodge, P.W., 1989. Properties of H II Region Populations in Galaxies. II - The HII Region Luminosity Function. *Astrophysical Journal*, 344:761.

Kerp, J., Winkel, B., and Kalberla, P.M., 2009. The Effelsberg Bonn HI Survey EBHIS. In *Proceedings of Science*, volume 89, pages 259–261.

Kim, K.T. and Koo, B.C., 2000. Radio Continuum and Recombination Line Study of UC HII Regions with Extended Envelopes. *The Astrophysical Journal*, 549(2):29.

Kolpak, M.A., Jackson, J.M., Bania, T.M., et al., 2003. Resolving the Kinematic Distance Ambiguity toward Galactic H ii Regions. *The Astrophysical Journal*, 582(2):756.

König, C., Urquhart, J.S., Csengeri, T., et al., 2017. ATLASGAL-selected massive clumps in the inner Galaxy. *Astronomy & Astrophysics*, 599:A139.

Kroupa, P., 2002. The Initial Mass Function of Stars: Evidence for Uniformity in Variable Systems. *Science (New York, N.Y.)*, 295(5552):82.

Kruijssen, J.M.D. and Longmore, S.N., 2013. Comparing molecular gas across cosmic timescales: The Milky Way as both a typical spiral galaxy and a high-redshift galaxy analogue. *Monthly Notices of the Royal Astronomical Society*, 435(3):2598.

Krumholz, M.R. and Bonnell, I.A., 2007. Models for the Formation of Massive Stars.

Krumholz, M.R., Dekel, A., and McKee, C.F., 2011. A Universal, Local Star Formation Law in Galactic Clouds, Nearby Galaxies, High-Redshift Disks, and Starbursts. *The Astrophysical Journal*, 745(1):69.

Krumholz, M.R. and Matzner, C.D., 2009. The dynamics of radiation-pressure-dominated H II regions. *Astrophysical Journal*, 703(2):1352.

Kuchar, T.A. and Bania, T.M., 1994. Kinematic distances of Galactic H II regions from H I absorption studies. *The Astrophysical Journal*, 436:117.

Kuiper, R., Klahr, H., Beuther, H., et al., 2010. Circumventing the radiation pressure barrier in the formation of massive stars via disk accretion. *The Astrophysical Journal*, 722:1556.

Kurtz, S., 2005. Hypercompact HII regions. *Proceedings of the International Astronomical Union*, 1(S227):111.

Kurtz, S., Cesaroni, R., Churchwell, E.B., et al., 2000. Hot molecular cores and the earliest phases of high-mass star formation. *Protostars and Planets IV*, pages 299–326.

Kurtz, S., Churchwell, E., and Wood, D.O.S., 2016. Ultracompact HII Regions II New High-resolution Radio Images. *TripleC*, 14(1):260.

Lada, C.J. and Lada, E.A., 2003. Embedded Clusters in Molecular Clouds. *Annual Review of Astronomy and Astrophysics*, 41(1):57.

Lada, C.J., Lombardi, M., and Alves, J.F., 2010. On the star formation rates in molecular clouds. *Astrophysical Journal*, 724(1):687.

Lépine, J.R.D., Cruz, P., Scarano, S., et al., 2011. Overlapping abundance gradients and azimuthal gradients related to the spiral structure of the Galaxy. *Mon. Not. R. Astron. Soc*, 417:698.

Li, J.J., Moscadelli, L., Cesaroni, R., et al., 2012. Massive star formation toward G28.87+0.07 (IRAS18411-0338) investigated by means of maser kinematics and radio to infrared continuum observations. *Astrophysical Journal*, 749(1):47.

Lockman, F.J., 2002. Discovery of a Population of H [CSC]i[/CSC] Clouds in the Galactic Halo. *The Astrophysical Journal*, 580(1):L47.

Longmore, S., Barnes, A., Battersby, C., et al., 2015. Using young massive star clusters to understand star formation and feedback in high-redshift-like environments. *EAS Publications Series*, 75-76:6.

Longmore, S.N., Kruijssen, J.M.D., Bastian, N., et al., 2014. The Formation and Early Evolution of Young Massive Clusters. *Protostars and Planets VI*, 1401(iii):4175.

Lumsden, S.L., Hoare, M.G., Oudmaijer, R.D., et al., 2002. The population of the galactic plane as seen by MSX. *Monthly Notices of the Royal Astronomical Society*, 336(2):621.

Lumsden, S.L., Hoare, M.G., Urquhart, J.S., et al., 2013. the Red Msx Source Survey: the Massive Young Stellar Population of Our Galaxy. *The Astrophysical Journal Supplement Series*, 208(1):11.

Martins, 1996. The Most Massive Stars in the Arches Cluster. *Astronomy & Astrophysics*, 308:573.

Martins, F., Schaerer, D., and Hillier, D.J., 2005. A new calibration of stellar parameters of Galactic O stars. *Astronomy & Astrophysics*, 436:18.

Marton, G., Tóth, L.V., Paladini, R., et al., 2016. An all-sky support vector machine selection of WISE YSO candidates. *Monthly Notices of the Royal Astronomical Society*, 458(4):3479.

Mattsson, L. and Andersen, A.C., 2012. On the dust abundance gradients in late-type galaxies - II. Analytical models as evidence for massive interstellar dust growth in SINGS galaxies. *Monthly Notices of the Royal Astronomical Society*, 423(1):38.

McClure-Griffiths, N.M., Pisano, D.J., Calabretta, M.R., et al., 2009. Gass: The parkes galactic all-sky survey I. Survey description, goals, and initial data release. *Astrophysical Journal, Supplement Series*, 181(2):398.

McKee, C.F. and Tan, J.C., 2003. The Formation of Massive Stars from Turbulent Cores. *The Astrophysical Journal*, 585(2):850.

Menten, K.M., Pillai, T., and Wyrowski, F., 2005. Initial Conditions for Massive Star Birth – Infrared Dark Clouds. *IAU Symposium Proceedings of the International Astronomical Union*, 227:23.

Misiriotis, A., Xilouris, E.M., Papamastorakis, J., et al., 2006. The distribution of the ISM in the Milky Way. A three-dimensional large-scale model. *Astronomy and Astrophysics*, 459:113.

Molinari, A.S., Swinyard, B., Bally, J., et al., 2010. Hi-GAL : The Herschel Infrared Galactic Plane Survey. *PASP*.

Moore, T.J.T., Urquhart, J.S., Morgan, L.K., et al., 2012. The effect of spiral arms on star formation in the Galaxy. *Mon. Not. R. Astron. Soc*, 426:701.

Mottram, J.C., Hoare, M.G., Davies, B., et al., 2011a. THE RMS SURVEY: THE LUMINOSITY FUNCTIONS AND TIMESCALES OF MASSIVE YOUNG STELLAR OBJECTS AND COMPACT H ii REGIONS. *The Astrophysical Journal Letters*, 730(6pp).

Mottram, J.C., Hoare, M.G., Lumsden, S.L., et al., 2007. The RMS survey: mid-infrared observations of candidate massive YSOs in the southern hemisphere. *Astronomy and Astrophysics*, 476(2):1019.

Mottram, J.C., Hoare, M.G., Urquhart, J.S., et al., 2011b. The RMS Survey: The Bolometric Fluxes and Luminosity Distributions of Young Massive Stars. *A&A*, 149:12.

Murphy, T., Sadler, E.M., Ekers, R.D., et al., 2010. The Australia Telescope 20 GHz Survey: The source catalogue. *Monthly Notices of the Royal Astronomical Society*, 402(4):2403.

Nakanishi, H. and Sofue, Y., 2006. Three-dimensional distribution of the ISM in the Milky Way galaxy: II. The molecular gas disk. *Publications of the Astronomical Society of Japan*, 58(5):847.

Neugebauer, G., Habing, H.J., van Duinen, R., et al., 1984. The Infrared Astronomical Satellite (IRAS) mission. *The Astrophysical Journal*, 278:L1.

Nguyên Luong, Q., Motte, F., Hennemann, M., et al., 2011. The Herschel view of massive star formation in G035.39–00.33: dense and cold filament of W48 undergoing a mini-starburst. *Astronomy & Astrophysics*, 535:A76.

Ossenkopf, V. and Henning, T., 1994. Dust opacities for protostellar cores. *Astronomy and Astrophysics*, 291:943.

Palla, F. and Stahler, S.W., 2008. *The Formation of Stars*. Wiley-VCH, Weinheim.

Paron, S., Ortega, M.E., Petriella, A., et al., 2012. The molecular clump towards the eastern border of SNR G18.8+0.3. *Astronomy & Astrophysics*, 547:A60.

Paulson, S.T. and Pandian, J.D., 2017. Probing Early Phases of High Mass Stars with 6.7 GHz Methanol Masers. *Proceedings of the International Astronomical Union*, 13(S336):323.

Poglitsch, A., Waelkens, C., Bauer, O.H., et al., 2008. The Photodetector Array Camera and Spectrometer (PACS) for the Herschel Space Observatory. volume 7010, page 701005. International Society for Optics and Photonics.

Price, S.D., Egan, M.P., Carey, S.J., et al., 2001. Midcourse Space Experiment Survey of the Galactic Plane. *The Astronomical Journal*, 121(5):2819.

Purcell, C.R., Hoare, M.G., Cotton, W.D., et al., 2013. The Coordinated Radio and Infrared Survey for High-Mass Star Formation. Ii. Source Catalogue. *The Astrophysical Journal Supplement Series*, 205(1):1.

Ragan, S., Henning, T., Krause, O., et al., 2012. The Earliest Phases of Star Formation (EPoS): a Herschel key program. *Astronomy & Astrophysics*, 547:A49.

Ragan, S.E., Moore, T.J., Eden, D.J., et al., 2016. The prevalence of star formation as a function of Galactocentric radius. *Monthly Notices of the Royal Astronomical Society*, 462(3):3123.

Rahman, N., Bolatto, A., and Collaboration, S., 2011. Spatially Resolved Molecular Gas Star Formation Law in CARMA Survey Towards Infrared-bright Nearby Galaxies (STING). *American Astronomical Society Meeting Abstracts #218*, 218:130.01.

Ramesh, B. and Sridharan, T.K., 1997. Reliable Galaxy-wide identification of ultracompact HII regions. *Monthly Notices of the Royal Astronomical Society*, 284:1001.

Reid, M.J., Menten, K.M., Zheng, X.W., et al., 2009. Trigonometric Parallaxes of Massive Star-Forming Regions. Vi. Galactic Structure, Fundamental Parameters, and Noncircular Motions. *The Astrophysical Journal*, 700(1):137.

Rigby, A.J., Moore, T.J., Plume, R., et al., 2016. CHIMPS: The 13CO/C18O (J = 3 $\rightarrow$ 2) Heterodyne Inner Milky Way Plane Survey. *Monthly Notices of the Royal Astronomical Society*, 456(3):2885.

Roberts, W.W., 1969. Large-Scale Shock Formation in Spiral Galaxies and its Implications on Star Formation. *The Astrophysical Journal*, 158:123.

Rodriguez-Fernandez, N. and Combes, F., 2008. Gas flow models in the Milky Way embedded bars. *Astronomy and Astrophysics, Volume 489, Issue 1, 2008, pp.115-133*, 489:115.

Roman-Duval, J., Heyer, M., Brunt, C.M., et al., 2016. DISTRIBUTION AND MASS OF DIFFUSE AND DENSE CO GAS IN THE MILKY WAY. *The Astrophysical Journal*, 818(2):144.

Roman-Duval, J., Jackson, J.M., Heyer, M., et al., 2009. Kinematic distances to molecular clouds identified in the galactic ring survey. *Astrophysical Journal*, 699(2):1153.

Roman-Duval, J., Jackson, J.M., Heyer, M., et al., 2010. Physical properties and galactic distribution of molecular clouds identified in the galactic ring survey. *Astrophysical Journal*, 723(1):492.

Rosolowsky, E., Dunham, M.K., Ginsburg, A., et al., 2010. The Bolocam Galactic Plane Survey – II. Catalog of the Image Data. pages 123–138.

Rygl, K.L.J., Brunthaler, A., Sanna, A., et al., 2012. Parallaxes and proper motions of interstellar masers toward the Cygnus X star-forming complex. *Astronomy & Astrophysics*, 539:A79.

Salpeter, E.E., 1955. The Luminosity Function and Stellar Evolution. *The Astrophysical Journal*, 121:161.

Sanders, D.B., 1986. Luminous infrared galaxies. In *Revista Mexicana de Astronomia y Astrofisica: Serie de Conferencias*, volume 6, pages 42–47.

Sandstrom, K.M., Leroy, A.K., Walter, F., et al., 2013. The CO-TO-H2 conversion factor and dust-to-gas ratio on kiloparsec scales in nearby galaxies. *Astrophysical Journal*, 777(1):5.

Schmidt, M., 1959. The Rate of Star Formation. *The Astrophysical Journal*, 129:243.

Schruba, A., Leroy, A.K., Walter, F., et al., 2011. A molecular star formation law in the atomic-gas-dominated regime in nearby galaxies. *Astronomical Journal*, 142(2).

Schuller, F., Csengeri, T., Urquhart, J.S., et al., 2017. SEDIGISM: Structure, excitation, and dynamics of the inner Galactic interstellar medium. *Astronomy & Astrophysics*, 601:A124.

Schuller, F., Menten, K.M., Contreras, Y., et al., 2009. ATLASGAL – The APEX telescope large area survey of the galaxy at 870 μm. *Astronomy and Astrophysics*, 504(2):415.

Shu, F.H., Adams, F.C., and Lizano, S., 1987. Star Formation in Molecular Clouds: Observation and Theory. *Annual Review of Astronomy and Astrophysics*, 25(1):23.

Siringo, G., Kreysa, E., Kovacs, A., et al., 2009. The Large APEX Bolometer Camera LABOCA. *Astronomy & Astrophysics*, 497:945.

Smith, M.D., 2014. Evolutionary tracks of massive stars during formation. *Monthly Notices of the Royal Astronomical Society*, 438(2):1051.

Springel, V., Di Matteo, T., and Hernquist, L., 2005. Modelling feedback from stars and black holes in galaxy mergers. *Monthly Notices of the Royal Astronomical Society*, 361(3):776.

Stahler, S.W. and Palla, F.F., 2004. *The formation of stars*. Wiley-VCH, Weinham, Germany, first edition.

Stanimirović, S., Putman, M., Heiles, C., et al., 2006. First Results from the Arecibo Galactic H i Survey: The Disk/Halo Interface Region in the Outer Galaxy. *The Astrophysical Journal*, 653(2):1210.

Stecker, F.W., Solomon, P.M., Scoville, N.Z., et al., 1975. Molecular hydrogen in the Galaxy and galactic gamma rays. *The Astrophysical Journal*, 201:90.

Talbot, R. J., J., 1980. Rate of star formation, dynamical parameters, and interstellar gas density in our Galaxy and M83. *The Astrophysical Journal*, 235:821.

Tan, J.C., Beltr, M.T., Caselli, P., et al., 2014. Massive Star Formation. In *Protostars and Planets VI*, volume astro-ph, page 21.

Thompson, M.a., Hatchell, J., Walsh, a.J., et al., 2006. A SCUBA imaging survey of ultracompact HII regions: The environments of massive star formation. 1026:1003.

Thompson, M.A., Serjeant, S., Jenness, T., et al., 2007. The SCUBA-2 "All-Sky" Survey. *Astronomy & Astrophysics*, 453(3):1003.

Thompson, M.A., Urquhart, J.S., Moore, T.J., et al., 2012. The statistics of triggered star formation: An overdensity of massive young stellar objects around Spitzer bubbles. *Monthly Notices of the Royal Astronomical Society*, 421(1):408.

Twarog, B.A., Ashman, K.M., and Anthony-Twarog, B.J., 1997. Some Revised Observational Constraints on the Formation and Evolution of the Galactic Disk. *The Astronomical Journal*, 114:2556.

Urquhart, J.S., Busfield, A.L., Hoare, M.G., et al., 2007a. The RMS survey 13 CO observations of candidate massive YSOs in the southern Galactic plane. *A&A*, 474:891.

Urquhart, J.S., Busfield, A.L., Hoare, M.G., et al., 2007b. The RMS Survey: Radio observations of candidate massive YSOs in the southern hemisphere. *Astronomy and Astrophysics*, 461(1):11.

Urquhart, J.S., Busfield, A.L., Hoare, M.G., et al., 2008a. The RMS survey: 13CO observations of candidate massive YSOs in the northern Galactic plane. *Astronomy and Astrophysics*, 487(1):253.

Urquhart, J.S., Csengeri, T., Wyrowski, F., et al., 2014a. ATLASGAL – Complete compact source catalogue: 280°< < 60°. *Astronomy & Astrophysics*, 568:A41.

Urquhart, J.S., Figura, C.C., Moore, T.J.T., et al., 2014b. The RMS survey: Galactic distribution of massive star formation. *Monthly Notices of the Royal Astronomical Society*, 437(2):1791.

Urquhart, J.S., Hoare, M.G., Lumsden, S.L., et al., 2008b. The RMS Survey: A Galaxy-wide Sample of Massive Young Stellar Objects. *ASPC*, 387:381.

Urquhart, J.S., Hoare, M.G., Purcell, C.R., et al., 2009. The RMS survey: 6 cm continuum VLA observations towards candidate massive YSOs in the northern hemisphere. *Astronomy and Astrophysics*, 501:539.

Urquhart, J.S., König, C., Giannetti, A., et al., 2018. ATLASGAL - Properties of a complete sample of Galactic clumps. *Monthly Notices of the Royal Astronomical Society*, 473(1):1059.

Urquhart, J.S., Moore, T.J., Hoare, M.G., et al., 2011. The Red MSX Source survey: Distribution and properties of a sample of massive young stars. *Monthly Notices of the Royal Astronomical Society*, 410(2):1237.

Urquhart, J.S., Moore, T.J., Menten, K.M., et al., 2014c. The almost ubiquitous association of 6.7-GHz methanol masers with dust. *Monthly Notices of the Royal Astronomical Society*, 446(4):3461.

Urquhart, J.S., Moore, T.J., Schuller, F., et al., 2013a. ATLASGAL - environments of 6.7 GHz methanol masers. *Monthly Notices of the Royal Astronomical Society*, 431(2):1752.

Urquhart, J.S., Moore, T.J.T., Csengeri, T., et al., 2014d. ATLASGAL - towards a complete sample of massive star forming clumps. *Monthly Notices of the Royal Astronomical Society*, 443(2):1555.

Urquhart, J.S., Thompson, M.A., Moore, T.J.T., et al., 2013b. ATLASGAL - properties of compact H II regions and their natal clumps. *Monthly Notices of the Royal Astronomical Society*, 435(1):400.

Vallee, J.P. and P., J., 2014. Catalog of observed tangents to the spiral arms in the Milky Way galaxy. *The Astrophysical Journal Supplement, Volume 215, Issue 1, article id. 1, 9 pp. (2014).*, 215.

van der Tak, F. and Menten, K., 2005. Very compact radio emission from high-mass protostars. II. Dust disks and ionized accretion flows. *Astronomy & Astrophysics*, 437(3):947.

Vutisalchavakul, N., Evans II, N.J., and Heyer, M., 2016. STAR FORMATION RELATIONS IN THE MILKY WAY. *The Astrophysical Journal*, 831(1):73.

Walsh, A.J., Burton, M.G., Hyland, A.R., et al., 1998. Studies of Ultracompact HII Regions - II. High-Resolution Radio Continuum and Methanol Maser Survey. *Monthly Notices of the Royal Astronomical Society*, 301:640.

Watson, M., 2010. Assessing the Performance of Sub-Millimetre Compact Object Detection Algorithms. *Masters Thesis*, page 1.

Weingartner, J. and Draine, B., 2001. Dust Grain–Size Distributions and Extinction in the Milky Way, Large Magellanic Cloud, and Small Magellanic Cloud. *The Astrophysical Journal*, 548(1):296.

Wienen, M., Wyrowski, F., Schuller, F., et al., 2012. Ammonia from cold high-mass clumps discovered in the inner Galactic disk by the ATLASGAL survey. *Astronomy & Astrophysics*, 544:A146.

Wilson, T., 1972. 4830 MILz Observations of the Formaldehyde Molecule in the Direction of Discrete Radio Sources. *Astronomy and Astrophysics*, 19:354.

Wilson, T.L. and Pauls, T., 1984. Astronomy and astrophysics. *Astronomy and Astrophysics*, 138:225.

Wolfire, M.G. and Cassinelli, J.P., 1987. Conditions for the formation of massive stars. *The Astrophysical Journal*, 319:850.

Wong, T. and Blitz, L., 2002. The Relationship between Gas Content and Star Formation in Molecule-rich Spiral Galaxies. *The Astrophysical Journal*, 569(1):157.

Wood, D.O.S. and Churchwell, E., 1989. The morphologies and physical properties of ultra-compact H II regions. *The Astrophysical Journal Supplement Series*, 69:831.

Wouterloot, J., Brand, J., Burton, W., et al., 1990. IRAS Sources beyond the Solar Circle. *Astronomy & Astrophysics*, 230:21.

Wouterloot, J., Brand, J., and Henkel, C., 1988. Star Formation in the outer Galaxy. *A&A*, 191:323.

Wright, E.L., Eisenhardt, P.R.M., Mainzer, A., et al., 2010. The Wide-field Infrared Survey Explorer (WISE): Mission Description and Initial On-orbit Performance. *The Astronomical Journal, Volume 140, Issue 6, article id. 1868-1881 (2010).*, 140.

Xu, J.L., Zavagno, A., Yu, N., et al., 2019. The effects of ionization feedback on star formation: A case study of the M16 H II region. *Astronomy & Astrophysics*.

Yuan, J., Wu, Y., Ellingsen, S.P., et al., 2017. High-mass Starless Clumps in the inner Galactic Plane: the Sample and Dust Properties. *The Astrophysical Journal Supplement Series*, 231(1):11.

Zavagno, A., Anderson, L.D., Russeil, D., et al., 2010. Star formation triggered by H II regions in our Galaxy. *Astronomy and Astrophysics*, 518:L101.

Zinnecker, H. and Yorke, H.W., 2007. Toward Understanding Massive Star Formation. *Annual Review of Astronomy and Astrophysics*, 45(1):481.

Zoonematkermani, S., Helfand, D.J., Becker, R.H., et al., 1990. A catalog of small-diameter radio sources in the Galactic plane. *The Astrophysical Journal Supplement Series*, 74:181.